TRANSPORT OF TRACE METALS

IN NEARSHORE SEDIMENTS

by

WILLIAM R. MARTIN

A.B., Brown University, 1973

B.S., University of Washington, 1979

SUBMITTED IN PARTIAL FULFILLMENT

OF THE REQUIREMENTS FOR THE DEGREE OF

DOCTOR OF PHILOSOPHY

at the

MASSACHUSETTS INSTITUTE OF TECHNOLOGY

and the

WOODS HOLE OCEANOGRAPHIC INSTITUTION

APRIL, 1985

Signature of Author _____
Joint Program in Oceanography, Massachusetts Institute of Technology and Woods Hole Oceanographic Institution, and the Department of Earth, Atmospheric, and Planetary Sciences, Massachusetts Institute of Technology

Certified by _____
F.L. Sayles, Thesis Superviser

Accepted by _____
Cindy Lee, Chairman, Joint Committee for Chemical Oceanography, Massachusetts Institute of Technology/ Woods Hole Oceanographic Institution.

ABSTRACT

The focus of this thesis is on rates of transport of metals both across the sediment/water interface and within the sediment column of nearshore sediments. The early diagenesis of several first-row transition metals exhibiting a variety of behaviors in the ocean -- Mn, Fe, Co, Ni, and Cu -- has been studied intensively at a site in Buzzards Bay, Mass. By limiting the study to a single site, independent measurements over the seasonal cycle of the concentrations of the metals in pore water, of the pore water constituents important to metal cycling, and of particle and solute transport rates could be made at the same site. In addition, a direct, in situ study of the interaction of chemical and transport processes was undertaken using radiotracer techniques. Thus, the study emphasizes the mechanisms of metal cycling near the interface of nearshore sediments.

Transport rates were estimated using excess ^{234}Th distributions for particle transport, and pore water ^{222}Rn deficit distributions for solute transport. Particle transport rates, modeled by analogy to Fickian diffusion, ranged from $7\text{-}80 \times 10^{-8}$ cm^2/sec, with excess ^{234}Th reaching to 2-2.5 cm below the interface. There was a significant seasonal variation in rates, with a warm-season average of 40×10^{-8} cm^2/sec and a cold-season average of 20×10^{-8} cm^2/sec. ^{234}Th-derived mixing rates were applied to Mn distributions through a mass balance model of Mn cycling. It was found that a particulate flux due to bioturbation, from the net dissolved Mn removal layer to a net dissolved Mn production layer ajdacent to the interface, was as large as 38% of net dissolved Mn production. Mixing of particulate Fe sulfides may have a similar importance for Fe cycling.

Solute transport was estimated using measured $^{222}Rn/^{226}Ra$ disequilibrium. The pore water ^{222}Rn deficit could be explained using a model including vertical molecular diffusion and exchange with overlying seawater via exchange of pore water with bottom water in rapidly flushed burrows. Cores taken in all seasons could be split into three groups: (1) December through March: the ^{222}Rn deficit was explained by vertical molecular diffusion alone; (2) early summer (June): irrigation affected the ^{222}Rn profile to a depth of at least 20 cm; (3) late summer/fall: irrigation was still important near the interface, affecting ^{222}Rn profiles to depths of 10-12 cm. ^{222}Rn deficits were adequately explained by an exchange parameter (α) which decreased exponentially with depth below the interface, but not by a constant-α model. Previous studies have explained irrigation using a constant exchange parameter throughout the irrigated layer. For comparative purposes, an α averaged over the upper 20 cm of the sediment column was calculated at the Buzzards Bay site: the range of depth-averaged α values found, $4\text{-}12 \times 10^{-7}$ sec^{-1}, is in agreement with values reported previously for a variety of nearshore sediments, using pore water SiO_2 as a tracer, of

$1\text{-}20 \times 10^{-7}$ sec^{-1}. ^{222}Rn-derived irrigation rates were applied to pore water Mn and Fe distributions. It was estimated that irrigation may contribute 20-40% of the dissolved Mn flux across the interface and about 20% of the dissolved Fe flux.

Study of pore water metal chemistry at the Buzzards Bay site included measurements of pore water Mn and Fe during all seasons, and measurements of Co, Cu, and Ni in two cores: one under late winter conditions when the interface is most oxidizing; one when sulfate reduction was very important in the upper centimeter of the sediments. Fe regeneration sufficient to produce enrichments on water column particles was observed only during periods of summer and fall when the interface was reducing; otherwise, oxidation of Fe to insoluble Fe(III) limited Fe fluxes. Mn, Co, Cu, and Ni fluxes varied inversely to Fe fluxes; the primary control on fluxes of these elements was their limited solubility in reducing marine systems. The control was least important for Mn and Co; fluxes of Ni and Cu were significantly greater than zero only when sulfate reduction was unimportant in the upper centimeter of the sediment column. Fluxes of Mn were sufficient to affect the water column Mn distribution, with enrichments on water column particulates of up to 10,000 ppm inferred from calculated fluxes. Tentative estimates of the turnover time of dissolved Co, Cu, and Ni in the water column relative to the benthic flux indicated that the flux may be a significant contributor to the coastal Co cycle (turnover time = 1 yr), but is less likely to be important to Cu and Ni cycles (turnover times greater than 2 yrs).

<u>In situ</u> radiotracer migration experiments were carried out at the Buzzards Bay site. ^{54}Mn, ^{59}Fe, ^{60}Co, and ^{63}Ni were released into the sediments at depths ranging from 2.5 to 7 cm below the interface. The order of mobilities was Mn>>Fe>Co,Ni, which is similar to the solubility trend for these metals in reducing marine systems. ^{63}Ni and ^{60}Co were essentially particle-bound in these experiments; apparent diffusion coefficients calculated from thier dispersion rates agreed with particle mixing rates from excess ^{234}Th distributions. Solid:solution distribution coefficients were calculated from ^{54}Mn dispersion and found to agree with directly measured values. The coefficient was approximately 15 (dpm/gm solid ÷ dpm/gm pore water) in the upper 0.5 cm and below 5 cm, and 5-10 from 0.5 to 5 cm. Distribution coefficients for ^{59}Fe were approximately 120 below 0.5 cm. Although the trend of the distribution coefficients is clear, the quantitative results from these expreiments are preliminary, in that the model used to explain metal ion dispersion, when applied to the nonreactive tracer, ^{36}Cl, could only explain a portion of the ^{36}Cl distribution. The agreement between calculated and directly measured ^{54}Mn distribution coefficients, as well as the way the distributions of tracers varied as a function of apparent diffusion coefficient and time, provides evidence in favor of the adequacy of the model used.

TABLE OF CONTENTS

LIST OF TABLES

LIST OF FIGURES

ACKNOWLEDGEMENTS

I first developed an interest in pore water chemistry while working with Jim Murray as an undergraduate at the University of Washington; my interest grew into a thesis project and, finally, a thesis in part because of the support of my thesis advisor at WHOI, Fred Sayles. Without his technical and scientific advice, the project never would have gotten off the ground. The other members of my thesis committee, Kirk Cochran and Ed Boyle, provided invaluable advice in their fields of expertise. The thesis itself benefitted substantially from the thoughtful reviews of all the thesis committee members.

One person alone cannot do all the work that goes into a thesis, and I have had more than my share of help. All the members of the Sayles lab -- Charlie Olson, Wayne Dickinson, Lary Ball, Barb Brockhurst, Elsa Chase, JoAnn Olmstead, and Scot Birdwhistell -- were more than generous with their time and with advice on all aspects of the project, from equipment design to analytical procedures to helping with the analyses themselves.

The really hard work of the last three years has been the sampling in Buzzards Bay. The people who helped with SCUBA diving deserve special mention. Charlie Olson, Lary Ball, Hovey Clifford, and Will Clarke willingly dove with me and for me, under the best and worst of conditions. Dick Colburn's patience and expertise on the Asterias made our Buzzards Bay expeditions both successful and enjoyable. Ann McNichol labored with me through too many long and arduous glove bag sessions, and Bruce Brownawell did some time, too. The project literally could not have been done without their help.

Even if a student could finish a thesis without the friendship, encouragement, and support of those around him, it wouldn't be worth it. All of my fellow Joint Program students, and all of the people with whom I've worked, have made my stay at WHOI a pleasure. The organizers of the local weekend (and evening, and weekday) sports scene know, too well, the ordering of my priorities. Finally, Ann has provided the support and encouragement I've needed to get through the drudgery and frustration. Last, but most important, my parents and family have given unfailing support throughout an incredibly long academic career. I can't remember a single time when they questioned the worth of what I was doing, even when I doubted it myself.

Financial support for parts of this work have come from: National Science Foundation grant # OCE-82-16425; Department of Commerce, NOAA, National Sea Grant College Program, under grant # NA80-AA-D-00077 (R/P/7); from the Coastal Research Center of the Woods Hole Oceanographic Institution; and from the WHOI Education Office.

Chapter I

General Introduction

Introduction

Oceanic budgets for first-row transition metals have been a subject of research since early observations of trace metal enrichments in pelagic sediments. In general, these metals are not significantly enriched in nearshore muds but become more enriched from Atlantic clays to Pacific clays and reach their highest concentrations in the sediments of active ridge crests (Turekian & Imbrie, 1966; Chester & Aston, 1976; Elderfield, 1976). Explanations for these enrichments have been slow in coming because of the difficulty of making accurate measurements of dissolved trace metal concentrations. Recently, improvements in sampling and analytical techniques (Boyle & Edmond, 1975; Bruland & Franks, 1979) have prompted extensive oceanic sampling, and a fairly large body of data on the seawater distributions of these elements is now available. As a result, processes determining their oceanic distributions are becoming better understood: the role of biological cycling has been studied in some detail (Boyle et al., 1981; Bruland, 1980; Collier, 1981); the important role of the redox chemistry of Fe and Mn has been demonstrated

(Spencer & Brewer, 1971; Bender et al., 1977; Froelich et al., 1979), as has the importance of Fe and Mn oxides as scavengers, along with terrigenous and biogenic particles, of other trace metals (Murray & Brewer, 1977; Parks, 1975). However, sampling at oceanic boundaries -- in rivers and the coastal ocean, in the atmosphere, at the sediment/seawater interface, in ocean-floor hydrothermal solutions-- is only beginning to provide enough accurate data to enable a quantitative assessment of the relative importance of the various sources of metals to the oceans. In particular, only a few studies of pore water metal chemistry have included trace elements: Klinkhammer and coworkers (Klinkhammer, 1980; Klinkhammer et al., 1982) and Sawlan & Murray (1983) have reported measurements of Ni and Cu in pelagic and hemipelagic sediments, and studied their oxic and suboxic diagenesis; Elderfield et al. (1981a) and Emerson et al. (1984) have studied Ni and Cu diagenesis through pore water measurements in nearshore sediments. Only one study of Co pore water chemistry has so far been reported (Heggie & Lewis, 1984).

The primary goal of the study presented here is to examine the ability of early diagenesis in nearshore sediments to convert particulate metals to dissolved form and to return them to the water column. The approach that has been taken is to choose first row transition metals exhibiting a variety of behaviors in the ocean -- Mn, Fe, Cu, Ni, and Co -- and to study their diagenesis intensively at a single site. In this way, independent measurements of the concentrations of the metals in pore water, of the pore water constituents important to metal cycling, and of solute and particle transport rates could be made at the same site. In

addition, a direct study of the interaction of chemical and transport processes was undertaken using radiotracer techniques. Thus, the emphasis of this study has been on the mechanisms of metal cycling near the interface of nearshore sediments. Once cycling mechanisms are understood well, results from a few well-characterized study sites can be used to draw general conclusions about the role of nearshore sediments in the transport of metals from the continents to the open ocean.

The first chapter of this thesis presents a review of recent work relating to the early diagenesis of metals in nearshore sediments. Two aspects of the study of early diagenesis are important to understanding metal cycling: the study of the transport processes affecting the distributions of particles and solutes near the sediment/water interface, and the study of the chemistry of metals in seawater and reducing marine systems. Recent work in these areas will be reviewed separately: first, transport processes will be described; then, work on the marine chemistry of Mn, Fe, Cu, Ni, and Co will be discussed.

Transport Processes

Transport processes affecting early diagenesis can be divided into two general groups: processes effecting the transport of bulk sediments and of particles alone, and processes transporting water and solutes. Many of the processes transporting bulk sediments and particles occur near the sediment/water interface and are important determinants of the distribution of solid substrates for microbial activity; many of the results of these processes can be described through an analogy of the processes to Fickian diffusion. The second group of processes -- those transporting water and solutes -- are quite complex, in that simple one-dimensional diffusion models have proven inadequate for describing their effects. Nonetheless, an adequate description of them is essential to the quantitative description of early diagenesis in nearshore sediments.

In this section, the development of models describing transport processes in nearshore sediments will be discussed. First, simple models that have been used to describe particle and bulk sediment transport near the sediment/water interface will be discussed; this discussion will be followed by a treatment of the development of methods of describing solute transport.

Solid Phase and Bulk Sediment Transport.

Early studies of particle mixing considered a simple case: the dispersion of a nonreactive, instantaneous-source tracer deposited in the deep sea. The most important result of the mixing process was the spreading of the thin layer of tracer as it was buried, a result which could be explained by imagining an infinitely rapidly mixed layer at the sediment surface (Berger & Heath, 1968). Guinasso & Schink (1975) succeeded in extracting a mixing parameter from the sedimentary record of these instantaneous-source tracers by modeling their profiles as the result of a process analogous to Fickian diffusion, an analogy drawn earlier by Goldberg & Koide (1962). With the introduction of a variable mixing parameter, the interaction of mixing processes and competing chemical processes became evident: if the competing processes are slow relative to mixing, then the tracer they are acting on will be uniformly distributed throughout the mixed layer; the more rapid the competing process, the steeper the gradient of the tracer in the mixed layer will be, despite the homogenizing effect of mixing. Particle-associated radioactive elements have become the primary tools for the study of particle mixing: in steady state, their gradients in the mixed layer of sediments are produced by a simple combination of radioactive decay, mixing, and burial. Because the effects of mixing on a tracer's profile vary with the rates of processes consuming the tracer, tracers with different half-lives are useful for determining different ranges of mixing rates: ^{230}Th ($t_{1/2}$ = 75,200 yrs) and ^{14}C ($t_{1/2}$ = 5700 yrs)

have been used to measure slow mixing rates; ^{210}Pb ($t_{1/2}$ = 22.3 yrs), ^{234}Th ($t_{1/2}$ = 24.1 days), and anthropogenic tracers with known input functions (in particular, Pu) have been used to detrmine more rapid rates (Nozaki et al., 1975; Demaster & Cochran, 1982; Aller & Cochran, 1976; Aller & Demaster, 1984). The original analogy of sediment particle mixing to Fickian diffusion has held up well for near-surface mixing: the observable consequences of this process are the result of a large number of small-scale, randomly oriented mixing events. The model cannot explain the transfer of particles over distances of 10-20 cm by falling in empty burrows or by feeding organisms: these events are isolated in time and space, and are not effectively averaged over the lifetime of tracers used to measure mixing. In addition, particle transport by "conveyor-belt" species, who feed at depth in the sediments and deposit ingested particles at the sediment surface, cannot be described by the Fickian diffusion analogy; Robbins (1984) has recently introduced a model to explain the effects of conveyor-belt transport on the distributions of particle tracers. Another important problem that has limited the use of the mixing model is that, when mixing is slow, burial by sedimentation becomes significant, and independent information on sedimentation rates is needed.

These problems have not prevented the modeling of particle mixing processes, and the use of a suite of tracers has led to quantitative esitmates of the variability of mixing rates in deep-sea and nearshore sediments. Demaster & Cochran (1982), in a study of differing sediments in widely separated areas, found ^{210}Pb-derived mixing rates

ranging from 1.3×10^{-9} to 8×10^{-9} cm^2/sec in surface mixed layers 7 to 15 cm in vertical extent. Aller & DeMaster (1984) used ^{234}Th and ^{210}Pb to derive a mixing rate of 9×10^{-7} cm^2/sec in a surface mixed layer 5 cm deep in NW Atlantic continental rise and Panama Basin sediments. In nearshore sediments, seasonally varying particle mixing rates of 10^{-8} to 10^{-6} cm^2/sec have been measured using ^{234}Th in Long Island Sound sediments; the rapidly mixed layer was about 5 cm deep, with slower particle mixing to 10-12 cm. (Aller & Cochran, 1976; Aller et al., 1980). Nozaki et al (1977) and Aller & Demaster (1984) have used pairs of isotopes with differing half-lives ($^{210}Pb/^{14}C$ and $^{234}Th/^{210}Pb$) to show the decrease in particle mixing rates with depth in the sediment column in deep-sea sediments; Benninger et al. (1979) demonstrated the use of a suite of four tracers to show the variability of mixing rates downcore in nearshore sediments.

Solute Transport

The transport of bulk sediment by bioturbation and wave and current scouring has an important direct influence on solute distributions only in a few cases: as has been shown, the mixing coefficients describing the process range from about 10^{-9} to 10^{-6} cm^2/sec, while molecular diffusion coefficients in sediments are about

10^{-6} to 10^{-5} cm^2/sec. In most cases, it is molecular diffusion and irrigation processes that influence solute distributions directly.

The effects of irrigation processes are most pronounced in nearshore sediments underlying shallow, highly productive water columns. There, they are driven by an abundant and active benthic fauna supported by a rapid supply of organic matter to the sediment surface; they are the result of the metabolic activities of tube-dwelling macroinfauna which pump burrow water and overlying seawater, keeping their burrows flushed of the breakdown products of their metabolic activities and supplied with O_2 (Aller & Yingst, 1978; Aller et al., 1983). Currents and the pumping action of waves and tides can also contribute to irrigation, particularly when tube and burrow structures are present. Irrigation processes have been seen to cause enhanced transport across the sediment/water interface, to cause flattening of pore water gradients in the presence of chemical reactions, and to cause subsurface extrema in solute profiles in the absence of chemical reactions. Models of solute distributions during early diagenesis must be able to explain these features.

A simple diagenetic equation for a solute concentration, C, assuming constant porosity, a constant diffusion coefficient, and negligible burial advection, shows how irrigation is included in diagenetic models:

$$\partial C/\partial t = D_{sed}(\partial^2 C/\partial x^2) + I + \Sigma R \qquad (I.1)$$

D_{sed} = diffusion coefficient, corrected for tortuosity, porosity
I = irrigation rate term
ΣR = reaction rate terms

The effects of the irrigation process on the profiles of pore water constituents have been described as diffusion in the vertical direction; as a horizontal diffusive process within a microenvironment defined by rapidly flushed burrows plus the sediments between the burrows; as an advective process; and, in a nonmechanistic way, as an exchange via burrows between bottom water and sediment pore waters.

The simplest way to treat irrigation is as a vertically oriented diffusive process. The diagenetic equation remains one dimensional, with flux described by

$$\partial F/\partial x = -\{D_{sed}(\partial^2 C/\partial x^2) + D_i(\partial^2 C/\partial x^2)\}$$

D_i = apparent diffusion coefficient describing irrigation rate

so that C(x) is given by

$$\partial C/\partial t = D_{app}(\partial^2 C/\partial x^2) + \Sigma R$$

Models of this sort have been used to describe fluxes across the sediment/water interface. Martens and coworkers (1980) measured the pore water concentration gradients (dC/dx) and the flux across the sediment/water interface (J) of a nonreactive tracer independently to define an apparent diffusion coefficient,

$$D^i_{app} = \frac{J_{i(meas)}}{\phi(dC/dx)_{pore\ water, x=0}}$$

(ϕ = porosity)

By assuming that the relative enhancement over molecular diffusion is the same for all dissolved species, they could calculate "effective" diffusion coefficients for all species which could in principle be combined with pore water concentration gradients to predict fluxes. Goldhaber et al (1977) used a similar simple one dimensional model to explain pore water profiles with diffusion/reaction equations . By assuming that the mixed layer (zone 1) overlies a molecular-diffusion layer (zone 2), they could calculate an effective diffusion coefficient from a flux continuity requirement at the boundary between the layers (at depth L):

$$D_{app} = \frac{D_{molec}(dC/dx)_{zone\ 2,\ x=L}}{(dC/dx)_{zone\ 1,\ x=L}}$$

However, pore water profiles are rarely as simple as the simple two-layer case. Often, irrigation processes produce extrema in solute profiles which cannot be explained by chemical reactions as well as constant profiles in the presence of reactions. When a simple, diffusion-type model of irrigation is applied, the coefficient which correctly explains the flux across the interface often cannot explain the pore water profile (Aller, 1980c). In these cases, models calling for a "nonlocal source" term (Emerson et al., 1984; Boudreau, 1984) allowing exchange between nonadjacent volume elements -- in particular, pore water well below the sediment/seawater interface and overlying water -- have been more successful. The connection allowing the exchange is burrows of the macroinfauna. For simplicity, burrow water is assumed similar to

overlying water. Exchange is then accomplished either by diffusion across the burrow wall or by advection through the wall. The flux of a solute across the wall is determined by an exchange parameter and the burrow/pore water concentration difference.

Aller (1980) developed a model in which nonlocal exchange is achieved by radial diffusion into vertically oriented burrows. Thus, the diagenetic equation is two dimensional, and the irrigation term in (I.1) is

$$I = \left(\frac{D_{sed}}{r}\right) \cdot \frac{\partial}{\partial r}\left\{r \frac{\partial C}{\partial r}\right\}$$

The transport process operating is molecular diffusion, and enhanced exchange over vertical molecular diffusive exchange is achieved by the decrease in diffusion distance caused by burrows below the sediment/water interface holding water that is rapidly exchanged with overlying seawater. Aller found that his model predicted both pore water concentration profiles and fluxes across the sediment/water interface (Aller, 1980a, 1980b). The drawback of the model is that it requires substantial knowledge of the local fauna: if one solute profile is used to determine the average burrow spacing (which fixes the very important radial diffusion distance), then knowledge of local fauna must provide the average burrow radius and length. If an _in situ_ reaction rate is to be determined, then knowledge of burrow spacing must be gained independently, either from another profile or from measured faunal abundance.

Other models describe the nonlocal exchange differently. They have been inspired by the "biopumping" models of Hammond & Fuller (Hammond & Fuller, 1979; Smethie et al., 1981) and of McCaffrey et al (1980) and Luedtke & Bender (1979). These original models specified advective exchange between burrows and the sediments they occupy; thus, as in Aller's model, exchange through burrows between pore water and overlying water depends on the pore water/overlying water concentration difference. The mechanism of increasing the flux over a diffusive flux is quite different: the model implies vertical pore water advection toward the sediment/water interface to balance input of water through burrows. These models have been applied as box models, predicting fluxes using transport parameters derived from in situ incubations and ^{222}Rn tracer (Hammond & Fuller, 1979), pore water ^{222}Rn measurements (Smethie et al., 1981), or laboratory incubations and ^{22}Na (McCaffrey et al.,1980; Luedtke & Bender, 1979) along with average pore water concentrations in the burrow-containing zone. Thus, the models cannot predict pore water profiles. However, they do imply a fairly simple diagenetic equation, with irrigation term (see eqn. I.1)

$$(P(x)/\phi)(C_{OL}-C)$$

$P(x)$ = vol. of water flowing through burrows, $cm^3_{water}/cm^3_{sed}.sec$
C_{OL} = concentration in overlying water

The advection velocity required to balance the flow of water through burrow walls increases as the sediment/water interface is approached, and is given by

$$v = - \frac{\int_{x_0}^{x} P(x)dx}{\phi}$$

x_0 = burrow length, from interface to bottom of burrow

The applicability of these models may be limited. Since burrow linings and fine-grained sediments are both rather impermeable to advective flow (Aller, 1982; Smethie et al., 1981), they may apply only in sandy sediments containing unlined burrows.

It can be shown that, if a linear approximation to dC/dr at the burrow wall holds, Aller's radial diffusion model reduces to a nonlocal source model with an irrigation term similar to that in the biopumping models (Boudreau, 1984; Emerson et al., 1984)

$$I = - \alpha(x) \cdot (C - C_{o_L})$$

Thus, with an intuitively appealing simplification, a simple model allowing rapid exchange between pore water in the burrowed zone of sediments and overlying water has been made. Because it is likely that the rate of exchange of pore water solutes with overlying water varies with depth below the interface, a positive feature of this model is that it is relatively simple to include a depth-dependent α in it. Using Boudreau's relationship (Boudreau, 1984), the approximation to physical reality can be assessed with measurement of Aller's benthos-describing parameters. The model has been applied both to pore water data and to benthic flux data. Estimates of α are found to vary over a relatively small range in a variety of coastal sediments, from about $1\text{-}20 \times 10^{-7}$ sec^{-1} (Emerson et al, 1984).

The work on modeling pore water profiles in nearshore sediments has demonstrated that both fluxes and pore water profiles can be explained if diffusive exchange with overlying water is allowed both vertically and horizontally via rapidly flushed animal burrows. The important effect of a sediment component's chemistry on its transport has also been shown. Obviously, since solute transport is faster than solid phase transport, reactions causing solid/solution phase changes are critical. Further, the position in the sediment column of solute production is an important determinant of the mode of transport of a sediment component: vertical diffusion dominates for solutes with large pore water gradients near the sediment/water interface, while irrigation processes dominate for other components (McCaffrey et al.,1980; Emerson et al., 1984). In addition, reactions near the sediment/water interface, unresolved by pore water measurements, may be an important factor in sediment/seawater exchange (Klump & Martens, 1981). Aller (1980c, 1983) has shown that reaction type can influence the effects of irrigation on profiles and fluxes of solutes, since its effects on solutes produced by zero-order and first-order reactions differ. Another factor which is beginning to be examined (Aller, 1983; Aller et al., 1983) is the chemistry of the burrow lining and of the zone immediately surrounding the burrow: both may have important effects on the rates of transport of particular solutes across burrow walls.

Pore Water Chemistry

In the preceding discussion of transport processes in sediments, it was shown that estimates of particle and bulk sediment mixing coefficients in marine sediments range from about 10^{-9} to 10^{-6} cm^2/sec. Sediment molecular diffusion coefficients for dissolved first-row transition metals, on the other hand, are on the order of $3x10^{-6}$ cm^2/sec. Even in the absence of irrigation, solute transport is considerably more rapid than transport of particle-bound species. Thus, the ability of a nearshore sedimentary system to recycle metals to the water column will be significantly influenced by chemical factors determining the rate and position in the sediment column of solid/solution phase changes. In this section, knowledge of solid/solution exchanges of metals gained from previous water column, deep-sea sediment, and nearshore sediment studies will be reviewed.

First, it is useful to put the discussion in perspective with a simple model of the behavior of metals in nearshore sediment systems. The model is qualitative in intent, and is built on several rather strong assumptions. To emphasize the relationship between transport and reaction, solute transport is assumed to occur by vertical molecular diffusion only. Because the metals under study here often have pore water profiles in nearshore sediments featuring near-interface maxima, vertical diffusion is the primary transport process affecting them. Two types of reaction are considered: reactions which produce dissolved metal ions from particulate sources at rate P ($moles/cm^2.sec$), and those causing

removal of the metals from solution and limiting their concentration to C_E (moles/cm^3). These reactions are assumed to occur rapidly in narrow sediment layers. While this assumption is shown to be justifiable by pore water metal profiles in reducing, nearshore sediments, it should be kept in mind that pore water profiles reflect the net result of competing reactions, and that both dissolution and precipitation may occur throughout the portion of the sediment column included in the model. Thus, the "production" layer is a layer in which dissolved metal production is clearly the dominant process, and the "removal" layer is a layer dominated by the consumption of the dissolved metal. The strongest assumption of the model is that the production layer occurs above the removal layer in the sediment column: as will be shown in Chapter III, this assumption appears to be valid for Mn, Co, Cu, and Ni, but is clearly violated for Fe. Important model variables are illustrated in Figure I.1.

In steady state, under the conditions of this model, a mass balance may be written for the production layer,

$$P = F_{OUT} + F_D \qquad (I.2)$$

Dissolved metal production (P) is balanced by the flux from sediments to overlying water (F_{OUT}) and the flux from the production layer down into the sediments (F_D). As long as solubility control is important, the "solubility-limited" concentration of the dissolved metal (C_E, the metal concentration in the removal layer) will be less than the concentration in the production layer, C_P, and F_D will be directed out of the production

Figure I.1

A Model Dissolved Metal Concentration Profile

A hypothetical dissolved metal concentration profile in a nearshore sediment system.

C_{OL} = concentration of the dissolved metal in overlying seawater

C_P = concentration of the dissolved metal at its maximum, in the net dissolved metal production layer

C_E = concentration of the dissolved metal in the net metal precipitation layer

L_p = distance from the sediment/water interface to the net dissolved metal production layer

L_r = distance from production to precipitation layer.

In the figure:

A = sediment/water interface
B = dissolved metal production layer
D = metal precipitation layer

Figure I.1

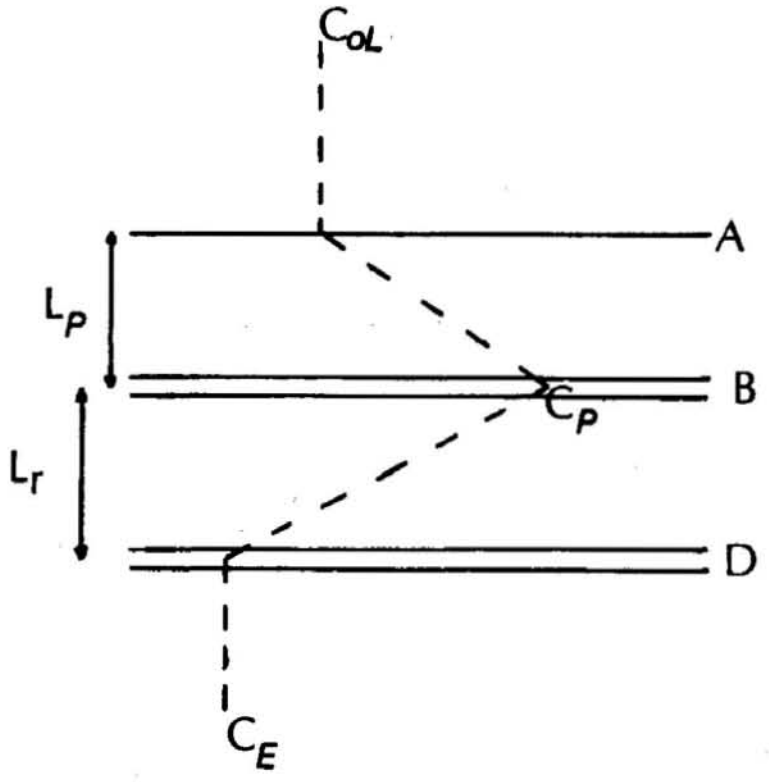

layer:

$$(I.3) \qquad F_D = \phi D_{sed}\frac{(C_P - C_E)}{L_r}$$

(L_r is the distance from the production layer to the removal layer; concentration terms are defined in Figure I.1. ϕ is porosity, D_{sed} is the sediment diffusion coefficient for the dissolved metal). The flux of the dissolved metal out of the sediments is given by:

$$(I.4) \qquad F_{out} = \phi D_{sed}\frac{(C_P - C_{OL})}{L_P}$$

(L_P is the distance from the sediment/water interface to the production layer). (I.2), (I.3), and (I.4) can be combined to give an expression for the dissolved metal concentration in the production layer,

$$(I.5) \qquad C_P = \frac{1}{W}\cdot\{(\phi D_{sed}/L_p)\cdot C_{OL} + (\phi D_{sed}/L_r)\cdot C_E\} + \frac{P}{W}$$

$$W = \frac{\phi D_{sed}}{L_p} + \frac{\phi D_{sed}}{L_r}$$

From (I.2) and (I.3), the importance of solubility control to metal recycling can be seen: since, if solubility control is important, $C_p > C_E$, the second term on the RHS of (I.2) is a downward flux, and the more stringent the solubility control (smaller C_E) and the closer the precipitation layer is to the interface (smaller L_r), the larger is the downward flux and the smaller is the flux out of the sediments. (I.2) and (I.4) show that, with transport by vertical mixing alone, the flux out of the sediments increases as the production rate of dissolved metal

ion increases and as the production layer is closer to the interface (smaller L_p). From (I.5) it can be seen that the maximum concentration of the metal ion (C_P) is determined by a transport-weighted average of the overlying water and saturation concentrations and by the ratio of the production rate and transport rate terms. Thus, the chemical factors which, along with the mixing regime, determine the amount of sediment/water column recycling of metal ions are (1) the rate and position in the sediment column of the production of dissolved metal ions, (2) the solubility limits on metal ion concentrations, and (3) the depth in the sediment column at which these solubility limits take effect.

The Production of Dissolved Metals in Sediments

An important determinant of the production in the sediments of dissolved metal ions is the form in which the particulate metal arrives at the sediment surface. While metals trapped in clay mineral lattices are unreactive and likely to be buried, metals associated with oxides and with biogenic material may be reactive. Further, the distribution of the metals between different reactive phases may influence the position in the sediment column of dissolved metal production.

The major sources of the transition metals included in this study to the coastal ocean are continental, with rivers being particularly important. Gibbs (1977), in a study of the Amazon and Yukon Rivers, has inferred, from measurements designed to show the phases with

which the metals carried by rivers are associated, that about 45% of Fe, 30% of Mn, 35% of Ni, 20% of Cu, and 50% of the Co transported in these rivers are present in clay mineral lattices and are therefore unreactive. Studies of the estuarine behavior of these metals, while not readily extrapolated from the particular estuaries studied, have yielded some generalizations: a large fraction of riverine Fe appears to be removed from the water column in estuaries by coagulation of colloidal material (Boyle et al., 1977); total Mn is approximately conservative, but there is considerable cycling between dissolved and particulate forms within the estuary (Graham et al., 1976; Evans et al., 1977); and Cu, Ni, and Co are approximately conservative (Sholkovitz et al., 1978; Sholkovitz & Copland, 1980; Boyle et al., 1982). Thus, a significant fraction of the transition metals present in rivers is associated with potentially reactive phases.

Recent work on the oceanic distributions of the first row transition metals has yielded a great deal of information about the cycling of metals between different phases in the water column. Most of the information is based on correlations of metal cycling behavior with the cycling behavior of organism soft and hard parts and of oxide phases. Thus, it does not demonstrate directly the association of metals with specific carrier phases. However, the work has proved to be very valuable in explaining the early diagenesis of metals because it has identified the phases with which the metals are regenerated.

The elements are involved to varying degrees in biological cycles. Collier (1981), by analyzing various leachates of planktonic

material, showed that significant fractions of all of these metals except Fe are cycled with the soft parts of organisms; he did not find significant amounts on siliceous or calcareous tests. Nonetheless, a well-known feature of oceanic Ni distributions is the correlation of dissolved Ni with both phosphate and silicate concentrations (Sclater et al., 1976; Bruland, 1980; Boyle et al., 1981), indicating that a fraction of Ni, if not directly associated with siliceous tests, is at least cycled in a similar way. Cu also shows some features of the nutrient-type metal distribution (Bruland & Franks, 1983). However, its involvement in water column biological cycles is obscured by the facts that it is scavenged onto particles throughout the water column and that its major site of regeneration is the sediment/water interface (Boyle et al., 1977). The distributions of Mn, Fe, and Co show little evidence of involvement in biological cycles.

The cycling of Mn and Fe between dissolved and particulate phases depends directly on variations in redox potential. Mn and Fe are present in the ocean largely in oxidized form, and their distributions in the eastern Pacific are indicative of the high reactivity of oxide phases: Klinkhammer & Bender (1980) argued that the dissolved Mn maximum in the O_2 minimum could be explained by rapid response to small pE and pH changes, maintaining equilibrium with an oxide phase; Landing & Bruland (1980) postulated that <u>in situ</u> MnO_2 reduction may contribute, along with input of Mn from slope sediments, to the dissolved Mn maximum; and Martin & Knauer (1984) used measurements of dissolved Mn and of Mn on trapped and suspended particles to show that 30% of the excess Mn in the

O_2 minimum was regenerated *in situ* to maintain equilibrium with oxides or with a surface phase. Gordon et al. (1982) found an Fe maximum within the O_2 minimum which may be explained by processes similar to those producing the Mn maximum.

Measurements of metals in the pore waters of pelagic and hemipelagic sediments, where the sites of oxic and suboxic diagenesis are often well separated in the sediment column, have also given important clues as to the phases with which the first-row transition metals are cycled. Klinkhammer et al. (1982), in a study of pore waters from siliceous sediments (MANOP site S), found that, during oxic diagenesis, Ni was regenerated with a similar Ni/Si ratio to that found for water column regeneration, and Mn showed only slight regeneration. Oxic diagenesis is the major means of regeneration of Cu (Klinkhammer et al., 1982; Callender & Bowser, 1980; Sawlan & Murray, 1983). A direct effect of suboxic diagenesis, occurring deeper in the sediments after O_2 is depleted, is the reductive dissolution of first Mn, then Fe oxides as they are used as electron acceptors during microbial oxidation of organic matter, producing large pore water concentrations of these elements and providing the major means of their sedimentary cycling (Froelich et al., 1979). The major part of the Ni and Co which are regenerated in sediments is dissolved during this process: Ni and Co pore water and solid phase profiles are closely related to those of Mn (Klinkhammer, 1980; Sawlan & Murray, 1983; Heggie & Lewis, 1984; Graybeal & Heath, 1984).

To summarize this discussion of the phases with which the cycling of the first row transition metals is associated: a significant

fraction of the metals reaching the coastal ocean from continental sources is in reactive form; because of differences in the estuarine and oceanic chemistry of the metals, they reach the sediments in different reactive forms, and may be cycled in different ways. (1) Cu is cycled with organic matter, with the sediment/water interface the site of most Cu regeneration; (2) Ni is apparently cycled with both soft and hard parts of organisms in the water column, but most of the Ni that is dissolved during early diagenesis is associated with Mn oxides; (3) the cycling of Mn, Fe, and Co is dominated by their association with oxide phases.

One requirement for the recycling of a fraction of the flux of particulate metals reaching the sediment surface to the water column is that conditions near the sediment/water interface favor dissolution of the metal-carrying phases. Previous studies of early diagenesis in nearshore sediments (Goldhaber et al., 1976; Klump & Martens, 1980; Aller, 1980a,b,; Emerson et al., 1984; Elderfield et al., 1981a,b) have shown that there are two direct effects of benthic microbial activity on carrier phases. First, soft parts of organisms, and any associated metals, are solubilized near the sediment/water interface by metabolic activities of benthic organisms. The evidence for this effect is the large increase in nutrient concentrations over bottom water that is often observed at the sediment/water interface, with steep gradients often continuing to several cm below the interface. Second, rapid depletion of O_2 during organic matter degradation in nearshore sediments leads to the use of Mn (IV) and Fe(III) as electron acceptors during organic

matter oxidation within mm or cm of the interface, allowing important recycling of these metals and perhaps of associated Ni and Co to the overlying water column. In addition to the direct effects of microbial activity, there are changes in water composition across the sediment/water interface which may have important effects on metal cycling. There is a large drop in redox potential which favors dissolution of metal oxides independently of direct action of organisms. There is also a large drop in pH accompanying organic matter and sulfur oxidation. This pH drop favors dissolution of oxides and desorption of metals from solid surfaces (Balistrieri & Murray, 1984). The pH drop also favors dissolution of carbonate tests; observed increases in carbonate alkalinity and dissolved silicate confirm that the dissolution of organism hard parts occurs.

Solubility Controls on Metal Concentrations in Reducing Sediments

It has been shown that conditions favoring the dissolution of particulate metals are likely to occur near the surface of nearshore sediments: thus, one condition for the recycling of metals to the water column is met. A second factor influencing the regeneration of metals during early diagenesis is solubility control of dissolved metal concentrations: the rapid metabolism occurring near the interface of nearshore sediments leads to the buildup of anionic breakdown products of organic matter degradation and sulfate reduction close to the sediment/water interface. High concentrations of phosphate, sulfide, and

carbonate ions may severely limit the recycling of metal ions. In Figure I.2, calculations of the free metal ion concentrations in equilibrium with likely solid phases under conditions existing near the sediment/water interface are shown. The compilation of constants in Jacobs (1984) was used for these calculations; phosphate mineral constants were taken from Aller (1980a). Calculations such as these involve many assumptions, the most important of which are (1) that pure solid phases are precipitating, and (2) that the free metal ion concentrations shown in Figure 2 are similar to the equilibrium total dissolved metal concentrations. Since it is unlikely that pure phases precipitate in sediments, these equilibrium calculations are unlikely to reflect, quantitatively, the actual sedimentary conditions. Inorganic complexation is likely to have the largest effect on Cu among these metals (Jacobs & Emerson, 1982); the effect of organic complexation is not well known. Despite these limitations, several of the general features of the results of these calculations have been observed. Work in anoxic basins (Jacobs & Emerson, 1982; Jacobs, 1984; Kremling, 1983) has shown: (1) Mn and Fe are more soluble in reducing systems at low S(-II) concentrations than they are in oxic systems; and the concentrations of Mn, Fe, and Co increase on the reducing side of the oxic/anoxic boundary before decreasing at higher sulfide levels; (2) while the concentration of Ni is not greatly changed across the oxic/anoxic boundary, that of Cu decreases steadily, even at elevated sulfide levels, when cuprous sulfide complexes have been hypothesized to stabilize dissolved Cu. The calculations shown in Figure I.2 also illustrate the possibility of

Figure I.2

Metal Solubilities in Reducing Marine Systems

Calculations of free metal ion activities in equilibrium with pure phases that may exist in nearshore sediments. For Mn and Fe, carbonates and phosphates are considered as well as sulfides. For carbonate and phosphate calculations, the range of dissolved anion concentrations observed in the upper 3 cm of the sediments at the Buzzards Bay site was used in the calculation:

$$CO_3^{2-} : 5 - 50\ \mu M$$

$$PO_4^{3-} : 0.02 - 2\ \mu M$$

pH = 7.3 was used for the calculations. For the sulfide equilibrium calculations, $HS^- = 10^{-5}\mu M$ was assumed. For each metal, the range of equilibrium metal ion activities shown was obtained from the range of sulfide phase equilibrium constants compiled by Jacobs (1984). "a" is the predicted total dissolved Cu concentration if, because of extensive complexation by sulfides, $Cu_T = 10^8 \bullet Cu^+$ (Jacobs & Emerson, 1982). All constants were obtained from Jacobs (1984), except phosphate constants from Aller (1980). The figure is adapted from a figure in Jacobs (1984).

Figure I.2

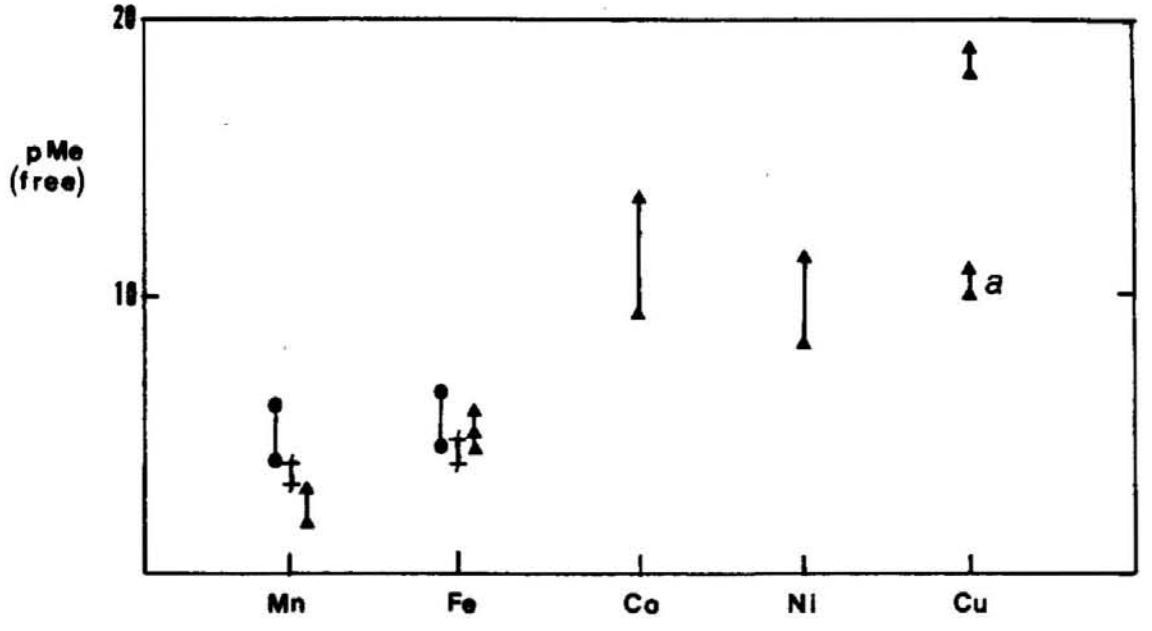

● Phosphate

\+ CO_3^{--}

▲ HS^-

a $Cu_t = 10^{-6}$ Cu^+

solubility control on the dissolved Mn and Fe concentrations by phases other than sulfides. Aller (1980a,b) and Murray et al. (1978) have shown that saturation with respect to Mn and Fe phosphates may exist at the phosphate maximum near the sediment/water interface; this saturation does not appear to persist deeper in the sediments, but precipitation of Ca phosphate may occur there (Aller, 1980a), and Mn and Fe may coprecipitate. Siderite ($FeCO_3$) does not appear to control the concentration of Fe in reducing sediments (Aller, 1980b). Rhodocrosite ($MnCO_3$) saturation may be reached; in addition, Mn has been found in association with $CaCO_3$ in reducing sediments (Pedersen & Price, 1982). Thus, solubility control in reducing marine systems appears to be due primarily to sulfides for all of these elements except Mn; control on Mn, at least in low-sulfide conditions near the sediment/water interface, may be due to phosphate minerals or carbonate minerals. Mn and Fe are more soluble in reducing systems than Ni, Co, and especially Cu. Because of the rapid buildup of organic matter degradation products and of sulfide near the interface in nearshore sediments, solubility controls may place an important limitation on the regeneration of metals at the interface of nearshore sediments.

In terms of the model presented at the beginning of this section, work on the riverine, estuarine, and oceanic water column chemistry of Mn, Fe, Ni, Cu, and Co has shown that a supply of reactive particulate metals to the sediment/water interface is likely; studies of diagenesis in nearshore sediments have shown that conditions of low redox potential and pH which favor solubilization of metals occur near the

sediment/water interface. On the other hand, buildup of sulfide, phosphate, and carbonate ions may limit the concentration of metal ions, and especially of Cu, very near the sediment/water interface. Thus, the ability of sediments to recycle Ni, Cu, and Co may depend on rather small variations in sediment conditions. No study of Co in nearshore sediment pore waters has been reported, but two studies including Ni and Cu have shown variable behavior, especially for Cu. While Emerson et al.(1984) showed quite large Cu and Ni maxima in pore waters at the sediment surface in Puget Sound, Wash., sediments, Elderfield et al. (1981a,b) found only intermittent maxima in Narragansett Bay, R.I., sediments, and concluded that these elements were not recycled to the water column. Given the importance of oxic diagenesis to the sedimentary cycling of Cu and the disappearance of O_2 in the upper mm of nearshore sediments, these previous studies may have been limited by the 1cm, and sometimes 2cm, sampling intervals used: finer sampling at the interface may reveal more generally occurring production of dissolved trace metals in nearshore sediments.

Earlier in this section, the possible importance of reactions at the sediment surface which may trap metal ions in the sediments was briefly mentioned. The occurrence of a thin oxic layer at the sediment/water interface may inhibit the flux of some metals at some times of year: both Mn and Fe are oxidized fairly rapidly at marine oxic/anoxic boundaries, Fe in minutes (Murray & Gill, 1978) and Mn in days (Emerson et al., 1979); thus, Mn and Fe may precipitate at the interface, and particle-reactive metals may be taken out of solution with

them. Nonetheless, studies of Mn cycling in coastal systems have shown the importance of nearshore sediments to the transport of Mn away from coasts (Trefry & Presley, 1982; Yeats et al., 1979); a study of Fe in Puget Sound, Wash., showed that Fe is returned to the water column from nearshore sediments (Murray & Gill, 1978). Fine-interval pore water sampling will be helpful in showing whether removal of metals from solution in a thin oxic layer at the sediment surface has an important effect on metal cycling in nearshore systems.

Outline of Thesis Work

Important processes affecting oceanic metal distributions appear to occur in the coastal ocean. Heggie (1982) demonstrated that elevated dissolved Cu levels exist on the Bering Sea continental shelf, and that the sediment/seawater interface is a likely source for the excess Cu; Boyle et al. (1981), Bruland (1980), and Kremling (1983) have shown that an increase in Cu concentration approaching continents is a general phenomenon in the N. Atlantic and N. Pacific. Kremling (1983) and Landing & Bruland (1980) found a similar result for Mn, and Martin & Knauer (1984) attributed the majority of excess Mn observed in the E. Pacific O_2 minimum to a continental shelf source. In addition, increases in metal concentration as salinity decreases approaching a continent have been found for Cu in the Gulf of Mexico (Boyle et al., 1984), Co in the NE Pacific (Knauer et al., 1982) and for Mn, Cu, and Ni in the NW

Atlantic (Bruland & Franks, 1983); Bruland & Franks found that the zero-salinity extrapolation of the metal-salinity correlations agreed within a factor of two to five with effective river end-member values. In short, there is ample evidence that metals cross the coastal ocean from rivers to contribute to oceanic dissolved metal concentrations. Given the high particle concentrations in the coastal ocean, the high particle-reactivity of the transition metals, and the shallow water column, it is reasonable to postulate a significant role for coastal sediments in this transport across the coastal ocean. It remains to be seen whether sedimentary recycling of metals is general to all the first row transition metals, and what the specific conditions favoring sedimentary recycling are.

Thus, this study is designed to explain mechanisms of metal cycling in reducing, nearshore sediments. In particular, it is designed to show under what specific chemical and mixing regimes nearshore sediments are likely to return dissolved metals to the water column. Then, if recycling mechanisms are understood, detailed measurements at relatively few sites can be used to predict the general involvement of nearshore sediments in oceanic metal cycles.

There are three parts to the study.

(1) A detailed sampling program has been carried out to determine the chemical characteristics relevant to transition metal transport at a silty clay sediment site in Buzzards Bay, Mass. Redox conditions have been followed using pore water Mn, Fe, and SO_4 measurements. The extent of organic matter degradation has been determined with measurements of

carbonate system components and phosphate, and the occurrence of organism hard part dissolution has been established with pore water carbonate system and silicate measurements. Saturation with respect to solid phases was examined with calculations of PO_4^{3-}, CO_3^{2-}, and HS^- concentrations based on pore water measurements of alkalinity and total CO_2, reactive phosphate, and sulfide. Finally, the trace metals, Ni, Cu, and Co, have been measured in the pore waters. Based on indications of the importance of near-interface processes, the smallest practical sampling interval, 0.5cm, was adopted near the interface. Sampling was carried out at four times of year to determine whether the annual cycle of biological activity is important to metal cycling.

(2) At the same site, uranium-series disequilibrium measurements have been made to characterize the mixing regime. Particle mixing rates were derived from $^{234}Th/^{238}U$ disequilibrium measurements in the upper few cm of the sediment column, and irrigation rates were measured by the $^{222}Rn/^{226}Ra$ disequilibrium method. These radiochemical measurements have been made throughout the seasonal cycle of biological activity. Thorium measurements were made on the same samples used for pore water chemistry characterization; Radon measurements were made on separate cores taken simultaneously with and within about 1 meter of the pore water chemistry cores.

(3) Again at the same site, <u>in situ</u> ion migration experiments were carried out. These experiments are unlike previous radiotracer studies of

metal ion mobility in sediments (McCaffrey et al., 1980; Luedtke & Bender, 1979; Adler, 1981) in two respects. First, the experiments were carried out in a relatively undisturbed sedimentary system rather than in the laboratory or in a larger simulated sedimentary system (the MERL microcosms) to ensure that they reflect in situ conditions as closely as possible. The extensive characterization of the chemistry and mixing at the experimental site is important to the interpretation of the results of the ion migration experiments. Second, while previous tracer experiments have examined metal transport following tracer introduction into the water overlying sediments, in these experiments, the metal isotopes were released directly into the reducing sediments, below the sediment/water interface. Because the results of radiotracer experiments can be influenced by the mode of introduction of tracer into the experimental system, these experiments complement the results of previous experiments. Transport of a transient tracer is dependent on the particle and solute mixing rates as well as on the solid/solution partitioning of the tracer. Thus, these experiments can answer questions concerning the relative solubilities of the metals under study, yielding distribution coefficients and perhaps rates of solid/solution exchange reactions. Further, they can show directly how the ambient mixing processes and chemistry interact to transport dissolved metal ions in reducing sediments.

Chapter II

Measurements of Particle Mixing and Solute Transport Rates Using Uranium-series Disequilibrium

Introduction

In this chapter on transport processes within the sediment column at the Buzzards Bay study site, data necessary for analysis of the early diagenesis of Mn, Fe, Ni, Cu, and Co in nearshore sediments will be presented. Three requirements must be met in order to define the transport regime at the study site. First, the rates of particle and solute transport, and their seasonal variability, must be determined so that fluxes of chemical constituents within the sediment column and across the sediment/seawater interface can be calculated. Second, the mechanisms of transport must be determined: transport mechanism is particularly important for solutes, since the relative importance of vertical diffusive processes and of nonlocal exchange processes can have significant influence on calculated fluxes. Finally, the vertical distribution of transport rates in the sediment column must be determined.

In this chapter, the calculation of transport parameters from uranium series disequilibrium measurements is discussed, and results of measurements of the $^{234}Th/^{238}U$ and $^{222}Rn/^{226}Ra$ systems are presented. The transport parameters derived here will be applied to a

discussion of the sedimentary chemistry of Mn, Fe, Ni, Cu, and Co in Chapter 3 and to the determination of metal mobility through tracer migration experiments in Chapter 4.

Study Site

While the action of waves and currents has an important direct influence on transport in the upper centimeter of the sediment column, it is the benthic fauna which is most important to determining rates and mechanisms of transport processes. Aller (1977) has reviewed the factors which determine the interaction between the macrobenthos and sediments. The makeup of the benthic community is of primary importance: the number density and size of infaunal organisms; the relative numbers of filter feeders, which move large volumes of water, and of deposit feeders, which are more efficient particle movers; the relative numbers of mobile and sedentary organisms; and the permeability of burrow walls to solute transport are all important to the mechanisms and rates of transport processes. Environmental factors which influence the composition and activity of the benthos include grain size, sediment stability, the supply of organic matter, and temperature.

The study site is located just northwest of the Weepecket Islands, at 41°31.25 N, 70°45.7 W (Figure II.1). In relation to previous studies in Buzzards Bay: the site is at the same location as station 49

Figure II.1

The Buzzards Bay Study Site

"x" marks the position of the study site. The dashed line in the figure outlines the region of fine-grained sediments in Buzzards Bay. From Moore, 1963.

Figure II.1

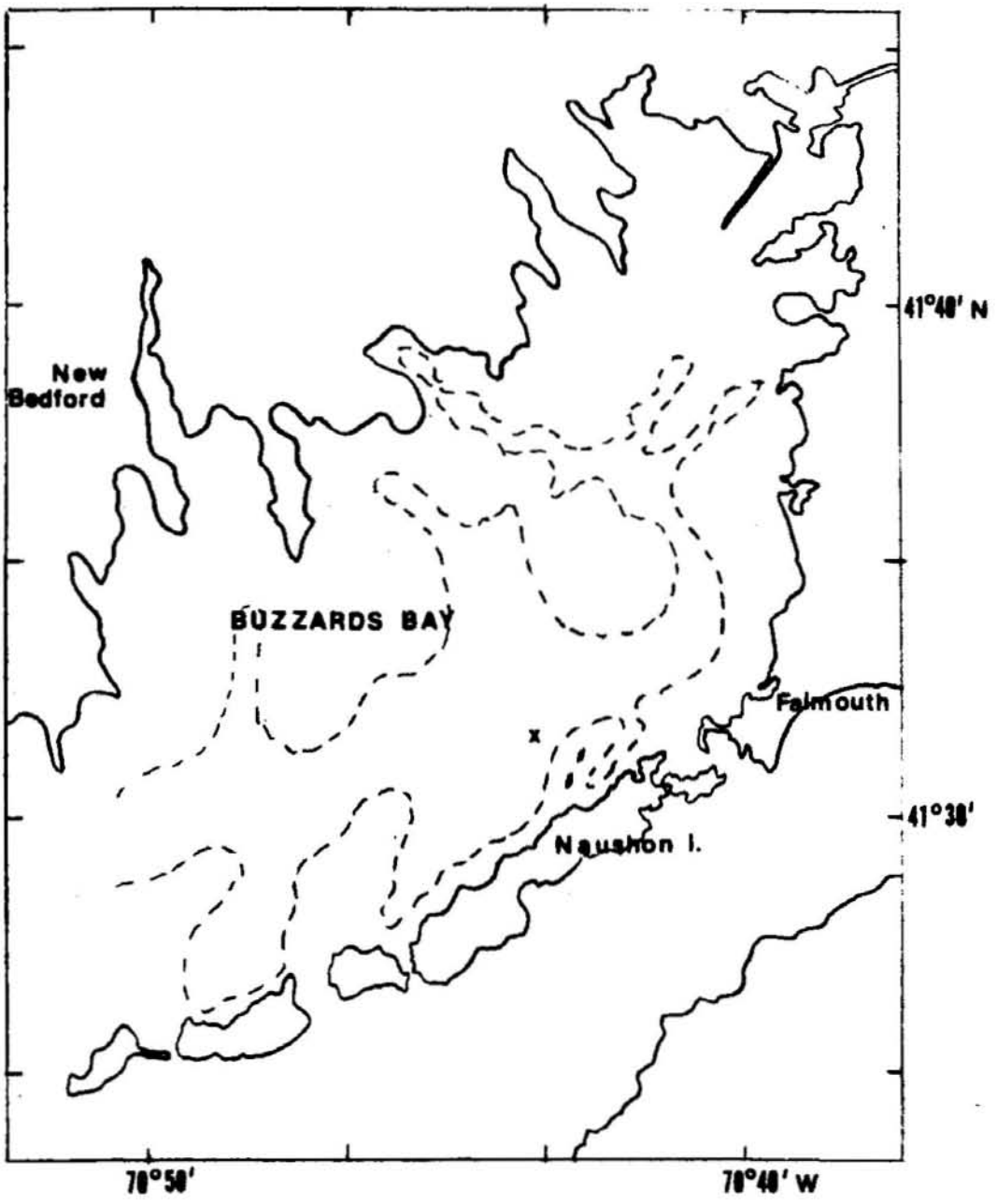
New Bedford
BUZZARDS BAY
Falmouth
Naushon I.
41°48' N
41°38'
70°50'
70°48' W

in Moore's bottom sediment study (Moore, 1963), lies between stations K and L of Sanders' benthic community study (Sanders, 1958), and is near station 31 of the 1982-83 hydrographic study (Rosenfeld et al., 1984). Water depth is 15 m. Bottom currents are relatively slow, and the sediments are about 17% clay and 93% silt/clay (Sanders, 1958; Moore, 1963); traveling from the study site towards the Weepecket Islands, the percentage of sand in the sediments increases rapidly. The fauna of fine-grained Buzzards Bay sediments is dominated by deposit feeders: the communities at Sanders' stations L and K are 5-20% filter feeders, 70-90% deposit feeders. The dominant species are the mobile polychete, Nephtys incisa (20-30%) and the small bivalve, Nucula proxima (10-40%) (Sanders, 1958). In a laboratory study using artificially laminated sediments, Rhoads (1967) found that the Buzzards Bay soft-bottom community extensively reworked the upper 2 cm of the sediment column in a few days, and that Nephtys created occasional disturbances to a depth of 10 cm.

Three environmental factors which, in addition to sediment texture, are important determinants of biological activity are water temperature, the supply of organic matter, and the redox environment. The activity of the macrobenthos tends to be closely related to water temperature (Aller, 1977); temperature was monitored during this study (Figure II.2). The annual temperature range is from about 2°C to 22°C (Sanders, 1958), with the minimum occurring in late winter and the maximum in late summer; the temperature increase in April-June is quite rapid. Primary productivity is about 100 gm C fixed/yr, and its cycle parallels the temperature cycle, with a broad minimum from December

Figure II.2

The seasonal temperature cycle in bottom water at the Buzzards Bay site

Figure II.2

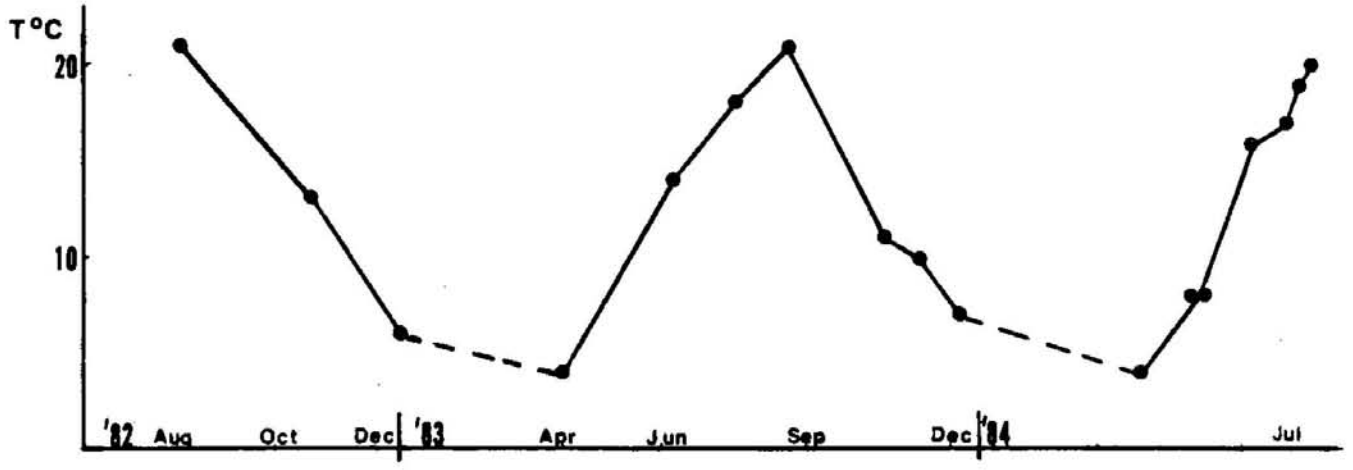

through April (about 100 mg C/m^2 day) and levels 5 to 8 times the minimum from June through October (Roman & Tenore, 1978). Sedimentary redox horizons are closely related to the activities of the macrobenthos, both as a determinant of organisms' activity and as a result of it. Mn(IV) is reduced in the upper 0.5 cm of the sediments at the study site, indicating that O_2 must be substantially depleted in the upper few mm; the first appearance of S(-II) in the pore waters is typically at 2.5-5 cm. The buildup of S(-II) in the pore water in the upper 20 cm of the sediment column varies seasonally, being smallest in early summer and greatest in late summer/early winter.

In summary, the study site is a clayey silt sediment underlying 15 m of water. The bottom community is dominated by deposit feeders, and can be described as a Nephtys-Nucula association (Sanders, 1958). As is typical of temperate, nearshore systems, there is considerable seasonal variability in temperature and productivity, and a seasonal cycle of biological activity should be observed. The sediments are reducing, and the absence of O_2 and presence of S(-II) may influence the depth in the sediments at which the effects of burrowing organisms are observed.

Determination of Transport Rates from Uranium Series Disequilibrium

Radioactive disequilibrium between a daughter nuclide and its much longer-lived parent can be used to establish time scales of processes occurring over a period of about five daughter half-lives. In a closed system, the parent-daughter disequilibrium would disappear at a rate determined by the daughter's half-life, but in an open system, processes causing loss or gain of the daughter to the system can maintain the disequilibrium in steady state. In the latter case, given a measurable difference in parent and daughter activities, simple steady-state models can be applied to measure rates of the processes causing gain or loss of the daughter. Here, measurements of radioactive disequilibrium will be applied to transport processes in nearshore sediments; with the importance of seasonality and of rapid, short-lived biological processes in these environments, isotopes with short half-lives are most useful for establishing time scales. ^{234}Th and ^{222}Rn have the required short half-lives; further, the half-lives of their respective parents are relatively long, so that disequilibrium is both measurable and relatively easy to model (Table II.1).

TABLE II.1

Isotope Half-Lives

Half-lives of the isotopes used in the transport studies described in Chapter II. "Ratio" is the ratio of the daughter's half-life to the parent's half-life.

Isotope	Half-life	Ratio
^{222}Rn	3.825 d.	6.5×10^{-6}
^{226}Ra	1622 yr.	
^{234}Th	24.1 d.	1.5×10^{-11}
^{238}U	4.5×10^{9} yr.	

$^{234}Th/^{238}U$ Disequilibrium

Because ^{234}Th is particle-bound in sediments, its vertical distribution in the sediment column is determined (in steady state) by a balance between radioactive decay and processes transporting particles vertically in the sediments. Thus, the distribution of excess ^{234}Th with depth in the sediments is a good tracer of processes mixing sedimentary particles. A measurable excess of ^{234}Th occurs in nearshore sediments because of the combination of the short residence time of ^{234}Th in coastal seawater relative to its soluble parent, ^{238}U, and the shallow coastal water column. ^{234}Th is rapidly scavenged onto particles in coastal seawater, and the particles reach the sediments at a rate which produces a sedimentary excess ^{234}Th inventory that is nearly equal, on average, to the water column ^{238}U inventory (Aller et al., 1980). At a salinity of 30°/oo, with a 15 m water column, an average excess ^{234}Th inventory of about 3 dpm/cm^2 should be produced. Aller et al. (1980) have described the processes which produce lateral heterogeneity of the sedimentary excess ^{234}Th inventory: resuspension of sediments and lateral transport of resuspended material tend to cause the largest inventories to be found in regions of fine-grained sediments and rapid biological activity. Fine-grained, nearshore sediments are therefore well suited to the measurement of rapid particle mixing rates using the distribution of excess ^{234}Th.

Excess ^{234}Th decays with a 24 day half-life. Therefore, its vertical distribution in the sediment column results from the sum of

particle mixing events over about a three month period and is most sensitive to variations in mixing rates in the range, 10^{-8} to 10^{-6} cm^2/sec. In a study of particle mixing rates in Long Island Sound sediments, Aller & Cochran (1976) and Aller et al. (1980) measured rates varying from $1x10^{-8}$ to $1.6x10^{-6}$ cm^2/sec in the upper 5 cm of the sediment column; in Panama Basin and NW Atlantic continental rise sediments, Aller & DeMaster (1984) found similar rates, about $9x10^{-7}$ cm^2/sec.

Methods

Each Core was taken by SCUBA divers who placed a 20 cm diameter core liner into the sediments and sealed the core top; the core was lifted to a boat, where the bottom was sealed. Great care was taken not to disturb the sediment/water interface, and its physical appearance, along with the chemical and radiochemical results, indicate that the efforts were successful. Cores were extruded and sectioned in 0.5 cm intervals. After samples were centrifuged and pore water removed for chemical analysis, the remaining mud was dried at 100°C, crushed, and homogenized; 5-10 gm were taken for $^{234}Th/^{238}U$ analysis. The analytical procedure used was as follows: (1) Samples were leached with hot 8N HNO_3. Two samples from the 7/82 core were also leached with hot 6N HCl; no significant difference between the two procedures was seen:

0-0.5cm	HCl leach	$^{234}Th=7.82\pm0.29$ dpm/gm
	HNO_3 leach	7.80 ± 0.20
0.5-1cm	HCl leach	5.74 ± 0.24
	HNO_3 leach	5.03 ± 0.15

(2) Except for the 26/3/84 core, when ^{228}Th and ^{232}U were added as yield monitors, ^{229}Th and ^{236}U were used; no significant difference was observed between the results obtained with the different yield monitors.

(3) Two AG-1x8 100-200 mesh columns in nitrate form were used to obtain a pure Th sample. U/Th separation was achieved by washing U off the column with 8N HNO_3; Th was eluted with dilute HCl.

(4) Samples were prepared for counting by electrodeposition onto stainless steel planchets using the method of Talvitie (1971). Counters were calibrated using a $^{238}U/^{234}Th$ source.

The primary source of analytical uncertainty is counting error; it is the total of counting errors that is reported with the data in Table II.2 (Appendix II.1). An additional source of uncertainty is the choice of a supported ^{234}Th value. ^{238}U activity was measured in two cores, 28/7/82 and 20/10/82: there appears to be a slight depletion in ^{238}U activity in the upper centimeter of the sediment column (Table II.2 and Figure II.3), but it is essentially constant below that, at about 2 dpm/gm dry wt. ^{234}Th activity decreases to a somewhat higher, approximately constant value of about 2.5 dpm/gm dry wt. This discrepancy between two different measures of the supported ^{234}Th activity may be due to artifacts of the leaching procedure (Aller & Cochran, 1976) or to the presence of a ß-emitting impurity remaining in the Th fraction after the anion exchange separations. As no samples were totally dissolved prior to Th and U analysis, no final conclusion can be reached as to the source of the discrepancy. Nonetheless, both ^{238}U and ^{234}Th reach

Figure II.3

Th-234/U-238 Results

Results from cores taken from 20/10/82 to 26/3/84. The horizontal axis in each core is the activity, in dpm/gm dry wt, of ^{234}Th or ^{238}U. Figures A and B include ^{238}U and ^{234}Th profiles. Figures C-G show ^{234}Th profiles only. The dashed line in each figure shows the supported ^{234}Th value assumed for each core.

Figure II.3

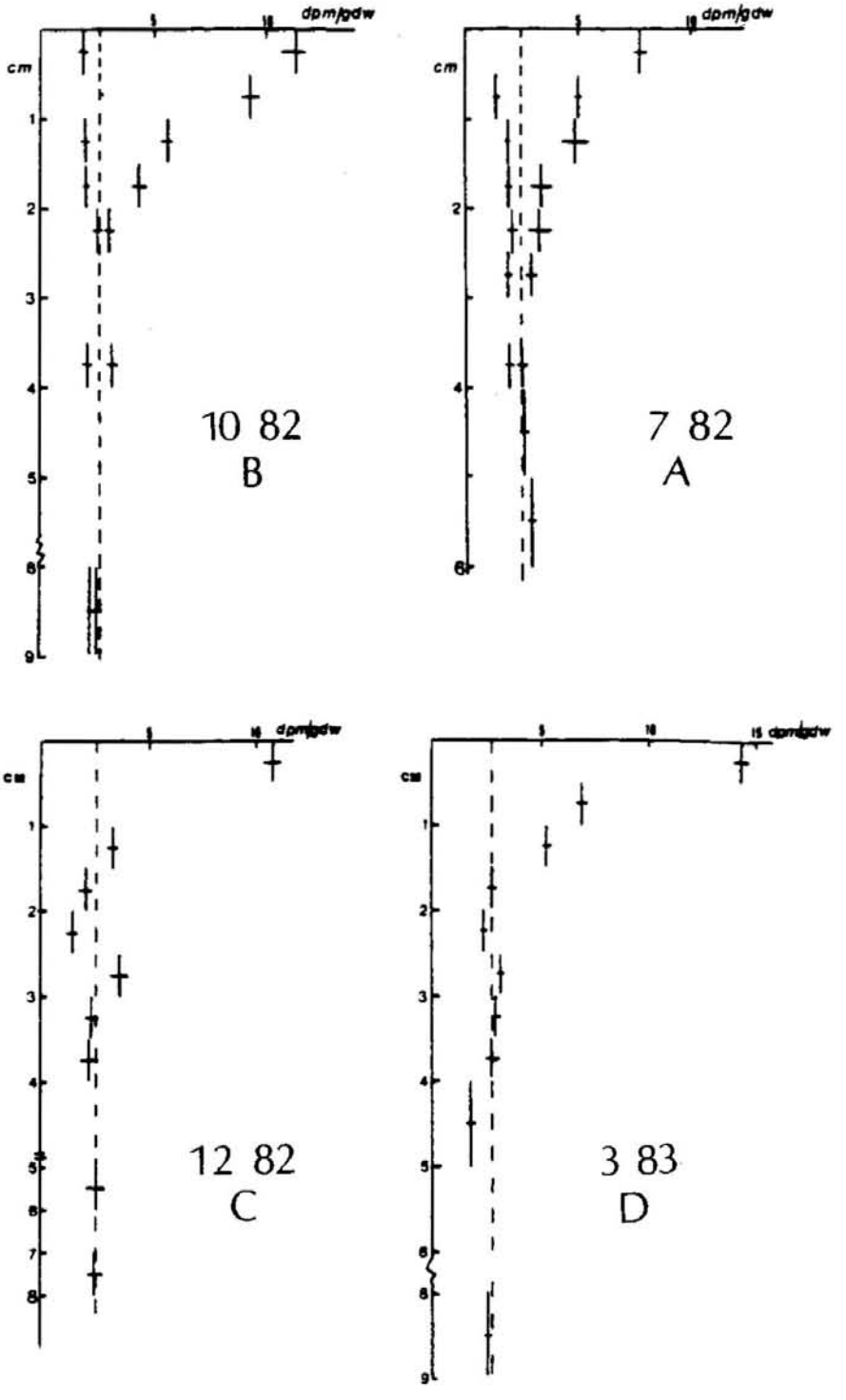

Figure II.3 (cont)

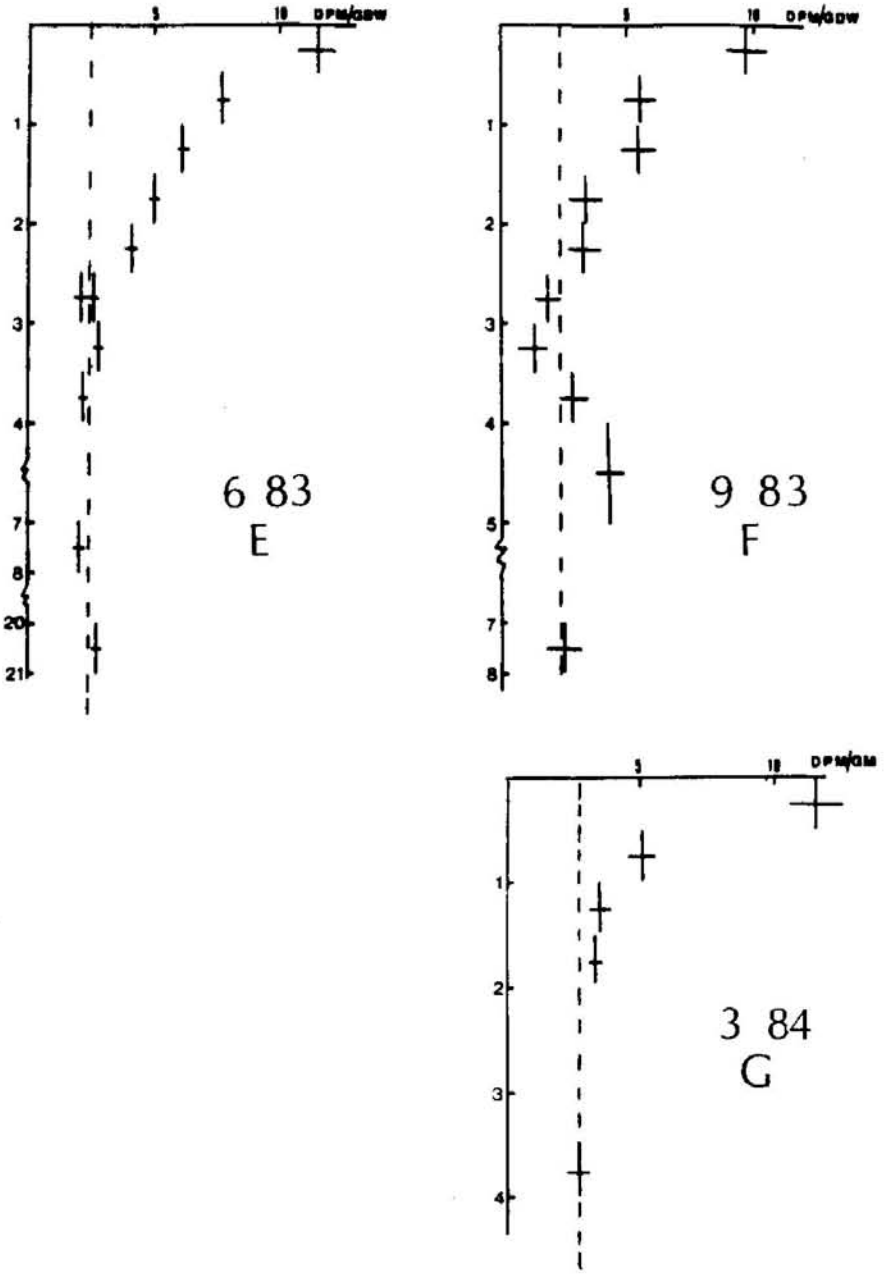

constant values below 3-4 cm, and ^{238}U is approximately constant throughout the sediment column; thus, no systematic error in derived mixing coefficients should be introduced by assuming that the deep ^{234}Th activity measured reflects supported ^{234}Th. Supported ^{234}Th values resulting from this assumption, and used for calculations of excess ^{234}Th, are listed in Table II.3 (Appendix II.1); the reported errors reflect the resulting uncertainty.

Results and Discussion

Consideration of the composition of the Buzzards Bay benthic fauna and of the seasonality of temperature and productivity in Buzzards Bay lead to the qualitative prediction that the sediments should be extensively reworked in the upper 2 cm, and that the reworking should be most rapid in the warm months, from June through October, and least rapid in the cold months, December through April. These reworking processes, given an approximately constant supply of ^{234}Th to the sediment surface, produce a vertical distribution of ^{234}Th in the sediments depending on a balance between (1) particle transport processes exchanging high-activity particles from the sediment surface with low-activity particles from deeper in the sediments and (2) radioactive decay. Sediment burial is unimportant because the decay of ^{234}Th is rapid relative to the burial rate of less than 3 mm/yr (Farrington

et al., 1977) in the area of the study site. An exponential decrease of ^{234}Th activity from the sediment/water interface downward should result from this balance, with a scale length depending on the rate of particle transport. Quasi-exponentially decreasing excess ^{234}Th profiles are observed at the Buzzards Bay study site (Table II.2 and Figure II.3). As predicted given a coupling of organism activity to the annual cycles of temperature and productivity, the profile scale length varies seasonally: excess ^{234}Th is present to depths of 1.5-2 cm below the sediment/water interface in March and December cores, and is present to 2-2.5 cm in the warmer months (June through October); in addition, the curvature of the profiles is greater in the cold months than in the warmer months. It is notable that the depth of the region of rapid particle transport agrees with the results of Rhoads (1967), who observed directly a 2 cm reworked layer in sediments occupied by the Buzzards Bay macrobenthos; it is also notable that the depth of the ^{234}Th excess at this Buzzards Bay site, dominated by Nucula proxima and Nephtys incisa, is less than was found in fine-grained sediments in Long Island Sound (Aller & Cochran, 1976), where Nephtys and Yoldia limatula, a larger bivalve than Nucula, dominate. However, because a 4-cm mixed layer has been observed in the Nephtys-Nucula dominated sediments of the New York bight apex (Cochran & Aller, 1979), the difference in depth of rapid particle reworking may not be related to the change in dominant macrofauna from Nucula to Yoldia.

The excess ^{234}Th profiles can be modeled quantitatively by considering particle transport in the upper 2-3 cm of the sediment column as a diffusive process transporting solution and particles together, so

that the driving force for diffusion is the gradient of ^{234}Th activity in dpm/volume of bulk sediment (this is "bioturbation" as described by Berner, 1980). Then, the diffusive flux of ^{234}Th is given by

$$J = -D_B \frac{d}{dx}\{(1-\phi)\rho_s A\}$$

D_B= bioturbation coefficient
ϕ= porosity
ρ_s=solid density
A= excess ^{234}Th activity, dpm/gm dry wt.

If burial advection is ignored and D_B considered constant, then the steady-state distribution of excess ^{234}Th is described by

$$D_B \frac{d^2A^*}{dx^2} - \lambda A^* = 0$$

λ=decay constant for ^{234}Th
$A^*=A(\rho_s(1-\phi))$, ^{234}Th excess in dpm/cm^3 sed.

with boundary conditions

$$A^*(x=0) = A_0^*$$
$$A^*(x\rightarrow\infty) = 0$$

It should be noted that the assumption of a constant D_B is not generally consistent with variable porosity, and that the two assumptions are only approximately consistent in these sediments (Aller et al. (1980) discuss the validity of the assumptions). However, since it is impractical to try to fit a model with variable D_B to the few data points that are obtained in the region of measurable excess ^{234}Th using 0.5 cm sampling intervals, the constant-D_B model is used. Then, D_B

can be determined from

$$\ln A^*(x) = \ln(A_0^*) - (\lambda/D_B)^{1/2}x$$

Directly measurable variables are $A^*(x)$ and the inventory of excess ^{234}Th, which can be related to D_B and A_0^* by integrating $A^*(x)$ over x,

$$I = (D_B/\lambda)^{1/2}A_0^*$$

Excess ^{234}Th inventories, along with D_B and A_0^* determined from $A^*(x)$, are shown in Table II.4. The results are generally consistent with the proposed model. Since ^{234}Th integrates particle mixing over about a three month period, and since times of rapid changes in environmental conditions are late spring and fall, cores most likely to show steady-state conditions are 7/82, 10/82, and 9/83 for the warm months, and 31/3/83 and 26/3/84 for the cold months. Using results from these five cores: (1) there is approximately a factor of two change in the average bioturbation mixing coefficient, from 24×10^{-8} cm^2/sec in the cold months to 44×10^{-8} in the warm months, and (2) the ratio of inventory to surface excess ^{234}Th activity shows the expected trend, with I/A_0^* greater, the larger the mixing coefficient. The average summer I is 3.3 dpm/cm^2, with A_0^*=2.2 dpm/cm^3, while the average winter I and A_0^* are 2.4 dpm/cm^2 (March, '83: no inventory for March, '84, could be calculated because an insufficient number of samples

TABLE II.4

Results from model fits to excess Th-234 profiles

The table includes ^{234}Th inventories (I) calculated from measured excess ^{234}Th and mixing coefficients (D_B) and surface ^{234}Th values (A_o) calculated from model fits to the data. Inventories could not be calculated for the 15/12/82 and 26/3/84 cores because an insufficient number of samples were taken. Errors listed with D_B are propagated from the uncertainty in the least squares fit to the linearized excess ^{234}Th data.

Core	A_o dpm/cm3	I dpm/cm2	D_B cm2/sec
28/7/82	2.15	3.60	47±10
20/10/82	2.72	3.62	33±10
15/12/82	3.18		9.0
31/3/83	2.90	2.4	34±4
8/6/83	2.97	3.7	81±8
7/9/83	1.75	3.0	53±30
26/3/84	2.80		14±6

was taken-- however, from the samples analyzed, I is unlikely to exceed the March, '83, level) and 2.85 dpm/cm^3, respectively. The December, '82, core, despite having been taken less than three months after the completion of the period of rapidly falling temperature and productivity, is fully characteristic of the winter cores, with high A_0^* (3.18 dpm/cm^3) and low D_B (7×10^{-8} cm^2/sec). The low mixing rate measured in this core may reflect patchiness in benthic biological activity -- although the cores were all taken within less than 50 m of each other, considerable variability occurs on small scales in these sediments -- and it may also reflect a faster-than-anticipated response to declining water temperature in the fall. If the December, '82, core is included in the cold season D_B average, the average becomes 19×10^{-8}cm^2/sec.

Interpretation of the June, '83, core poses some problems. First, June is at the beginning of the summer warm period, and rapid bioturbation beginning in June would not mix ^{234}Th down into the sediments quickly enough to produce this profile; this core appears to have been taken in an area of very high population density. Second, despite the high mixing coefficient, there is quite a low I/A_0^* ratio. This appears to occur because excess ^{234}Th has reached the bottom of the rapidly mixed layer, as is evidenced by the presence of a sharp drop in the excess ^{234}Th activity at 2.5 cm following the smooth decrease in activity to that point. If the bottom of the mixed layer is reached, the boundary condition requiring $A_0^*(x \to \infty)=0$ is no longer valid in the mixed layer, and the simple relationship between I, A_0^*,

and D_B no longer holds: since the particles brought to the surface from the bottom of the mixed layer no longer have zero activity, it is expected that the effect of the change in boundary conditions will be to raise A_o^* relative to I for a given D_B.

The important results of the ^{234}Th measurements undertaken here can be briefly summarized. With the exception of the June, '83, core, the data are consistent with the simple mathematical model proposed by Aller et al. (1980) as a means of deriving bioturbation mixing coefficients from excess ^{234}Th profiles. Thus, the data agree with the interpretation of particle mixing processes by analogy to Fickian diffusion with the concentration gradient of activity in the bulk sediment volume as a driving force. These data illustrate, within the restrictions on interpretation imposed by spatial variability of benthic biological activity, that there is an annual cycle of particle mixing rates at the Buzzards Bay site, with D_B averaging 24×10^{-8} cm^2/sec in the cold months and 44×10^{-8} in the warm months. The range of D_B observed is considerably greater than the difference between the averages, with a minimum of 7×10^{-8} cm^2/sec and a maximum of 80×10^{-8}. The variation in the mixing coefficient over time is shown in Figure II.4. Finally, the depth of penetration of excess ^{234}Th, which is the depth to which rates of particle mixing exceeding about 10^{-8} cm^2/sec occur, is 1.5-2 cm at this site during the cold months and 2-2.5 cm during the warm months.

Figure II.4

The Seasonal Trend of the Bioturbation Mixing Coefficient at the Buzzards Bay Site

Figure II.4

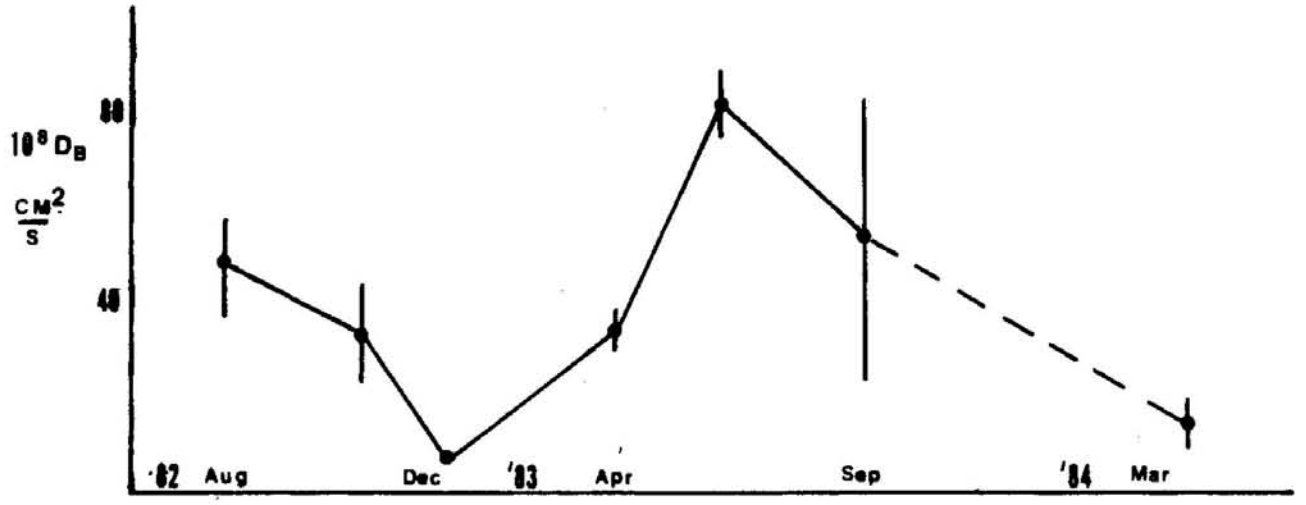

$^{222}Rn/^{226}Ra$ Disequilibrium

Whereas $^{234}Th/^{238}U$ disequilibrium is a useful tracer of particle mixing in sediments, $^{222}Rn/^{226}Ra$ disequilibrium is a useful tracer of solute transport. In this case, disequilibrium is produced when some of the ^{222}Rn produced by decay of solid phase and surface-adsorbed ^{226}Ra is released into pore water and when a fraction of the Rn released escapes to the overlying water unaccompanied by its parent. Thus, the disequilibrium occurs in the form of a ^{222}Rn deficit in sediment pore waters; since ^{222}Rn has a half-life of 3.8 days, solution phase transport events integrated over a period of about two weeks are timed using the ^{222}Rn deficit as a tracer.

Following the early work of Broecker (1965), Key et al. (1979) demonstrated several important features of the $^{222}Rn/^{226}Ra$ system. In particular, they showed theoretically that the shape of the pore water supported ^{222}Rn profile has important consequences for the transport parameters determined from the ^{222}Rn deficit, and that the profile shape depends on porosity, grain size, and the distribution of sedimentary ^{226}Ra between ^{226}Ra in equilibrium with ^{230}Th and ^{238}U; ^{226}Ra in equilibrium with unsupported, surface-adsorbed ^{230}Th; and unsupported ^{226}Ra scavenged from the water column by sedimenting particles. In the fine-grained, oceanic sediments they examined, they found that supported pore water ^{222}Rn levels were 30-60% of total sediment ^{226}Ra and that supported pore water ^{222}Rn profiles were generally exponential in shape and could be described by an equation

of the form,

$$P = P_\infty - (P_\infty - P_0) \cdot e^{-L x} \qquad (II.1)$$

(P_∞ = asymptotic supported Rn, P_0 = supported Rn at the sediment/water interface).

Over the last ten years, $^{222}Rn/^{226}Ra$ disequilibrium has been measured in a wide range of marine sedimentary environments. The maximum observable signal is the maximum supported ^{222}Rn in the sediments, which has been found to vary from 0.2 to 6 dpm/gm of dry sediment: 0.2-0.9 dpm/gm dry wt in estuarine sediments (Hammond et al., 1977; Hammond & Fuller, 1979); 0.5-1.6 dpm/gm dry wt in California Borderland sediments (Berelson et al., 1982); 0.4 dpm/gm dry wt in sand and silty sand sediments on the Washington continental shelf (Smethie et al., 1981); and 1-6 dpm/gm dry wt in sediments underlying deep water columns (1500-5000m) in the Gulf of Mexico and the tropical N. Atlantic (Key et al., 1979). Signals usable for solute transport rate or benthic flux determinations were obtained in all the above cases. $^{222}Rn/^{226}Ra$ disequilibria greater than could be explained by transport of pore water ^{222}Rn by molecular diffusion alone were found by Hammond & Fuller (1979) in San Francisco Bay sediments, by Smethie et al. (1979) in Washington continental shelf sediments, and by Martens & Klump (1980) in nearshore sediments permeated by bubble tubes. While Hammond & Fuller and Smethie et al explained solute transport by using biopumping models, Martens & Klump used a one-dimensional enhanced diffusion model.

In this study, Rn/Ra disequilibrium measurements have been used

to determine rates and mechanisms of solute transport at the Buzzards Bay study site: to determine the magnitudes of transport parameters and their seasonal variability and to determine the applicability of a fairly general model allowing transport of solutes by vertical diffusion and by the nonlocal exchange mechanism described by Emerson et al. (1984).

Methods

The procedure for $^{222}Rn/^{226}Ra$ disequilibrium measurements follows quite closely the method described by Key et al. (1979). Samples ranging in weight from 10-30 gm (total sediment weight) were placed in glass bottles containing 200 ml seawater and a magnetic stirring bar, stoppered, and sealed using silicone sealant (for the 12/10/82 core, samples were sealed in gas washing bottles instead). The sediment was slurried by vigorous stirring, and Rn was transfered to counting cells using the method described in Mathieu (1977). The ^{222}Rn activity measured from this extraction, after decay correction back to sampling time, was the *in situ* pore water ^{222}Rn activity. Following storage for 2-6 weeks for ^{222}Rn ingrowth, samples were again slurried for extraction of supported ^{222}Rn. ^{222}Rn scintillation counting was done on Applied Techniques model DRC-MK-6 Dual Radon Counter.

Seven cores for Rn measurement were taken by SCUBA divers over a two-year period. Except for the 12/10/82 core, they were taken along with cores for $^{234}Th/^{238}U$ and pore water chemistry measurement. The Rn core was taken as close as possible to the Th/ pore water chemistry core,

always within 1m of it. The Rn core was hand-carried to the boat, where it was sampled immediately; the time required for sampling and sealing of sample bottles was 15-20 min. Two somewhat different procedures were used for sampling. The 12/10/82 and 31/3/84 cores were collected in 7 cm diameter core liners and extruded at 2 cm intervals; samples were sealed in bottles following removal of the outer parts of the sediment sections. All subsequent cores were collected in a 16 cm diameter PVC core liner and were sampled *via* open-ended syringes inserted through holes in the core liner which had been taped shut during emplacement in the sediment. Two samples were taken from each 2 cm interval; they were usually combined, but some were kept separate for replicate analyses.

Results of pore water ^{222}Rn analyses (*in situ* ^{222}Rn and supported ^{222}Rn, called "Ra_E" here following Key et al., 1979) are shown in Table II.5 (Appendix II.2). Results are presented in dpm/cm^3 pore water, the unit used for modelling of profiles; the directly measured quantity was dpm/gm sediment, which was converted to the reported unit using

$$A(dpm/cm^3 \text{ pore water}) = A(dpm/gm \text{ sed}) \; (\rho_w + (1-\phi)\rho_s/\phi)$$

ρ_w= pore water density = 1.02 gm/cm^3
ρ_s= density of solids = 2.62 gm/cm^3
ϕ= porosity; measured porosity values were used

A summary of replicate determinations is reported in Table II.6. The data in this table are separated into four groups:

(1) twice-run Ra_E. 14 samples were analyzed twice for supported ^{222}Rn. The differences between the two runs should reflect the sum of

TABLE II.6

Reproducibility of Ra-E, in situ Rn-222, and Rn-222 deficit

For groups 1 through 3, values reported are the difference between two replicate measurements as a percentage of the mean of the two measurements. In Group 4, values reported are the difference between measurements on two replicate samples, in dpm/cm^3 pore water.

Group 1: Twice-Run Ra_E (as % of mean)		
Core Date:	31/3/83	Reproducibility: 3.7, 6.6, 7.1
		3.9, 7.8, 8.5
	8/6/83	6.6, 21, 3.3
	7/9/83	4.7, 11.7, 7.3
	16/12/83	1.8, 9.6
Group 2: Replicate Ra_E (as % of mean)		
	31/3/83	6.7
	7/9/83	5.4
	16/12/83	2.0, 2.3
	26/3/84	2.2, 12
	8/6/84	6.8
Group 3: Replicate Rn (as % of mean)		
	7/9/83	21
	16/12/83	22, 11
	26/3/84	8.4, 19
	8/6/84	6.2
Group 4: Replicate Rn Deficit (in dp,/cm^3 pore water)		
	7/9/83	.008
	16/12/83	.017, .010
	26/3/84	.010, .008
	8/6/84	.004

counting errors, irreproducibility in the extraction procedure, and variability in blanks. The values reported are the differences between the pairs of analyses as a percentage of the mean of the two. If all samples are included, the average spread is 7.4±4.7%; if the "flier" from 8/6/83 is excluded, the average is 6.4±2.8%.

(2) Replicate Ra_E samples. Two syringes were filled from each 2 cm section.The two sampling holes were separated by a horizontal distance of 15 cm along the core liner; because of the curvature of the core liner, syringes inserted through the two holes came within 1-2 cm of each other at the center of the core. Differences between the samples from the two syringes reflect the errors in (1) above as well as weighing errors (probably insignificant) and sediment heterogeneity. The average spread of 7 pairs analyzed is 5.3±3.6%.

(3) Replicate Rn samples. Of the duplicate analyses described in (2) above, in situ pore water Rn was analyzed in 6 pairs. The average spread is 15±7%. There are several reasons why the spread is greater than for the Ra_E measurements: in situ pore water Rn depends on solute transport processes which may produce short-term, small-scale heterogeneity, while supported Rn does not; if there is irreproducibility in the extraction procedure, it is more likely to occur during the first extraction, when the sediments in their natural state are broken up by stirring; the most likely handling errors result in loss of Rn during initial sampling and placing in sample bottles, and would therefore only show up in the in situ pore water Rn analysis; and there is some uncertainty introduced by the decay corrections needed to calculate in situ pore water Rn.

(4) Replicate Rn deficit determinations. The variable which is directly related to transport processes is the Rn deficit (supported Rn minus *in situ* Rn). Reproducibility of deficit determinations was evaluated for the 6 samples discussed in (2) and (3) above, and is reported as the absolute difference between replicate samples in dpm/cm^3 pore water. The mean difference is .010±.004. A direct method of determining the error in Rn deficit determinations is to look at samples which "should" be in secular equilibrium: the 31/3/83, 15/12/83, and 26/3/84 cores are consistent with transport by molecular diffusion alone (see discussion below); thus, below 10 cm, ^{222}Rn and ^{226}Ra should be in secular equilibrium. Measured deficits in these samples are both positive and negative, and their magnitudes are 5-15% of measured Rn, which is consistent with experimental error ((2) above). Deficits of less than 0.02 dpm/cm^3 are probably not significant, and larger deficits, up to 0.04 dpm/cm^3, may only be significant if they are observed in several samples.

A component of the errors just discussed is the analytical blank, which is made up of blanks from the extraction lines and of bottle blanks. Two extraction lines were used, and they have blanks of 0.080±0.023 and 0.045±0.015 dpm ^{222}Rn. Bottle blanks average 0.294±0.028 dpm ^{222}Rn. Since, in most cases, samples are 2-5 dpm, the variability in blanks is less than about 2% of sample activity. The only significant exception is the 0-1cm, 8/6/84 sample, for which, because of its low activity, the error introduced by variability in blanks is about 10%.

Results and Discussion

The $^{222}Rn/^{226}Ra$ disequilibrium measurements reported here were undertaken to provide information on the rates and mechanisms of solute transport processes at the Buzzards Bay study site. Variability in transport rates is reflected in the magnitudes of transport parameters, which are obviously important to flux calculations; variability in transport mechanisms can also be important. If transport processes include diffusive transport perpendicular to the sediment/water interface and exchange via tube and burrow structures with overlying water, described by the product of an exchange parameter and the concentration difference between pore water and overlying water (Emerson et al., 1984), then the flux of a solute across the sediment/water interface is given by

$$J_0 = -\phi D_{sed}(dC/dx)_{x=0} - \int_0^{x^*} \phi \cdot \alpha(C(x)-C_{OL})dx$$

α = exchange parameter, in sec^{-1}
x^* = depth of irrigated layer in sediments
C_{OL} = concentration of solute in overlying water, amt/cm^3
D_{sed} = molecular diffusion coefficient for the solute

(a negative flux is out of the sediments). The diffusive term is likely to dominate the calculated flux if the concentration gradient at the sediment/water interface is large; the nonlocal exchange term will be important if α is large or if there is a large solute concentration difference between pore water below the upper few cm of the sediment column and overlying water. Clearly, for many solutes, it is important to determine whether exchange of pore water and overlying water is

significant relative to direct diffusive exchange across the sediment/water interface. Thus, the $^{222}Rn/^{226}Ra$ disequilibrium data have been interpreted both in terms of vertical diffusive transport and, when the shape of the Rn profile has justified it, in terms of nonlocal exchange.

In steady state, if pore water advection is insignificant and if porosity (ϕ) and the diffusion coefficient (D_{sed}) are assumed constant, then ^{222}Rn profiles can be explained in a model including both vertical diffusion and nonlocal exchange by

$$(II.2) \qquad D_{sed}\frac{d^2C}{dx^2} - (\lambda+\alpha)C + \lambda(P_\infty - \Delta P e^{-Lx}) = 0$$

C= ^{222}Rn activity, in dpm/cm^3 pore water

D_{sed} = the solute molecular diffusion coefficient, corrected for porosity, tortuosity, and variations in temperature (cm^2/sec)

α= nonlocal exchange parameter, sec^{-1}. Exchange of ^{222}Rn between pore water and overlying water is described by the product of α and the pore water/overlying water concentration difference. For ^{222}Rn, the overlying water concentration is essentially zero, and the nonlocal exchange term is $-\alpha C$.

P_∞, ΔP, L describe the supported ^{222}Rn profile, and are obtained by being varied to fit the observed profile (see equation II.1 for their definitions)

λ = decay constant for ^{222}Rn

The boundary conditions applied are:

$$(1) \quad C\ (x=0) = 0$$

$$(2) \quad C\ (x=x_s) = P_\infty\lambda/(\lambda+\alpha)$$

(x_s is the maximum sampling depth). If $\alpha = 0$, this model is identical to that proposed by Key et al. (1979). Two effects of a nonzero α on the pore water ^{222}Rn profile are important. At each depth in the irrigated layer (that is, the layer in which $\alpha > 0$), the ^{222}Rn deficit is greater than that produced by vertical molecular diffusion alone. In addition, secular equilibrium between ^{222}Rn and ^{226}Ra is not reached in the irrigated layer as, below the zone in which exchange with overlying water via vertical diffusion is important, ^{222}Rn production is balanced by the sum of radioactive decay and loss to overlying water by irrigation (boundary condition (2)). For the balance expressed by boundary condition (2) to hold exactly, the ^{222}Rn gradient must be constant at the base of the sampled layer (x_s).

To explain the $^{222}Rn/^{226}Ra$ disequilibria observed at the Buzzards Bay site, the model described by equation II.2 must include an α that varies with depth below the sediment/water interface. Thus, equation II.2 has been solved numerically, with $\alpha = \alpha_0 \cdot \exp(-x/\alpha_1)$. If equation II.2 is approximated at n+1 points along the x-axis such that $x_i = (i-1)\Delta x$, then, using a centered-difference approximation to d^2C/dx^2, the equation can be approximated by

$$(II.3) \qquad C_{i-1} - (A_i(\Delta x)^2 + 2) + C_{i+1} = B_i(\Delta x)^2$$

$$A_i = \frac{\alpha_i + \lambda}{D_{sed}}$$

$$B_i = (\lambda/D_{sed}) \cdot (\Delta Pe^{-L \times i} - P_\infty)$$

with boundary conditions

$$(1)\quad C_0 = 0$$

$$(2)\quad C_n = P_n \bullet \lambda/(\alpha_n + \lambda)$$

The numerical model results in a system of n equations which can be solved by standard techniques (Hornbeck, 1975). In this case, the system was solved in three steps. First, the tridiagonal coefficient matrix (A) was rewritten as the product of a lower and an upper diagonal matrix (L and U, respectively). Thus, the equation system was rewritten,

$$(LU)C = b$$

(C_i are the unknown concentrations; b is the right-hand side of equation II.3). This equation was solved for the product vector, y = UC, using the relationship,

$$y_i = \{b_i - (y_{i-1})(l_{i,i-1})\}/l_{ii}$$

(y_i and b_i are the components of the vectors, y and b; l_{ij} are the components of the matrix, L). Then, the concentrations, C_i, were obtained from UC = y using

$$C_i = y_i - (u_{i,i+1})(C_{i+1})$$

The model has been fit to the Ra/Rn data from the Buzzards Bay site using a grid-search method (Bevington, 1969) and two adjustable parameters, α_0 and α_1. A grid spacing (Δx) of 0.05 cm was used to obtain the fits; the results were checked for adequate convergence of the numerical solution by recalculating the model profile using Δx = .025

cm. The maximum differences in the two calculated solutions, observed for the June, '84, core, were about 3%.

The $^{222}Rn/^{226}Ra$ data are presented in Table II.5 (Appendix II.2) and in Figure II.5. Based on the general shape of the profiles and on a preliminary analysis using equation II.2 with $\alpha = 0$ and D_{sed} as an adjustable parameter (Table II.7), the data have been divided into three groups. The first group, including March and December cores, is consistent with solute transport by vertical molecular diffusion alone. The Rn profiles in the second and third groups cannot be explained by vertical molecular diffusion alone. In the second group (the June cores), irrigation appears to occur to depths exceeding 20 cm, greatest depth sampled; in the third group (September and October cores), irrigation affects the Rn profiles to a depth of about 10 cm.

The first data group includes the December, 83, core and the two March cores: the data show small ^{222}Rn deficits near the sediment/water interface, with ^{222}Rn and ^{226}Ra approximately in secular equilibrium at depths greater than 6 cm below the interface. This result is consistent with transport of solutes by molecular diffusion.

Molecular diffusion coefficients, corrected for tortuosity and porosity, have been approximated using the data for Rn diffusion in water as a function of temperature of Broecker & Peng (1976) and the relationship between the formation factor, F (the ratio of the resistivity of bulk sediment to the resistivity of the interstitial fluid), and porosity found at the study site. Resistivity data, obtained by F. Sayles (pers. comm.) in October, 1981, indicate that F is

Figure II.5

Rn-222/Ra-226 Measurements at the Buzzards Bay Site

In situ pore water ^{222}Rn data are represented by the dashed vertical bars in the figure. Supported pore water ^{222}Rn data are represented by solid vertical bars. The unit of both quantities is dpm/cm^3 pore water.

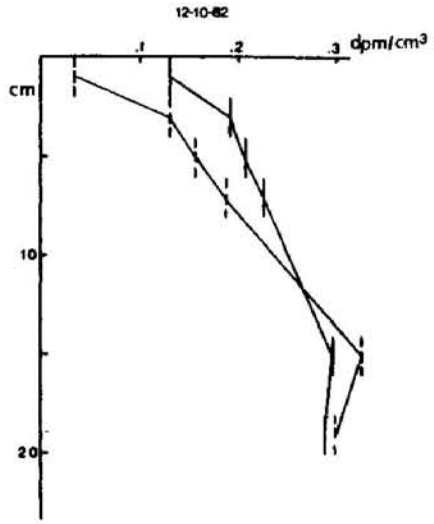
12-10-82
.1
.2
.3
dpm/cm3
cm
10
20

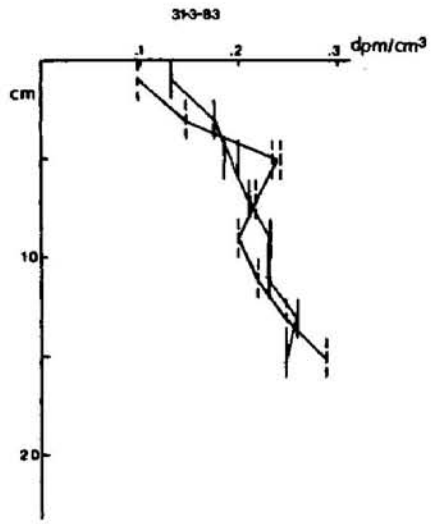
31-3-83
.1
.2
.3
dpm/cm3
cm
10
20

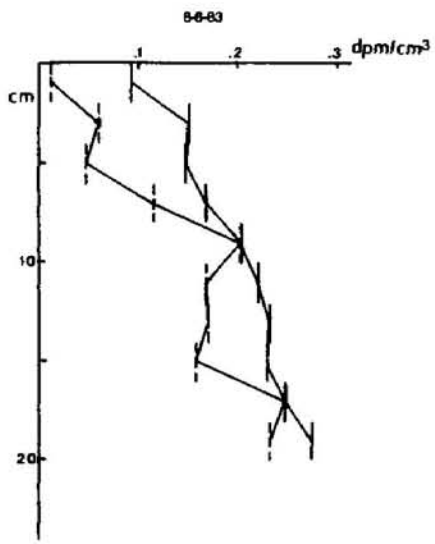
8-6-83
.1
.2
.3
dpm/cm3
cm
10
20

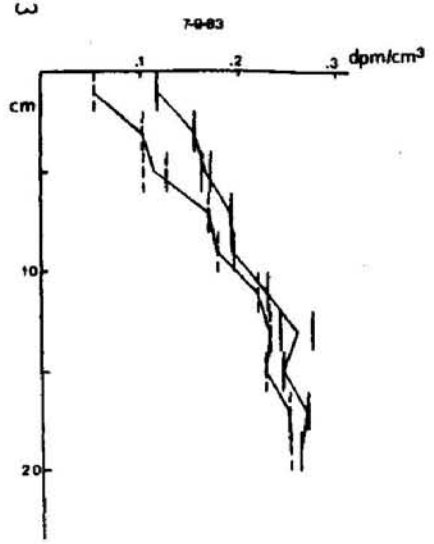
7-9-83
.1
.2
.3
dpm/cm3
cm
10
20

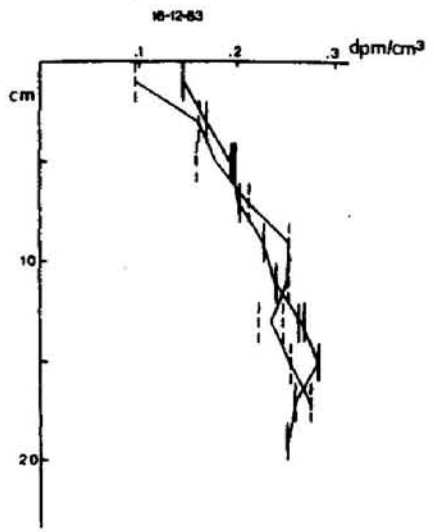
16-12-83
.1
.2
.3
dpm/cm3
cm
10
20

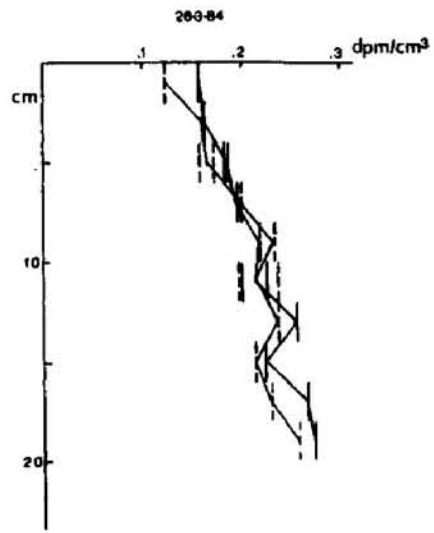
26-3-84
.1
.2
.3
dpm/cm3
cm
10
20

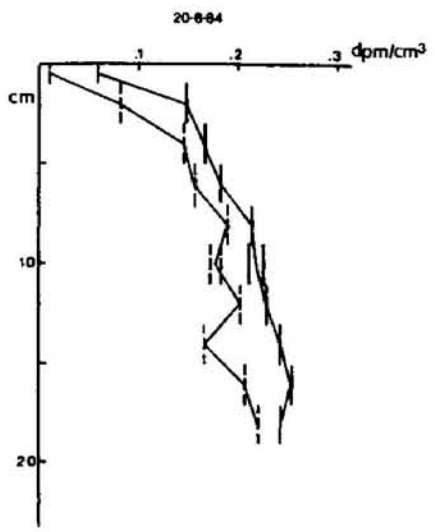
20-6-84
.1
.2
.3
dpm/cm3
cm
10
20

approximately constant at 2.0±0.2 (2σ) between 2 and 35 cm below the interface. Detailed porosity measurements, made on a total of six cores, during all seasons, between 7/82 and 9/83 (Figure II.6), indicate that there is no systematic seasonal variability in porosity profiles. They can be explained adequately by an average porosity profile,

$$\phi = .737 + .159 \cdot e^{-.187x}$$

Following Andrews & Bennett (1981), who studied the diffusivity of fine-grained nearshore sediments on the Scotian shelf, porosity and formation resistivity factor have been related through $F = C \cdot \phi^{-K}$, with $C = 1$. $K = 2.5 \pm 0.3$ was found at the Buzzards Bay site using $F = 2.0$ and $\phi = .758$ (the average ϕ between 2 and 30 cm below the interface). Then, an average D_{sed} in the sampled region of the sediment column (0-20 cm) was calculated using

$$D_{sed} = \frac{D_{pw}}{\phi_{AV} F} = .64 D_{sw}$$

(D_{pw} is the molecular diffusion coefficient in pore water, assumed equal to the molecular diffusion coefficient in seawater. $\phi_{AV} = .778$). The porosity data in Figure II.6 clearly show that the use of an average D_{sed} is an approximation. Using the calculated F and ϕ from the time-averaged porosity profile, D_{sed} can be seen to vary by about 15% from 1-20 cm below the sediment/water interface, with most of the variation occurring in the upper 4 cm. This variation is not much greater than the 10% uncertainty in the average of the formation factor

Figure II.6

Porosity at the Buzzards Bay Site

A. Porosity Profiles

B. Porosity data, plotted with the time-averaged porosity profile,

$$\phi = .737 + .159e^{-.187x}$$

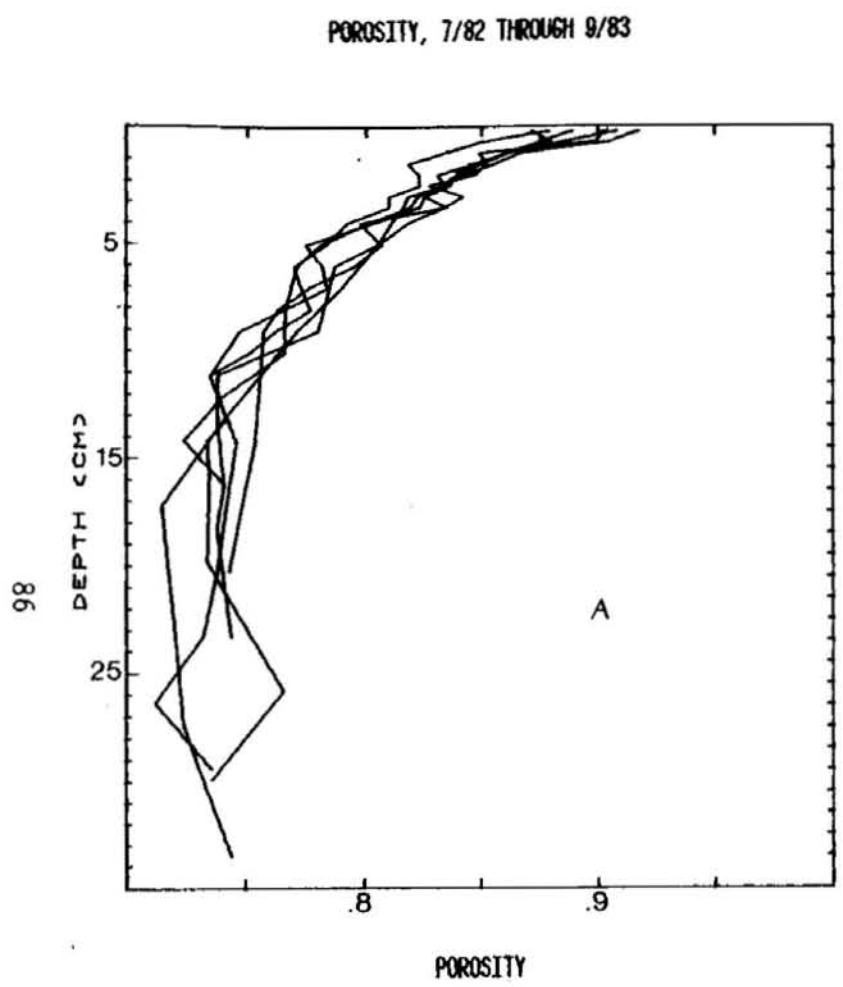
POROSITY, 7/82 THROUGH 9/83
DEPTH (CM)
5
15
25
.8
.9
POROSITY
A

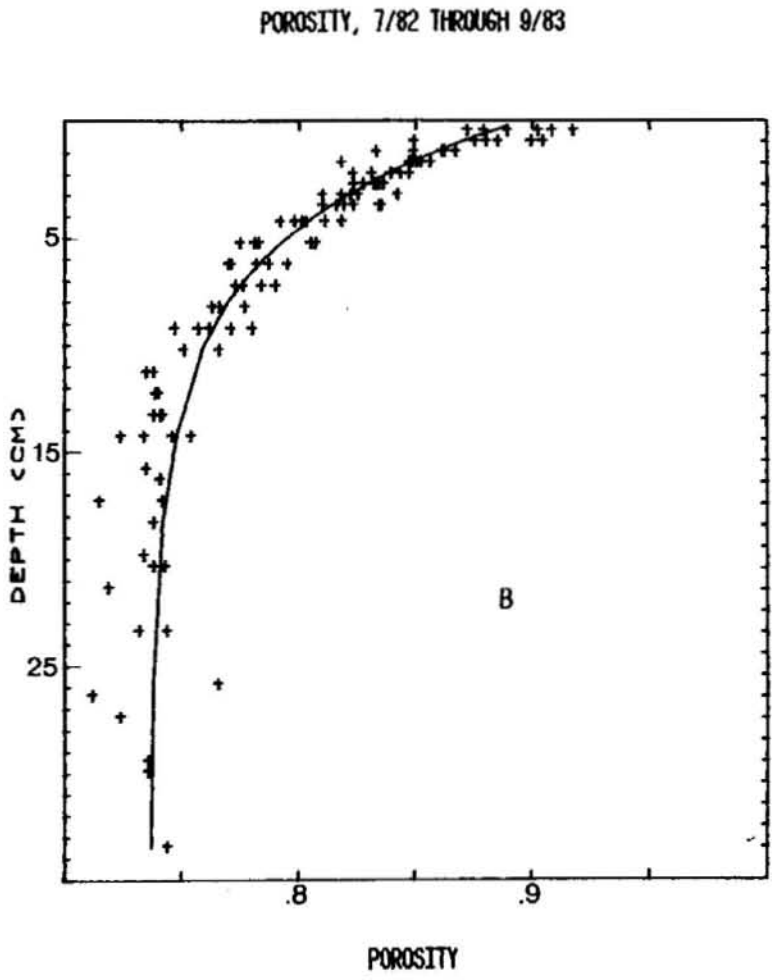
POROSITY, 7/82 THROUGH 9/83
DEPTH (CM)
5
15
25
.8
.9
POROSITY
B

measurements. Thus, use of a depth-averaged D_{sed} does not add significantly to the error in the analysis of the $^{222}Rn/^{226}Ra$ data.

Calculated D_{sed} are shown in Table II.7. Also shown in Table II.7 are the results obtained by fitting the Rn data using equation II.2 with α = 0 and D_{sed} adjusted to fit the data (the best-fit D is called "D_{app}"). In addition, in Figure II.7A, the data from the three cores in the first group are plotted with fits to the supported ^{222}Rn profiles and the in situ ^{222}Rn profiles expected if solute transport is by molecular diffusion. From these results, it can be seen that the Rn deficits measured were generally consistent with, but somewhat smaller than, predicted by molecular diffusion. Sampling error is the most likely cause of this small discrepancy: since cores were taken in a nontransparent, PVC core liner, and sampled through holes in the core liner at levels fixed before coring, it is likely that small overpenetration of the cores occurred, so that actual depths below the interface are somewhat greater than the recorded depths. Sampling was done with the cores sealed to prevent escape of Rn; because removal of sediment during sampling caused a slight change in the position of the interface within the core liner, accurate corrections for overpenetration could not be made. In March, '84, when the results showed this error to be most significant, the divers taking the core had observed directly a slight overpenetration. Given the steep in situ Rn gradients present in the upper 4 cm of these cores, an overpenetration of 1 cm would explain the difference between the observed results and the results predicted by the molecular diffusion model. It is notable that the core showing the smallest discrepancy, the March, '83, core, was sampled by extruding from a transparent core liner through which the

TABLE II.7

Modeling results for Rn-222/Ra-226 profiles.

The first column indicates the date the core was taken; the second is the temperature of bottom water at the time of coring. The third column shows molecular diffusion coefficients interpolated from the data of Broecker & Peng (1976) for Rn diffusion in water as a function of temperature. The fourth column is D_{sed}, the molecular diffusion coefficient for Rn corrected for tortuosity and porosity. The fifth column is the apparent diffusion coefficient derived by fitting the Rn data using equation II.2 with $\alpha = 0$, using D as a fitting parameter. E is the ratio, D_{app}/D_{sed}. The seventh and eighth columns are the best-fit α using the numerical model of equation II.3, in which α varies exponentially with depth below the sediment/water interface, $\alpha = \alpha_0 \exp\{-x/\alpha_1\}$. Units of D are cm^2/sec; units of α are sec^{-1}.

Date	°C	D-mol $\times 10^6$	D-sed $\times 10^6$	D-app $\times 10^6$	E	$\alpha 0$	$\alpha 1$
12/10/82	15	10.5	6.7	26	3.9	3.5×10^{-6}	2.63
31/3/83	4	7.7	4.9	1.9	0.39	-	-
8/6/83	14	10.2	6.5	120	18	4.8×10^{-6}	5.26
7/9/83	16	10.8	6.9	33	4.8	1.8×10^{-6}	4.34
15/12/83	7	8.4	5.4	2.1	0.39	-	-
26/3/84	4	7.7	4.9	0.69	0.15	-	-
8/6/84	16	10.8	6.9	48	7.0	3.7×10^{-7}*	∞

*..These values determined from a model with $\alpha(x)$ = constant. When $\alpha(x) = \alpha_0 \exp\{-x/\alpha_1\}$ was used to fit the data, $\alpha_0 = 3.4\times10^{-7}$ and $(\alpha_1)^{-1} = -.01$ were obtained.

Figure II.7

Model Fits to Rn-222/Ra-226 Data

In figures 7A through 7C, pore water Rn is represented by open circles, Ra_E by X. The data from the first group of cores are shown in Figure 7A; the second group is shown in Figure 7B; the third group is shown in Figure 7C. Curve I in each case is the best-fit supported pore water ^{222}Rn (Ra_E) based on $P=P_\infty-\Delta Pe^{-Lx}$. Curve II in Figure 7A is the in situ pore water ^{222}Rn with solute transport by vertical molecular diffusion and the best-fit supported Rn. In Figures 7B and 7C, Curve II is the in situ pore water ^{222}Rn obtained with the numerical model of equation II.3, in which solute transport is by vertical molecular diffusion and nonlocal exchange, with the exchange parameter allowed to vary with depth below the sediment/water interface.

Figure II.7A

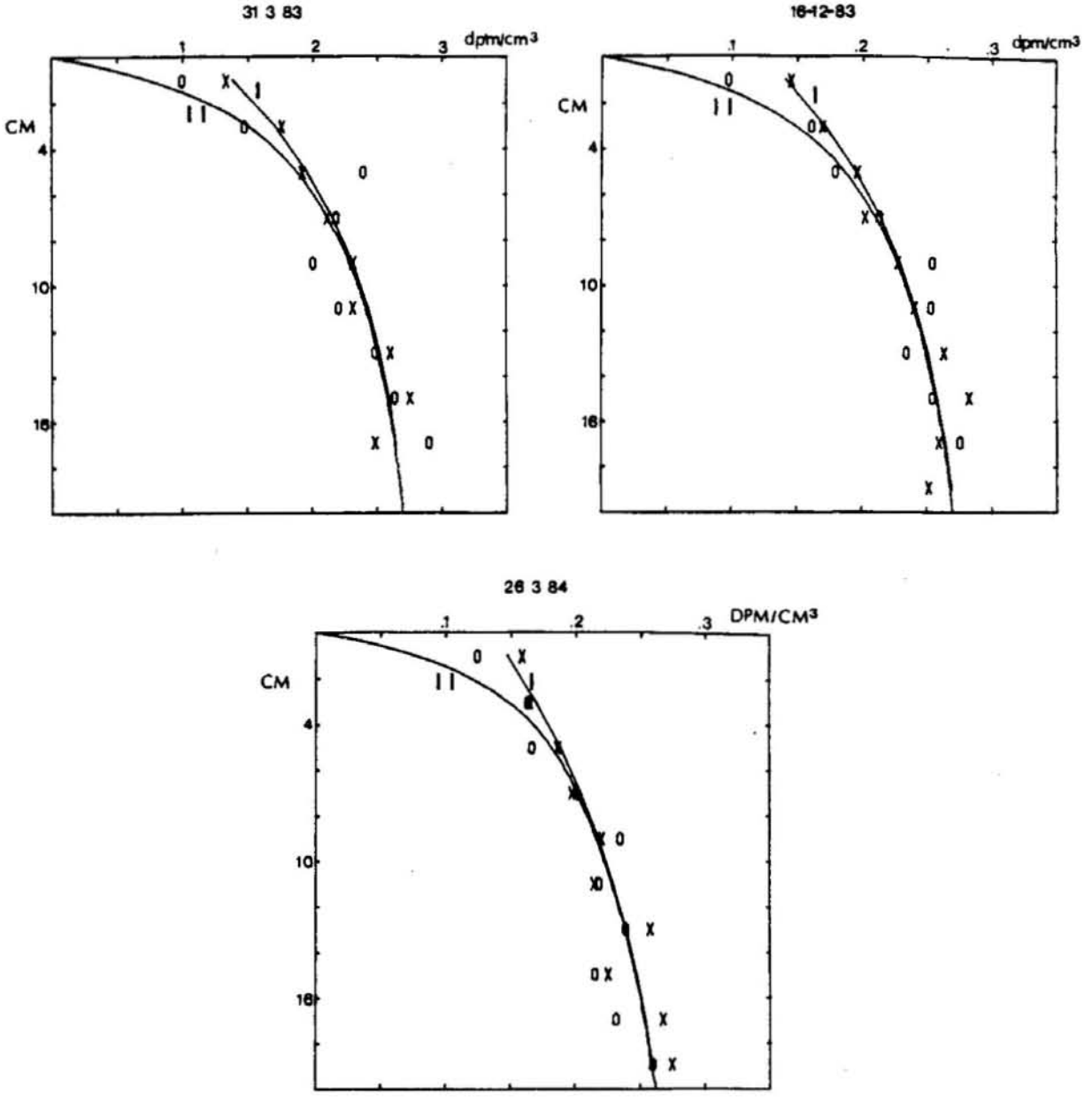

Figure II.7B

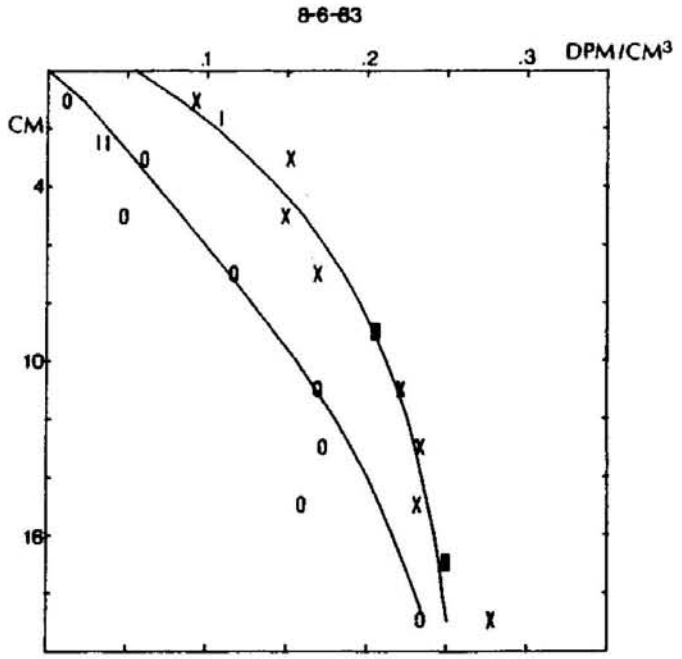

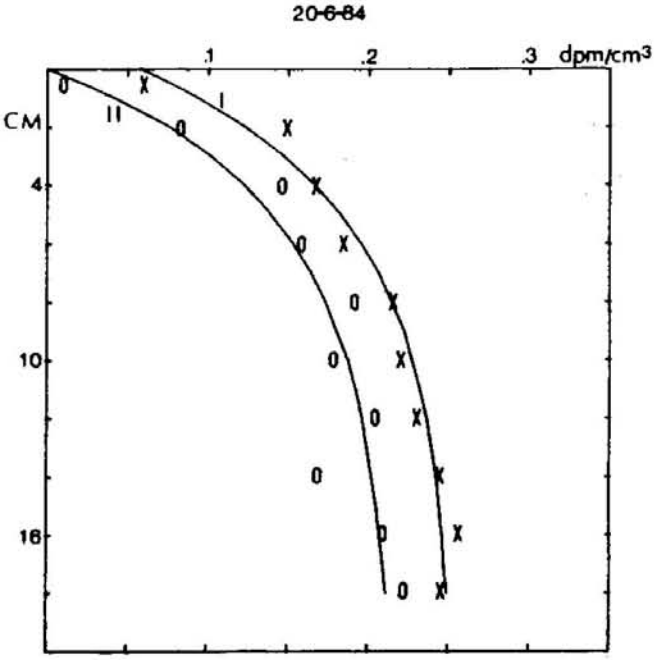

Figure II.7C

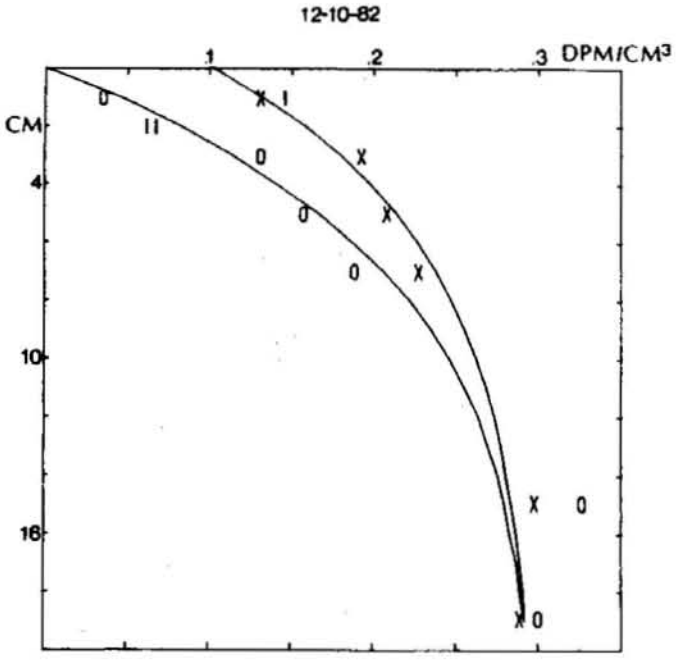
12-10-82
.1
.2
.3 DPM/CM³
CM
4
10
16
I
II
0
X

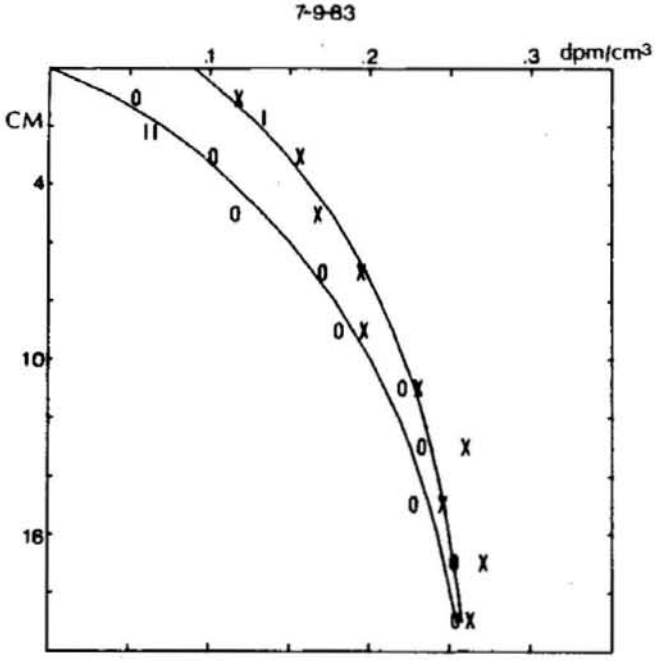
7-9-83
.1
.2
.3 dpm/cm³
CM
4
10
16
I
II
0
X

position of the interface was easily observable.

The June cores make up the second data group. In both June cores, significant deficits (based on the criteria discussed in the methods section) occur to at least 20 cm below the sediment/water interface. As is shown in Table II.7, molecular diffusion coefficients exceeding those estimated for Rn at the study site by a factor of 7 (June, '84) to 18 (June, '83) would be required to optimize the model fit to the Rn data if irrigation is not allowed. Even using these extremely large values for D_{sed}, neither profile is fit well; in particular, the approximately constant deficits observed in June, 84, cannot be explained by a vertical diffusion model. Because these deficits are significantly larger than those observed at depth in other cores obtained during this study, they cannot be explained as an artifact of the slurrying procedure used for measuring pore water Rn (Hammond & Fuller, 1979; Berelson et al., 1982). Instead, they are readily explained by including nonlocal exchange with overlying seawater in the model. The result obtained by using α as a fitting parameter, with D_{sed} the molecular diffusion coefficient corrected for tortuosity and porosity, is shown in Figure II.7B. The profile is fit quite well when when α is constant with depth below the sediment/water interface and equal to $3.7 \times 10^{-7} sec^{-1}$, a value that is consistent with the results obtained by Emerson et al. (1984) when they applied the nonlocal exchange model to solutes other than ^{222}Rn in a variety of nearshore locations. This result was obtained using the analytical solution to equation II.2 with constant α. When the numerical model (equation II.3) was used, a similar result was obtained: $\alpha_0 = 3.4 \times 10^{-7} sec^{-1}$ and $(\alpha_1)^{-1}$ slightly negative, but essentially indistinguishable from

zero. The June, 83, core is a more complicated case, as it shows alternating regions of small ^{222}Rn gradients (0-6cm and 10-15cm) and steep ^{222}Rn gradients. When a vertical diffusion model was applied, a very large enhancement over molecular diffusion was required to produce the deficits observed at depth: the best-fit D was 18 times the molecular diffusion rate. On the other hand, a molecular diffusion/nonlocal exchange model with $\alpha = (4.8 \times 10^{-6}) \exp(-x/5.3)$ sec^{-1} explained the deficits quite well (Figure II.7B). The details of the Rn profile in this rapidly irrigated sediment column are not explained by the model; it is likely that individual transport events have produced discontinuities in pore water Rn gradients too rapidly (or too recently, if the steady-state assumption is relaxed) to be smoothed by diffusion.

The third data group includes the October, '82, core and the September, '83, core. They are characterized by smoothly varying in situ Rn profiles, with significant Rn deficits extending to approximately 10 cm below the interface. For smoothly varying in situ Rn profiles to be observed, it is necessary that the individual transport events occurring during the 2-week period which is integrated to produce the Rn profile be averaged effectively. The data from these late summer cores were fit using the "enhanced diffusion" construct to demonstrate that solute transport is more rapid than is allowed by molecular diffusion at the in situ temperature: D_{app} is enhanced over the sediment molecular diffusion coefficient (D_{sed}) by a factor of 3.9 in October, '82, and by a factor of 4.8 in Septmeber, '83. When the molecular diffusion/nonlocal exchange model was used to fit the data (Figure II.7C), it yielded scale

lengths for the depth variation of the nonlocal exchange parameter (α_1 in Table II.7) of 2.6 cm (October, '82) and 4.3 cm (September, '83), and α_o values of $3.5 \times 10^{-6} sec^{-1}$ (October, '82) and $1.8 \times 10^{-6} sec^{-1}$ (September, '83). In order to compare these data with previous studies, the nonlocal exchange parameter has been averaged over the upper 20 cm of the sediment column. The average α is similar for both these cores (4.6×10^{-7} sec^{-1} and $3.9 \times 10^{-7} sec^{-1}$ for 10/82 and 9/83, respectively); these values are similar to that found for the June, '84, core, but significantly less than was found in June, '83 ($12 \times 10^{-7} sec^{-1}$). Previous studies (Emerson et al., 1984), using a constant-α model and SiO_2 as an irrigation tracer, estimated α at $1\text{-}20 \times 10^{-7}$ sec^{-1} at a variety of nearshore sediment sites. The data from the seven cores sampled for Rn at the Buzzards Bay site suggest that the two fall cores represent intermediate transport between the cold months, when irrigation is unimportant, and the early summer, when rapid exchange of pore water with water in burrow structures occurs to depths exceeding 20 cm; in the two fall cores, irrigation is an important determinant of the ^{222}Rn profile to only about 10 cm.

The general results of the solute transport study using $^{222}Rn/^{226}Ra$ disequilibrium as a tracer can be briefly summarized. Transport rates follow a distinct seasonal trend. The measured rate is consistent with transport by molecular diffusion in the cold months, December through March; sediment irrigation has a significant effect on the pore water ^{222}Rn profile to depths of at least 20 cm in two cores taken in June; and irrigation is important to about 10 cm in two fall

cores. The variability of the irrigation rate both over time and with depth below the sediment/water interface has been quantified using numerical solutions to a model which describes irrigation by the nonlocal exchange mechanism proposed by Emerson et al. (1984). The results are summarized in Figure II.8, which shows the variability of the nonlocal exchange parameter (α) with depth below the interface. The magnitude of α at the sediment/water interface varies considerably, ranging from $4 \times 10^{-7} sec^{-1}$ (6/84) to $48 \times 10^{-7} sec^{-1}$ (6/83); the two fall cores have intermediate values. The large difference between the two June cores may be explained by the fact that, while sulfate reduction was not important near the interface in 6/83, there was evidence for the existence of significant concentrations of sulfides near the interface in 6/84 (these results are discussed in detail in Chapter 3). The two June cores are similar in that they both show important irrigation in the 10-20 cm depth interval. In this way, they are in sharp contrast to the two fall cores, in which α drops to very small values by 10 cm below the interface. Of course, it must be kept in mind that, since no study of spatial heterogeneity was undertaken, generalizations about time trends of transport rates and mechanisms are based only on observations of similar results during the same seasons of different years. Nonetheless, application of the variable-α model to $^{222}Rn/^{226}Ra$ disequilibrium measurements appears to show significant trends in solute transport processes at the Buzzards Bay study site.

Figure II.8

The Variation of α with depth below the sediment/water interface

A summary of the results obtained by applying a model explaining solute transport by the combination of vertical molecular diffusion and nonlocal exchange, with the nonlocal exchange parameter (α) varying exponentially with depth below the sediment/water interface.

Figure II.8

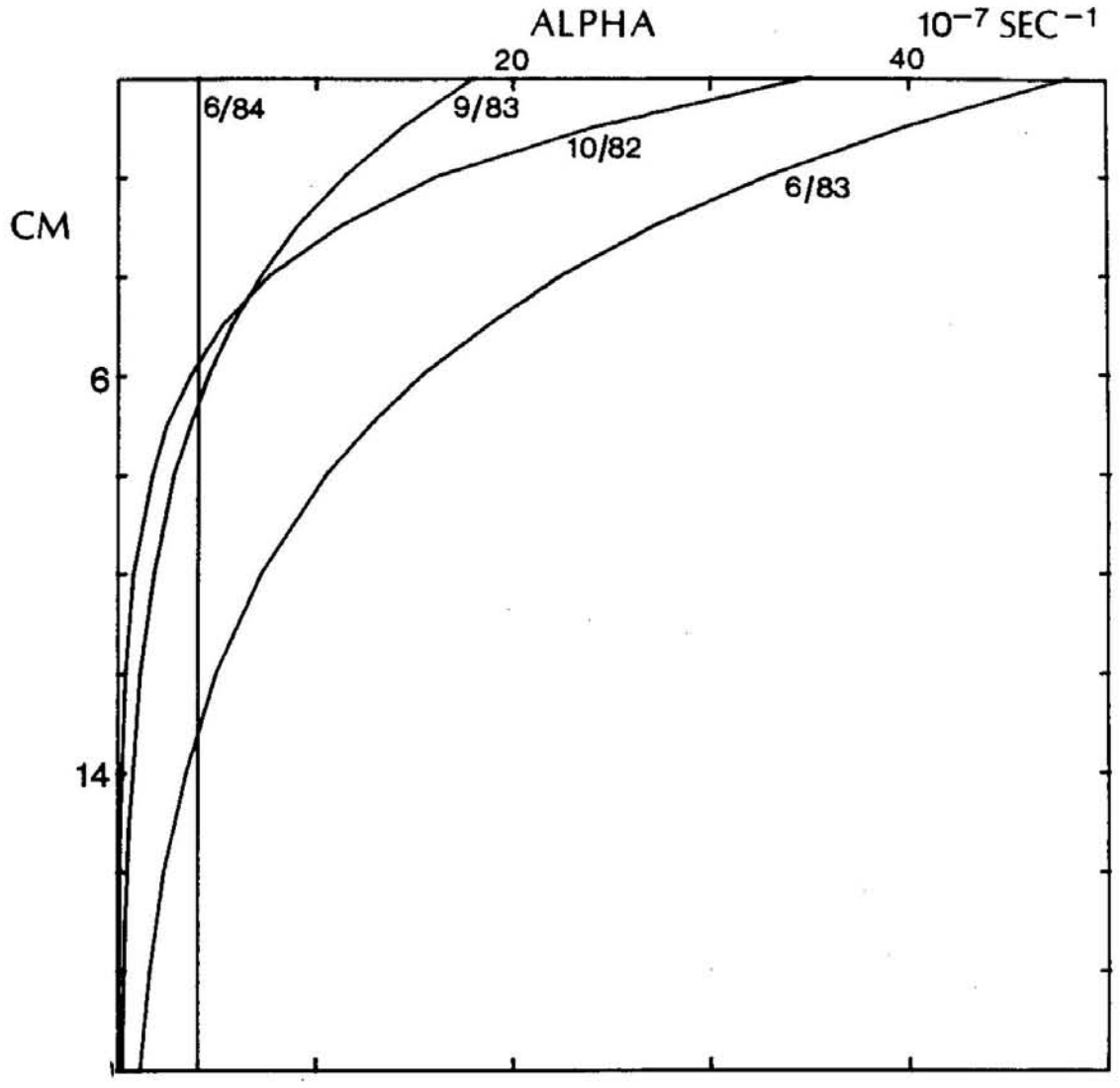

Summary and Conclusions

Both particle and solute transport rates at the Buzzards Bay study site follow the trend predicted from seasonal variability in biological activity. ^{234}Th-derived particle mixing rates range over an order of magnitude, with a warm season average (44×10^{-8} cm^2/sec) about two times the cold season average (24×10^{-8}cm^2/sec). Solute transport rates derived from pore water ^{222}Rn measurements show similar overall variability, but, due the nonconstancy of irrigation rates with depth, the variability is more difficult to quantify. Solute transport can be modeled by vertical diffusion in winter; in late summer, transport in the upper 10 cm of the sediment column is too rapid to be explained by molecular diffusion, but can be explained by invoking nonlocal exchange of pore water solutes with overlying seawater; in two early summer cores, transport was found to be consistent with nonlocal exchange over the upper 20 cm of the sediment column.

In addition to transport rate and mechanism, the depth below the sediment/water interface to which enhanced transport occurs has been examined. Rapid particle mixing measurable using the ^{234}Th excess occurs to depths of 1.5-2.5 cm at the study site. The depth of solute transport between pore water and overlying seawater may vary dramatically: when solute transport is by molecular diffusion, Rn deficits are observed to only 6-8 cm; in fall, when irrigation is important, Rn deficits are observed to 10-12 cm; finally, when nonlocal exchange is most effective, it connects pore waters with overlying

seawater to the bottom of the sampled interval, at 20 cm below the sediment/seawater interface. The effects of irrigation on other solutes may be important to depths in excess of the depth at which a ^{222}Rn deficit is observed: ^{222}Rn is affected by irrigation events occurring over only about a 2 week period; when longer time scales are considered, irrigation may occur to depths in excess of 20 cm.

Appendix II.1

TABLE II.2

Th-234/U-238 data for cores collected from 28/7/82 to 26/3/84

Depths are in cm; activities are in dpm/gm dry weight. Errors reported are total 1 σ counting errors, including uncertainties in backgrounds, efficiencies, and yield measurements.

Sample cm	Porosity	U-238 dpm/gdw	Th-234 dpm/gdw	Excess Th-234 dpm/gdw
28/7/82				
0-0.5 A	.879		7.82±0.29	5.30±0.28
0-0.5 B			7.80±0.20	5.28±0.19
0.5-1 A	.849	1.41±0.10	5.74±0.24	3.23±0.22
0.5-1 B		1.65±0.11	5.03±0.15	2.50±0.12
1-1.5	.833	1.98±0.12	4.92±0.64	2.41±0.63
1.5-2	.818	1.98±0.19	3.42±0.54	0.91±0.54
2-2.5	.823	2.08±0.24	3.29±0.57	0.75±0.56
2.5-3	.823	1.93±0.19	2.95±0.23	0.43±0.21
3.5-4	.810	1.97±0.25	2.53±0.21	0.016±0.19
4-5			2.51±0.19	-0.02±0.17
5-6			2.90±0.21	0.38±0.19
20/10/82				
0-0.5	.872	1.94±0.06	11.27±0.51	8.64±0.51
0.5-1	.880		9.29±0.42	6.68±0.41
1-1.5	.862	1.98±0.13	5.63±0.28	3.01±0.27
1.5-2	.847	2.01±0.12	4.39±0.34	1.77±0.33
2-2.5	.831	2.49±0.15	3.02±0.22	0.41±0.21
3.5-4	.816	2.06±0.15	3.18±0.24	0.56±0.23
4-5			2.62±0.19	0.00±0.18
8-9		2.11±0.09	2.42±0.20	-0.21±0.19

Sample cm	Porosity	U-238 dpm/gdw	Th-234 dpm/gdw	Excess Th-234 dpm/gdw
15/12/82				
0-0.5	.908		10.78±0.46	8.19±0.44
1-1.5	.862		3.38±0.34	0.80±0.30
1.5-2	.850		2.02±0.35	-0.55±0.32
2-2.5	.839		1.42±0.34	-1.16±0.31
2.5-3	.832		3.65±0.46	1.07±0.43
3-3.5	.825		2.37±0.36	-0.20±0.33
3.5-4	.823		2.25±0.40	-0.33±0.37
5-6	.775		2.58±0.39	0.00±0.36
7-8			2.45±0.42	-0.12±0.39
31/3/83				
0-0.5	.917		14.33±0.35	11.7±0.34
0.5-1	.904		6.90±0.25	4.25±0.24
1-1.5	.867		5.22±0.20	2.56±0.19
1.5-2	.856		2.66±0.15	0.00±0.13
2-2.5	.843		2.38±0.17	-0.29±0.16
2.5-3	.833		3.14±0.17	0.47±0.15
3-3.5	.822		2.95±0.14	0.29±0.12
3.5-4	.819		2.78±0.23	0.12±0.22
4-5	.801		1.78±0.19	-0.88±0.18
8-9	.766		2.53±0.17	-0.12±0.15
8/6/83				
0-0.5	.889		11.6±0.8	9.09±0.78
0.5-1	.875		9.62±0.36	7.13±0.35
1-1.5	.861		6.12±0.24	3.63±0.22
1.5-2	.848		5.02±0.24	2.53±0.22
2-2.5	.839		4.13±0.22	1.64±0.20
2.5-3 A	.836		2.61±0.20	0.11±0.18
2.5-3 B			2.19±0.23	-0.30±0.21
3-3.5	.825		2.81±0.20	0.32±0.18
3.5-4	.835		2.25±0.19	-0.24±0.16
7-8			2.12±0.22	-0.36±0.20
20-21			2.77±0.22	0.28±0.20

Sample cm		Porosity	U-238 dpm/gdw	Th-234 dpm/gdw	Excess Th-234 dpm/gdw
7/9/83					
0-0.5		.902		9.73±0.75	7.34±0.68
0.5-1		.899		5.59±0.64	3.20±0.55
1-1.5		.849		5.51±0.65	3.12±0.57
1.5-2		.852		3.43±0.69	1.04±0.61
2-2.5		.847		3.32±0.64	0.93±0.56
2.5-3		.827		1.88±0.59	-0.51±0.50
3-3.5		.842		1.30±0.59	-1.09±0.49
3.5-4		.835		2.87±0.62	0.48±0.53
4-5		.818		4.32±0.64	1.93±0.56
7-8				2.43±0.68	0.04±0.60
26/3/84					
0-0.5	A	.895*		12.2±1.2	9.5±1.2
	B			10.4±1.7	7.8±1.7
0.5-1	A	.882		4.84±0.65	2.15±0.62
	B			5.50±0.80	2.81±0.77
1-1.5	A	.856		3.41±0.56	0.72±0.52
	B			3.57±0.64	0.88±0.61
1.5-2	A	.845		3.32±0.30	0.63±0.23
3.5-4	A	.823		2.73±0.50	0.044±0.46
	B			2.60±0.71	-0.085±0.68

* Porosity was not measured for this core; the values shown are averages calculated from all the cores taken at the study site.

TABLE II.3

Supported Th-234 estimates

The supported ^{234}Th estimates in this table are based on ^{234}Th activities below the rapidly mixed layer. These values were used to calculate excess ^{234}Th. Unit= dpm/gm dry wt.

Core	Supported Th-234
28/7/82	2.52±0.21
20/10/82	2.62±0.19
15/12/82	2.58±0.39
31/3/83	2.66±0.15
8/6/83	2.49±0.09
7/9/83	2.39±0.32
26/3/84	2.69±0.20

Appendix II.2

TABLE II.5

Rn-222/Ra-226 Disequilibrium Results

Pore water ^{222}Rn ("Rn"), supported pore water ^{222}Rn ("Ra_E"), and the pore water Rn deficit from cores taken from 12/10/82 to 8/6/84. Depths are in cm; activities are in dpm/cm^3 pore water.

	Depth	Ra_E	Rn	Deficit
12/10/82				
	0-2	.131	.035	.096
	2-4	.192	.131	.061
	4-6	.208	.157	.051
	6-8	.227	.188	.039
	14-16	.297	.326	-.029
	18-20	.288	.299	-.011
31/3/83				
	0-2	.133	.099	.034
	2-4	.176	.147	.029
	4-6A	.186	.243	-.057
	4-6B	.205,.192	.234	-.036
	6-8	.203,.218	.218	-.008
	8-10	.237,.228	.200	.032
	10-12	.240,.222	.220	.011
	12-14	.260	.248	.012
	14-16	.237,.258	.289	-.040
8/6/83				
	0-2	.0898,.0959	.012	.081
	2-4	.168,.136	.061	.075
	4-6	.149	.048	.101
	6-8	.169	.117	.052
	8-10	.205	.205	.000
	10-12	.221	.169	.052
	12-14	.233	.172	.061
	14-16	.231	.159	.072
	16-18	.249	.249	.000
	18-20	.272,.281	.233	.043

	Depth	Ra_E	Rn	Deficit
7/9/83				
	0-2	.118	.054	.064
	2-4	.156	.102	.054
	4-6A	.168,.176	.128	.044
	4-6B	.153,.172	.104	.059
	6-8	.194	.170	.024
	8-10	.196	.180	.016
	10-12	.230	.220	.010
	12-14A	.265,.285	.232	.043
	12-14B	.242		
	14-16	.245	.227	.018
	16-18	.270	.252	.018
	18-20	.262	.253	.009
16/12/83				
	0-2	.145	.097	.048
	2-4	.169	.161	.008
	4-6A	.194	.159	.035
	4-6B	.198	.198	.000
	6-8	.202	.213	-.011
	8-10	.229,.225	.254	-.027
	10-12	.240	.253	-.013
	12-14A	.268	.246	.022
	12-14B	.249,.274	.221	.040
	14-16	.282	.254	.028
	16-18	.259	.275	-.016
	18-20	.251		
26/3/84				
	0-2	.158	.124	.034
	2-4	.164	.163	.001
	4-6A	.188	.173	.015
	4-6B	.184	.159	.025
	6-8	.197	.201	-.004
	8-10	.220	.234	-.014
	10-12A	.227	.238	-.011
	10-12B	.201	.197	.004
	12-14	.257	.238	.019
	14-16	.225	.215	.010
	16-18	.267	.231	.036
	18-20	.274	.259	.015

20/6/84

Depth	Ra_E	Rn	Deficit
0-1	.060	.010	.050
1-3	.149	.083	.066
3-5	.167	.146	.021
5-7	.184	.158	.026
7-9	.215	.191	.024
9-11A	.227	.184	.043
9-11B	.212	.173	.039
11-13	.230	.204	.026
13-15	.244	.168	.076
15-17	.256	.209	.047
17-19	.245	.222	.023

Chapter III

The Pore Water Chemistry of Mn, Fe, Cu, Ni, and Co at the Buzzards Bay site

Introduction

There have been few studies of the regeneration of trace metals at the surface of nearshore sediments. One reason for the small number of studies is the fact that there is evidence from oceanic trace metal distributions that several of the metals behave conservatively in coastal seawater. The evidence includes observations of roughly linear, negative metal:salinity correlations as continents are approached from the open ocean (Boyle, et al., 1981, 1984; Bruland & Franks, 1983), with the measured metal:salinity correlations predicting the concentrations of the metals in river end-members to within a factor of three to five (Bruland & Franks, 1983). In contrast to these results from oceanic metal distributions are studies of particle-reactive elements in nearshore areas showing that they may be rapidly scavenged from coastal seawater. ^{234}Th results, for example, show that this reactive element is removed with a time scale of a few days from the water column of Long Island Sound (Aller & Cochran, 1976). In addition, studies in a simulated

coastal environment, carried out in MERL tanks (Santschi et al., 1980), indicate that Fe is removed on a similar time scale to that of ^{234}Th and that inputs of Mn and Co, while scavenged somewhat more slowly, are still removed to the sediments in less than thirty days. Thus, since the metals included in this study are particle-reactive, and since productive, coastal seawater is particle-rich, if the residence time of seawater in the coastal environment is long enough, metals may be removed from seawater, reaching the sediment/water interface in particulate form. If the postulated removal of metals from the water column is indeed important, then the two sets of results -- those from oceanic distributions of metals suggesting that they behave conservatively in coastal seawater, and those from nearshore systems showing rapid removal of the metals -- would be reconciled if there is rapid recycling of metals to the water column as a result of early diagenesis in nearshore sediments.

There is some indirect evidence that coastal sediments return metals to the water column. Yeats et al (1979) demonstrated that fluxes from the sediments produced very large enrichments of Mn in particulate matter in near-bottom waters in the Gulf of St. Lawrence, and Murray and Gill (1978) showed a similar effect for Fe in Puget Sound, Washington. Heggie (1982) determined concentration gradients in the deep water of the Bering Sea continental shelf implying a sedimentary source of dissolved Cu.

Except for Mn, work involving direct measurement, either through pore water concentration measurements or flux chamber experiments, of

metal fluxes across the sediment/water interface in nearshore sediments has been rare. The sediment/seawater flux calculations resulting form several of the studies are summarized in Table III.1. In general, Mn fluxes are found to be significant to coastal Mn budgets. Fe fluxes are highly variable, being significant when the oxic layer at the sediment surface is very thin. Fluxes of Ni and Cu, depending strongly on the presence or absence of sulfide near the sediment/water interface, can vary greatly in magnitude and are not always directed out of the sediments (Aller, 1980b; Elderfield et al., 1981a,b; McCaffrey et al., 1980; Emerson et al., 1984). No study of benthic fluxes in coastal sediments has included Co.

The goal of this study of the pore water chemistry of Mn, Fe, Ni, Cu, and Co in coastal sediments has been to expand the data set describing fluxes of metals across the sediment/water interface. Dense sampling of sediment pore waters near the sediment/water interface, where rapid reactions require high sampling resolution, has been employed. Measurements of particle and solute transport rates, using nonreactive tracers, were made at the same site as the pore water study site. These measurements were made, in part, to eliminate ambiguities as to whether solutes are removed from pore water to overlying seawater or to solid phases near the interface. Samples were taken during different seasons so that a range of temperature, biological productivity, and redox conditions occurring in nearshore sediments underlying oxygenated bottom water could be sampled. Through detailed study of a single site, a surprising range of environmental conditions can be seen, and enough

Table III.1

Dissolved Fluxes of Transition Metals Across the Sediment/Water Interface from some Previous Studies in Nearshore Sediments

Study	Fluxes			
	Mn ($\mu mol/cm^2.sec$)	Fe	Cu ($nmol/cm^2.sec$)	Ni
Emerson et al, 1984 Quartermaster Harbor, Washington	$6x10^{-8}$	$2x10^{-7}$	$4.9x10^{-7}$	$1.2x10^{-7}$
Elderfield et al,1981 Narragansett Bay, R.I.	$.2-4x10^{-7}$	-	(small, variable direction)	
Trefry & Presley,19 Mississippi Delta	$4.8-5.4x10^{-7}$	$5.7x10^{-7}$	-	-
Aller (1980b) Long Island Sound	$1-2x10^{-6}$	$.1-7x10^{-8}$	-	-
Graham et al (1976) Narragansett Bay, R.I.	$4.2x10^{-7}$	-	-	-

constraints can be placed on the environmental system to elucidate the mechanisms determining fluxes of metals across the sediment/water interface.

Study Site

The general features of the Buzzards Bay study site were discussed in Chapter 2 and will only be briefly reviewed here. The site contains silty clay sediments, and lies under 15 m of water. The macrobenthos is a Nephtys-Nucula association, with abundance fairly typical of the fine-grained sediments in Buzzards Bay. Seasonal variability in environmental conditions is important, as temperature and productivity both have maxima in summer to early fall, and minima from December to April. The response of the macrobenthos to the variations in temperature and in the supply of organic matter to the sediment surface was discussed in chapter 2: both particle mixing by bioturbation and solute transport by irrigation reach their fastest rates during the summer; during the cold months, solute transport occurs by molecular diffusion, while particle transport occurs at a rate 2 to 8 times slower than during the summer.

The topic of this chapter is the chemistry of the upper few centimeters of the sediment column, and its response to seasonal

variations; some general observations of the sediment surface are pertinent. A light brown, oxidized layer of sediments is typically visible during the winter and spring. In 1983, this layer persisted through June; by the time the September core was taken, the sediment surface had darkened noticeably. In 1984, the sediment surface became dark much earlier, being darkish brown with black patches by the time the June core was taken (20/6/84). These variations in redox conditions near the sediment/water interface, coupled with variations in transport rates and mechanisms, are of primary importance in determining the fluxes of Mn, Fe, Cu, Ni, and Co across the sediment/water interface.

Methods

Cores were taken by SCUBA divers who placed a 20 cm diameter core liner into the sediments and sealed the core top; the cores were then lifted to a boat, where the bottoms were sealed. Both the physical appearance of the sediment/water interface and the chemical and radiochemical analyses of near-interface samples indicate that undisturbed cores were collected using this technique. Cores were returned to the laboratory where they were extruded, at 0.5 cm intervals to 4 cm and at 1 cm intervals below that, in a nitrogen-filled glove bag. Separate samples were taken from each section for nutrient and metal analyses. Samples were centrifuged for 15 min at 3500 rpm and

pressure-filtered through 0.4 μm Nuclepore polycarbonate filters in a nitrogen-filled glove bag. Temperature was not controlled during the sampling procedure, and artifacts related to temperature changes are possible: if they are present they should be minimal for summer and fall cores, but more important for winter cores, when the water/laboratory temperature difference was 15-20°C.

Samples were routinely taken for ΣCO_2 (or, for the 12/82 core, pH), alkalinity, phosphate, sulfide, and metal analyses. Nitrate and silicate analyses were done for the 12/82 core; SO_4 analyses were done for the 12/82 and 9/83 cores. To minimize degassing effects, ΣCO_2 samples were always taken first, filtered directly into a 1 cc syringe, and analyzed immediately by gas chromatography. Alkalinity samples were analyzed the day after sampling; phosphate samples were preserved in dilute H_2SO_4 and analyzed the next day; sulfide samples were preserved by precipitation as ZnS. Standard analytical methods were used for all analyses. The method of Gilboa-Garber (1971) was used for sulfide analyses, with a methylene blue solution calibrated by the method of Fonselius (1976) as a standard. Reactive phosphate, nitrate, and silicate were measured by colorimetric analysis (Strickland and Parsons, 1972). Alkalinity was measured by automated Gran titration. Sulfate was measured by precipitation of $PbSO_4$ and subsequent analysis of Pb by flame atomic absorption spectrophotometry. Precision was somewhat variable from core to core for ΣCO_2, and is estimated at 3.1±1.1%; precision for alkalinity was 0.6%, for sulfide 4.8%, for phosphate 3% (10% for samples at less than 10μM concentration), for sulfate 1.3%.

Metal Analyses

Rigorous cleaning procedures were followed for all materials used for sectioning cores and for filtering and storing trace metal samples. Plastic sectioning utensils were soaked in 2 N reagent grade HCl for several days prior to leaching in hot 0.5 N redistilled HCl for 12-24 hrs. Filter holders, syringe barrels, and sample storage vials were leached in hot 2 N reagent grade HCl for 12-24 hrs, in cold 2 N HNO_3 for several days, and finally in hot redistilled 0.5 N HCl for 12-24 hrs. 0.4μm Nuclepore polycarbonate filters, and gaskets for filter holders, were soaked in 1 N redistilled HCl for 24 hrs, then in clean (distilled, deionized, and redistilled) water for 24 hours prior to final rinsing with clean water. Rubber tips of syringe plungers were cleaned by rinsing with 6 N HCl and soaking in dilute redistilled HCl; however, since this procedure may not effectively leach the rubber tips, care was taken not to contact samples with them during filtering: pore water trace metal samples were poured from centrifuge tubes to syringe barrels, leaving a head space over the sample, before inserting the syringe plunger. 3-4 ml of sample were used to rinse filters prior to collecting samples.

All metal analyses were carried out by graphite furnace atomic absorption spectrometry using deuterium arc background correction, on a Perkin-Elmer model 4000 spectrophometer with HGA 400 furnace. Direct injection of pore water samples was employed; samples were calibrated against spiked seawater at the same dilutions and with the same matrix

modification as were used for samples. Fe and Mn were usually run at 1:201 and 1:61 dilutions, with the most concentrated Fe samples run at greater dilution; no matrix modification was necessary. All of the Cu, Ni, and Co samples and a few Mn samples were analyzed after being made 1.8% in ascorbic acid (Hydes, 1980). Detection limits, estimated as twice the variability in the absorbance of an unspiked sample of the seawater used for calibration (this measure is the sum of the variability in the analytical blank and the variability in the background absorbance), were approximately 0.1μM for Mn (except about 10nM for 1:5 dilutions of pore water), 0.8μM for Fe, 3nM for Cu, 5nM for Co, and 7nM for Ni. Reproducibility was estimated by running replicates of the same filtered sample and by running separately filtered aliquots of samples taken from the same sediment section. For Mn, reproducibility by both estimates was about 5%, while for Fe it was about 7%. Occasional Fe samples showed greater variabilty: in most cases, these samples were found to contain solids, and it is likely that the contaminant Fe was leached from sediment grains, which had leaked around filters, at the low pH (~2) at which the samples were stored. Reproducibility for Cu was about 11% throughout the range of concentrations measured; for Ni, the difference between replicates ranged from 1.5 to 10 nM, and averaged 5.2nM; for Co, the range was 1.2-4.9nM and averaged 3.2nM. It is important to note that, using a direct injection of seawater technique, there is uncertainty in absolute concentrations measured due to possibly uncorrected background absorbance. To calculate the concentrations reported here, the assumption was made that 0 absorbance = 0 concentration. A limit on the error due to

this assumption can be inferred from the lowest concentrations calculated in this way: for Cu, the lowest three concentrations calculated were 1.0-1.4nM, for Ni, 2.7-4.8nM, and for Co, 1.5-2.6nM; these values are all lower than the reported detection limits. Thus, although direct injection analysis of Cu, Ni, and Co is not sensitive enough for seawater analysis, it is sufficient to demonstrate the major features of the pore water profiles presented here, with concentrations ranging from the detection limits up to 40nM for Ni, 20nM for Cu, and 30nM for Co (Appendix III.2 and Figure III.1).

Results and Discussion

To characterize a sediment system's ability to recycle metals to the water column, it is necessary to: (1) characterize the mechanisms producing dissolved metals, (2) determine the phases limiting the dissolved metal concentrations and the conditions under which saturation is reached, (3) determine the spatial relationships in the sediment column between dissolved metal production and consumption, and (4) determine the rates at which the dissolved metals are transported.

A total of seven cores were taken from 12/82 to 6/84 to study the first three of the four problems stated. Of these, six will be discussed in detail. The seventh, the 12/83 core, was taken after a period of several large storms during which its pore water constituents

Figure III.1

Pore Water Analysis Results

Figures III.1A-G show the results of pore water analyses carried out on cores from the Buzzards Bay study site. In the pore water metal concentration plots and in the pore water H_2S plots, samples in which concentrations were below detection limits are shown by triangles.

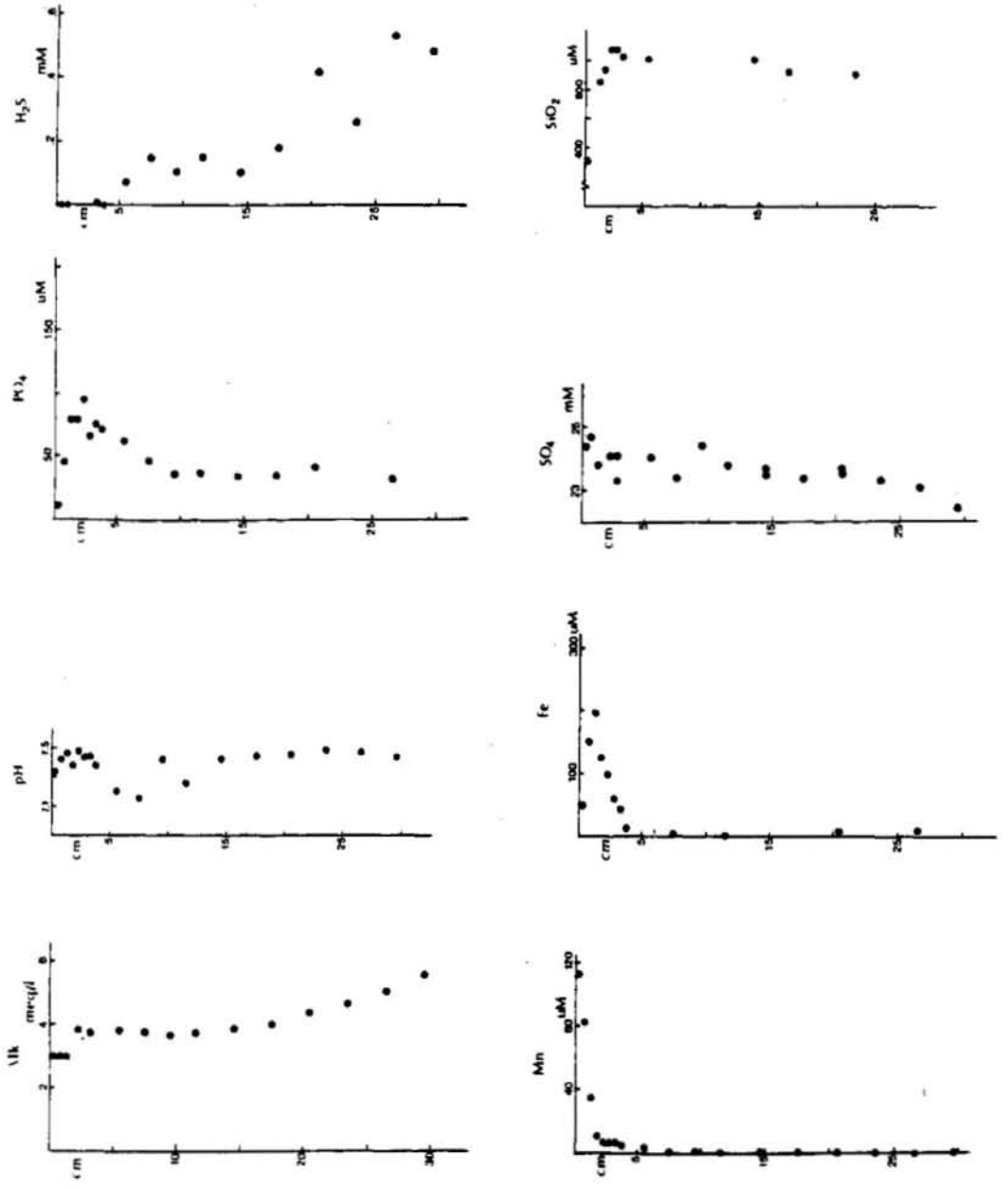

Figure III.1A: 15/12/82

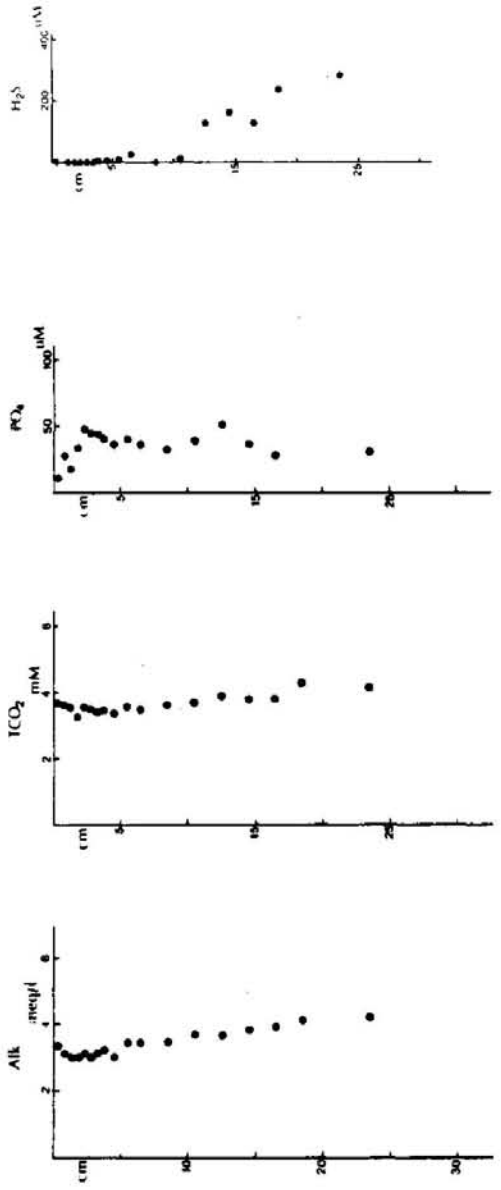

Figure III.1B: 31/3/83

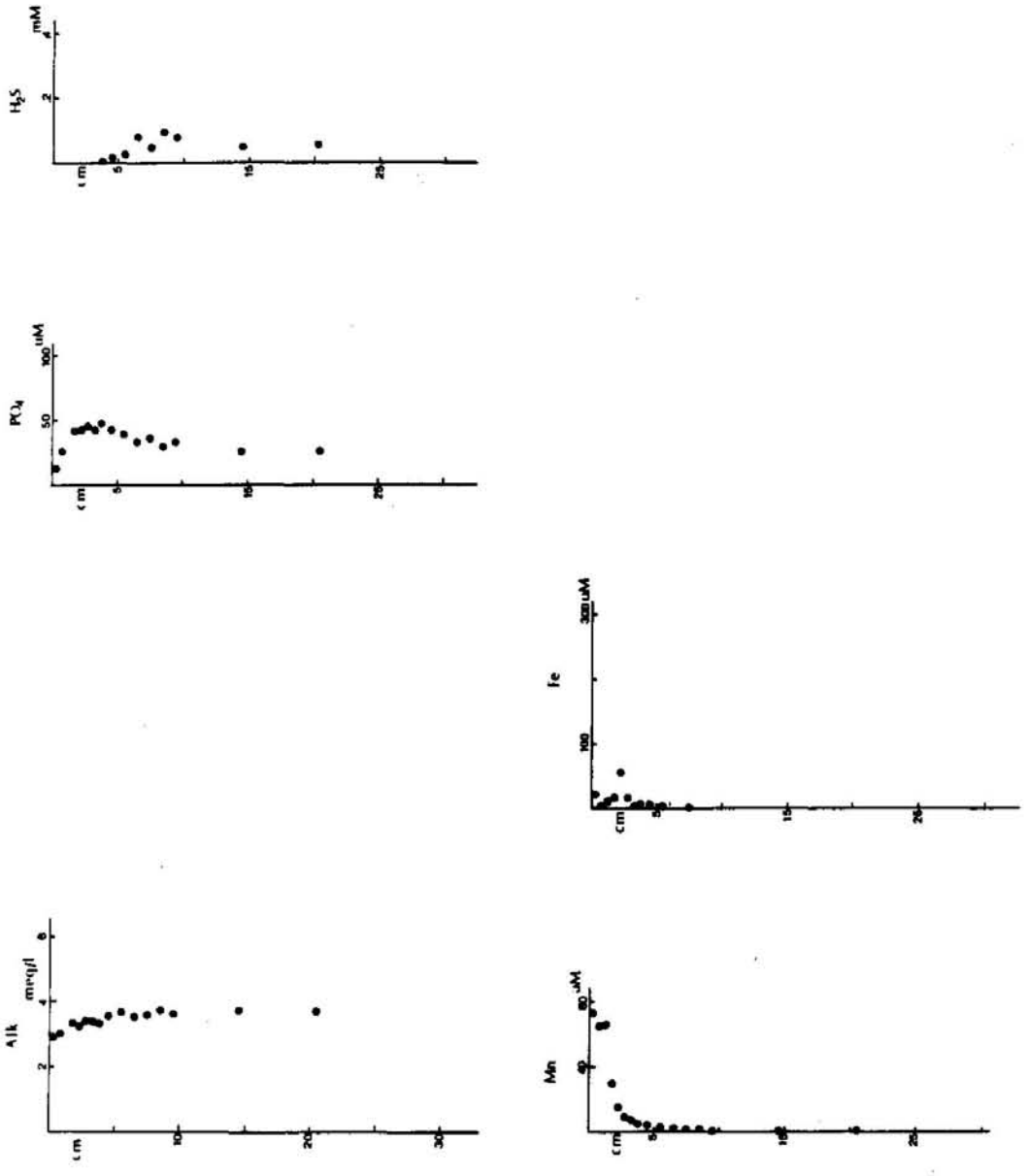

Figure III.1C: 8/6/83

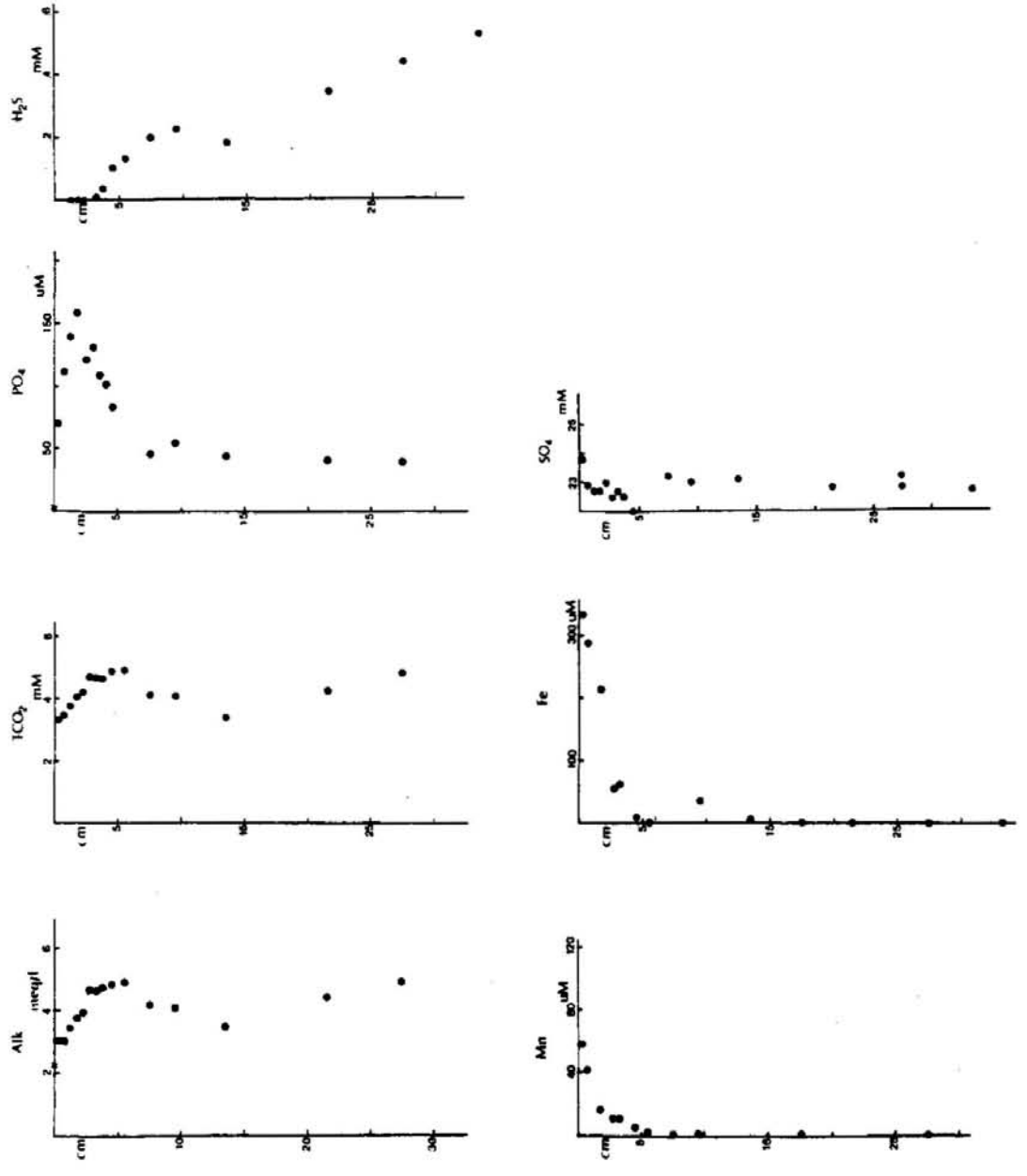

Figure III.1D: 7/9/83

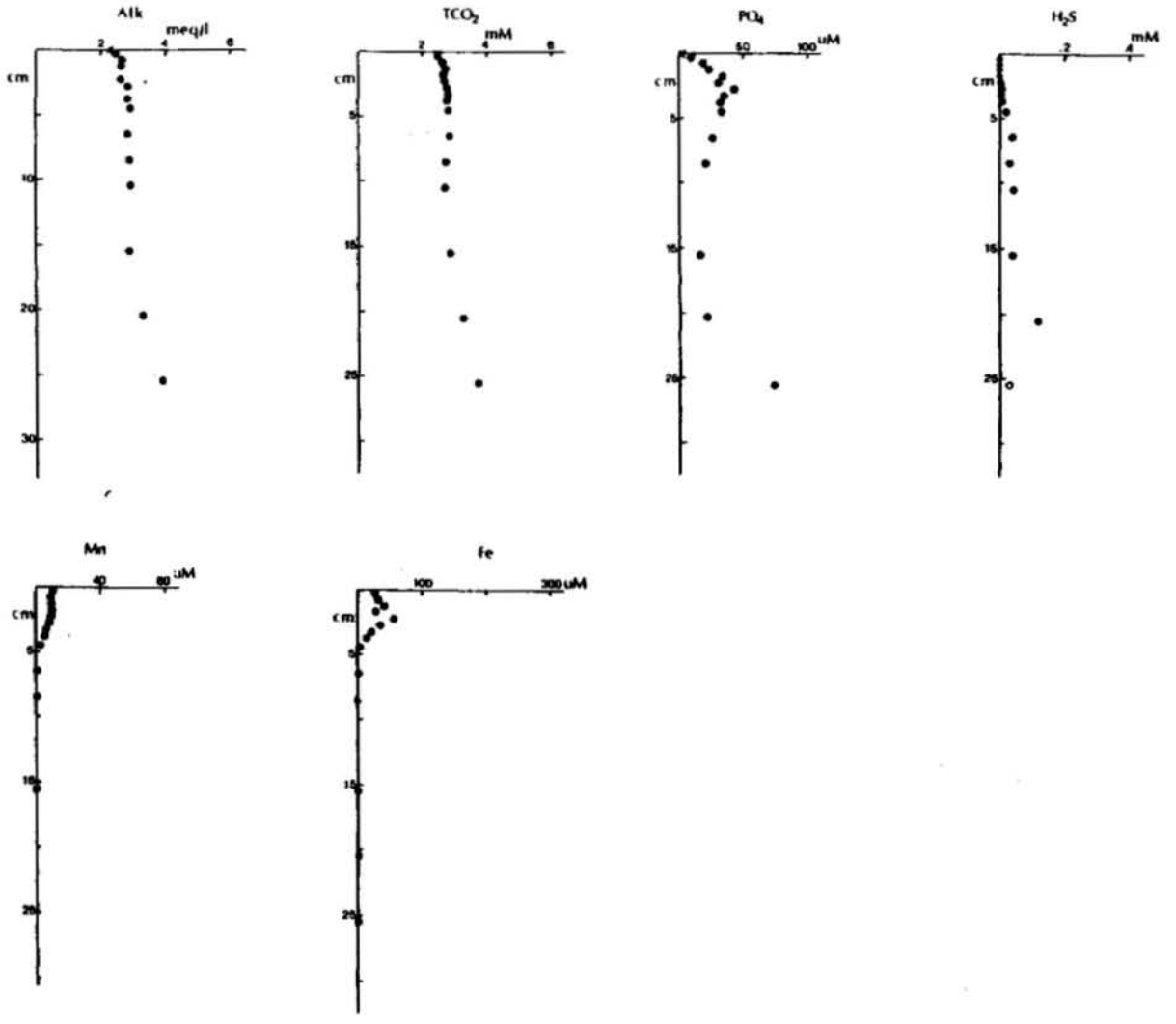

Figure III.1E: 16/12/83

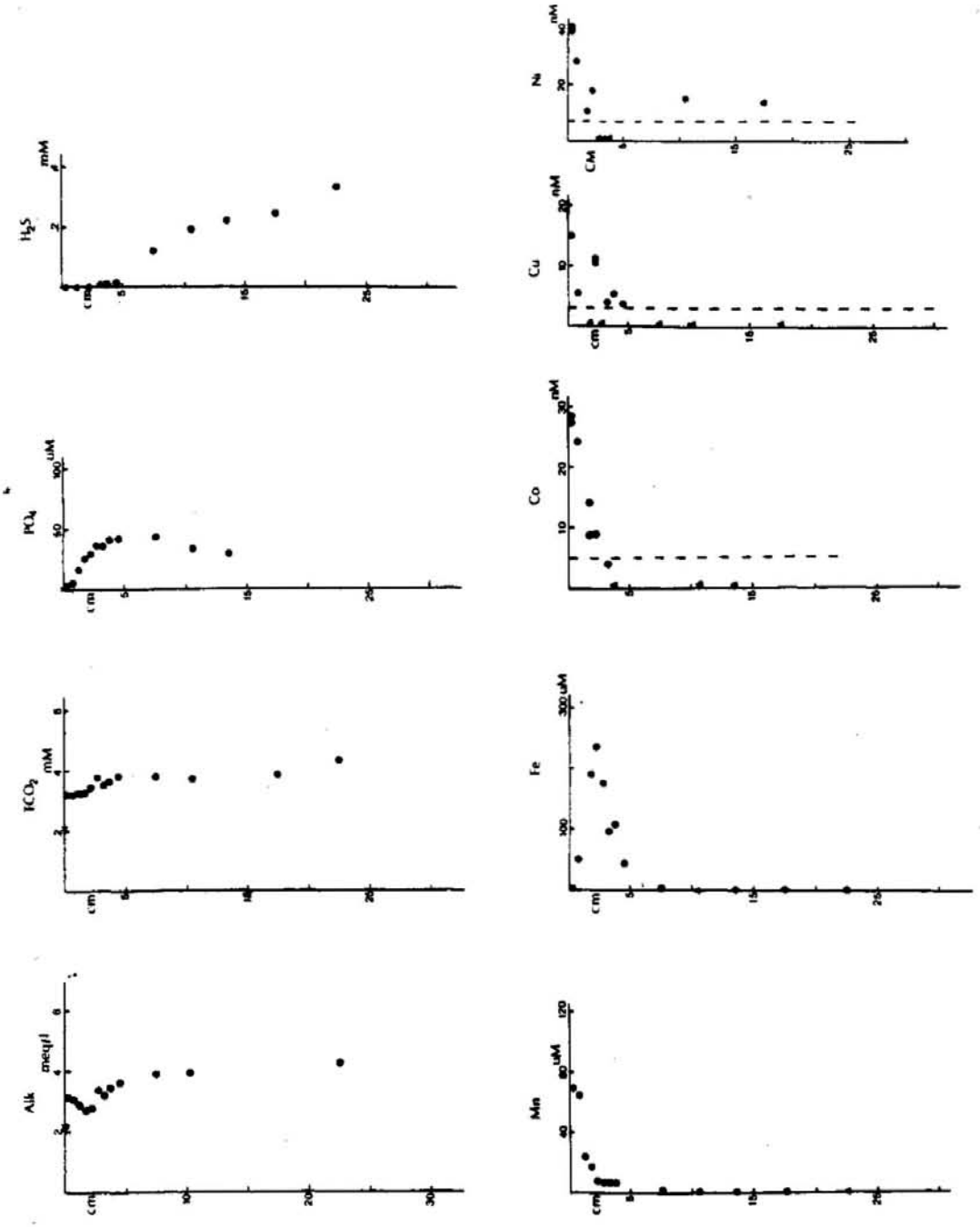

Figure III.1F: 26/3/84

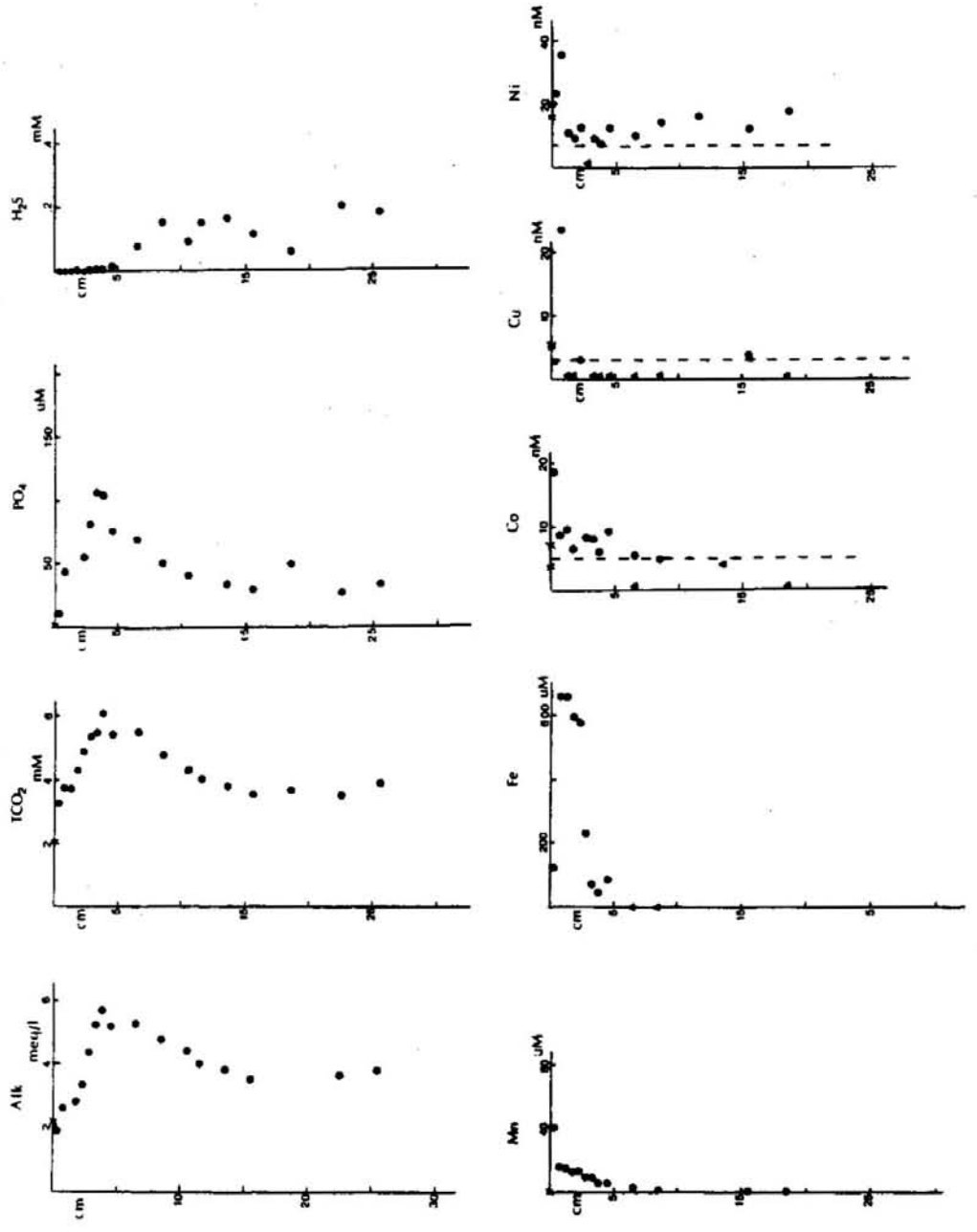

Figure III.1G: 20/6/84

were almost certaintly depleted by irrigation. Because the accompanying $^{222}Rn/^{226}Ra$ measurements did not show Rn depletion in the sediments, the irrigating event must have occurred about two weeks before sampling. Since the water temperature and supply of organic matter are low in December, the system was approaching a new steady state slowly. Because many of the arguments presented in this chapter depend on a steady-state approximation, this core will not be discussed further. Of the other six cores, two were taken in March, two in June, one in September, and one in December. Ni, Cu, and Co were measured in the 3/84 and 6/84 cores; Fe and Mn were measured in all but the 3/83 core; and sulfide, phosphate, and two carbonate system parameters were measured for all but the 6/83 core (for which ΣCO_2 is missing). Sulfate was measured in the 12/82 and 9/83 cores. Results are presented in Appendix III.1 and in Figures III.1A-G.

A Chemical Model for Metal Cycling between Dissolved and Solid Phases in Nearshore Sediments

This section presents a summary of the chemical processes driving metal cycling at the Buzzards Bay study site. These processes are clearly dependent on interactions of metal cycles with the cycles of organic matter and sulfur. It is the involvement of metals in the oxidation of organic matter, both directly (for Mn and Fe) and indirectly (for Cu, Ni, and Co), that leads to dissolution of particulate metals; and it is the buildup of

the products of the oxidation of organic matter by sulfate that limits the solubility of the metals in reducing sediments. In the model, the sediments consist of two layers. The first is a thin upper layer dominated by the effects of organic matter oxidation by O_2, NO_3, and Mn(IV). The second layer is dominated by the effects of sulfate reduction.

The upper layer of the sediment column, extending 0.5-1.5 cm below the sediment/water interface, is defined by the region of net production of dissolved Mn. The layer is characterized by evidence for the production of dissolved Mn, Ni, Cu, and Co, by the absence of dissolved H_2S, and by relatively low concentrations of PO_4. That dissolution of a fraction of the metal content of sedimenting particles occurs in this layer is expected from the results of work on the early diagenesis of transition metals in deep-sea sediments. Cu is regenerated primarily during oxic diagenesis in deep-sea sediments (Klinkhammer et al., 1982; Callender & Bowser, 1980; Sawlan & Murray, 1983), while Mn, Co, and Ni are returned to solution during the oxidation of organic matter by Mn(IV) (Klinkhammer, 1980; Sawlan & Murray, 1983; Heggie & Lewis, 1984). Although zones in which organic matter is oxidized by O_2, NO_3, or Mn(IV) are not resolved by 0.5 cm sampling intervals at the Buzzards Bay site, the important point is that all three reactions occur in the upper 0.5-1.5 cm, producing maxima in dissolved metal concentrations very near the sediment/water interface.

Although it is unlikely that the dissolution of the tests of organisms contributes significantly to pore water trace metal concentrations, a significant characteristic of this upper layer of the

sediment column is that it is a site of extensive dissolution of $CaCO_3$ and SiO_2. $CaCO_3$ dissolution is indicated by enrichments over bottom water in pore water Ca^{2+} concentrations near the surface of the sediments (A. McNichol, pers. comm.). In addition, the upper 3 cm of the sediment column is consistently undersaturated with respect to $CaCO_3$ (Figure III.2). One dissolved SiO_2 profile, taken in 12/82, indicates very rapid dissolution of siliceous tests near the sediment/water interface (Figure III.1A).

The thickness of this layer of net dissolved metal production is limited by the onset of sulfate reduction, and can be expected to show a seasonal trend: the rate of microbial activity shows a distinct temperature dependence, with minimum activity at the lowest temperature (Aller, 1980a). Therefore, the rate of organic matter oxidation increases as temperature increases during the summer (and also as the supply of organic matter increases: Roman & Tenore, 1978), and sulfate reduction becomes important nearer the sediment/water interface from late spring through early fall. Sulfate reduction influences the cycling of Mn, Ni, Cu, and Co through the production of H_2S, PO_4, ΣCO_2, and alkalinity. The increase in PO_4 concentration with sulfate reduction may limit the solubility of Mn near the sediment/water interface through the formation of a Mn-containing phosphate mineral; solubility of the other metals is most likely limited by the presence of sulfide. The absence of detectable sulfide (>3μM) in the upper 3 cm of all cores except 6/84 and 9/83 suggests that scavenging by solid sulfides may be the mechanism for removal from solution of the sulfide-forming metals,

Figure III.2

Calcite Saturation

Degree of saturation with respect to calcite at the Buzzards Bay site. The horizontal axis is Ω, the ratio of the ion concentration product (icp) to the equilibrium ion concentration product (K). Ω = 1.0 is calcite equilibrium determined from the constant of Ingle (1975). Ω = .91 coincides with calcite saturation according to the seawater equilibrium constant determined by Mucci (1983). The data shown are from the March, '83, September, '83, March, '84, and June, '84, cores. The circles are the average Ω found at each depth; the bars represent the range of Ω in these cores at each depth. Open circles are shown for depths at which only one Ω value was calculated. The line from 12-30cm is the depth-averaged Ω in that region, 0.8±0.2.

Figure III.2

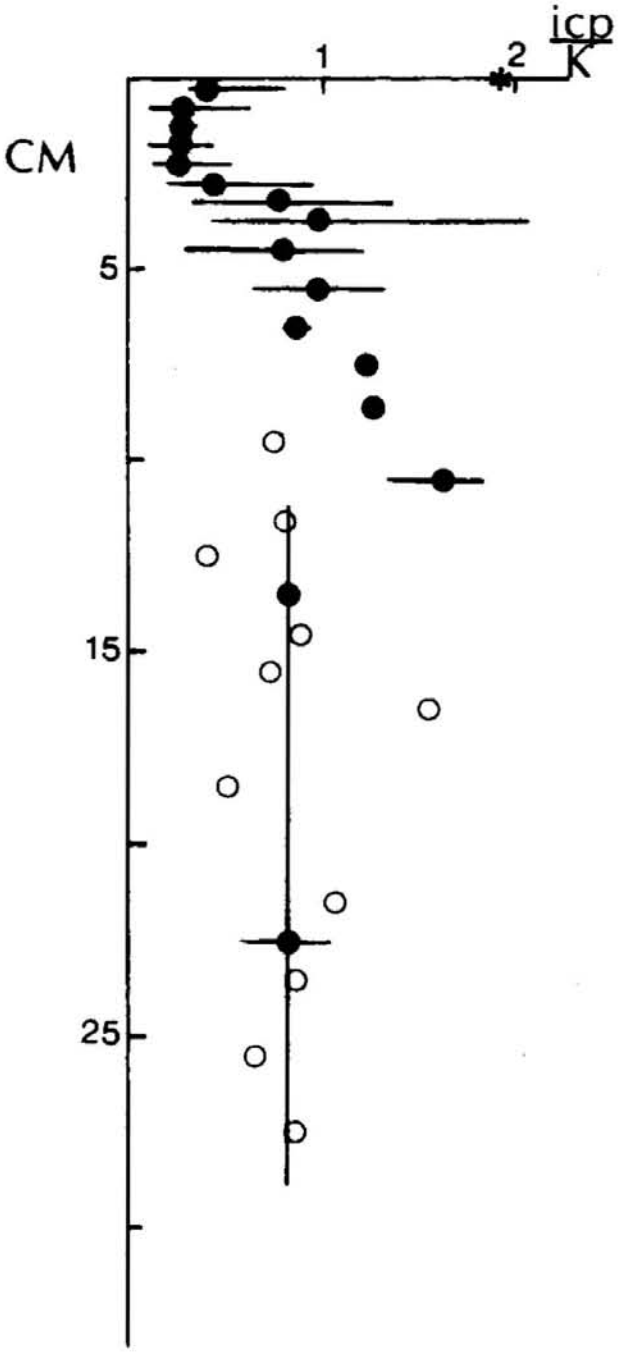

Cu, Ni, and Co. Solid sulfides are likely to be present near the sediment/water interface. Since Fe(III) is used before sulfate for organic matter oxidation, reduced iron must be present at the onset of sulfate reduction, and dissolved H_2S may be quantitatively removed by reaction with ferrous iron to form iron monosulfides and pyrite in the upper 3 cm of the sediment column. Pyrite and FeS have been found to occur, even at the sediment/water interface, in nearshore sediments (Berner, 1970; Goldhber et al., 1977; Aller, 1980a,b; Giblin & Howarth, 1984). Studies of the mechanisms of pyrite formation have shown that it can be rapid under conditions extant near the surface of nearshore sediments (Berner, 1970; Rickard, 1975).

The formation of iron sulfides near the sediment/water interface makes the cycling of iron between particulate and dissolved phases complex. When pyrite and FeS form near the interface, they can be mixed throughout the bioturbated layer (0-2.5cm), and may come into contact with O_2. Then, FeS and pyrite can be oxidized to SO_4, with release of Fe^{2+} to solution; this Fe^{2+} can either remain in solution or be oxidized to insoluble Fe(III) (Aller, 1980b; Giblin & Howarth, 1984). Thus, the iron cycle in nearshore sediments includes the reduction of ferric iron during organic matter oxidation to form soluble ferrous iron; reaction of ferrous iron with sulfur to form insoluble sulfides; mixing of the sulfides in the bioturbated layer, reaction of a fraction of them with O_2, and further release of Fe into solution. In reducing sediments, dissolved iron concentrations are limited by the solubility of iron phosphates or carbonates in the absence of sulfide (Martens et al.,

1978; Suess, 1979) and by sulfides when dissolved H_2S is present (Aller, 1980a,b).

The primary feature of the chemical model proposed here to explain the cycling of metals in nearshore sediments is the importance of reactions between the metals, organic matter, and sulfur. Dissolved Mn, Ni, Cu, and Co are produced during the oxidation of organic matter near the sediment/water interface. A fraction of the dissolved metals returns to overlying seawater; the rest is removed from solution by reaction with the PO_4, CO_2, or H_2S produced during the oxidation of organic matter by sulfate. Of the reduced metals removed to solids in the upper 2.5 cm of the sediment column, a fraction may be returned to the surface layer of the sediments by biologically driven particle mixing. The Fe cycle is complex, with dissolved Fe production both from Fe(III) and reduced iron minerals. The concentration of dissolved iron in near-surface sediments is controlled by oxidation in the presence of O_2 and by equilibrium with phosphate minerals in its absence. Ultimately, iron is buried as ferrous sulfides and in clay mineral lattices.

Pore Water Chemistry of Iron

Iron is a major component of nearshore sediments (the sediments from the Buzzards Bay site are approximately 2.8% Fe by weight), and its direct involvment with the organic matter and sulfur cycles causes rapid dissolution of particulate iron at most times of the year. Nonetheless, iron fluxes to overlying water vary over a large range during the seasonal cycle (eg Aller, 1980b). This fact is due primarily to the rapid oxidation of Fe(II) to Fe(III) in the presence of oxygen. Because of this reaction, the occurrence of significant fluxes to overlying water is limited to times when oxygen is consumed rapidly at the sediment/water interface by organic matter oxidation and when there are pore water iron gradients steep enough to produce fluxes of dissolved iron to the interface that are large relative to the Fe(II) oxidation rate.

The features which appear to have the greatest influence on dissolved iron profiles are (1) the combination of Fe(III) reduction and oxidation of sulfur in FeS and FeS_2 to produce dissolved Fe, (2) the occurrence of removal processes between the sediment/water interface and the dissolved iron maximum, and (3) rapid removal of dissolved iron below its maximum. The net result of these processes at the Buzzards Bay site is an iron maximum whose magnitude varies dramatically, from 50μM in 6/83 to over 600μM in 6/84, with steep gradients on either side of the maximum. It appears likely that O_2 diffusing into the sediments across the sediment/water interface removes dissolved Fe above its maximum: the

effect is evident in all cores except 9/83 and 12/82. There is a systematic variation in the depth of Fe removal by this process. It is deepest in the 6/83 aand 3/84 cores (when a light brown oxic layer was clearly visible at the sediment surface during coring), shallower in the 6/84 core, and not evident (probably because it is not resolved by the 0.5 cm sampling interval) in the 12/82 and 9/83 cores. Below its maximum, dissolved Fe is rapidly removed by the precipitation of ferrous minerals. To explain the observed iron profiles and use them to find the mechanisms producing iron fluxes across the sediment/water interface, it is necessary to explain the variability in the magnitude of the dissolved iron maximum and the variability in the depth below the interface at which the maximum is reached.

Control of dissolved iron concentrations by equilibrium with ferrous minerals is demonstrably significant in these sediments. The sequence of phases controlling the maximum dissolved iron concentration has been documented before (Aller, 1980a,b; Elderfield et al., 1981a; Martens et al., 1978): in the absence of oxygen, vivianite ($Fe_3(PO_4)_2$) saturation limits the dissolved iron concentration until dissolved H_2S is present; then, dissolved iron appears to be in equilibrium with an iron monosulfide phase. The occurrence of this sequence at the Buzzards Bay site is illustrated in Figure III.3. The figure shows the negative log of the ion concentration products, $(Fe^{2+})^3(PO_4^{3-})^2$, $(Fe^{2+})(HS^-)/a_H$, and $(Fe^{2+})(CO_3^{2-})$, relative to their respective equilibrium values. Saturation with respect to vivianite was reached in all cores except the rapidly irrigated 6/83

Figure III.3

Saturation of Pore Waters with Respect to Reduced Fe phases

The phases considered are vivianite ($Fe_3(PO_4)_2$), siderite ($FeCO_3$), and the sulfides, greigite, mackinawite, and amorphous FeS. Constants for siderite and the sulfides are from Jacobs (1984). The vivianite constant is from Aller (1980a). Activity coefficients used to correct thermodynamic constants to seawater ionic strength are:

$\gamma(Fe^{2+})$ = .23 (Davison, 1980)

$\gamma(HS^-)$ = .45 (Davison, 1980)

$\gamma(PO_4^{3-}) = 10^{-4.4}$ (Martens, et al., 1978)

$\gamma(CO_3^{2-})$ = .021 (from the Davies equation: Stumm & Morgan, 1970; and 9 % free: Garrels & Thompson, 1960).

The dashed line in each figure represents saturation with respect to the solid phase considered. A special symbol, X, is used for the $Fe_3(PO_4)_2$ product in June, '83; ΣCO_2 was not measured for this core, and the calculations are based on estimated pH values.

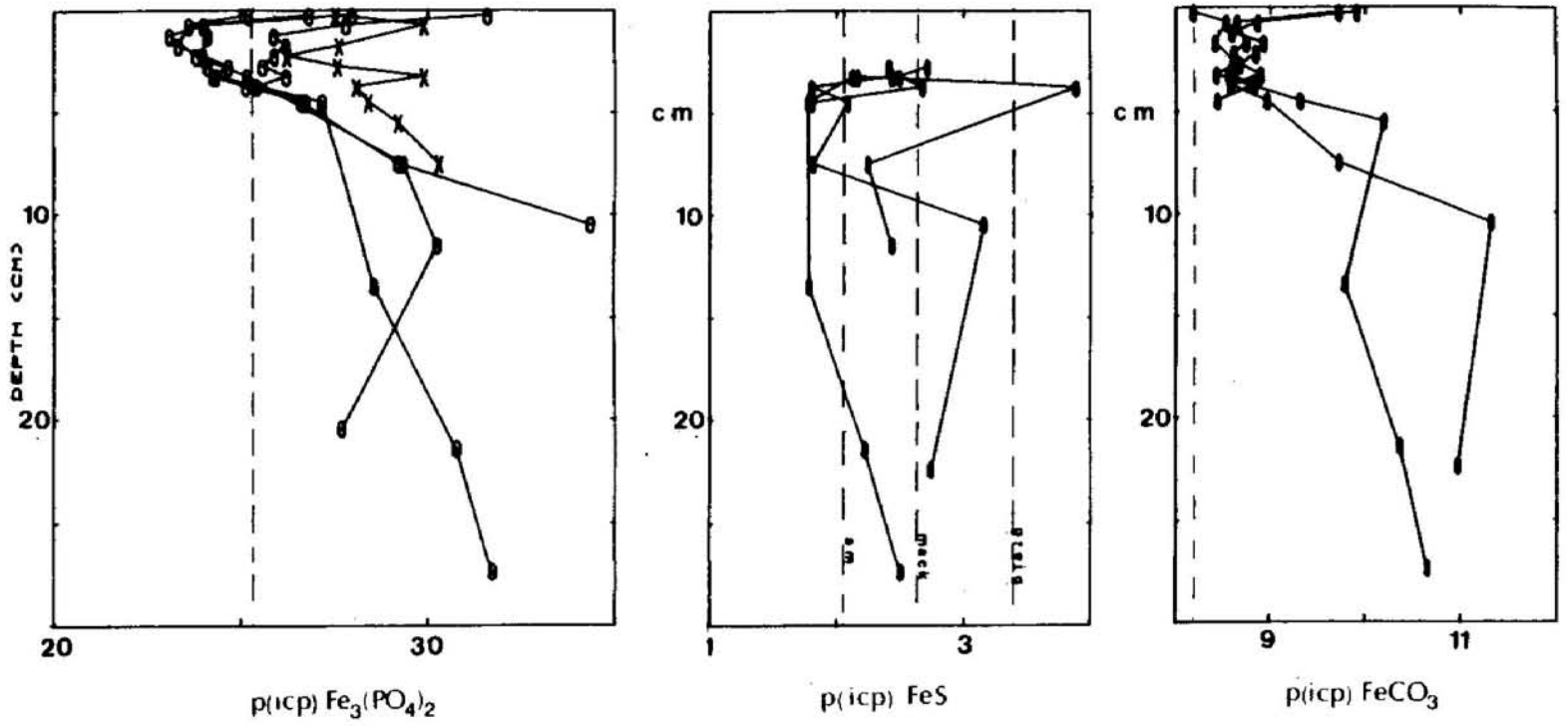
DEPTH (CM)
10
20
20
30
p(icp) $Fe_3(PO_4)_2$
cm
10
20
1
3
p(icp) FeS
cm
10
20
9
11
p(icp) $FeCO_3$

core. In cores having elevated phosphate and dissolved iron concentrations, considerable apparent supersaturation occurred. This may reflect error in the calculations, but it may also reflect a relationship between the rates of dissolved Fe and PO_4 production and vivianite precipitation or the association of Fe^{2+} with dissolved or colloidal organic matter. An association between iron and organic matter in nearshore sediments has been demonstrated by Krom & Sholkovitz (1977) and by Elderfield (1981).

Figure III.3 shows that, as soon as detectable sulfide is present in pore waters, dissolved Fe is at saturation with respect to an iron monosulfide phase. At that point in the sediment column, the pore waters become undersaturated with respect to vivianite. The sequence of reactions is shown in more detail for the 6/84 core in Figure III.4. Fe and PO_4 are clearly removed from solution in the 1-2.5 cm region, where pore waters are supersaturated with repect to vivianite. When, below 3.5 cm, dissolved sulfide levels begin to increase, Fe is removed preferentially to sulfide phases, and the pore waters become undersaturated with respect to vivianite.

Thus, equilibrium with respect to solid phases clearly exerts some control on the maximum dissolved iron concentrations observed at the study site. However, it cannot be the only control: although similar degrees of saturation with respect to vivianite are reached in several cores, at similar depths, there is considerable variation in both the magnitude of the dissolved iron maximum (200-600μM) and in its position relative to the sediment/water interface (0-0.5 cm to 2-2.5 cm).

Figure III.4

Iron-Phosphate-Sulfide Correlations

Dissolved Fe, phosphate, and sulfide concentrations in the pore waters, 6/84 core. Also shown is the ion concentration product for vivianite, calculated from the Fe and PO_4 data. Saturation with respect to vivianite is indicated by the dashed line.

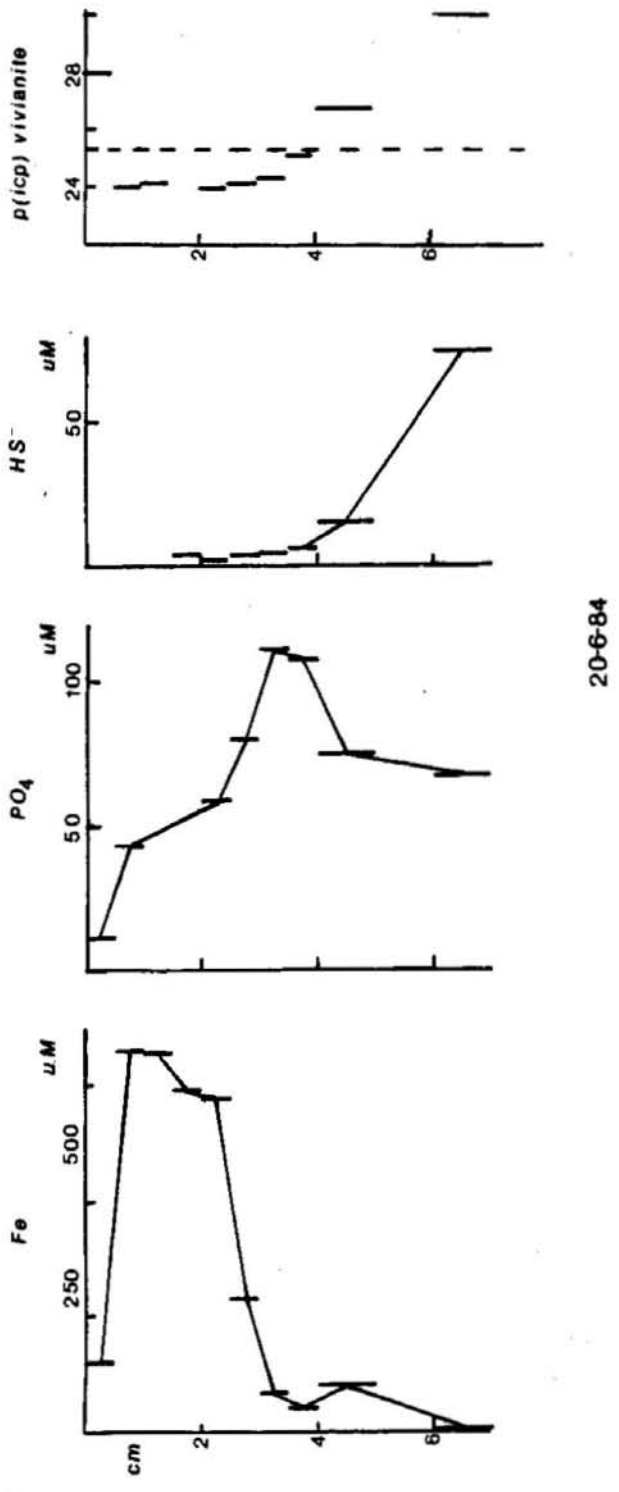
p(icp) vivianite
28
24
2
4
6
HS⁻
uM
50
PO4
uM
100
50
Fe
uM
500
250
cm
2
4
6

20-6-84

The other control on the position and magnitude of the dissolved iron maximum is the production rate of dissolved iron from particulate sources. One mode of production is the reduction of Fe(III) during microbial degradation of organic matter. Its rate and position in the sediment column are closely related to the rate of benthic metabolic activity, which varies with water temperature and the supply of organic matter; the seasonal variation of both parameters leads to rapid metabolism during the summer and early fall, and to slower metabolism during winter and spring (Goldhaber et al., 1977; Aller, 1977; Elderfield et al., 1981a). Fe (III) reduction occurs after Mn(IV) reduction and before SO_4 reduction in the sequence of microbially catalyzed organic matter oxidation reactions (Froelich et al. 1979). Thus, the observation from SO_4 profiles of SO_4 consumption at 1.5 cm in 12/82 and at 0.5-1 cm in 9/83 (Figure III.1) agrees with observations of Fe maxima at 1-1.5 cm in 12/82 and at 0-0.5 cm in 9/83. In addition, the inference from ΣCO_2, alkalinity, and PO_4 profiles of rapid sulfate reduction in the upper 3 cm agrees with the observation of a large Fe maximum at 0.5-1 cm in 6/84. A similar inference that SO_4 reduction is relatively unimportant in the upper 3 cm in 6/83 and 3/84 agrees with the observation of the Fe maximum at 2-2.5 cm in these cores. Data concerning the magnitudes and the positions relative to the sediment/water interface of observed dissolved iron maxima are summarized in Table III.2.

If dissolved Fe production depended only on the microbially catalyzed reduction of Fe(III), it would be expected to show a seasonal trend similar to temperature and productivity trends. However, it does

Table III.2

Dissolved Fe maxima and Fluxes From Sediments to Overlying Seawater

Both the diffusive flux across the sediment/water interface (J_o) and the nonlocal exchange flux (I_t) have been calculated. J_o is calculated by:

$$J_o = - \phi \cdot D_{sed} (\Delta C / \Delta x)_{x=0}$$

$$\phi = 0.9$$

$$D_{sed} = \phi^2 \cdot D_{molec}$$

The nonlocal exchange flux is calculated over the upper 10 cm of the sediment column,

$$I = -\int_0^{10} \phi \cdot \alpha (C - C_w) dx$$

C_w = overlying water conc. = 0

Date	conc at max μM	position of max cm	conc 0-0.5 cm μM	J0 10^{-7} μmol/sec	I	I/J0
12/82	196	1-1.5	49.0	5.3	0	0
6/83	55	2-2.5	21.4	3.2	2.0	.63
9/83	332	0-0.5	332	48	8.2	.17
3/84	237	2-2.5	3.5	0.38	0	0
6/84	661	0.5-1	120	18	4.6	.19

not: the most striking example is the 3/84 core, which, having relatively small buildup of the products of organic matter oxidation despite the absence of pore water flushing by irrigation, shows evidence of slow rates of organic matter oxidation in its pore water alkalinity, ΣCO_2, and PO_4 profiles, but has a large dissolved Fe maximum and evidence of rapid dissolved Fe production. The other source of dissolved Fe is its release to solution during the oxidation of sulfur in FeS and pyrite. Evidence for the occurrence of sulfur oxidation in nearshore sediments has been found by other workers: it has been invoked to explain low rates of accretion of sulfide minerals relative to rates of sulfate reduction (Howarth, 1984; Goldhaber et al., 1977; Aller, 1980a); to explain the existence of FeS and pyrite sulfur gradients despite particle mixing in the bioturbated layer of sediments (Aller, 1980a); and to explain correlations between dissolved Fe and alkalinity concentrations in sediment pore waters (Giblin & Howarth, 1984; Aller, 1980b). Oxidation of FeS/pyrite sulfur requires oxygen. Thus, its occurrence is limited to zones near the sediment/water interface where bioturbation can bring reduced sulfur into contact with O_2 diffusing across the interface and to isolated regions below the zone of onset of sulfate reduction to which irrigation supplies O_2. It appears unlikely that sulfur oxidation could change the position of the dissolved iron maximum sufficiently to alter the flux of dissolved iron across the interface, since the extent of the maximum is limited from above by Fe oxidation (the end product of FeS/pyrite oxidation can be Fe(III) as well as Fe(II)), and from below by the presence of dissolved H_2S. However, it may have a significant

effect on the magnitude of the Fe maximum, particularly in winter and spring.

Evidence for the occurrence of dissolved iron production through sulfur oxidation has been sought through alkalinity: dissolved iron correlations. Dissolved iron production through sulfur oxidation has a distinctive pore water signature, in that it consumes alkalinity while producing dissolved iron (Giblin & Howarth, 1984; Aller, 1980b). The oxidation of pyrite to Fe^{2+} + SO_4^{2-} consumes two equivalents of alkalinity per mole of pyrite oxidized; if Fe^{2+} is also oxidized, to Fe(III), four equivalents of alkalinity are consumed per mole of pyrite oxidized. In contrast, the production of dissolved iron by microbially catalyzed Fe(III) reduction produces alkalinity (Bender & Heggie, 1984).

Inspection of dissolved iron and alkalinity profiles from the study site indicates that there is a rough negative correlation between their curvatures. Curvature of pore water profiles is related to solute production and consumption in a system in which diffusion and reaction are dominant processes by

$$D \cdot d^2C/dx^2 = -P$$

(P= production, in amt./cm^3.sec; D= diffusion coefficient). Negative curvature ($d^2C/dx^2<0$) implies production ($P>0$), positive curvature consumption. Results of calculations of production of dissolved iron and alkalinity using finite difference approximations to second derivatives are shown in Figure III.5 for the 3/84 and 6/84 cores. Obviously, the calculations are crude, since analytical errors (7% for Fe, 0.6% for Alk, 3% for CO_2) are

Figure III.5

Dissolved Fe, Alkalinity, and ΣCO2 Production

Apparent dissolved Fe, Alk, and ΣCO_2 production for the 3/84 and 6/84 cores. Negative values indicate apparent consumption.
The depth ranges over which the second derivatives were averaged are indicated by the vertical bars in the figure; the errors propagated through the calculation are indicated by the error bars shown. For alkalinity, the error is no greater than the size of the symbol used.

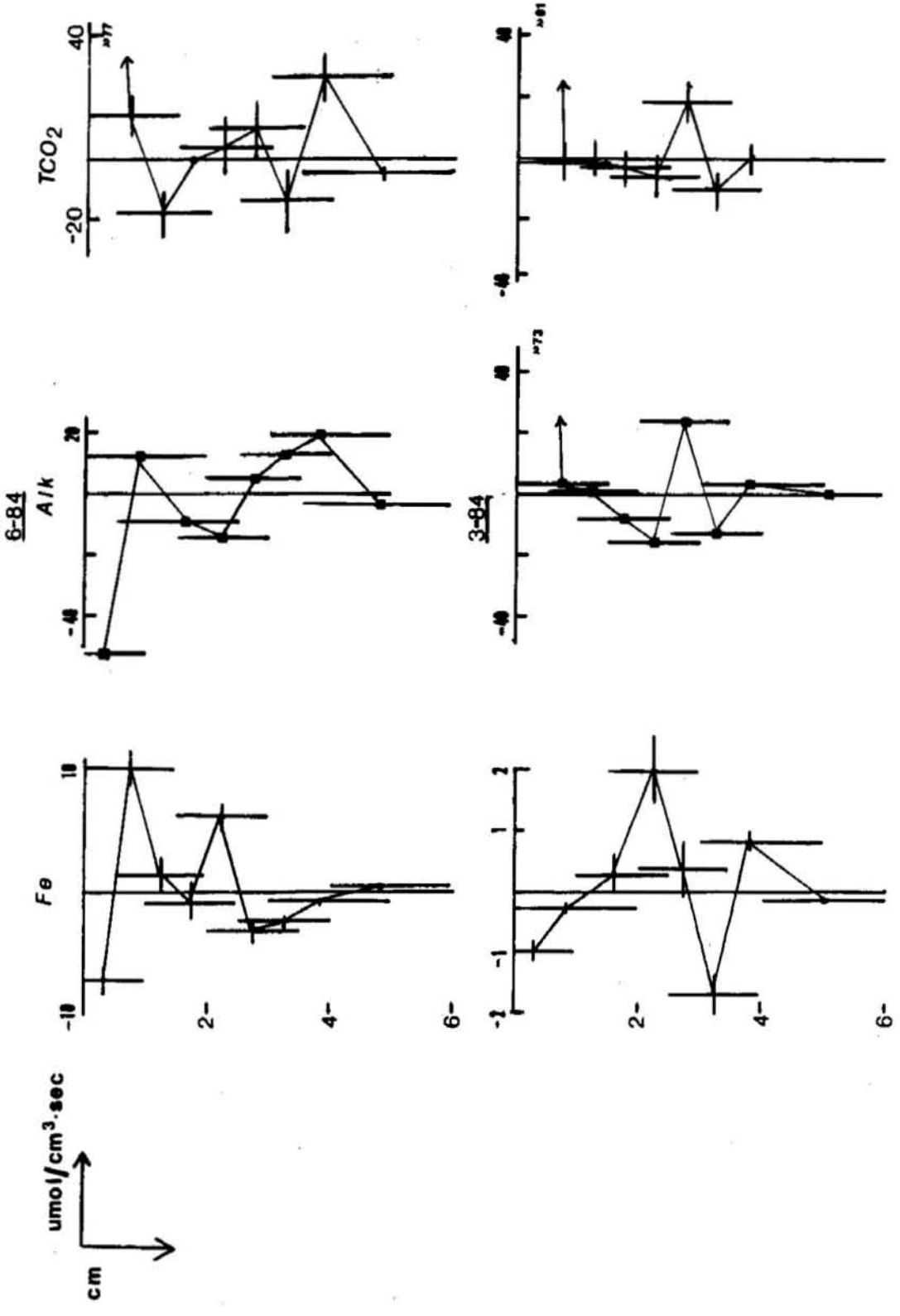
6-84
3-84
TCO_2
Alk
Fe
40
-20
2300
2273
2281
20
-40
18
-18
2
1
-1
-2
2-
4-
6-
umol/cm³·sec
cm

compounded during the calculation and since depth-averaging over three sample intervals is required to calculate d^2C/dx^2 in each sample interval. The depth ranges over which the second derivatives were averaged are indicated by the vertical lines in Figure III.5, and the errors propagated through the calculation are indicated by the error bars shown. Despite the limitations of the calculation, results consistent with FeS/pyrite oxidation were obtained from the 6/84 core. Black patches, presumably due to the presence of iron sulfides, were clearly present in the upper 2 cm of the core, and were also visible at the sediment/water interface when the core was taken. The very large alkalinity consumption calculated at the sediment/water interface ($52.7\pm1.6 \times 10^{-6}$ $\mu eq/cm^3.sec$) indicates significant sulfide oxidation there; in this case, iron appears to be oxidized as well. The net dissolved Fe consumption in the same interval was $8\times10^{-6}\mu mol/cm^3.sec$, which would imply an alkalinity consumption of only 16 (of the same units) during oxidation of Fe(II) to Fe(III), confirming that the alkalinity consumption was due in part to sulfur oxidation. An interval of concurrent alkalinity consumption and dissolved Fe production was present in the 6/84 core at 2-2.5 cm. In this interval, $-P_{Alk}/P_{Fe} = 2.4\pm0.6$, consistent with the oxidation of pyrite to $Fe^{2+} + SO_4^{2-}$.

Results from the other cores taken were similar to those shown for the 3/84 core, in which $-P_{Alk}$ was much greater than would be implied by the calculated P_{Fe} (3/84, 2-2.5 cm: $-P_{Alk}/P_{Fe} = 7.9\pm1.7$). In these cores, apparent alkalinity consumption was often

correlated with apparent ΣCO_2 consumption. Since, at the depth horizons shown, the $(Ca^{2+})(CO_3^{2-})$ product indicated that pore water (CO_3^{2-}) was only at 10-50% of saturation with respect to calcite, the apparent consumption of ΣCO_2 must have been due to sample heterogeneity (equivalent to conservative mixing of waters with varying Alk and ΣCO_2, with the proportions of the different component waters changing at different depth horizons). In principle, a true P_{Alk} could be calculated by subtracting $P_{\Sigma CO_2}$; however, the error in $P_{\Sigma CO_2}$ makes this operation meaningless (for example, for 3/84, 2-2.5 cm, the resulting $-P_{Alk}/P_{Fe} = 4.8 \pm 4.2$). Thus, while apparent $P_{Alk}:P_{Fe}$ correlations were often seen in cores from the study site, only in 6/84, when the combination of highly reducing conditions very near the sediment/water interface, exposure of iron sulfides at the interface, and rapid irrigation (as indicated by $^{222}Rn/^{226}Ra$ disequilibrium) made conditions favorable for sulfur oxidation, was the alkalinity signal implied by the calculated Fe^{2+} production rates large enough to be correlated quantitatively with Fe^{2+} production.

Although the relative importance of the two sources of dissolved Fe remains unresolved, the two combine to produce Fe maxima ranging from 50-150μM above 3 cm below the sediment/water interface throughout the year. It is likely that Fe(III) reduction is most important during the summer/early fall, when there is also evidence of rapid sulfate reduction (6/84, 9/83, and, to a lesser extent, 12/82). FeS/pyrite oxidation may explain such features as the large dissolved Fe maximum in 3/84 and the extremely large maximum in 6/84.

The rate of dissolved iron production is one of two key parameters in the determination of iron fluxes across the sediment/water interface, since it produces steep gradients near the interface. The other key factor is the penetration of oxygen into the sediments. The combination of these factors produces a distinct seasonal trend in near-interface dissolved iron concentrations (Table III.2), and therefore in Fe fluxes across the interface. Calculated iron fluxes are shown in Table III.2: by far the largest fluxes occur when rapid organic matter oxidation makes the sediment surface very reducing during the summer and fall (6/84, 9/83); the smallest fluxes occur in late winter and spring, when the sediment surface is less reducing (3/84). In the 6/83, 6/84, and 9/83 cores, the calculated nonlocal exchange flux is also important because the large subsurface iron concentrations are greater than or comparable to the interfacial dissolved Fe concentration. The applicability of a nonlocal exchange flux to iron profiles is questionable, however, since the ability of oxygenated seawater to carry dissolved iron out of sediments is uncertain. Because of this and because the 0.5 cm sampling intervals used in this study may not resolve a thin oxic layer at the sediment surface, calculated iron fluxes are quite likely to overestimate the true flux. The range of diffusive fluxes calculated at the Buzzards Bay site is 0.4×10^{-7} $\mu mol/cm^2.sec$ (3/84) to 50×10^{-7} $\mu mol/cm^2.sec$ (9/83).

Pore Water Chemistry of Manganese

The oxidation of organic matter by Mn(IV) occurs in the upper 0.5 cm of the sediments at the Buzzards Bay site at all times of year, and a dissolved Mn maximum is always observed in the upper 0.5 cm of the sediment column (Figure III.1). Since the overlying water Mn concentration (about 0.075μM) is very small compared to the pore water concentration, there is always a Mn flux out of the sediments.

The Mn profiles reported in Figure III.1 show relationships to dissolved iron profiles and to the importance of sulfate reduction. In the cores showing the least evidence of sulfate reduction (6/83 and 3/84), a zone of net dissolved Mn production (judged by the curvature of the dissolved Mn profile) extends to 1-1.5 cm below the interface. In the more reducing cores, the zone of net dissolved Mn production does not exceed 1 cm: it extends to the 0.5-1 cm sample in 12/82, and, in the most reducing cores (9/83 and 6/84), it extends to less than 0.5 cm from the interface, and does not appear to be resolved by the 0.5 cm sampling interval. In each core (except perhaps 6/84), a zone of rapid net dissolved Mn removal appears to coincide with rapid net dissolved Fe removal.

The dissolved Mn profiles observed at the Buzzards Bay site are qualitatively similar to the dissolved Cu profiles found in deep-sea sediments by Klinkhammer, et al. (1982) and Callender & Bowser (1980). Mn-rich particles fall to the sediment surface, and microbially catalyzed Mn(IV) reduction causes release of Mn to solution. A dissolved Mn maximum

in the upper few mm of the sediments results, and steep gradients between the Mn maximum and both the overlying seawater and underlying pore water lead to fluxes in both directions. In terms of the model used in Chapter 1 to explain the fluxes of metal ions produced in a thin layer near the sediment/water interface, the steady-state flux to overlying water (F_{OUT}) is determined by its balance with the production rate of dissolved metal in the surface layer (P) and the flux to the underlying pore water (F_D):

(III.1)
$$F_{OUT} = P - F_D$$
$$F_D = \phi \cdot D_{sed} \cdot (C_P - C_E)/L$$

where C_P is the concentration of dissolved metal in the production layer. Below the production layer, concentration decreases approximately linearly to the solubility-limited concentration, C_E, at depth L below the sediment/water interface. If C_E is approximately constant, the variables which are most important in determining F are L and P. Both may vary with environmental conditions. L may decrease as the occurrence of sulfate reduction approaches the sediment/water interface during the summer, causing increased concentrations of anions with which Mn may form solid phases; since L is likely to be a function of the precipitation rate of Mn-containing solids, it is probably through variations in the Mn precipitation rate that L changes. P may increase from low winter rates as increased temperature and supply of organic matter fuel an increase in metabolic rates during the warm months. In this section, the effects of variations in these parameters and in

transport parameters on the Mn flux across the sediment/water interface will be examined. Mass balances in the net dissolved Mn production and removal layers will be used to examine the supply of Mn to the production layer, the rate of production of dissolved Mn, and the chemical mechanisms for dissolved Mn removal.

Mn Mass Balances

The boundary between the net dissolved Mn production layer (Layer 1) and the net dissolved Mn removal layer (Layer 2), at depth x_1 below the sediment/water interface, and the depth of the bottom of Layer 2 (x_2), were chosen by inspection of Mn profiles (model parameters are illustrated in Figure III.6). x_1 is the depth of the sample interval beneath which the profile curvature indicates net dissolved Mn removal is occurring; x_2 is a region of approximately constant Mn gradient which occurs somewhere between about 2 and 5 cm below the interface in each of the cores.

The steady-state mass balance used for Layer 1 is illustrated by equation III.1 with F_{OUT} equal to the sum of the diffusive flux across the sediment/water interface and the nonlocal exchange flux,

$$(III.2) \quad F_{OUT} = \phi \bullet D_{sed} \bullet (C_1 - C_{OL})/(0.5\Delta x_1) + \Sigma_{i=1}^{n} \phi_i \bullet \alpha_i \bullet (C_i - C_{OL})\Delta x_i = J_O + I_P$$

Figure III.6

The Mn Mass Balance Model

L_1 denotes layer 1, extending from the sediment/water interface to x_1; L_2 denotes layer 2, which is between the depths, x_1 and x_2. Irrigation fluxes are: I_P, the flux between layer 1 and overlying water; and I_r, the flux between layer 2 and overlying water. J_0 is the diffusive flux across the sediment/water interface. F_D is the dissolved Mn flux from layer 1 to layer 2.

The particulate fluxes are shown by double arrows. F_A is the accumulation flux of Mn. F_{UP} is the particulate Mn flux from layer 2 to layer 1 due to the bioturbating activities of infauna.

Figure III.6

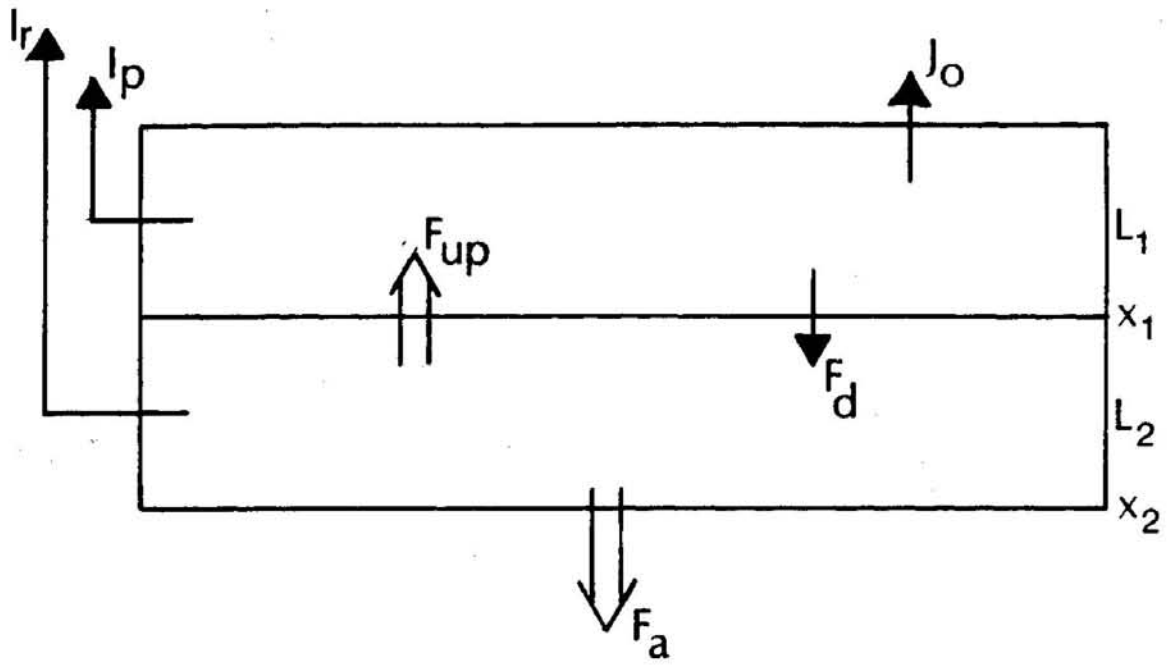

(there are n sample intervals in Layer 1, each of thickness Δx_i and concentration C_i; C_1 and Δx_1 denote the concentration in the sample interval immediately adjacent to the sediment/water interface and the thickness of that interval, respectively. ϕ is porosity, D_{sed} is the molecular diffusion coefficient, corrected for tortuosity and porosity; α is the nonlocal exchange transport parameter; C_{OL} is the overlying water Mn concentration. The first term, J_o, is the diffusive flux across the sediment/water interface, and the second term, I_P, is the nonlocal exchange flux from the production layer).

The fluxes occurring into and out of the dissolved Mn removal layer, Layer 2, are (1) a solution phase Mn flux out of Layer 1, (2) a solution phase flux due to nonlocal exchange with overlying water, (3) a flux out of the bottom of the layer, assumed equal to the Mn accumulation rate at the study site, and (4) a particulate phase Mn flux from Layer 2 to Layer 1 driven by bioturbation and the particulate Mn concentration change resulting from precipitation of the dissolved flux from Layer 1. The dissolved Mn flux from Layer 2 to Layer 1 cannot simply be buried because, as will be shown later, the solute flux out of Layer 1 is significantly greater than the Mn accumulation rate. Thus, the Layer 2 mass balance is described by

(III.3) $$F_D = I_R + F_A + F_{UP}$$

I_R. I_R is the nonlocal exchange flux, which removes dissolved Mn from Layer 2 by exchange with water overlying the sediments. The value for the nonlocal exchange transport parameter, α, is derived from the

$^{222}Rn/^{226}Ra$ disequilibrium measurements described in Chapter II.

There are two important assumptions inherent in the use of this transport model to calculate Mn fluxes. The first is that the permeability of burrow walls to Mn transport is equal to their permeability to Rn. The validity of this assumption depends on several factors, including the redox level of the burrow wall (if O_2 is present in burrow waters, some Mn may be trapped by oxidation within the burrow wall: Aller, 1977), and the presence or absence of a burrow lining (Aller, 1983). In addition, it is assumed that the concentration of Mn in the burrow water is the same as the Mn concentration in the overlying seawater (which is essentially zero relative to the much larger pore water concentrations). Neither of these assumptions is likely to be quantitatively correct. However, because Mn(II) oxidation occurs over a period of days in seawater (Emerson et al., 1979), if burrow flushing is reasonably rapid, then the calculated nonlocal exchange flux should approximate a true flux.

The nonlocal exchange flux is calculated by

$$I_R = \int_{x1}^{x2} \phi \bullet \alpha (C - C_{OL})\, dx$$

Using equation III.6 (see below) to describe the dissolved Mn profile in Layer 2 and the expression for α determined in Chapter II,

$$\alpha = \alpha_0 \exp(-x/\alpha_1)$$

the nonlocal exchange flux is:

$$\text{III.3A} \quad I_R = \phi\alpha_0\left(\left(\frac{\Delta C_1 e^{\gamma x_1}}{1/\alpha_1+\gamma}\right)\bullet E_1 - (\alpha_1 \Delta C_{OL})\bullet E_2\right)$$

$$E_1 = \exp\{-(1/\alpha_1+\gamma)x_1\} - \exp\{-(1/\alpha_1+\gamma)x_2\}$$

$$E_2 = \exp\{-x_1/\alpha_1\} - \exp\{-x_2/\alpha_1\}$$

ϕ is the average porosity in Layer 2, determined from the porosity profiles shown in Chapter II. The other variables in equation III.3A are described in the text below.

F_A. F_A is the Mn accumulation rate; based on a sediment Mn concentration of 350 ppm, a dry bulk density of 0.65, and a sedimentation rate of 0.3 cm/yr (Farrington et al., 1977), $F_A = 4.0 \times 10^{-8}$ $\mu mol/cm^2.sec$. It is important to note that this calcultation is based on a ^{210}Pb-derived apparent sedimentation rate, obtained at a nearby site in Buzzards Bay, and is an upper limit to the true Mn accumulation rate. Because of this, model results shown below have been calculated using this apparent F_A and an accumulation rate ten times lower (in the latter case, the magnitude of this flux, compared to the other fluxes in the model, is negligible).

F_{UP} is the particle flux from Layer 2 to Layer 1, $F_{UP} = D_B \bullet (\Delta C/\gamma^{-1})$. D_B is the bioturbation mixing coefficient from $^{234}Th/^{238}U$ disequilibrium measurements, γ^{-1} is the scale length of the solution phase Mn removal profile (see below). ΔC is the particulate Mn concentration difference between the top of Layer 2 and the bottom of Layer 1 required to balance the Mn budget in Layer 2.

F_D is the solution phase Mn flux from Layer 1 to Layer 2.

The two unknowns which will be calculated from III.1 and III.2 are P, the dissolved Mn production rate, and ΔC, the particulate Mn concentration difference across the Layer 1: Layer 2 boundary.

The Mn Removal Layer

Layer 2 will be considered first. Following the procedure used by Klinkhammer et al. (1982) to model Cu removal in oxic sediments, Mn removal is modeled as a first-order process. Then, in steady state,

$$D \cdot d^2C/dx^2 = k_{app} \cdot (C - C_E) \qquad \text{(III.4)}$$

The term, k_{app}, is a first-order removal rate constant. C_E, a second fitting parameter, is, conceptually, the dissolved Mn concentration at which no further net Mn precipitation occurs in Layer 2.

Choosing the upper and lower boundaries of the Mn removal zone (x_1 and x_2) and applying the boundary conditions, $C(x_1) = C_1$ and $(dC/dx)_{x2} = F_2$ (F_2 is determined from the dissolved Mn profile),

$$\Delta C = \Delta C_1 \cdot e^{\gamma(x-x1)} + G \cdot (e^{-\gamma(x-x1)} - e^{\gamma(x-x1)}) \qquad \text{(III.5)}$$

$$\Delta C = C - C_E$$

$$\Delta C_1 = C_1 - C_E$$

$$G = \frac{(\Delta C_1 \cdot e^{\gamma(x-x1)} - F_2/\gamma)}{e^{\gamma(x2-x1)} + e^{-\gamma(x2-x1)}}$$

$$\gamma = (k_{app}/D_{sed})^{1/2}$$

Then, the solution phase flux from Layer 1 into Layer 2 is

$$F_D = -\phi \cdot D_{sed} \cdot (dC/dx)_{x1} = \phi D_{sed} \gamma \cdot (2G - \Delta C_1)$$

The model inputs and the best-fit values of C_E and γ are shown in Table III.5A. It can be seen that G is very nearly equal to ΔC_1 so that, to a good approximation,

(III.6)
$$\Delta C = \Delta C_1 \cdot e^{-\gamma(x-x1)}$$
$$F_D = \phi D_{sed}(C_1 - C_E)/\gamma^{-1}$$

These simplifications show that the simple model of equation III.1 holds with L set equal to the scale length of the dissolved Mn removal profile (γ^{-1}) and $C_P = C_1$. Thus, since γ^{-1} is directly related to the rate of precipitation of Mn with solid phases, the hypothesized relationship of L to the Mn precipitation rate is demonstrated by equation III.6.

Mn can be removed from the solution phase of Layer 2 either by exchange of pore water with overlying water through animal burrows (nonlocal exchange) or by removal to a solid phase. Elderfield et al. (1981a) speculated that nonlocal exchange was an important removal mechanism in bioturbated Narragansett Bay sediments. At the Buzzards Bay site, the nonlocal exchange transport parameter has been measured using $^{222}Rn/^{226}Ra$ disequilibrium (Table II.7, Chapter 2). The Mn loss by nonlocal exchange has been calculated using equation III.3A with the

best-fit C_E and γ. The results (I_R in Table III.3B) show that nonlocal exchange, while significant in the summer and fall, does not remove the entire downward flux of dissolved Mn into Layer 2 of these sediments, as I_R varies from 0 to 45% of F_D. Because of the assumptions inherent in the calculation of the nonlocal exchange flux, this calculation is more likely to overestimate than to underestimate dissolved Mn removal by nonlocal exchange. Dissolved Mn must be removed to a solid phase.

Although saturation with respect to pure Mn phases has been found to be possible in some nearshore sediments (Aller, 1980a,b), pure Mn phases can be ruled out with some confidence at this site. Rhodocrosite ($MnCO_3$), reddingite ($Mn_3(PO_4)_2$), and the sulfides, alabandite and haurite (MnS), have been considered as potential Mn phases. The seawater constant of Johnson (1982) was used for rhodocrosite calculations. The reddingite constant from Aller (1980a) and sulfide constants from the tabulation of Jacobs (1984) were used with $\gamma(Mn^{2+})$ = .18 (from the Davies equation at seawater ionic strength and % free = .75: Carpenter, 1983). $\gamma(HS^-)$ and $\gamma(PO_4^{3-})$ were the same as used for the Fe calculations. Only in the March, 84, core did Mn approach saturation with respect to rhodocrosite; it never exceeded 3% of saturation with respect to reddingite; and it was consistently undersaturated with respect to the Mn sulfides considered. There may be significant error in these calculations, but since they show no consistent ion product variations in the dissolved Mn removal layer, precipitation of pure Mn phases appears unlikely. Several mixed phases

Table III.3A
Mn Removal Layer Model Parameters

Model inputs: x_1, x_2, F_2, and C_I are as defined in the text, and are chosen from the dissolved Mn profile.
Model outputs: γ^{-1} is the scale length of the solute profile in the removal layer. C_{eq} and γ define the solute removal rate by

$$\text{removal rate} = k_{app}\,(C-C_{eq})$$

$$k_{app} = \gamma^2 \cdot D_{sed}$$

k, the rate of removal of solute to the solid phase, is k_{app} after it has been corrected for removal of solute by irrigation:

$$k = \frac{\int_{x1}^{x2} k_{app}(C-C_{eq})dx - \int_{x1}^{x2} \alpha(C-C_{OL})dx}{\int_{x1}^{x2} (C-C_{eq})dx}$$

$$= \frac{F_D - I_R}{\phi(\Delta C_I/\gamma)\cdot(1-\exp\{-\gamma(x_2 - x_1)\}}$$

	Inputs				Output		
Date	x1	x2	F2	CI	γ	Ceq	k
12/82	0.75	3.25	-0.36	82.4	2.08	5.25	1.3
6/83	1.25	5.50	-1.44	65.9	1.74	4.11	0.57
9/83	0.75	3.25	0	41.6	1.43	9.51	0.56
3/84	0.75	3.75	-0.52	64.3	2.15	6.86	1.4
6/84	0.25	2.25	0	40.4	4.89	13.7	9.1

Units: x_1, x_2 : cm
F_2 : 10^{-3} μmol/cm^4
C_I, C_{eq} : 10^{-3} μmol/cm^3
γ : cm^{-1}
k : 10^{-5} sec^{-1}

Table III.3B

Mass Balance in the Mn Removal Layer

The table includes values for the terms in

$$(III.2) \qquad F_D = I_R + F_A + F_{UP}$$

(terms are defined in the text). ΔC is calculated from

$$F_{UP} = D_B \cdot G = D_B(\Delta C/\gamma^{-1})$$

(G is the gradient in the particulate Mn concentration required to balance the Mn budget in Layer 2). D_B values are from the excess ^{234}Th values reported in Chapter II.

Date	F_D	I_R	F_A	F_{UP}	D_B	G	ΔC
12/82	3.7	0	0.40	3.3	9	3.7	250
			0.04	3.7		4.1	290
6/83	3.1	1.4	0.40	1.3	81	0.14	13
			0.04	1.7		0.21	17
9/83	1.5	0.48	0.40	0.62	53	0.12	12
			0.04	1.0		0.19	19
3/84	2.8	0	0.40	2.4	14	1.7	115
			0.04	2.8		2.0	130
6/84	4.3	0.11	0.40	3.8	40*	0.95	28
			0.04	4.2		1.05	31

*.. This value for D_B is estimated from the average "warm-water" value measured for the Buzzards Bay site.

Units: G : $\mu mol/cm^4_{sed}$
ΔC : ppm
D_B : 10^{-8} cm^2/sec
Fluxes: 10^{-7} $\mu mol/cm^2.sec$

Table III.3C

Mass Balance in the Mn Production Layer

Values are shown for the terms in the production layer mass balance,

$$P = F_D + F_{OUT},$$

$$F_{OUT} = I_P + J_0$$

(equation III.2). F_D is determined from the solute flux at $x = x_1$. Also included in the table are:

(1) I_T, the nonlocal exchange flux from pore water to overlying water, over the upper 10m cm of the sediment column. It is determined as described for I_P in equation III.2.

(2) R, the fraction of dissolved Mn production that is returned to overlying water,

$$R = (J_0 + I_T)/P$$

Date	F_D	F_{OUT}	P	I_P	J_0	I_T	R
12/82	3.7	16	20	0	16	0	.80
6/83	3.1	15	18	0.37	11	4.8	.88
9/83	1.5	9.1	11	0.69	8.4	1.2	.87
3/84	2.8	9.9	13	0	9.9	0	.76
6/84	4.3	5.9	10	0.07	5.8	.20	.58

Units of all fluxes are 10^{-7} $\mu mol/cm^2.sec$

have been reported for Mn, in particular (Mn,Ca) and (Mn,Ca,Mg) carbonates (Pedersen & Price, 1982; Boyle, 1983; Suess, 1979). In the upper 3-4 cm of these sediments, where Mn removal is required, coprecipitation of Mn with $CaCO_3$ is unlikely. Probably because of inputs of acid from oxic organic matter diagenesis and from oxidation of Fe sulfides, the upper 4 cm of the sediment column is consistently undersaturated with respect to calcite (Figure III.2). In addition, near-interface pore water has excess Ca^{2+} over bottom water (A. McNichol, pers. comm.), indicating that $CaCO_3$ dissolves at the sediment/water interface. Coprecipitation of Mn with Fe phosphates is a possibility for which there is circumstantial evidence. There is a correlation of x_1 (the depth below which net Mn removal occurs) with the depths at which pore waters are supersaturated with respect to vivianite: there is deeper penetration of the dissolved Mn production layer in the 3/84 and 6/83 cores than in the 9/83, 12/82, and 6/84 cores, which three are all supersaturated with respect to vivianite near the sediment/water interface. Unfortunately, because of the complex nature of iron cycling in this region of the sediment column, pore water data cannot be used to calculate possible Mn/Fe ratios in solids. As was discussed in the iron chemistry section, there is evidence of significant sulfate reduction coincident with the zone of vivianite saturation. Thus, since HS^- does not appear in solution until 2-3 cm, Fe sulfides must be forming, and there is a possibility of Mn removal with Fe sulfides as well as with Fe phosphate. The data do not allow elimination of either possibility.

First-order rate constants for the removal of dissolved Mn to solids have been calculated by correcting the apparent constants (k_{app}), obtained from the fit of equation III.5 to Mn data, for removal by irrigation processes. The calculation and results are shown in Table III.3A. The variations, except for the 6/84 core, are probably not significant, with a range of 0.6-1.4x10^{-5}sec^{-1}. In fact, the relatively small constant calculated for the 9/83 core may be an underestimate: because of the rapid rate of organic matter oxidation evident in this core, the 0.5 cm sampling interval may not resolve the Mn production layer well, and considerable curvature in the Mn profile may have been missed. The rate calculated for the 6/84 core, 9.5x10^{-5} sec^{-1}, is clearly faster than the others. The 6/84 core has extremely elevated dissolved Fe levels (up to 650μM), elevated PO_4 concentrations, and evidence of rapid Fe phosphate removal in the upper 2 cm (Figure III.4). Sulfate reduction is also occurring, and the presence of black patches at the sediment/water interface indicates that Fe sulfides are present. The more rapid rate constant for dissolved Mn removal may be due to more rapid precipitation of the solid phase in which Mn is included.

The Mn mass balance for Layer 2 has been calculated according to equation III.3, and the results of the calculation are shown in Table III.3B. The balance shows that the most important removal flux from Layer 2 must be the particulate Mn flux back to Layer 1. Some possibly significant assumptions have gone into the calculation, from this particulate Mn flux, of the predicted particulate Mn concentration

difference across the Layer 2/Layer 1 boundary. Although a concentration difference of at least 3-9% of the total Mn concentration is predicted at all times, the elevated 12/82 and 3/84 differences may depend on non-steady state conditions: the variability in Mn profiles shows that the assumption of steady state is not strictly valid, but the data do not permit quantitative estimation of the error involved. The calculated ΔC also depends on the approximation, $(dC/dx)_{x=x1} \approx \Delta C/\gamma^{-1}$, that is, that the scale length of the dissolved Mn removal profile reflects the distance over which the particulate Mn concentration gradient occurs. A shorter Δx would require smaller concentration differences. A final assumption is that the D_B calculated from excess ^{234}Th profiles, averaged over the upper 2-2.5 cm of the sediments, is valid in the depth zone of interest (0.5-1.5 cm). If D_B decreases with depth below the interface, the calculations done here would overestimate the required concentration difference. Despite these possible errors, the prediction of solid phase Mn concentration variations of 3-75% may be testable by solid phase Mn measurements.

The Mn Production Layer

The mass balance in the net dissolved Mn production layer (equations III.1 and III.2 and Table III.3C) shows that the upward flux of particulate Mn may be important in maintaining a dissolved Mn maximum at the sediment surface throughout the year. The upward particulate Mn

flux ranges from 6% (9/83) to 38% (6/84) of the net dissolved Mn production in Layer 1, being most important in the June, '84, core, but also important in the two cold-water cores analyzed, 12/82 and 3/84 (17% and 18% of net dissolved Mn production, respectively). Thus, according to this scenario, dissolved Mn production would result from dissolution of reduced Mn phases as well as from Mn(IV) reduction, perhaps helping to explain how the surface dissolved Mn maximum is maintained throughout the winter. The near-interface Mn cycling is still dependent on the rate of oxidation of organic matter, however, as Fe(III) and SO_4 reduction are necessary for producing the conditions for near-interface dissolved Mn removal. These conditions appear to persist throughout the year, although they occur deeper in the sediments at the end of winter (see the 3/84 and 6/83 dissolved Mn profiles). Calculated net production rates of dissolved Mn in Layer 1 reflect the year-round persistence of the dissolved Mn maximum. The variability in production rates is small, from 1.0×10^{-6} to 2.0×10^{-6} μmol $Mn/cm^2.sec$. There is no distinct seasonal trend. In fact, given the potential errors in the calculations of F_D and F_{OUT} arising from the use of a 0.5 cm sampling interval, rather than a smaller one, the variability is probably not significant. This error may be greatest for the 9/83 core, when the Fe maximum occurred in the upper 0.5 cm. The true Mn maximum may have been greater than the observed maximum, which would increase F_D, F_{OUT}, and P.

There do appear to be variations in the Mn flux across the sediment/water interface, although the effects of finite sampling resolution must be kept in mind. The results (the sum of J_0 and I_T in

Table III.3C) show that the smallest flux, 6×10^{-7} μmol/cm².sec, occurred under the most reducing conditions (6/84), when removal of dissolved Mn occurred very close to the interface. This core probably reflects rather extreme reducing conditions at this study site, and the total observed variability in the dissolved Mn flux is still less than a factor of 3, from 6 to 16×10^{-7} μmol/cm².sec. There are important potential errors arising from use of a 0.5 cm sampling interval to calculate fluxes: Mn^{2+} oxidation to insoluble Mn(IV) may occur in a thin oxic layer at the sediment surface, causing calculated fluxes to be greater than the true flux (this effect would be most important for the 3/84 and 6/83 cores); on the other hand, especially when reducing conditions prevail at the sediment surface, the true Mn maximum may be greater than the 0-0.5 cm average Mn concentration. As discussed previously, the calculated nonlocal exchange flux may overestimate the true flux. The relative importance of these errors is difficult to evaluate without a direct flux measurement.

A final application of the Mn mass balance results is the calculation of the concentration of Mn in sedimenting particles needed to explain the Mn flux out of the sediments. This calculation has been applied previously to Cu balances in deep-sea sediments (Callender & Bowser, 1980; Klinkhammer et al., 1982). It requires that the product of the Mn concentration on sedimenting particles and the fraction of sedimenting Mn which accumulates be equal to the concentration of Mn in accumulating sediment. Since the fraction of Mn which accumulates is

$$\frac{F_A}{F_A + F_{OUT}}$$

(Table III.3B and C), the required Mn concentration in a thin enriched layer at the sediment surface, assuming the ^{210}Pb-derived apparent accumulation rate is accurate, ranges from 5400-10,000 ppm Mn. Although I have no particulate Mn data from Buzzards Bay, these enrichments are in keeping with those found in the deeper water column of the Gulf of St. Lawrence, where particulate Mn concentrations in the water column ranged from 1000 ppm in surface waters to values in excess of 15,000 ppm near the sediment/water interface; the apparent source of the excess Mn was a benthic flux of dissolved Mn (Yeats et al., 1979). If the true Mn accumulation rate is much lower than that used for this calculation, unrealistically large enrichments on sedimenting particles are calculated.

Pore Water Chemistry of the Trace Metals: Co, Ni, Cu

The Ni, Cu, and Co profiles obtained at the study site (3/84 and 6/84) bear a qualitative resemblance to the Mn distributions measured there. Net production of the dissolved form of all four of these metals occurs in a thin layer near the sediment/water interface, and rapid removal of the metals to solid phases occurs below the surface layer. The rates of production and consumption are different for the different metals. Both the surface layer mass balance (equation III.1) and the dissolved metal removal model (equations III.4 to III.6) used to explain observed dissolved Mn distributions can be applied to the trace metal data.

Model inputs were chosen using the same method as was described previously for Mn; inputs and model results are shown in Table III.4, and calculated parameters are shown in Table III.5. It is apparent from Table III.5 that, when apparent metal accumulation rates are used, unlike for Mn, the solute flux into the sediments (F_D) is much less than the sediment accumulation rate for each of these metals, so that a particulate metal flux from the removal layer to the production layer is not necessary. If the true metal accumulation rate is actually much less than that calculated using the apparent sedimentation rate, such a flux may still be necessary to balance the Layer 2 metal budgets. Similarly, since the flux across the sediment/water interface does not greatly exceed the accumulation rate in either case, no dramatic metal enrichment on sedimenting particles is needed to balance the dissolved metal flux

across the sediment/water interface.

The models are most readily applied to Co, whose pore water distributions are more regular than those of Ni and Cu (Figure III.1). The dissolved Co flux across the interface is similar for both 3/84 and 6/84. Despite the significant change to very reducing conditions from 3/84 to 6/84, with the consequent reduction in the thickness of the net dissolved Co production layer, the decrease in the dissolved Co flux is only about 20%, from 2.3×10^{-7} to 1.9×10^{-7} nmol/cm^2.sec. The effect of the more rapid removal of dissolved Co to the solid phase in 6/84 is seen in the fraction of the dissolved Co production that is returned to the overlying water: it drops from 82% in 3/84 to 56% in 6/84.

Similar processes appear to affect both Co and Mn: there is a linear correlation between the Mn and Co pore water concentrations in the upper 2 cm of the 3/84 and 6/84 cores (it is in the upper 2 cm that appreciable Mn and Co gradients exist), with $\Delta Co/\Delta Mn = .34 \times 10^{-3}$ mol/mol (Figure III.7). When two pore water components are linearly related, their fluxes are linearly related,

$$D_{sed}(\Delta C_A/\Delta x) = K \cdot D_{sed}(\Delta C_B/\Delta x)$$

(K is a constant of proportionality, D_{sed} is the diffusion coefficient. For simplicity, $D_A = D_B$ has been assumed; $D_{Mn} = D_{Co}$ is a good approximation: Li & Gregory, 1974). By applying this relationship to the upper and lower boundaries of a sediment layer, it can be shown that it implies that, within the layer, the production or removal rates of two components whose concentrations are linearly related are proportional,

Table III.4

Removal Layer Model Parameters: Co, Ni, Cu

The terms in the table are defined exactly as they were for the Mn model.

	Inputs				Output		
Date	x1	x2	F2	CI	γ	Ceq	k
A. Co							
3/84	0.75	3.75	0	24.2	0.91	0.36	0.24
6/84	0.25	3.75	0	18.6	3.90	7.50	6.2
B. Ni							
3/84	0.75	3.75	0	28.6	1.28	3.08	0.45
C. Cu							
3/84	0.25	3.25	0	15.1	3.00	2.60	3.7

Units: x_1, x_2 : cm

C_i, C_{eq} : 10^{-3} nmol/cm^3

γ : cm^{-1}

k : 10^{-5} sec^{-1}

Table III.5

Production Layer Model Parameters: Co, Ni, Cu

Terms are defined exactly as for the Mn model: see Table III.5C. $F_{OUT} \simeq J_0$ for these elements. F_A, the accumulation rate of the metal in the sediment column, is included in this table.

Date	F_D	J_0	I	P	R	F_A
A. Co						
3/84	4.7	23	0	28	.82	60
6/84	15	19	.43	34	.56	
B. Ni						
3/84	77	22	0	30	.73	260
6/84		8				
C. Cu						
3/84	9.4	10	0	19	.53	230
6/84		-3.7				

Units of all fluxes are 10^{-8} nmol/cm^2.sec

Figure III.7

Mn-Co Correlations

The correlation between dissolved concentrations of Mn and Co in the upper 2.5 cm of the sediments at the Buzzards Bay study site, 3/84 and 6/84 cores.

Figure III.7

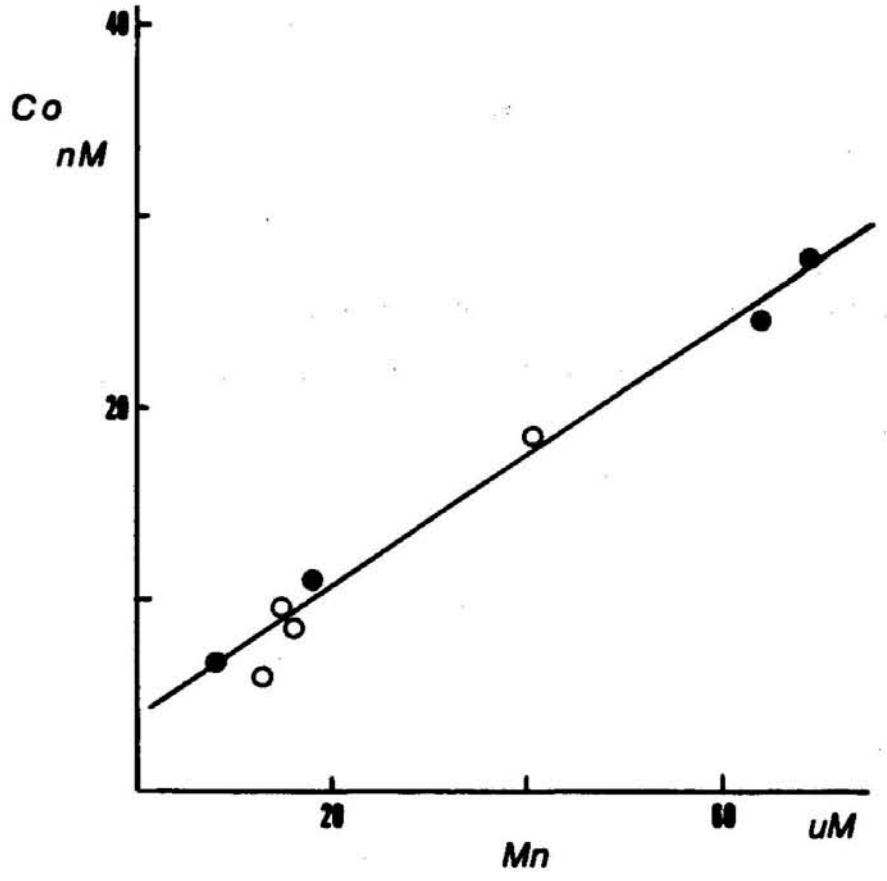

○ 6-84
● 3-84

Table III.6

Comparison of Results for Mn and Co

The terms compared in the table are: J_o, the diffusive flux across the sediment/water interface; P, the production rate of dissolved metal; F_D, the dissolved flux at $x = x_1$; R, the fraction of dissolved metal production which is returned to overlying water, and k, the rate constant for removal to the solid phase.

J_o, P, F_D are entered as Co/Mn x 10^3

R and k are entered as Co/Mn

Parameter	3/84	6/84
J_o	.23	.33
P	.22	.34
F_D	.17	.35
R	0.93	1.0
k	.17	.68

and that the ratio of their production (consumption) rates is equal to the slope of the linear relationship. A comparison of flux and removal rate results for Co and Mn in the 3/84 and 6/84 cores is shown in Table III.6. Agreement with $\Delta Co/\Delta Mn = .3x10^{-3}$ is good except that, in 3/84, Co appears to be removed from solution more slowly than Mn (thus, F_D and k are smaller for Co).

Results of the application of the dissolved metal removal model and the surface layer mass balance for Ni and Cu are shown in Tables III.4 and III.5. Uncertainties in the data prevented application of the model in 6/84. A large maximum at 0.5-1 cm is present for both Cu and Ni in this core. It coincides with a possible input of dissolved Fe from sulfide oxidation, and may be related to it; on the other hand, the maximum may merely be due to contamination. A similar, but smaller, feature is present at 2-2.5 cm in the 3/84 core. Elderfield et al. (1981a) noted similar features in Cu and Ni profiles from reducing sediments in Narragansett Bay, R.I., and demonstrated that these metals may be released to solution when sulfide-rich sediments are exposed to O_2-containing seawater.

The most important result arising from these calculations is that the fluxes of Cu and Ni across the sediment/water interface depend more strongly on the depth in the sediments of the occurrence of sulfate reduction than do the fluxes of Mn and Co. The Ni flux in 6/84 is a factor of three lower than in 3/84 (this decrease depends partly on the accuracy of the measured bottom water concentration of 17 nM for Ni;

there is no independent verification of this result); in fact, the 6/84 flux is very small, and may not be significantly different from zero. The Cu flux changes in direction, as the flux of dissolved Cu is out of the sediments in 3/84, but there is a small flux into the sediments in 6/84. The behavior of Ni is similar to that of Co in 3/84, with a similar removal rate constant (4.5×10^{-6} sec^{-1} compared to 2.4×10^{-6} sec^{-1} for Co) and a similar recycling efficiency (73% of dissolved Ni production is returned to the water column, compared to 82% for Co). However, for Cu, even in the less reducing 3/84 core, a more rapid removal rate (the rate constant is $37 \times 10^{-6} sec^{-1}$) and lower recycling efficiency (53%) are evident.

The trend of rates of removal from pore water to solid phases found in these sediments, Cu>Ni>Co, is similar to the behavior of these metals in anoxic basins and to predicted solubility trends. The results from trace metal measurements used in this discussion are from Jacobs & Emerson, 1982; Kremling, 1983; Jacobs, 1984. Cu is removed from the dissolved phase in marine anoxic basins, its concentration decreasing continuously from its value at the oxic/anoxic interface. Ni shows little change in concentration across the interface. Co, on the other hand, increases in concentration going from the oxic to the anoxic side of the interface; in this respect, its behavior is similar to that of Mn. Thus, observed behavior of these metals in anoxic basins is consistent with behavior observed in reducing sediments.

Estimates of the solubilities of Ni, Cu, and Co in the presence of a small amount of sulfide (HS^- = 1μM) at pH 7.3 have been made

using the constants compiled by Jacobs (1984). If αCoS is taken as the controlling solid phase for Co (Jacobs, (1984) and Kremling (1983) have reported results consistent with this hypothesis in anoxic basins), an equilibrium Co^{2+} concentration of 10 nM is predicted. For Ni, a wide range of concentrations is predicted from the solubilities of two NiS phases (αNiS and millerite), 0.3-79 nM. Following Jacobs & Emerson (1982), taking Cu to be in the +I oxidation state, with $Cu_T = 10^8 \cdot Cu^+$ (due to extensive complexation by sulfides), the equilibrium Cu concentration is predicted to be 0.05-0.6 nM. Again, if rate of removal from pore waters can be predicted from relative solubilities, the trace metal results found in Buzzards Bay sediments are consistent with the predicted solubility trend, Co~Ni>Cu.

Since HS^- concentrations were below the analytical detection limit in the zone of rapid removal of these metals, scavenging by Fe sulfides has been proposed as a removal mechanism. Since Co and Mn removal appear to be related, these two metals may be removed to the same phase, either a phosphate or a sulfide mineral (however, the pore waters are considerably undersaturated with respect to $Co_3(PO_4)_2$). The behavior of Fe in these sediments, and solid phase analyses of nearshore sediments reported by other workers (e.g., Aller, 1980a,b), indicate that Fe sulfides are likely to be present near the sediment/water interface; thus, sulfides which could act as scavengers of sulfide-forming metals are present. However, the data offer no proof of this mechanism, and it remains an unproved hypothesis.

The trace metal results reported here indicate that the

efficiency with which the sediments at the Buzzards Bay site recycle Co, Ni, and Cu to the water column decreases in the order, Co>Ni>Cu. While similar dissolved Co fluxes from sediments to overlying seawater were found for late winter conditions, when sulfate reduction is relatively unimportant in the upper 2-3 cm of the sediments, and for very reducing conditions, the flux of Ni was found to be considerably smaller under very reducing conditions, and the Cu flux changed from a return flux of dissolved Cu to the water column when conditions were less reducing to a flux of dissolved Cu into the sediments under very reducing conditions. These results depend on the adequacy with which interfacial metal concentrations are measured using a 0.5 cm sample interval. If a very thin oxic layer remains at the sediment surface when conditions are reducing, the benthic boundary layer may be a more important source of dissolved trace metals to the coastal ocean water column than has been reported in this study.

The most extensive study of pore water metal chemistry in nearshore sediments prior to this one is that of Elderfield et al. (1981a,b; Elderfield, 1981) in Narragansett Bay, R.I. Their study included Cu and Ni, but not Co. Their results are based on cores taken in late summer at a heavily polluted site at the mouth of the Providence River and at a site in Rhode Island Sound. They found the heavily polluted site to be very reducing near the interface throughout the year, with millimolar dissolved H_2S levels, PO_4 = 400 - 800 μM, and ΣCO_2 = 5 - 10 mM in the upper 5 cm of the sediment column. The pore water data from the Rhode Island Sound site indicated that it was

qualitatively similar to the Buzzards Bay site in late summer, with significant decreases in pore water SO_4 concentrations in the upper 5 cm, and with ΣCO_2 = 4 - 6 mM and PO_4 = 100 - 150 μM. Pore water Fe and Mn profiles were qualitatively similar to those measured at the Buzzards Bay site. The pore water Cu and Ni profiles from the Narragansett Bay study agree with the conclusion reached in this study, that, when sulfate reduction is important near the interface, benthic Cu and Ni fluxes tended to be very small and into the sediments. A contrasting study is that of Emerson et al. (1984), in which results obtained from a core taken in January in Quartermaster Harbor, Puget Sound, Washington, are reported. Although H_2S and PO_4 measurements were not shown for this core, alkalinity levels were less than 3mM in the upper 5 cm of the sediment column, and results from another January core showed PO_4 less than 40μM in the upper 5 cm. Thus, benthic metabolism was relatively slow near the interface, and, if the conclusions of the Buzzards Bay study can be extrapolated to other sites, conditions were favorable for significant fluxes of Cu and Ni from sediments to the water column. In fact, fluxes comparable to those observed in Buzzards Bay in March, '84, were measured, with the dissolved Cu flux 4.9×10^{-7} nmol/cm^2.sec and the dissolved Ni flux 1.2×10^{-7} nmol/cm^2.sec. Thus, results from the limited number of comparable other studies support the general conclusions of this trace metal study at a fine-grained sediment site in Buzzards Bay, Mass.

Conclusions

The dissolved metal data from the Buzzards Bay site indicate that the most important factor determining the variability in dissolved metal fluxes across the sediment/water interface is the variability in the depth of redox horizons. Fluxes of all the metals measured depend on this factor, but to different degrees and for different reasons.

The flux of dissolved Fe across the sediment/water interface varies dramatically (the observed variation during this study exceeded 100 x), with a seasonal pattern. Fe fluxes are greatest during periods of summer and fall when the interface is most reducing, smallest in winter and spring when sulfate reduction is least important near the interface. Fe redox chemistry is the primary determinant of its behavior. It is oxidized very rapidly in the presence of O_2 (Murray & Gill, 1978): dissolved Fe production must occur very near the sediment/water interface for there to be a large dissolved Fe flux out of the sediments. Irrigation may effect a significant dissolved Fe flux during the summer months: Fe is much more soluble in seawater under reducing conditions, and the dissolved Fe maximum usually occurs below the sediment/water interface. However, nonlocal exchange of Fe is small relative to the large diffusive fluxes that occur when the interface is reducing. In addition, O_2-containing burrow water may not be an effective transporter of dissolved Fe.

Cu fluxes also vary dramatically as the redox level of the interface varies. The Cu flux variation is inversely related to the Fe

flux variation. The dissolved Cu flux out of the sediments decreases as the interface becomes more reducing, and becomes negative when sulfide is present very near the interface. While Fe is more soluble near the interface of the sediments than in O_2-containing seawater, even when sulfide is present, Cu is much less soluble in the presence of sulfide. Thus, the Cu flux depends on the redox potential because of the very limited solubility of Cu sulfides.

The control on the Ni flux is similar to the control on the Cu flux. However, Ni is more soluble in marine systems in the presence of sulfides than is Cu. Work in anoxic basins (Emerson & Jacobs, 1982; Kremling, 1983; Jacobs, 1984) has shown that the dissolved Ni concentration changes little across the oxic/anoxic boundary. Thus, while Ni fluxes from nearshore sediments show similar trends to Cu fluxes, the variability is smaller than for Cu. In this study, the Ni flux varied by about a factor of three from the relatively oxidizing 3/84 core to the very reducing 6/84 core.

As is the case for Ni and Cu, dissolved Mn and Co production occurs in the upper 0.5 cm of the sediment column at the study site. However, the solubility control on the latter two metals at low sulfide concentrations is less strict than it is on Cu and Ni. Thus, although their fluxes decrease under very reducing conditions, the observed variability is relatively small -- less than a factor of two change for Co and less than a factor of three change for Mn were measured during this study, in which both relatively oxidizing and reducing conditions were observed.

In summary, Fe is cycled between particulate and dissolved phases differently than Mn, Co, Ni, and Cu in nearshore sediments. Dissolved Fe is produced below the sediment/water interface during most of the year, and its flux across the interface is limited by its rapid oxidation rate. Mn, Co, Ni, and Cu all are produced in the upper 0.5 cm of the sediment column, and their fluxes appear to be limited by their solubility in reducing systems. The solubility control is strict for Cu, and is progressively less strict for Ni, Co, and Mn.

An important limitation on calculated fluxes from nearshore sediments is the ability, given a 0.5 cm sampling interval, to resolve near-interface processes. The occurrence of a very thin oxic layer, unresolved given the sampling interval, may cause calculations of all of these fluxes, especially Cu fluxes, to be underestimated. In addition, there is the possibility of an overestimate, especially for Fe and Mn, due to their oxidation in the presence of O_2 at seawater pH.

Appendix III.1

Results of Pore Water Analyses

15/12/82

Dep (cm)	Alk meq/l	TCO2 mM	PO4 µM	H2S µM	SiO2 µM	SO4 mM	Mn µM	Fe µM
0-0.5	3.019	7.344	11.6	bd	356	24.40	113	49.0
0-.5B						24.40		
0.5-1	3.011	7.426	45.4	bd		24.69	82.4	150
1-1.5	3.002	7.467	78.5		625	23.78	35.1	196
1.5-2		7.382	78.5		669		11.2	125
2-2.5	3.864	7.490	94.1		739	24.07	7.90	98.4
2.5-3	7.437	65.4			740	23.28	7.54	58.9
2.5-3B						24.07		
3-3.5	3.743	7.447	74.9	6.90	714		7.36	43.0
3.5-4		7.377	70.6	0.60			5.47	13.6
5-6	3.821	7.204	61.3	71.6	704	24.01	3.94	
7-8	3.725	7.154	45.2	147		23.39	1.51	4.00
9-10	3.612	7.423	35.4	103		24.40	1.78	
11-12	3.703	7.255	36.7	150		23.78	0.88	1.83
14-15	3.829	7.468	33.4	106	704	23.45	1.06	
14-15B						23.67		
17-18	3.981	7.476	33.6	181	664	23.33	0.62	
20-21	4.311	7.461	40.0	417		23.67	0.62	8.66
20-21B						23.50		
23-24	4.580	7.490		260	654	23.28	0.35	
26-27	4.975	7.474	31.6	532		23.05	0.26	
29-30	5.480	7.443		483		22.43	0.26	9.28

31/3/83

Dep (cm)	Alk meq/l	TCO2 mM	PO4 µM	H2S µM
0.0		2.18		
0-0.5	3.354	3.69	11.06	bd
0.5-1	3.129	3.61	27.5	
1-1.5	3.002	3.52	17.4	bd
1.5-2	3.022	3.25	33.6	bd
2-2.5	3.116	3.55	48.0	bd
2.5-3	3.012	3.47	44.8	bd
3-3.5	3.133	3.39	43.6	bd
3.5-4	3.234	3.45	40.0	5.95
4-5	3.006	3.32	35.7	6.27
5-6	3.446	3.57	40.1	9.31
6-7	3.465	3.49	36.3	27.9
8-9	3.479	3.39	32.2	bd
10-11	3.686	3.67	39.3	13.8
12-13	3.653	3.87	50.7	129
14-15	3.813	3.77	36.6	164
16-17	3.898	3.77	27.7	129
18-19	4.103	4.25		240
23-24	4.211	4.13	30.6	284

8/6/83

Dep (cm)	Alk meq/l	PO4 µM	H2S µM	Mn µM	Fe µM
0-0.5	2.929	13.6		73.1	21.4
0.5-1	2.996	26.3		65.3	3.00
1-1.5				65.9	10.0
1.5-2	3.332	42.3		29.6	16.1
2-2.5	3.217	43.0		14.9	54.5
2-2.5	3.389	46.6		8.80	15.3
3-3.5	3.367	42.8		7.09	2.17
3.5-4	3.297	47.1	4.20	5.02	6.44
4-5	3.551	42.8	15.3	3.94	6.09
5-6	3.654	39.6	24.4	2.50	2.53
6-7	3.487	33.2	77.9	1.87	
7-8	3.547	36.6	45.8	1.51	0.75
8-9	3.675	30.1	91.5	1.51	
9-10	3.593	33.9	76.1	0.88	
14-15	3.682	28.7	48.5	0.53	
20-21	3.656	27.0	54.3	0.79	

7/9/83

Dep (cm)	Alk meq/l	TCO2 mM	PO4 µM	H2S µM	SO4 mM	Mn µM	Fe µM
0.0	2.238		2.06				
0-0.5	3.060	3.31	70.2		23.8	58.1	332
0.5-1	3.053	3.46	111		22.9	41.6	286
1-1.5	3.440	3.76	139	bd	22.7		
1.5-2	3.770	4.04	158	2.42	22.7	17.2	213
2-2.5	3.950	4.19	121	bd	23.0		
2.5-3	4.668	4.79	131		22.5	11.5	55.3
3-3.5	4.630	4.65	108	5.57	22.7	11.7	63.1
3.5-4	4.727	4.62	101	34.8	22.5		
4-5	4.823	4.84	82.6	99.1	22.0	5.99	9.35
5-6	4.900	4.89		131		2.73	1.11
7-8	4.183	4.09	45.2	196	23.2	1.55	
9-10	4.060	4.07	53.0	222	23.0	1.55	34.9
13-14	3.437	3.38	43.4	180	23.1		5.15
17-18						1.37	1.26
21-22	4.390	4.23	40.1	338	22.8		0.94
27-28	4.871	4.80	38.5	435	22.8	0.24	0.61
27-28B					23.2		
33-34				522	22.7		0.61

16/12/83

Dep (cm)	Alk meq/l	TCO2 mM	PO4 µM	H2S µM	Mn µM	Fe µM
0.0	2.218		2.30			
0-0.5	2.444	2.50	9.70	bd	11.1	26.5
0.5-1	2.649	2.63	19.0	bd	9.82	32.0
1-1.5	2.621	2.73	23.4	bd	10.4	35.9
1.5-2		2.66	33.2	bd	10.4	27.8
2-2.5	2.613	2.69	30.2	6.78	9.91	55.3
2.5-3	2.829	2.78	43.1	7.33	8.34	34.0
3-3.5		2.80	34.5	4.40	6.51	21.0
3.5-4	2.807	2.77	32.5	9.35	5.99	12.6
4-5	2.889	2.82	33.0	20.5	2.86	0.94
6-7	2.796	2.83	25.6	38.9	0.94	0.29
8-9	2.868	2.73	20.8	30.6	0.42	bd
10-11	2.897	2.79		42.4		
15-16	2.847	2.84	16.3	42.4	0.33	1.91
20-21	3.22	3.24	21.6	118		1.26
25-26	3.841	3.70	74.5	29.5		0.29

26/3/84

Dep (cm)	Alk meq/l	TCO2 mM	PO4 µM	H2S µM	Mn µM	Fe µM	Ni nM	Cu nM	Co nM
0.0	2.193	2.07	0.59						
0-0.5	3.125	3.20	3.56	bd	68.9	3.50	40.7	15.1	28.5
0-0.5B							39.2		27.3
0.5-1	3.056	3.19	6.72		64.3	50.7	28.6	5.44	24.2
1-1.5	2.888	3.24	16.6		24.2				
1.5-2	2.701	3.28	26.0	bd	17.6	191	10.9	bd	13.6
1.5-2B									8.70
2-2.5	2.787	3.43	29.9	bd	8.03	237	17.0	10.6	6.90
2-2.5B								11.3	
2.5-3	3.383	3.78	36.3		7.09	176	bd	bd	
3-3.5	3.194	3.53	36.4	5.49	6.82	95.9	bd	3.93	3.80
3.5-4	3.457	3.62	41.2	9.88	6.56	108	bd	5.44	bd
4-5	3.616	3.79	42.5	12.9		43.4		3.29	
7-8	3.871	3.78	43.8	118	1.69	3.46		bd	
10-11	3.917	3.69	33.5	191	0.78	bd	15.2	bd	bd
13-14			29.4	220	0.55	0.84			bd
17-18		3.80		246	0.28	bd	14.0	bd	
22-23	4.229	4.28		332	bd	bd			bd

20/6/84

Dep (cm)	Alk meq/l	TCO2 mM	PO4 µM	H2S µM	Mn µM	Fe µM	Ni nM	Cu nM	Co nM
0.0	2.180	2.080	1.70		0.076		19.8	5.42	7.00
0.0B	2.177	2.10	2.20				15.6	5.11	3.80
0-0.5	1.882	3.28	10.5	bd	40.4	120	23.1	2.76	18.6
0.5-1	2.587	3.74	43.2	bd	15.9	661	35.4		8.60
1-1.5		3.72		bd	14.8	658	10.8	bd	9.60
1.5-2	2.771	4.30		3.90	12.9	596	9.10	bd	6.40
2-2.5	3.320	4.88	59.0	bd	13.8	578	12.4	3.02	
2.5-3	4.349	5.33	80.4	4.00	9.64	232	bd		8.20
3-3.5	5.224	5.47	111	4.30	9.30	69.6	9.10	bd	8.00
3.5-4	5.683	6.09	108	6.30	6.01	42.8	7.50	bd	6.00
4-5	5.181	5.41	75.2	15.6	5.93	83.8	12.6	bd	9.20
6-7	5.232	5.49	67.8	75.1	bd	bd	10.2	bd	5.50
6-7B									bd
8-9	4.763	4.77	50.2	151	1.12	bd	14.2	bd	4.70
10-11	4.401	4.34	40.1	89.7					
11-12	3.972	4.03		150			16.1		4.00
13-14	3.798	3.82	33.4	161					
15-16	3.49	3.55	28.9	111	0.54		12.1	3.86	bd
18-19		3.68	48.4	55.5	0.43		17.7	bd	
22-23	3.658	3.56	28.7	199					
25-26	3.808	3.90	32.3	178					

Chapter IV

Ion Migration Experiments

Introduction

In Chapter 2, transport parameters describing particle and solute mixing at the Buzzards Bay site were derived from distributions of naturally occurring uranium-series radionuclides in quasi steady-state. In Chapter 3, these results were combined with measurements of the pore water concentrations of several first transition series metals to evaluate the degree to which metals reaching the sediment surface in particulate form are returned to the overlying water column during early diagenesis. The ability of the sediments to recycle the various metals was found to depend on the depth relative to the sediment/water interface at which the metals dissolve during early diagenetic reactions, on solubility controls of dissolved metal concentrations, and on the cycling of metals between particulate and dissolved forms within the sediment column.

In this chapter, the effects of the chemical properties of the metals on their transport are studied directly, through the use of radiotracer experiments. These experiments provide information on the solid:solution partitioning of Mn, Fe, Co, and Ni, which is related to their solubility in reducing sediments' pore waters and to the sorption

properties of sediment particles. They provide a means of directly testing the importance of particle and solute mixing to the distributions of metal tracers with variable solid:solution partitioning. The experiments also extend the determinations of particle mixing obtained from excess ^{234}Th by allowing measurements of particle mixing processes on shorter time scales and averaged over smaller areas of sediment than is possible using steady state distributions of an isotope with a 24 day half-life.

The radiotracer experiments were carried out in situ at the Buzzards Bay site described in the previous chapters. In these experiments, ^{54}Mn, ^{59}Fe, ^{60}Co, and ^{63}Ni were injected through a tracer release probe directly into the reducing sediments. Mn, Co, and Ni were introduced in dissolved form; Fe was introduced as freshly precipitated Fe(III) hydroxides. The experiments differ from previous radiotracer experiments carried out in nearshore sediments in that the metals were introduced directly into the sediments rather than into the water overlying the sediments (Luedtke & Bender, 1979; Adler, 1981); in this way, the experiments mimic more closely the way in which early diagenesis releases dissolved metals into the sediment column. Thus, because the results of radiotracer experiments can depend strongly on the mode of introduction of the tracer into the experimental system, these experiments complement previous studies of radiotracer mobility in coupled seawater/sediment systems.

Methods

Probe Design

The probe through which tracers were released into the sediments is illustrated in Figure IV.1. It is made of three parts: a 3/8" diameter by 14" long PVC rod which contains the release point and the chamber within which the tracer spike is held at the start of an experiment (the "source chamber"); a 1/4" i.d., 1/2" o.d. acrylic tube which fits over the upper 5 cm of the PVC rod, is sealed at both ends, and is filled with seawater which acts to transfer pressure exerted on a syringe to a piston at the top of the source chanber; and a disposable plastic syringe, connected to the top of the acrylic tube via a length of small-bore teflon tubing. Tracers were released into the sediments through 4 .016" diameter holes spaced at 90° to each other around the cylindrical probe. The holes meet at the center of the probe, from where they are connected to the source chamber by a 1" long x .030" diameter hole.

Experimental Method

The probe was prepared to begin an experiment by placing a small excess of the tracer-containing solution (the "source solution") into the source chamber, inserting the piston (a short piece of the rubber-tipped plunger from a 1cc syringe) into the source chamber, and expressing the excess solution through the release holes to remove air bubbles from the release mechanism. The release holes were flushed with

Figure IV.1

Tracer Release Probe

Figure IV.1

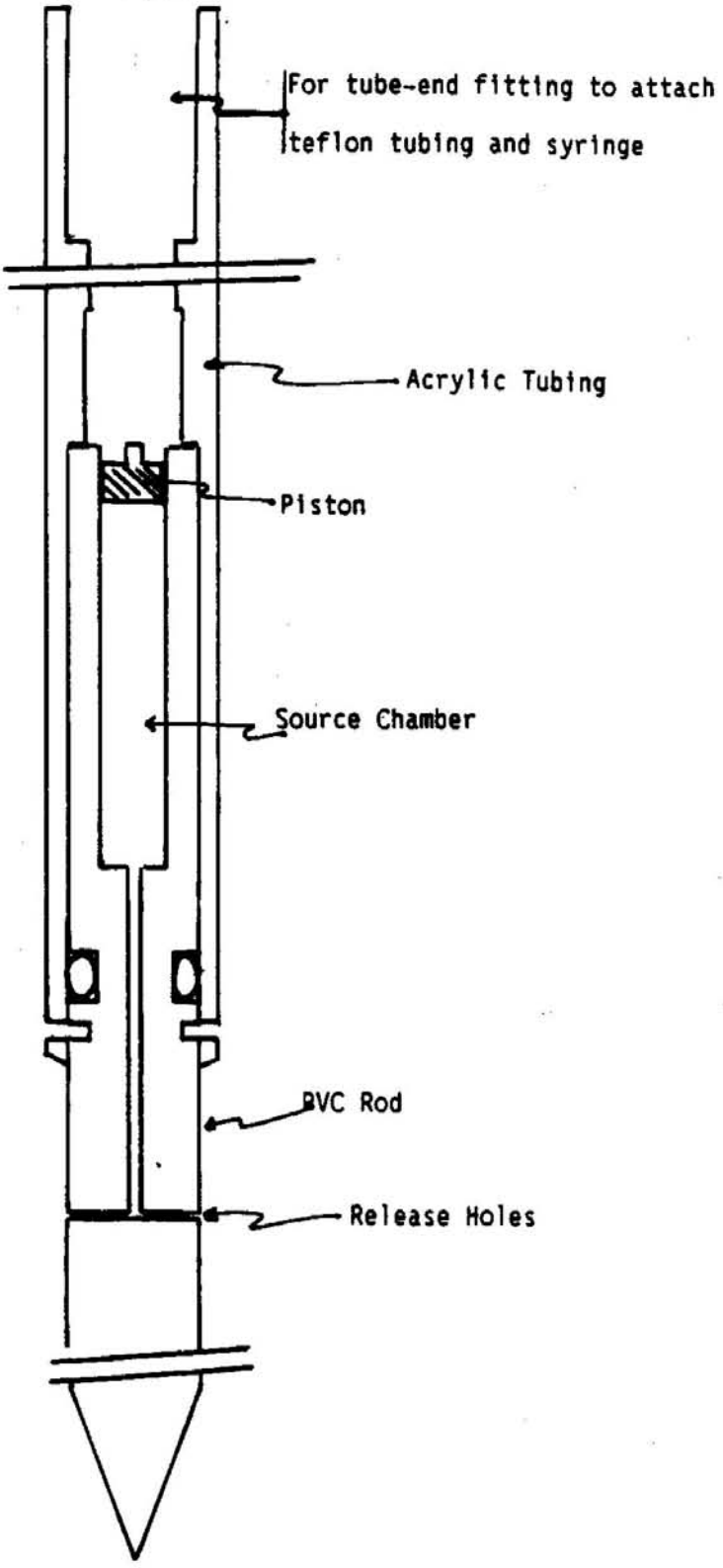
For tube-end fitting to attach
teflon tubing and syringe
Acrylic Tubing
Piston
Source Chamber
PVC Rod
Release Holes

seawater and the sides of the PVC rod were wiped clean with a moistened tissue to remove traces of the source solution from the probe exterior. Then, the acrylic tube was put over the PVC rod and fixed in place by pins inserted through the side of the tube into a groove in the PVC rod. The acrylic tube was filled with seawater, and teflon tubing and syringe were attached to the top of the assembled probe.

Probes were inserted into the sediments, and the source solution injected, by SCUBA divers. First, a tripod was placed in the sediments. A device fixing a 1/2" i.d. aluminum tube perpendicular to the sediment/water interface and a few inches above it was placed on the tripod; a probe was inserted vertically into the sediments, with release point at the desired depth, through this tube (the insertion mechanism was designed by L. Ball, WHOI). The source solution was injected into the sediments by exerting pressure on the syringe attached to the top of the probe. A release was judged successful if no obvious disturbance of the sediments was observed during the release and if no bubbles were seen escaping from the sediments in the area surrounding the probe. Following a successful release, teflon tubing and syringe were removed by cutting the tubing at the top of the probe. The probe and tripod were left in place. At the end of an experiment, a guide for inserting a 20 cm diameter core liner was placed on the tripod; the sediment surrounding the probe was cored with the probe in place. Cores were taken by the method described in Chapter 2.

Sampling Method

The heterogeneity of nearshore sediments inhabited by an abundant macroinfauna is well known (Aller, 1982); therefore, averaging over as many tube and burrow structures as possible in each sample taken is important for obtaining smooth profiles. The probe design adopted was chosen with this sampling feature in mind. Its cylindrical symmetry allows samples to be taken in rings of 0.5 cm vertical thickness and 0.5 cm radial thickness around the probe so that tracer activity averaged over a maximum area of sediment at each distance from the release point could be obtained.

Samples were taken by extruding a 0.5 cm vertical layer of sediment, then sampling each layer at 0.5 cm or 1 cm intervals measured radially from the probe. The vertical thickness of each layer was somewhat variable, and was measured precisely, using the probe as a fixed reference, after sampling each layer. For sampling each radial sediment layer, a rigid, rectangular piece of plexiglass was used as a guide. It had a hole at $\rho = 0$ (ρ = radial distance from the probe) just large enough to fit over the probe, and holes spaced at 0.5 cm intervals along it into which thin needles capable of cutting the sediment could be inserted. A ring was cut by placing a needle at the desired radial position, placing the sampling tool over the probe, and rotating it through 360°.

Samples were put in vials and stored at 4°C for later analysis. When samples were taken for ^{54}Mn distribution coefficient measurements (experiments 1C and 3C), they were flushed thoroughly with nitrogen

after being put in centrifuge tubes. They were centrifuged immediately, and pore water samples were removed for ^{54}Mn analysis.

Analytical Procedures

Because sample size was quite variable and because the ß-emitting isotope, ^{63}Ni, was included in the experiments, wet chemistry was necessary to prepare samples for γ and ß counting. Briefly, the analytical procedure consisted of five steps.

(1) Samples weighing 0.5-5gm were routinely leached in hot 8N HNO_3 following the addition of 5 mg of Mn, Ni, and Co carriers. Dried sediments were first leached for 1 hr with cold 8N HNO_3 in the sample vials (this procedure broke up the dried sediment into small particles and removed sediment from vial walls), then transfered quantitatively to beakers for hot 8N HNO_3 leaching. They were leached twice for 4 hours with 80 ml 8N HNO_3, and the leachates were combined. Leaches of a few samples with hot concentrated HCl after nitric acid leaching showed no additional ^{54}Mn, ^{59}Fe, or ^{60}Co activity; therefore, it was assumed that negligible amounts of activity remained in the sediments after 8N HNO_3 leaching.

Different leach procedures were tried for experiments 1C and 3C (these were short experiments, 4 days and 11 days long, respectively). Acetic acid leaches have been proposed as a means of obtaining a measure of surface-adsorbed and carbonate-fraction metals in deep-sea sediments (Lyle et al., 1984); it was felt, given the short duration of

experiments 1C and 3C, that tracers might be accessible to a 25% acetic acid leach. Thus, a group of samples from these experiments was leached with 25% acetic acid. It was found, after subsequent leaching with 8N HNO_3, that about 99% of ^{54}Mn, 75% of ^{59}Fe, 80-90% of ^{60}Co, and 85% of ^{63}Ni were released to solution by acetic acid leach (Table IV.1). Thus, in calculating ^{59}Fe, ^{60}Co, and ^{63}Ni activities for those samples which were leached only with 25% acetic acid, a multiplicative correction based on these leach experiments was applied; this correction is listed as "L" in Table IV.1. The error introduced in activities calculated by this procedure is estimated at 2-6%. No correction was applied for ^{54}Mn.

(2) Following leaching, hydrolyzable metals were precipitated with NaOH. The precipitates were washed twice with distilled, deionized water and taken up in 9N HCl. They were evaporated to about 500µl of 6N HCl; then 15 ml absolute ethanol were added to each sample. At this point, a yellow solid was often present in the sample; this solid turned white within minutes as Fe dissolved in the 0.2N HCl/97% ethanol solution. The entire sample, including solids, was loaded on an anion exchange column.

(3) The anion exchange procedure was adapted from the procedures of Fritz & Pietrzyk (1961) and Kraus & Moore (1953). Using this procedure, Ni, Mn, Co, and Fe can be collected in separate fractions. For this study, it was used primarily to separate Ni from the other transition metals; in addition, a separate Fe sample was often collected because, in samples

Table IV.1

Acetic acid vs HNO_3 leaches

A comparison of results obtained by leaching sediment samples with 25% acetic acid and with hot 8N HNO_3. F is the fraction of total tracer remaining in the solid phase after leaching with 25% acetic acid,

$$F = A_{HNO3}/(A_{HOAc} + A_{HNO3})$$

(A_{acid} = activity obtained from the acid leach)

L is the correction factor applied to samples leached only with acetic acid, so that

$$A_{total} \simeq (A_{HOAc})\bullet(L)$$

$$L = 1/(1-F)$$

Element	Experiment #1C		Experiment #3C	
	F	L	F	L
Fe	.260±.012 (2)	1.35±.02	.241±.047 (4)	1.32±.08
Co	.099±.023 (4)	1.11±.03	.195±.038 (4)	1.24±.06
Ni*#	.156±.026 (3,3)	1.19±.04		
Mn	.010±.003 (4)	-	.018±.010 (4)	-

The values in parentheses are the number of samples used to calculate the averages shown.

* The Ni average includes 3 samples from each experiment; all were averaged together since they were quite scattered, but each experiment had a similar mean value.

One sample was excluded from the average. For an unknown reason, this sample gave F = .571

with high ^{60}Co activities but low ^{59}Fe activities (these were primarily samples in which a large fraction of the initial ^{59}Fe had decayed away), the ^{60}Co 1173 and 1333 keV γ rays interfered with counting of the major ^{59}Fe γ rays at 1099 and 1292 keV. The anion exchange procedure is outlined in Table IV.2A; the separations and yields obtained for a representative sample, a 1.00 gm sediment sample to which 10 mg Ni, Mn, and Co carriers had been added, are shown in Table IV.2B.

(4) ^{63}Ni was prepared for liquid scintillation counting using a method developed by L. Ball (WHOI). The Ni fraction, a HCl/alcohol solution, was taken to near dryness; 9N HCl was added, and the fraction was taken to near dryness again. Then, it was taken to a volume of 15 ml with 0.5 N HCl. Following precipitation with NaOH and washing of the precipitate with distilled, deionized water (DDW), the precipitate (consisting of Ni, Mg, and Ca hydroxides) was dissolved by adding 0.5 ml of glacial acetic acid. DDW was added until the sample was 4 ml, and the sample was transfered to a scintillation vial using 15 ml of Instagel scintillation cocktail (Packard Instruments). Samples were counted on a Beckman LS 100C liquid scintillation counter using the ^{14}C window; counting efficiency was 52.5±1.8 (2σ)%, and background counts were about 25 cpm.

Two procedures were used to prepare samples for γ counting.The first procedure was used for samples in which ^{63}Ni activity was not determined. These samples were prepared for counting directly after leaching. They were taken to a small volume of concentrated HNO_3 and transfered to 50 ml centrifuge tubes. The samples

Table IV.2A

Anion Exchange Procedure

Column: 20 ml (11 cm height x 1.5 cm length) AG1-X8, 200-400 mesh (Biorad)

(1) Conditioning: 25 ml 0.2N HCl/93% EtOH
15 ml 0.2N HCl/97% EtOH
(2) Sample on: 15.5 ml 0.2N HCl/97% EtOH
(3) Ni elution: 2 x 20 ml 0.2N HCl/96% MeOH
(4) Mn + Co elution: 50 ml 4N HCl (10 ml + 2 x 20 ml)
(5) Fe elution: 50 ml 0.5N HCl (10 ml + 40 ml)

Table IV.2B

Separations and Yields

The separations and yields obtained using the anion exchange procedure for a 1.00 gm dry wt. Buzzards Bay sediment sample to which Ni, Mn, and Co tracers had been added. After leaching the sample with hot 8N HNO_3, the leachate contained:

Fe	27.5 mg
Mn	10.3
Co	10.0
Ni	10.0

The values in the table are the % of the total amount of the metal (each metal has a row in the table) found in each fraction collected (the columns in the table)

	Fraction		
Element	Ni	Mn + Co	Fe
Ni	100	0.03	0
Mn	0.04	98	0.002
Co	0.03	100	0.02
Fe	0.01	0.002	84.7

were evaporated to a volume of 2.5 ml in a water bath. Each sample was placed in a holder designed to enable precise placement of samples on Ge(Li) detectors, thus minimizing errors due to variable counting geometry. Counting efficiency was determined by spiking already-counted samples with the isotopes analyzed (^{54}Mn, ^{59}Fe, ^{60}Co) and recounting them: in this way the variability in counting efficiency included errors in sample and counting geometry. Efficiencies are reported in Table IV.3.

The second method for preparing samples for γ-counting was applied to samples which had undergone anion exchange separation, and for which there were separate Fe and Mn + Co fractions. Each fraction was transfered to a 50 ml centrifuge tube, Fe fractions with 0.5N HCl and Mn + Co fractions with dilute HNO_3. Samples were evaporated to 0.5 ml in a water bath. Efficiencies were determined as for the 2.5 ml samples, by adding spikes to already-counted samples, then recounting them.

Yields were determined by atomic absorption spectrometry. Ni and Co yields were measured against the Ni and Co carriers added to the samples at the start of the procedure; Fe and Mn yields were determined by comparing the Mn and Fe contents of samples immediately after leaching and after counting.

Activity levels measured in these experiments varied over a large range: about two orders of magnitude for ^{54}Mn and two to three orders of magnitude for ^{59}Fe, ^{60}Co, and ^{63}Ni. Analytical errors were the sum of errors due to counting statistics, counter calibration, and yield measurement errors. The error from the last two sources is

Table IV.3

Ge(Li) Detector Efficiencies

Samples were counted on two coaxial Ge(Li) detectors (Canberra): 52 mm diameter, 18% relative efficiency, 2 keV resolution. Efficiencies for both detectors are shown, for both 0.5 and 2.5 ml sample volumes.

Counter #	Mn-54 (834 keV)	Fe-59 (1099 keV)	Co-60 (1173 keV)
A. 2.5 ml samples			
1	.0196±.0002	.00801±.00013	.0104±.0002
2	.0173±.0010	.00681±.00027	.00974±.0004
B. 0.5 ml samples			
1	.0251±.0006	.0104±.0006	.0139±.0006
2	.0222±.0005	.00900±.0002	.0125±.0003

estimated at 5%; counting errors ranged from 2% for the samples with highest activity to 20% for the lowest activity samples. Thus, the range of analytical errors is about 7-25%.

Samples with low but measurable activity occasionally occurred at larger distances from the release point of an experiment than could be explained by processes dominating the tracer distributions. The activity in these samples may have been due to contamination problems caused by the large range of activities measured. These samples were excluded from apparent diffusion coefficient calculations because of the uncertainty in the origin of their activity levels and because they had an unduly large effect on the least-sqquares fits to the data.

Procedure for ^{54}Mn Distribution coefficient Measurement

Distribution coefficients for ^{54}Mn between solid and solution phases were measured as part of experiments 1C and 3C, the 4-day and 11-day experiments. The sediments were sampled as usual, but several samples (13 for 1C, 11 for 3C) were placed in 50 ml centrifuge tubes, flushed thoroughly with nitrogen, and centrifuged immediately. Using this procedure, sediments were exposed to air for about 15-20 minutes before Mn samples were purged of oxygen and sealed in nitrogen-filled tubes; thus, some dissolved Mn activity may have been lost to the solid phase through oxidation/adsorption. The magnitude of this effect is not known, but based on reports that sediment samples can be handled briefly in air without loss of dissolved Mn from the pore water (Emerson et al., 1984), the error is believed to be small. An aliquot of pore water was

removed to another centrifuge tube for ^{54}Mn counting. The following measurements were required to determine distribution coefficients:

A_W = activity in the pore water sample

A_R = activity remaining in the sample after removal of pore water

W = total sample weight

W_R = weight remaining after removing pore water sample

W_D = dry weight

Then, the following parameters could be calculated:

(1) dpm ^{54}Mn/gm pore water = $A_{WG} = A_W/(W-W_R)$

(2) Total ^{54}Mn activity in the pore water
$= A_{TW} = A_W \times (W-W_D)/(W-W_R)$

(3) dpm ^{54}Mn in solids/gm of dry solids
$= A_D = (A_W + A_R - A_{TW})/W_D$
(the contribution of sea salts to the dry weight was neglected in this calculation)

(4) Gravimetric distribution coefficient
$= K_{GRAV} = A_D/A_{WG} =$ ^{54}Mn/gm dw ÷ ^{54}Mn/gm pore water

Because very small pore water samples were obtained for these measurements (0.13 - 1.1 gm), the samples could not be filtered. Thus, there is the possibility of overestimation of the activity of ^{54}Mn in solution. However, from the assumption that any ^{60}Co present in the pore water is due to particulate matter, it can be shown that the possible contribution of particulate matter to measured ^{54}Mn activity is within the uncertainty in the determination of pore water ^{54}Mn (the maximum particulate ^{54}Mn contribution is 4-7% of pore water ^{54}Mn).

Because sample volumes for these measurements varied through a large range, Ge(Li) detectors had to be calibrated as a function of sample volume. The calibration curves were nonlinear, but could be fit quite accurately by a second-order equation.

Source Solutions

Ideally, in an experiment to study transport of metals under natural conditions, isotopic tracers would be added to the natural system in exactly the form in which the stable metals exist there. When the natural system is the reducing pore waters of nearshore sediments, the ideal experiment is impossible: the preservation of reducing pore waters -- in particular, the exclusion of O_2 and retention of H_2S and CO_2 -- while at the same time subjecting them to the handling necessary to introduce radiotracers, load them into a tracer release probe, and transport them to the experimental site is virtually impossible.

In this study, pore waters were approximated by local bottom waters to which radiotracers were added. To prepare source solutions, local bottom water, with its pH adjusted to 2.0, was added to a small amount of HCl solution containing the required amounts of ^{59}Fe, ^{54}Mn, ^{60}Co, and ^{63}Ni (all as +II chlorides, except Fe as +III chloride); in some cases (experiments 1C and 3C), ^{36}Cl (as HCl) was also present. Then, the pH of the spiked bottom water solution was adjusted to 5.0-5.5. Source solutions were generally used after an equilibration period of 24-48 hours; the source solution for experiment 3B was allowed to equilibrate for 30 days (long equilibration times were impractical

because of the 45 day half-life of ^{59}Fe). Raising the pH of the source solution to pH 5 caused a substantial fraction of the ^{59}Fe in the solution to precipitate. To quantify this effect, aliquots of some solutions were filtered through 0.2 μm and 0.4μm filters, and the activities of the γ-emitters, ^{59}Fe, ^{54}Mn, and ^{60}Co, were compared in filtered and unfiltered solutions (Table IV.4). ^{54}Mn and ^{60}Co were present primarily in dissolved form at pH 5, but only 7% of the ^{59}Fe activity passed through a 0.2 μm filter. Since these filtration experiments were carried out immediately before loading the unfiltered source solutions into probes (about 2 hours before deployment), it was concluded that ^{54}Mn and ^{60}Co were introduced into pore waters as dissolved Mn(II) and Co(II), while ^{59}Fe was introduced as freshly precipitated Fe(III). Filtration experiments were not performed for ^{63}Ni.

The perturbation of conditions within the sediments due to the addition of 250μl of source solution was minimal. If the bottom water used contained O_2 at 200μmol/l, introduction of 250μl implies the addition of about 50 nmol of O_2 to the sediments; and 250μl of seawater at pH 5 contains only about 2.5 neq of H^+. Compared to the amounts of reduced sulfur and alkalinity in the sediments, both of these additions are very small. The concentrations of Na^+ and Cl^- in the source solutions were significantly greater than those in local pore waters. From the amount of NaOH required to bring the solutions to pH 5, it is estimated that the Na^+Cl^- concentration was 1.5–2 M. While this may mean that codiffusion of Na^+ and Cl^- affected the ^{36}Cl

Table IV.4

Source Solution Filtration Experiments

Each Entry in the table is the ratio of activity in the filtered source solution to the activity in the corresponding unfiltered source solution. Experiments were carried out using 0.2μm filters at pH 2 and 5 and at pH 5 using a 0.45μm filter.

pH	Activity Ratio, filtered/unfiltered		
	Mn-54	Fe-59	Co-60
A. 0.2 μm filters			
2.0	1.06±.07	1.06±.10	1.05±.07
5.1	0.96±.07	.067±.034	1.05±.07
B. 0.45 μm filter			
5.0	0.91±.02	0.74±.03	0.94±.04

diffusion rate, codiffusion should not have affected the diffusion rates of the trace components, Fe, Mn, Co, and Ni.

An important consideration is the amount of each of the stable metals added to the system with the radiotracers. These amounts have been inferred from the specific activity of the isotopes listed by the suppliers; they are shown in Table IV.5A. While the amounts added were always small compared to the amounts present in an equal volume of sediment, the dissolved concentrations in the source solution were greater than ambient pore water concentrations for Co (by a factor of 20-25) and for Ni (by a factor of 4000). The dissolved Mn concentration in the source solution was always less than the pore water Mn concentration, by a factor of 5-50; although the Fe in the source solution was not dissolved, the total Fe concentration in the source solution was similar to the dissolved Fe concentration in ammbient pore water. Table IV.5B shows the concentration of dissolved metals in the pore waters where the source solutions were introduced. The concentrations were determined on cores taken at the study site during the course of the radiotracer experiments.

Because the time for equilibration of the tracers added with the ambient labile metal pools depends on the rates of reactions between the metal species present and the size of the labile metal pools, it cannot be evaluated directly. Thus, an important assumption of these tracer migration experiments is that the metals behave similarly to the metals in the natural metal pools. Because Ni, especially, and also Co, were added in dissolved concentrations significantly greater than

Table IV.5A

Stable Metals Introduced With Tracers

The amounts of stable metal introduced with tracers through the tracer release probe. Values are calculated from specific activities given by the suppliers of the isotopes.

Metal	Amount introduced (nmol)	Concentration in source solution(μM)
Mn	0.05	0.20
Fe*	0.36-2.3	1.4-9.2
Co	0.04	0.16
Ni	10	40

* Fe is introduced as a solid (see text)

Table IV.5B

Natural Metal Concentrations in Ambient Pore Waters

Values are estimated from measurements of dissolved metals on cores taken at the study site during the course of the radiotracer experiments

Date	Date	Depth	Mn μM	Fe μM	Ni nM	Co nM
3	3/4-30/4	2.25	8	240	10	7
6	3/4-30/4	7.75	1.7	3.5	15	3
3B	7/5-5/6	4.25	1-5	40	5	3
1C	2/7-6/7	3.25	9	70	9	8
3C	2/7-13/7	3.25	9	70	9	8
Ratio*			.02-.2	.04-2.5	4000	20-25

* Ratio = (conc. metal added)/(conc in ambient pore water)

ambient dissolved concentrations, their observed transport may represent only the short-term supersaturation at the source and consequent precipitation, rather than an equilibrium exchange between solids and solution. These irreversible reactions are less likely to be important for Mn and Fe, which were added in concentrations more representative of ambient dissolved concentrations.

Calibration of Injection Volume

The probe was designed to release 250μl of source solution into the sediments; this volume represents about 30% of the pore water volume in the sample taken closest to the release point (based on a sample of 0.5 cm radial thickness and 0.5 cm vertical thickness, a probe radius of 0.5 cm, and porosity = .75). An experiment was performed to confirm the volume of source solution released. The probe was loaded, by the standard procedure, with a solution of known Na concentration. Then, the probe was placed in a graduated cylinder containing a known amount of distilled water which was stirred with a magnetic stirrer. The probe was allowed to sit for 5 minutes to test for leakage of the source solution (leakage should be more important in a rapidly stirred solution than during an actual release into the sediments). A sample was taken from the graduated cylinder and, after the sample volume was replaced with distilled water, the source solution was injected. After allowing 3 minutes for the injection to become thoroughly mixed into the distilled water, a second sample was taken. Na concentrations were measured by flame atomic absorption spectrometry. Three experiments showed the

injection volume to be 251±3 µl; leakage was 1.5-3% of the injected quantity. A fourth experiment was less successful, as the source chamber was apparently poorly sealed. Leakage was 25% and the injection volume was 188µl. Thus, while improper loading of the source chamber can be a problem (this was an early experiment, and loading techniques were subsequently improved), the injection volume is generally quite precisely controlled.

Initial Tracer Distribution

Because the source solution is injected into the sediments, there is some uncertainty as to its initial distribution: it is this uncertainty which can ultimately limit the the interpretation of the tracer release experiments. Two experiments were performed to determine initial spatial distributions. The first was a laboratory experiment in which an injection (of ^{134}Cs) was made into a sediment core taken the day of the experiment; the core was sampled immediately after the injection was made. The second experiment was a 7-day deployment of a probe at the Buzzards Bay study site, with ^{36}Cl and ^{60}Co tracers injected. The first experiment was performed to test the spread of the tracer away from the release point as a result of the injection; in the second experiment, the inhomogeneity in the initial distribution caused by the release of the tracers through 4 holes spaced around the probe (at a single depth below the interface, from holes at 90° to each other) was investigated.

The results of the first experiment are shown in Table IV.6.

Table IV.6

Initial Distribution Test

Results obtained by sampling a core immediately following a release of ^{134}Cs through the tracer release probe. The release was into the sediment interval lying 5.5-6 cm below the sediment/water interface. The samples are identified by their position relative to the release interval at z_o = 5.5-6, ρ_o = 0-0.5. The positions shown are $z-z_o$, $\rho-\rho_o$.

Position	cpm	cpm/gm	cpm/cpm(0,0)	(cpm/gm)/(cpm/gm(0,0))
0,0	1550	1340	1.00	1.00
0,0.5	85.8	43.6	.055	.033
0,1.0	21.6	5.3	.014	.004
0.5,0.5	30.5	7.8	.020	.006

There was some spread of the tracer injected beyond the first sample interval (0.5 radially and 0.25 cm above and below the release), but the amounts of tracer were small: 5.5% and 1.4% of the tracer inventory in the first radial sample was found in the second (ρ = 0.50, z = 0), and third (ρ = 0.75, z = 0) samples, respectively. The tracer concentrations, normalized to that in the first sample, were .033 and .004. The spread of the tracer in the vertical direction was smaller, with an amount equal to 2% of the first-sample tracer content found in a sample at ρ = 0-1, z = 0.25-0.75.

^{36}Cl and ^{60}Co were released in the second experiment for a 7-day deployment. Results of the experiment are shown in Table IV.7 and in Figure IV.2. They show that there were significant variations in concentration of tracer between samples taken immediately in front of the release holes and samples taken in between the release holes. These inhomogeneities persisted for at least 7 days after the release, and were more important for the less rapidly dispersing tracer. When sample differences were calculated as the difference between the tracer concentrations in front of and between release holes, divided by the mean of the concentrations, the inhomogeneities amounted to 11-40% for ^{36}Cl (compared to 2σ counting errors of 2-5%) and 13-130% for ^{60}Co (relative to counting errors, due to variable sample geometry and to counting statistics, of 10-20%). In practice, these inhomogeneities are smoothed out by sampling complete rings around the probe, so that the average concentration in each interval is measured.

The potential errors due to the finite initial volume of the

Figure IV.2

Initial Distribution Eperiment

Results of a 7-day deployment to determine the inhomogeneity in the initial distribution of tracers injected into the sediments through the tracer release probe. The solid bars mark the activities of the actual samples taken. The samples with higher activities at each depth were taken directly outside the release holes, in the interval 0-0.5 cm from the edge of the probe. The samples with lower activity were taken between the release holes. The dashed bars are the weighted averages of the measured samples.

Figure IV.2

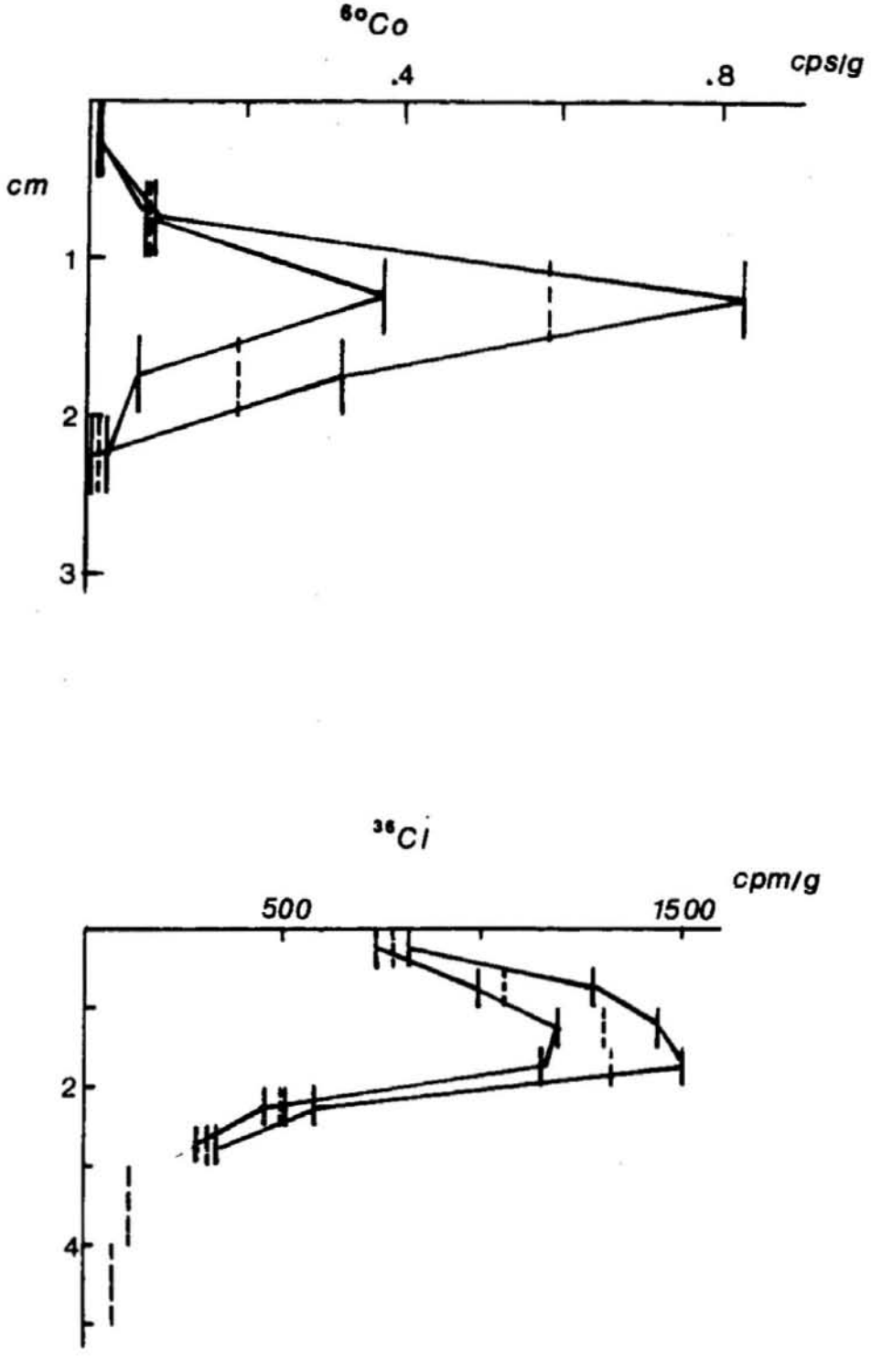

initial tracer distribution and to its inhomogeneity within the sample intervals are reduced as the spread of the tracers at the end of an experiment increases. Thus, in the experiments discussed in this chapter, uncertainties are least for ^{54}Mn distributions, greatest for ^{60}Co and ^{63}Ni; they are greater for the short experiments (1C: 4 days; 3C: 11 days) than for the longer experiments (which were 25-29 days long).

Results

In a total of five experiments, carried out from 3/84 to 7/84, ^{59}Fe, ^{60}Co, and ^{63}Ni were released into the sediments. The data pertinent to the deployments are listed in Table IV.7. The factor which limited the duration of the experiments was active erosion of the sediment surface immediately surrounding the probe, which occurred at average rates of 0.06-0.19 cm/day. In order that the sediment/water interface at the end of the experiments remain approximately representative of the undisturbed interface, experiment duration was limited to a maximum of 30 days. At the end of this period, the interface surrounding the probe remained similar in appearance to nearby sediments (i.e., if a light brown oxidized layer was present nearby, it was also present immediately adjacent to the probe), and the water content of near-surface samples was similar to water contents measured in undisturbed cores, but tended to be somewhat lower (65-70% compared to 70-75%). However, in experiments 1C and 3C, a small depression, a few mm in depth and 0.5-1 cm in radius, was noted immediately surrounding the probe.

The experimental ^{54}Mn, ^{59}Fe, ^{60}Co, and ^{63}Ni distributions are shown in Table IV.8 (Appendix IV.1) and in Figures IV.3 and IV.4. Figure IV.3 shows contour plots of the distributions. The horizontal axis in these plots is ρ, the radial distance from the probe; the edge of the probe lies along the vertical axis. The vertical

Table IV.7

Data Describing to Tracer Release Experiments

The "Release" and "Activity Maximum" columns in the table list the depths relative to the sediment/water interface of the introduction of tracers and of the activity maximum at the completion of the experiment. The difference between these two, divided by the duration of the experiment, gives the erosion rate.

Expt #	Dates	Length (days)	Release (cm)	Activity (cm)	Temp (°C)	Erosion (cm/day)
1C	2/7-6/7	4	3.25	2.5	18	0.19
3C	2/7-13/7	11	3.25	2.2	19	0.10
3B	7/5-5/6	29	4.25	2.5	12	0.06
3	3/4-30/4	27	2.25	0.3	6	0.07
6	3/4-30/4	27	7.75	5.7	6	0.08

Figure IV.3

Ion Migration Experiments: Contour Plots

Contour plots of the ion migration experiments described in Table IV.7. The contour intervals in all the plots are 80%, 60%, 40%, and 20% of the maximum tracer activity. The horizontal axis is ρ, the radial distance from the probe. The vertical axis lies along the edge of the probe, and is z, the distance below the sediment/water interface. The dots mark the centers of the sample intervals in which tracer activities were measured.

Figure IV.3A: Experiment 1C

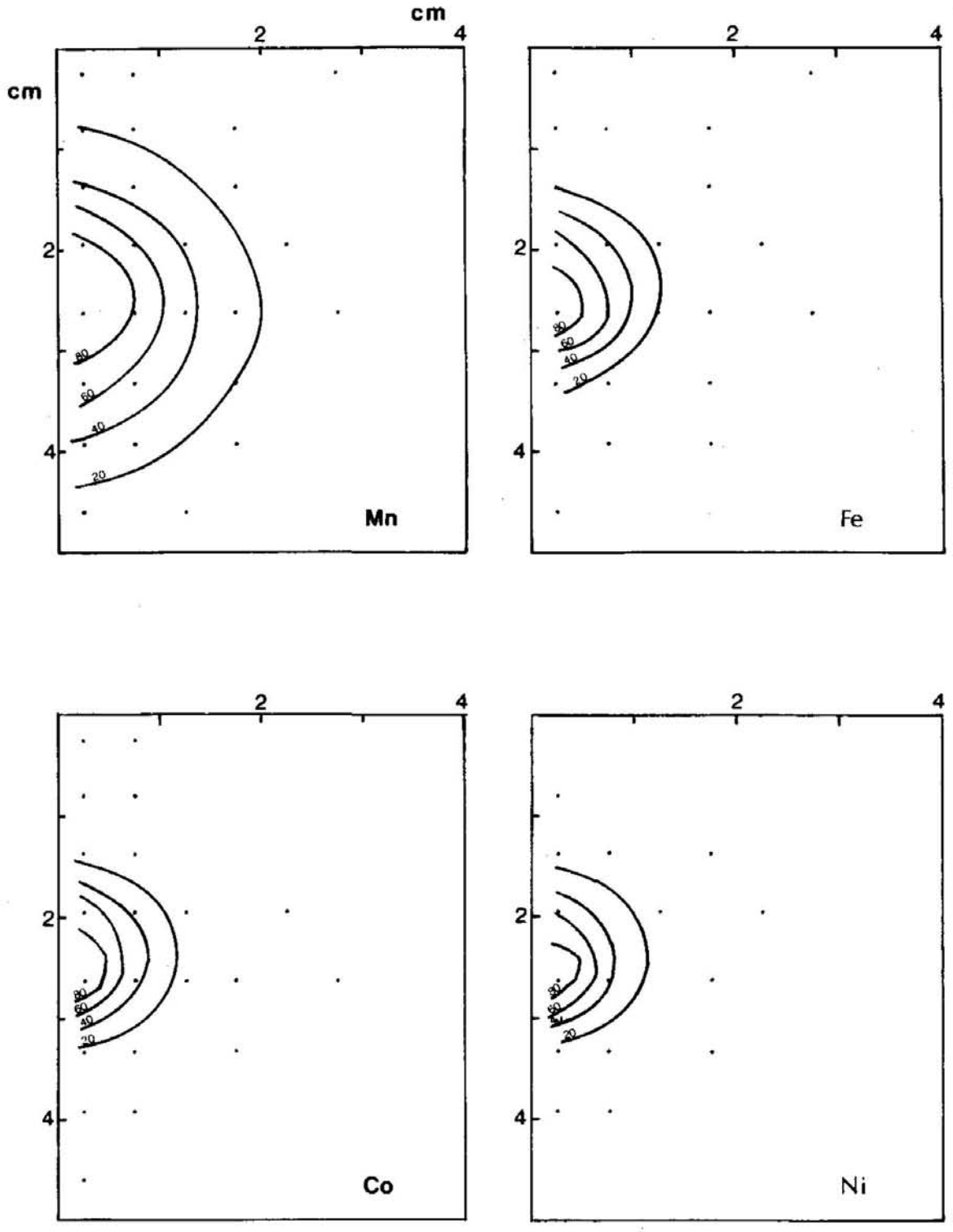

Figure IV.3 B: Experiment 3C

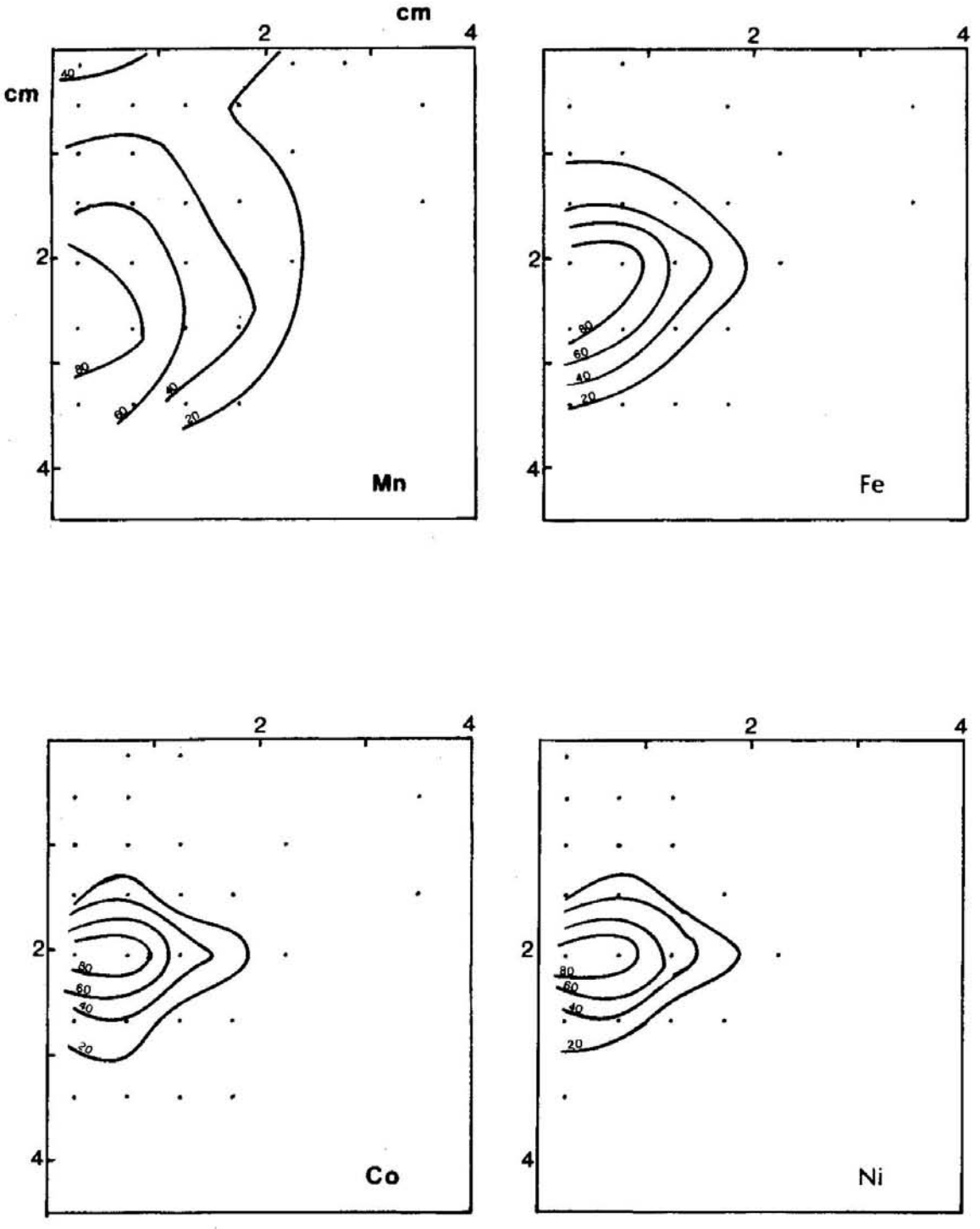

Figure IV.3C: Experiment 3

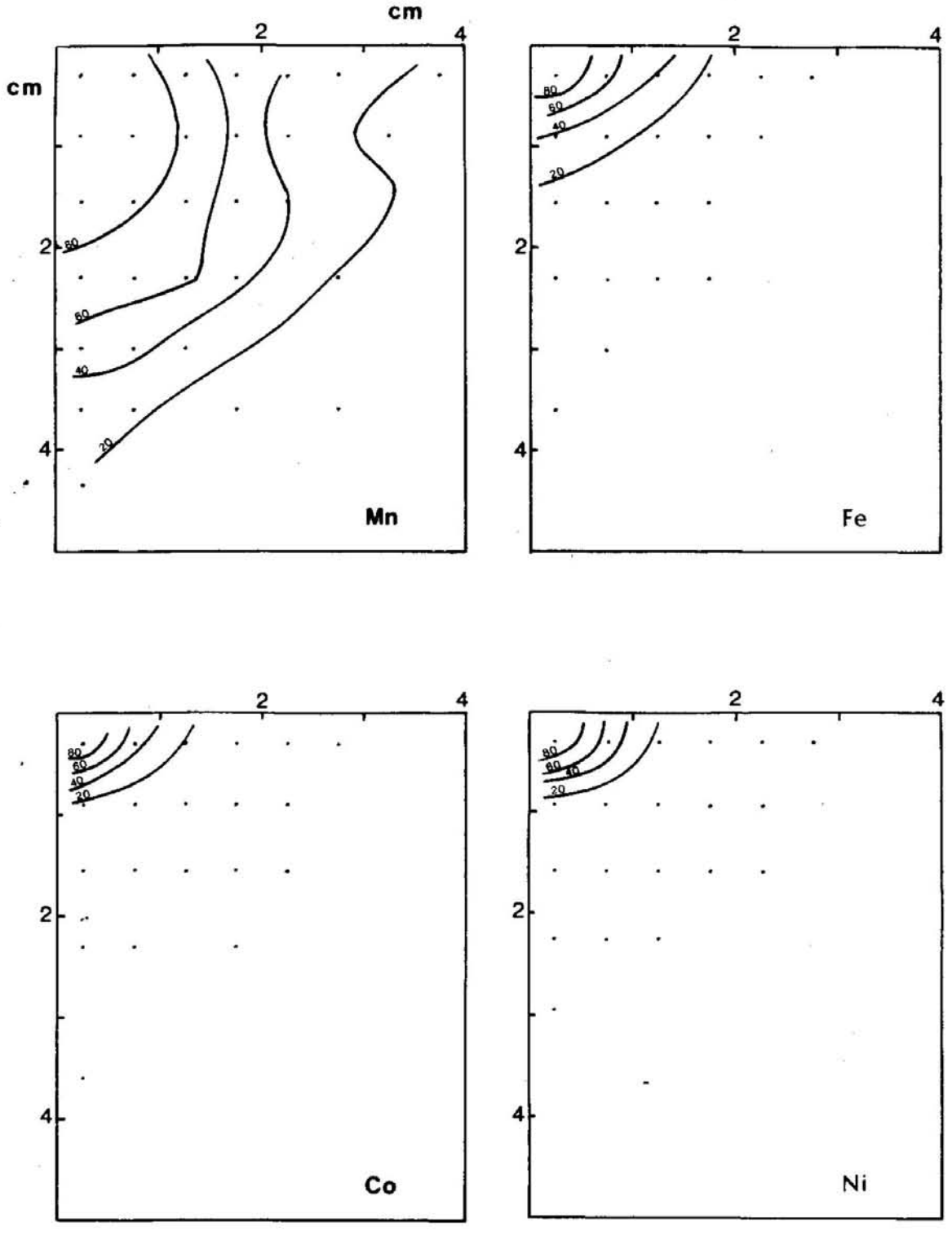

Figure IV.3D: Experiment 3B

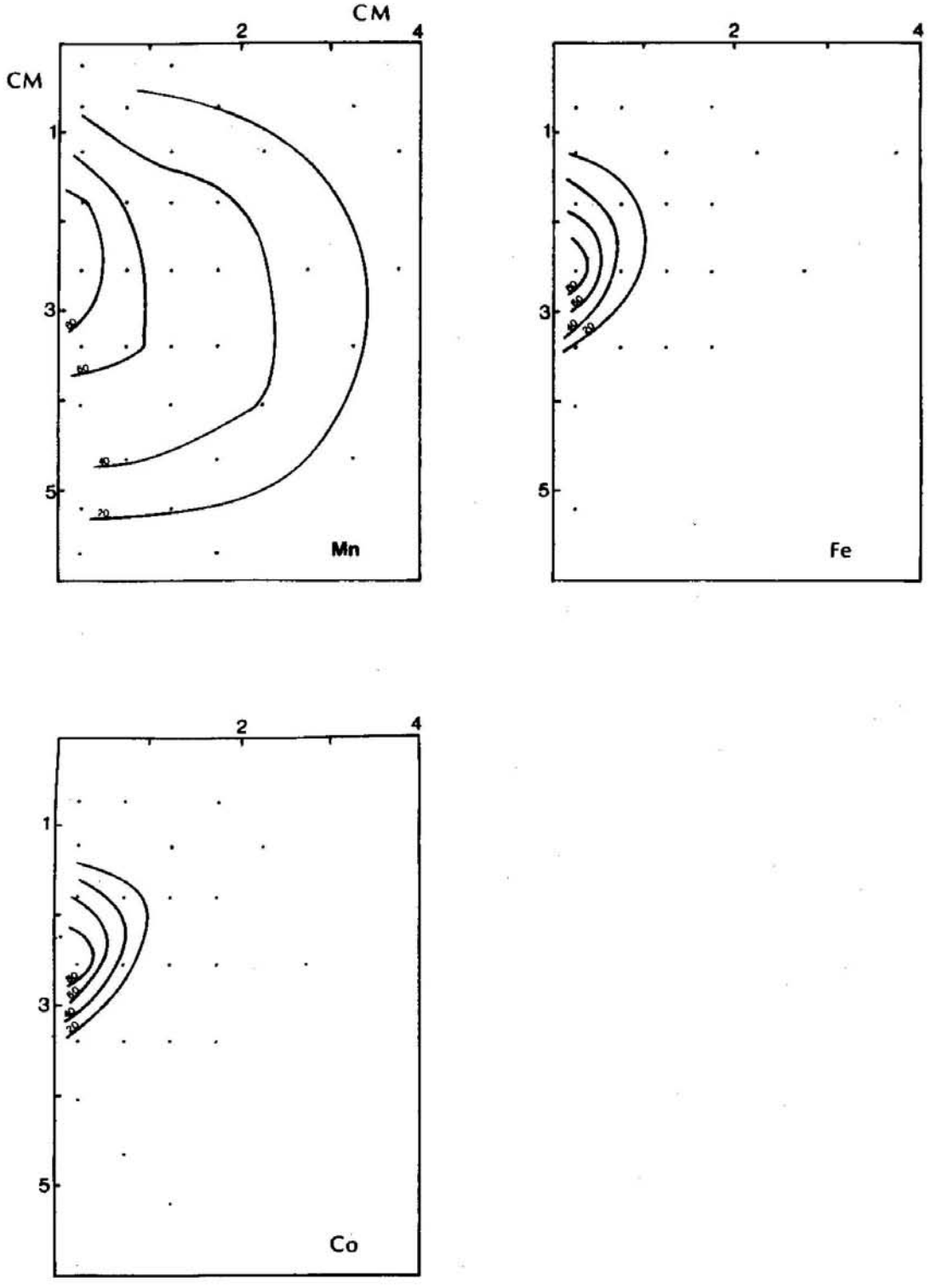

Figure IV.3E: Experiment 6

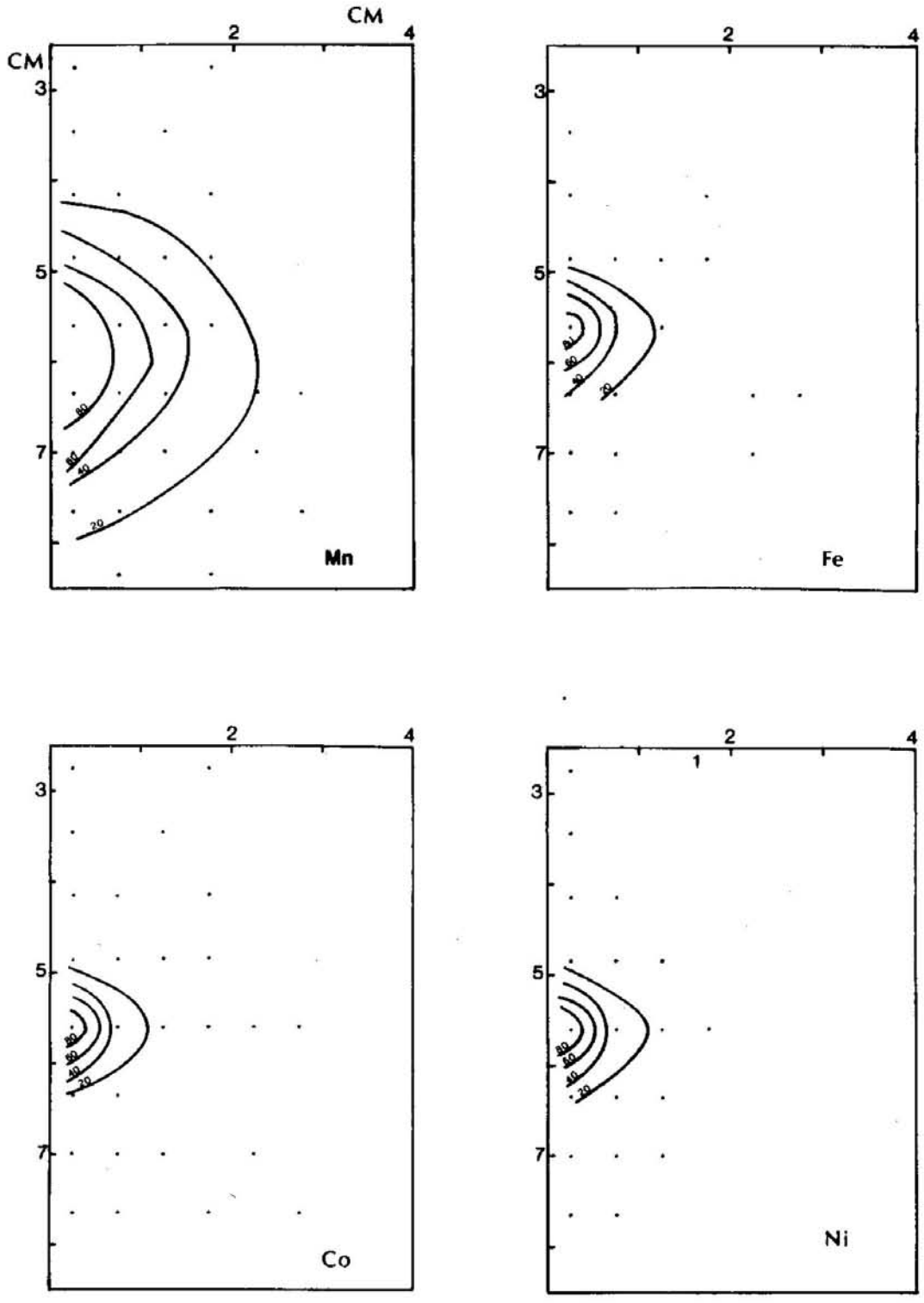

Figure IV.4

Ion Migration Experiments: Linearized Data

Results of the ion migration experiments described in Table IV.8. The vertical axis in each plot is the relative activity, i.e., the activity divided by the maximum activity measured for the tracer plotted in the experiment. The horizontal axis is the square of the distance of the midpoint of the sample interval from the position of the activity maximum. A tracer distribution obeying the model described by equation IV.2 perfectly will yield a single straight line when plotted in this way.

Key:

⬡ samples at ρ = 0.25 cm

□ ρ = 0.75

△ ρ = 1.25

● ρ > 1.25

The data from each depth horizon are joined together by solid lines when the horizon is at or below the release depth, and by dashed lines when the horizon is above the release depth.

Figure IV.4A: Experiment 1C

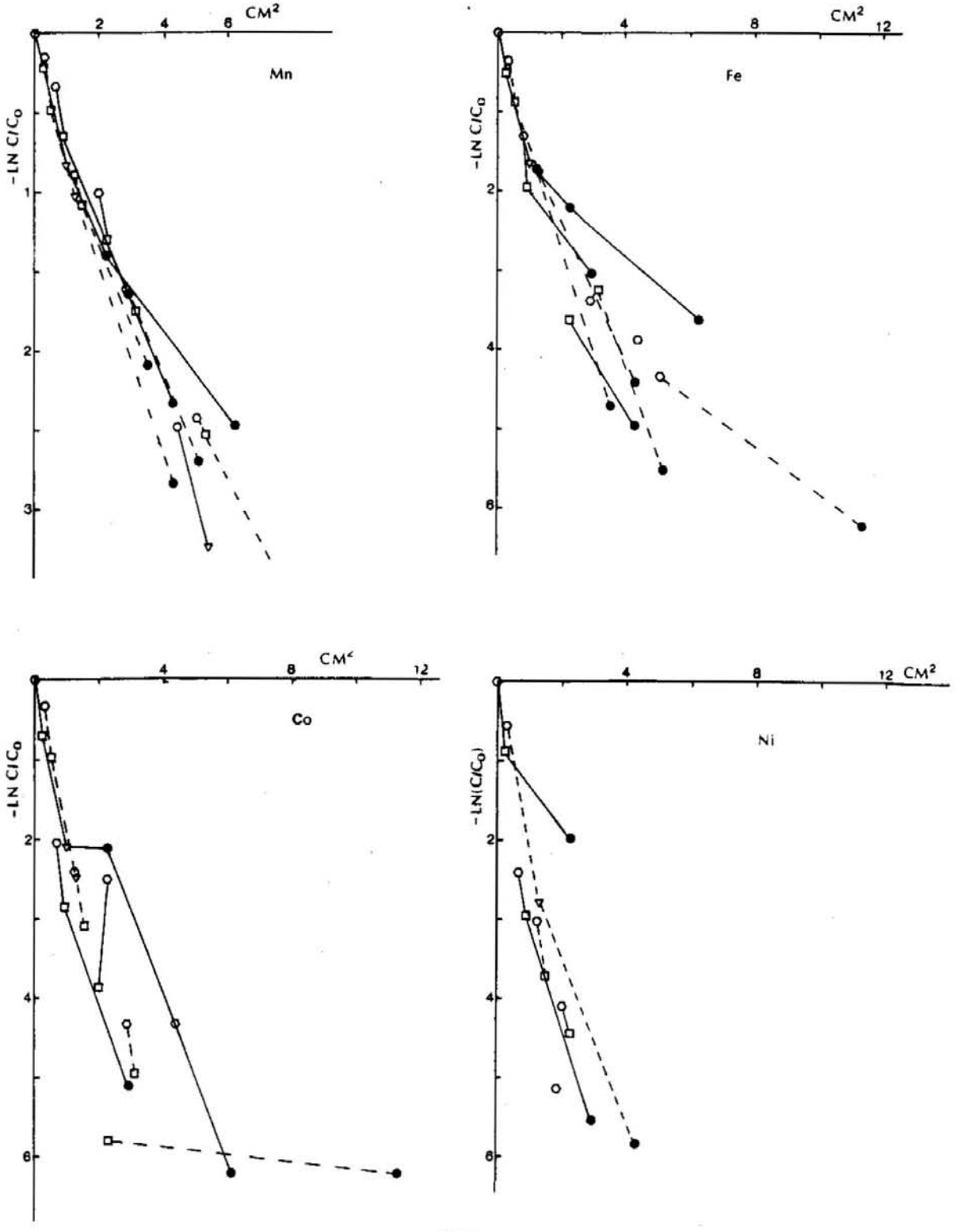

Figure IV.48: Experiment 3C

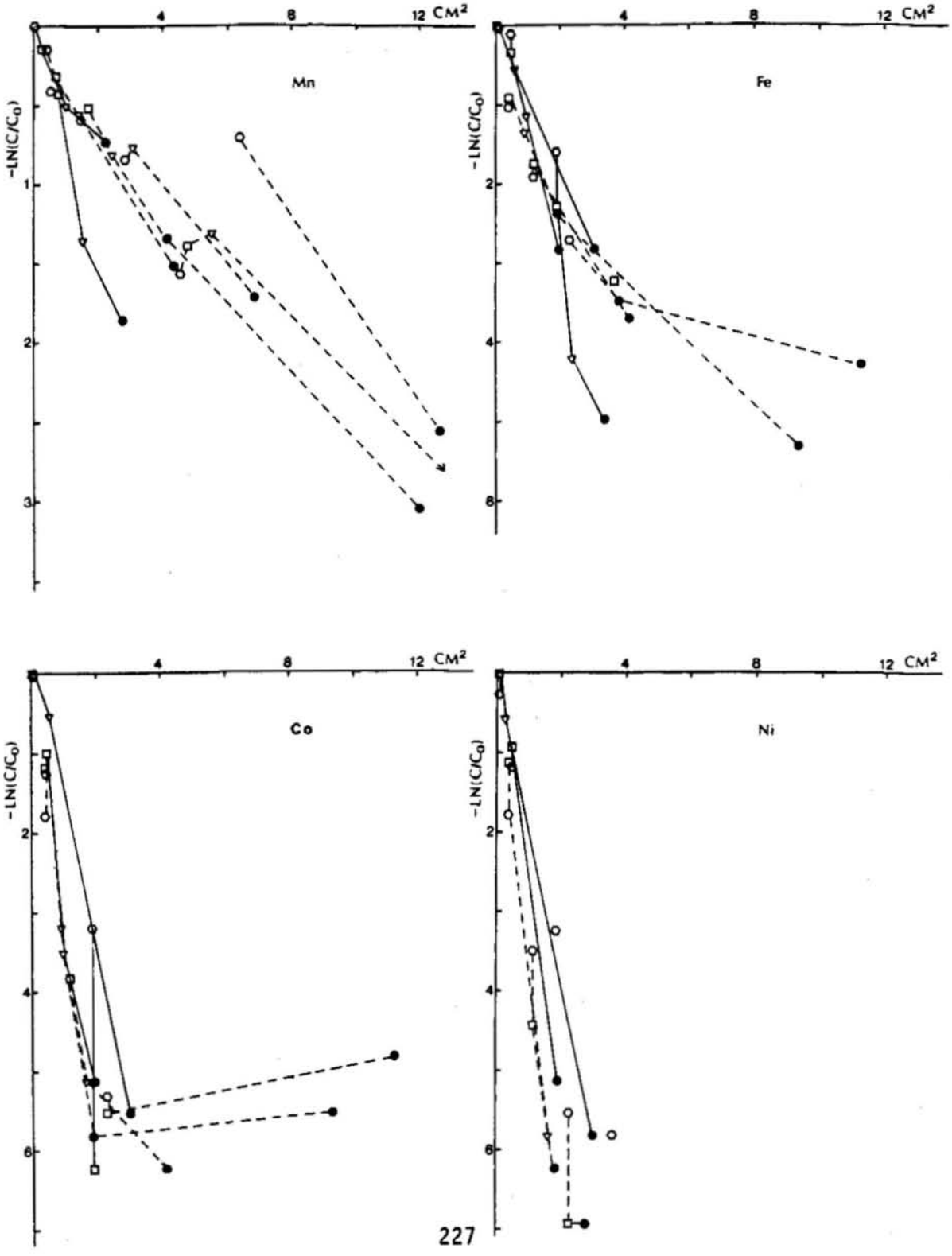

Figure IV.4C: Experiment 3

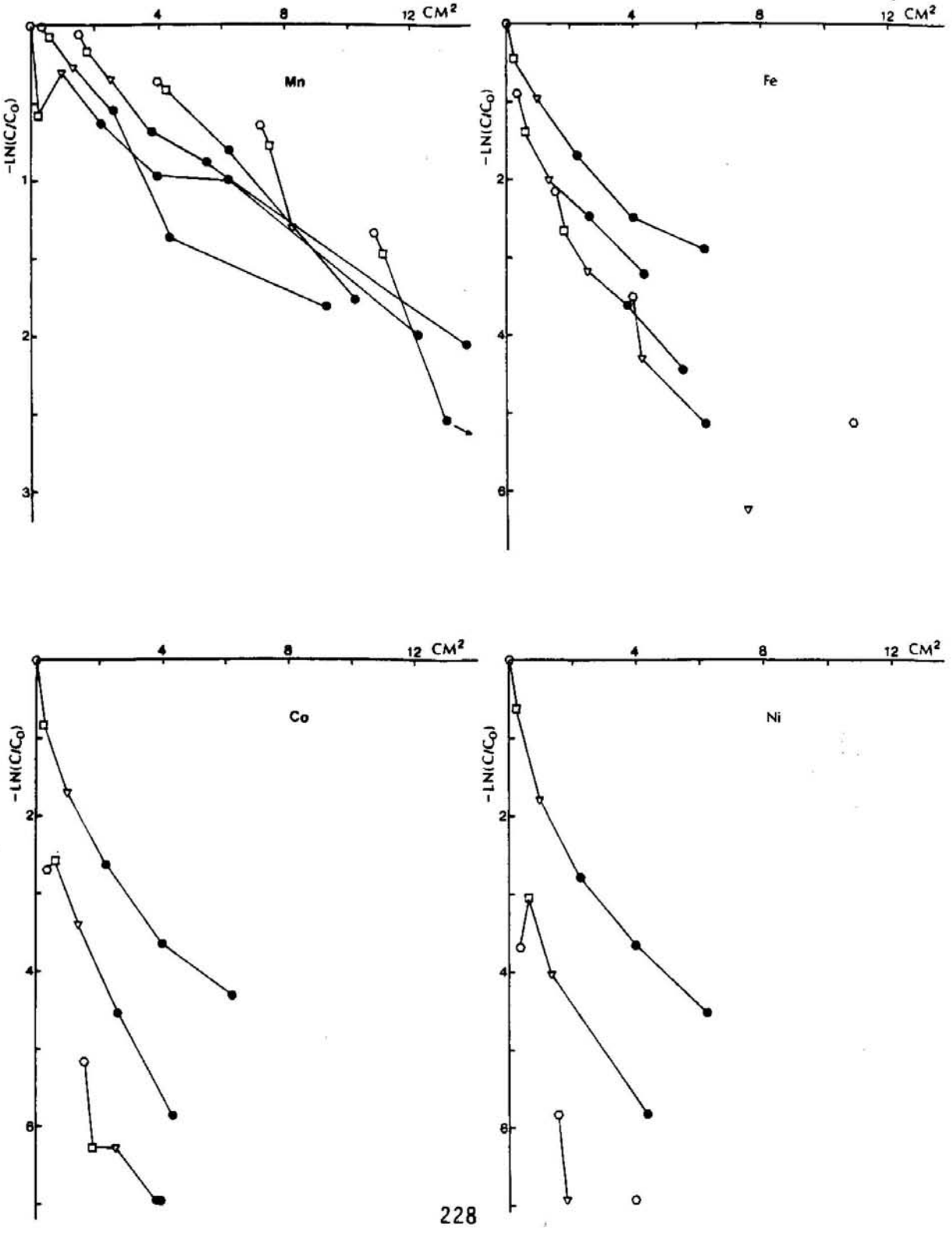

Figure IV.4D: Experiment 3B

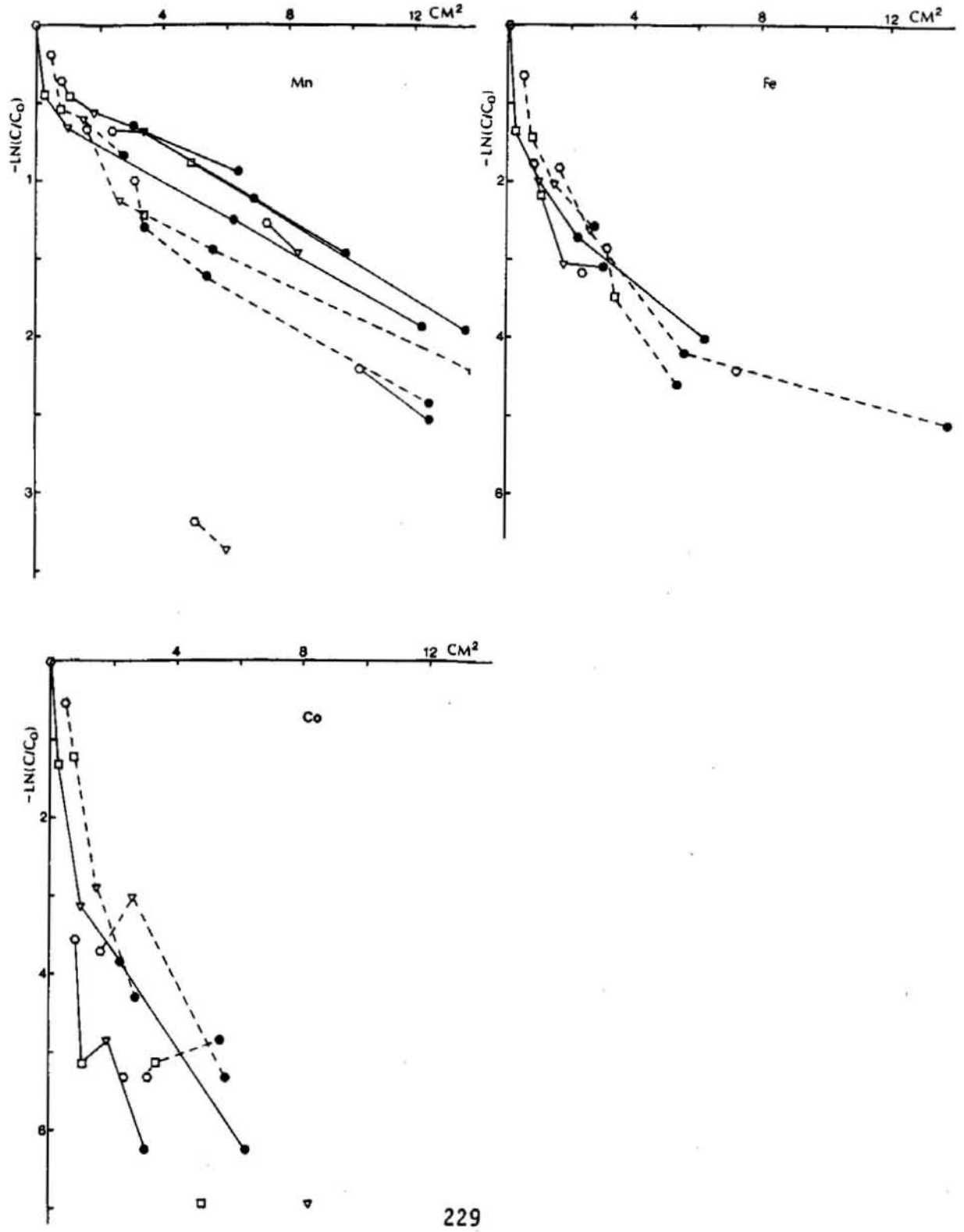

Figure IV.4E: Experiment 6

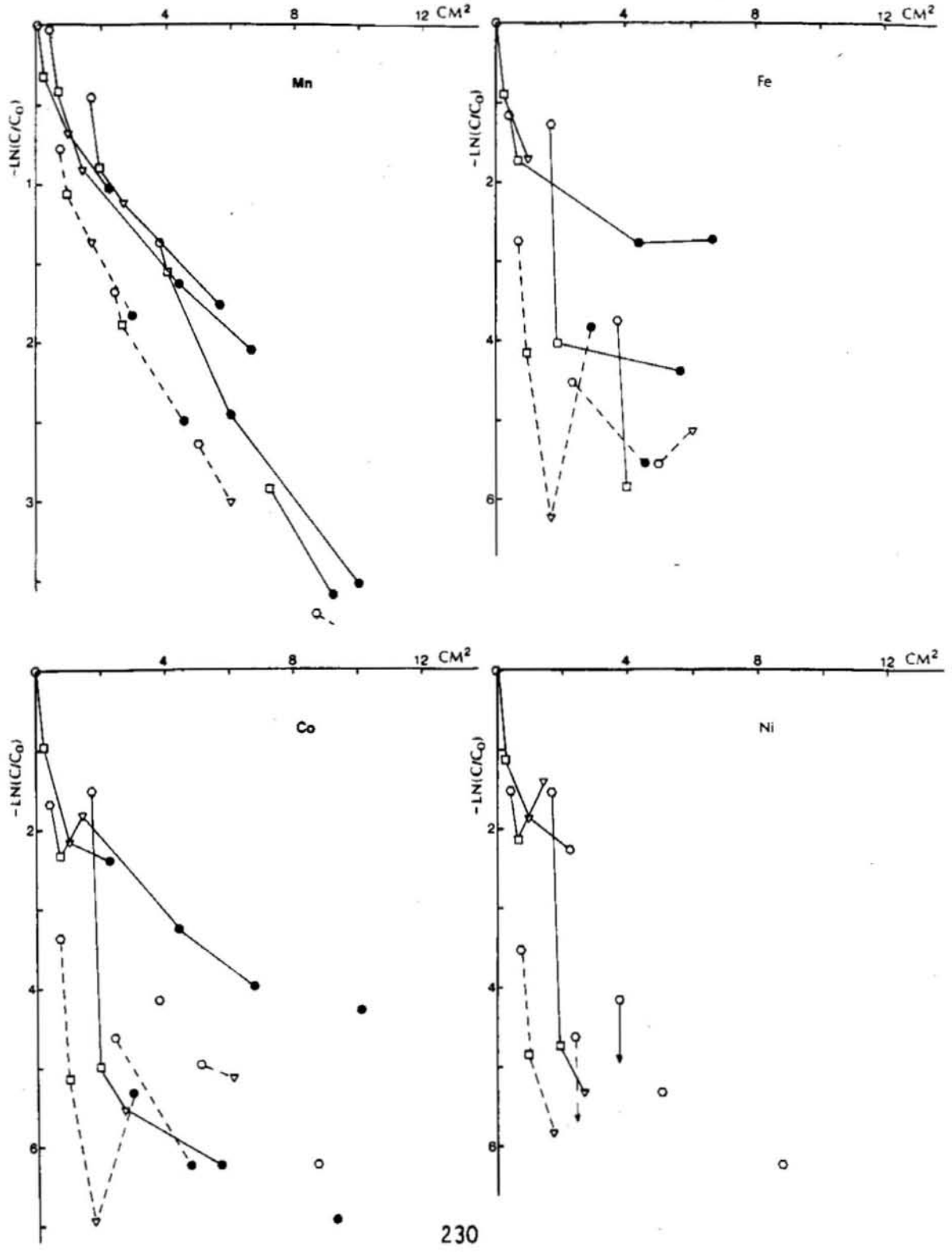

axis is z, the distance below the sediment/water interface. Figure IV.4 shows the data after linearization by application of the model used to calculate apparent diffusion coefficients. Apparent diffusion coefficients are determined from the slopes of the lines in this figure.

The contours drawn in Figure IV.3 are at 80%, 60%, 40% and 20% of the maximum tracer concentration. The plots show that, with the important exception of a secondary ^{54}Mn maximum at the sediment/water interface in experiment 3C, the distributions decrease regularly from their maxima at the release point. The Mn maximum at the sediment/water interface will be discussed in detail later; it is apparently due to oxidation of Mn(II) at the interface. The order of mobilities is apparent from these plots: $^{54}Mn >> ^{59}Fe > ^{60}Co, ^{63}Ni$. Dispersion of the tracers is generally isotropic: in particular, there is no evidence of preferential transport vertically along the probe, a potential artifact in experiments of this kind. The major exception to isotropic dispersion occurred in experiment 3C: there is evidence of enhanced transport along a horizontal axis away from the release point (at $z \simeq 2$ cm) and along a vertical axis at $\rho \simeq 0.75$ cm. These features are consistent with the presence of burrow structures in which transport is enhanced because of organism activity or because of the effects on solid:solution partitioning and on solute diffusion rates of increased porosity in burrows. The effect of the anisotropic dispersion is greatest on the distributions of the more slowly dispersing isotopes, especially ^{60}Co and ^{63}Ni, for which steep gradients are maintained for longer periods of time.

Figure IV.4 shows the experimental tracer distributions in linearized form. The linearization is achieved by plotting ln (activity) versus R^2, where R is the distance of a sample from the release point. If the release point is at (z_o,ρ_o), then $R^2 = (\rho-\rho_o)^2 + (z-z_o)^2$. In the figures, data from individual depth horizons (layers parallel to the sediment/water interface) are joined by lines to give an indication of the success with which the data can be described by a one-dimensional, point-source model of tracer migration. A data set described perfectly by this model would yield a single straight line. If this model is approximately correct, the slopes of the lines are inversely related to the product of the diffusion coefficient and the duration of the experiment. These figures show the same relationship as was shown in the contour plots: ^{54}Mn is much more mobile than ^{59}Fe, which is generally more mobile than ^{60}Co and ^{63}Ni. There is considerably more scatter in the ^{60}Co and ^{63}Ni data than in the ^{54}Mn and ^{59}Fe data. Sampling error may contribute to the scatter, as the slower dispersion rates of the less mobile tracers result in distributions covering a smaller volume of sediments, so that imperfect sediment cutting and imperfect averaging of inhomogeneities result in greater uncertainty than for the more widely spread tracers. The nature of particle mixing may also contribute to the scatter. Particle mixing by bioturbation is an erratic process and, for experiments of short duration, individual mixing events are likely to be poorly averaged, so that tracer distributions are irregular. The definition of a "short" experiment in this sense depends on the dispersion rate of the tracer

and on the spatial scale of the experiment. Short experiments are described by a small dimensionless time parameter, $T = D \cdot t/a^2$, where D is the dispersion coefficient, t is experiment duration, and a is the scale length of the experiment. In larger scale experiments carried out in the MERL microcosms, Adler (1981) found a similar patchiness in tracer distributions, and attributed it to the erratic nature of particle mixing processes.

This brief qualitative description of the data has shown some of the important features of the experimental results: the order of mobility is Mn>>Fe>Co, Ni, and the dispersion process is generally isotropic on the time and space scales of the tracer experiments. Limitations are imposed on the experiments by their short duration and the resulting limited areal extent of the distributions of the primarily particle-bound tracers, especially ^{60}Co and ^{63}Ni. In the rest of this chapter, the experimental data will be treated quantitatively, and the effects of sediment chemistry on the tracer distributions will be considered.

Calculation of Apparent Diffusion Coefficients

To calculate apparent diffusion coefficients from the experimental data, the tracer distributions were modeled as diffusion from a point source into an infinite volume. Mathematically,

(IV.1) $\partial C/\partial t = D_{app}(\partial^2 C/\partial R^2)$

$C(R > 0, t = 0) = 0$

$C(R = 0, t \rightarrow 0) \rightarrow \infty$

$\int_0^\infty C(R)dR = M$

(M is the amount of tracer introduced; the other variables are as defined previously). This equation, with the stated boundary conditions, has solution (Crank, 1975):

(IV.2) $C(R,t) = (M/(8(\pi D_{app}t)^{3/2}))\cdot \exp\{-R^2/(4D_{app}t)\}$

Thus, an apparent diffusion coefficient can be derived from the experimental tracer distributions using the slope of a plot of ln (C) vs. R^2.

The model system is an approximation of the actual experimental system, which has cylindrical symmetry around an impermeable barrier (the probe) at $\rho = 0.5$ cm. Three potentially significant sources of error due to the simplicity of the model system have been investigated.

(1) The volume of the probe has been ignored. This has little effect on the overall tracer distribution, since the probe volume amounts to a

maximum of about 10% of the total volume of an experiment. However, the exclusion of the probe may have a more significant effect near the origin of the distribution. Tracer which would occupy the probe's volume in the absence of the impermeable barrier may be present in the sample intervals closest to the release point, causing an excess tracer concentration in those intervals. This effect can be seen in the linearized plots in Figure IV.4: ln (C) decreases more rapidly near the origin than is predicted by the point source model. In practice, the calculated diffusion coefficients are not greatly affected by the inclusion of the points closest to the origin in the regression line.

(2) It has already been shown experimentally that the true source achieved using the tracer release probe is not a point source, but is distributed through a radial distance of about 0.5 cm. When tracer initially distributed through a finite volume is described by a diffusion coefficient calculated from a straight-line fit using a point-source model the true diffusion coefficient is overestimated. The error is shown in Figure IV.5; it ranges from 5% to 20%, with the largest error occurring for the smallest values of the dimensionless time parameter, $T = D \cdot t/a^2$.

(3) It has also been shown that there is inhomogeneity in the initial distribution caused by release of the source solution from four small holes rather than from a single hole. The effect of assuming a homogeneous initial distribution is that the tracer in the real system is actually diffusing into a larger volume than is assumed in the model. Thus, the tracer concentration decreases more rapidly near the probe

than would a tracer diffusing from a true point source.

The effects of the three simplifications are greater, the smaller is the dimensionless time parameter, $T = D \cdot t/a^2$, for a given experiment, that is, the shorter is the experiment or the slower is the dispersion rate of the tracer. In these experiments, the uncertainties are the greatest for ^{63}Ni and ^{60}Co, less for ^{59}Fe, and smallest for ^{54}Mn. ^{63}Ni and ^{60}Co are also the isotopes for which there is more likely to have been significant perturbation of the natural pore water/sediment system, due to the relatively large concentrations of stable metals injected at the start of the experiments. In addition, the imprecision in the measured ^{63}Ni and ^{60}Co distributions is rather large for most of the experiments carried out during this study.This is partly because of the nature of the processes dispersing these primarily particle-bound isotopes; a contributing factor is the relative importance of inhomogeneity in the initial distribution and of sampling errors in experiments with small T. It is clearly seen from the linearized data in Figure IV.4 that the errors causing scatter in the data at small values of T (in particular, in the ^{60}Co and ^{63}Ni data) produce uncertainties in the slopes of the best-fit lines similar to the error in the point-source approximation.

An important test of the experimental system is the release of a nonreactive tracer whose dispersion rate can be predicted from its known diffusion coefficient and the porosity and formation factor (described in Chapter II) of the sediments. ^{36}Cl was used as such a tracer in experiments 1C (4 days duration) and 3C (11 days duration).

Figure IV.5

The Error in the Point-Source Assumption

The error in the point-source assumption has been evaluated for a spherical initial distribution of 0.5 cm radius. D_{actual} is the diffusion coefficient that was used to generate a tracer distribution using a volume source model. D_{calc} is the diffusion coefficient derived from a straight-line fit to the volume source distribution, based on a point-source assumption. Points were calculated using two diffusion coefficients, 2×10^{-7} and 1×10^{-6} cm^2/sec, at several values of the dimensionless time parawmeter, $D \cdot t/a^2$.

Figure IV.5

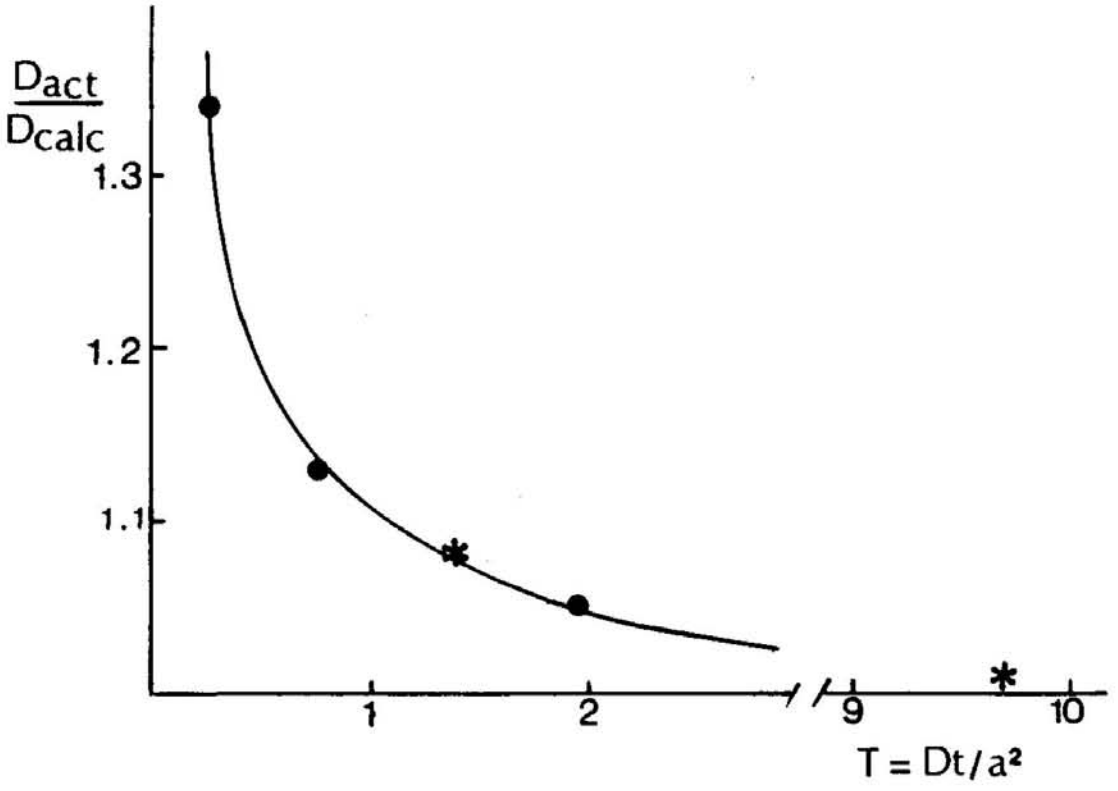

The results are shown in contour plots (Figure IV.6) and using the same linearization as was used for the metal ion migration experiments in Figure IV.7.

It is clear that, in experiment 3C, isotropic dispersion of ^{36}Cl did not occur, with enhanced transport near the release point along axes at $\rho = 0.75$ and $z = 2.0$. This result is similar to that observed in the ^{63}Ni and ^{60}Co distributions for this experiment. The nature of the process producing the ^{36}Cl distribution is difficult to discern, as it appears to have concentrated ^{36}Cl, allowing steep gradients to be maintained, rather than dispersing the tracer.

The ^{36}Cl results from experiment 1C are more important to the metal migration experiments. In this experiment, the contour plot shows regularly decreasing ^{36}Cl activity moving away from the release point. The ln (C) vs. R^2 plot, however, shows that the simple, one-dimensional model is inadequate to describe the experiment. There is a distinct break in the slope of ln (C) vs. R^2 when the data in individual depth horizons are joined by lines. The break occurs, for each horizon, at $\rho = 1.25$ cm, and the slope is smaller outside the boundary than inside it. Thus, according to the one-dimensional model, dispersion is apparently more rapid at distances greater than 1.25 cm from the probe than nearer to it. The reason for this break is not known. A change in the physical properties of the sediments sufficient to produce this large a change in their diffusivity is very unlikely: for instance, the porosity change across the region of interest is small, less than 3%. No likely chemical artifact has been discovered;

Figure IV.6

Cl-36 Results: Contour Plots

^{36}Cl distribution from experiments # 1C and 3C. the data are plotted in the same way as the metal ion tracer results in Figure IV.4

Figure IV.6

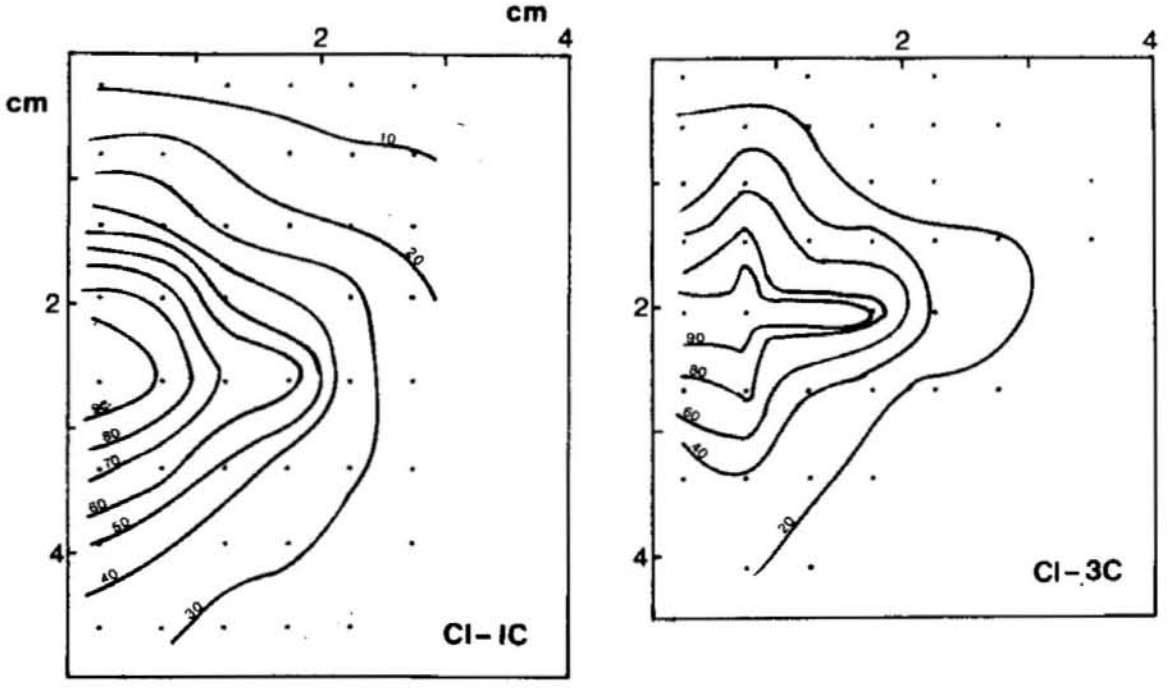

Figure IV.7

Cl-36 results: Linearized Data

Plots of ^{36}Cl distributions from experiments # 1C and 3C after application of the model of equation IV.2. The plots are identical in form to those for the metal ion migration experiments in Figure IV.5

Figure IV.7

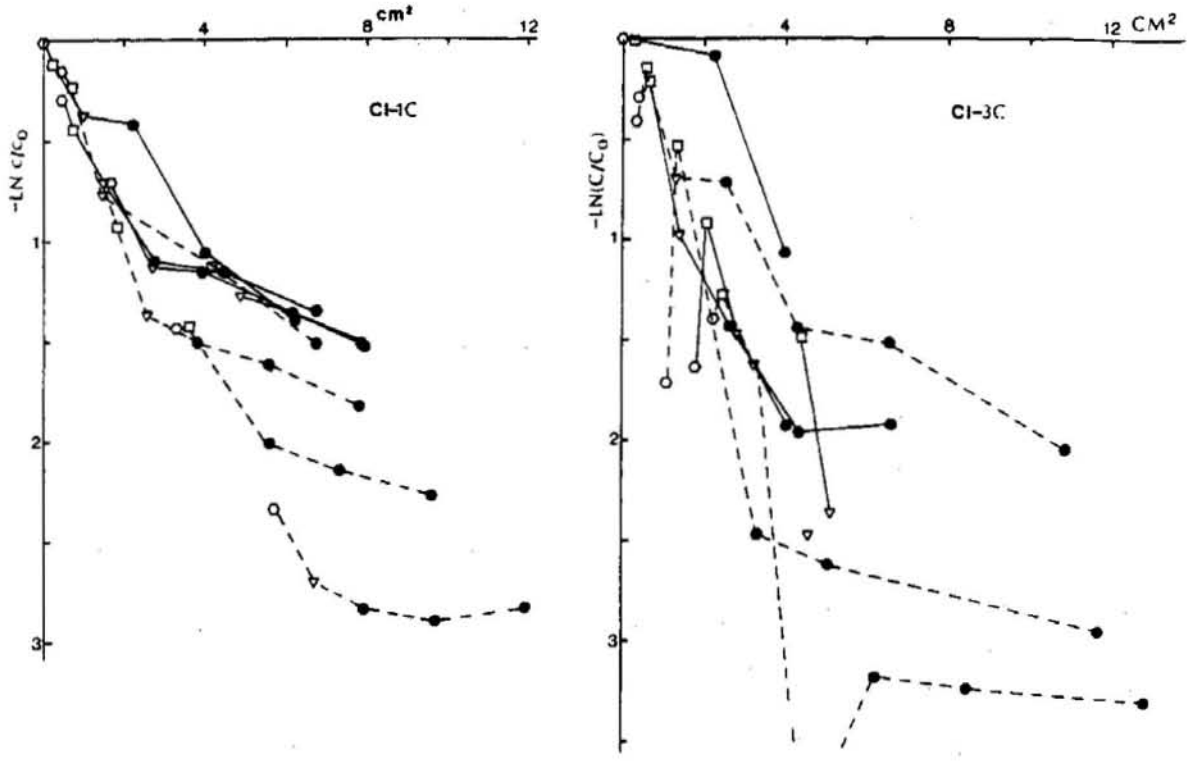

although codiffusion of Cl^- with Na^+ from the source solution is possible given the high NaCl concentration in the source solution, this effect is also too small to produce the observed data. The break in slope may result from the failure of the mathematical model to describe the effect of the presence of an impermeable barrier, the probe wall, on the tracer distribution. The ^{36}Cl results also depart from the simple, one-dimensional model in that the depth horizons are separated, above the release point, on the ln(C) vs. R^2 plots. The activities are lower relative to the model-predicted values, the closer to the horizon is to the sediment/water interface. This deviation from the model is most likely due to transport across the interface.

The slopes of the lines outside $\rho = 1.25$ cm, when used with equation IV.2, are roughly consistent with the known molecular diffusion coefficient for Cl^- (Li & Gregory, 1974), after it has been corrected for tortuosity and porosity by the relationship described in Chapter II (using $\phi = .81$, the average porosity in the upper 10 cm of the sediment column, and $F = \phi^{-2.5}$, from porosity and resistivity data). Calculated apparent diffusion coefficients are:

Depth horizon	D-app x 10^6 (cm^2/sec)
z>2.63	8.5
z=1.38	8.6
z=0.80	14
z=0.25	12

The calculated Cl^- diffusion coefficient for the experimental conditions is 12×10^{-6} cm^2/sec. Thus, the procedure used to obtain the Cl^- diffusion coefficient from the ^{36}Cl dispersion data yielded

results somewhat lower than the true Cl^- diffusion coefficient, with a maximum deviation of about 30%.

From the ^{36}Cl data and the metal ion migration data, the occurrence of the observed breaks in slope of the ln (C) vs. R^2 plots does not appear to depend directly on the chemical properties of the tracer used. Rather, it appears to depend strongly on the length of the experiment relative to the dispersion rate of the tracer. This quantity is described by the dimensionless time parameter, T (defined earlier in this section). In this sense, the 4-day ^{36}Cl experiment is "longer" than all the metal ion migration experiments. For instance, the experimental results indicate that T = 10 for a 30-day ^{54}Mn experiment, compared to T = 14 for the ^{36}Cl experiment. Only in the long ^{54}Mn experiments (#3B, especially; also #3 and #6) were breaks in slope and separations of depth horizons clearly evident. In experiments 3 and 6, exclusion of points at $\rho = 0.25$ and $\rho = 0.75$ from calculation of the best-fit line for the ln C vs. R^2 plots did not change the calculated apparent diffusion coefficient; in experiment 3B, while $D_{app} = 6.9 \times 10^{-7}$ cm^2/sec was calculated using a single line to fit all the data, results ranging from 8.4 - 10 x 10^{-7} were obtained by fitting the data from individual depth horizons beyond $\rho = 0.75$. Only slight breaks in slope were observed in the long ^{59}Fe experiments, and they did not change calculated apparent diffusion coefficients. For ^{60}Co and ^{63}Ni, some curvature was observed in experiment 3, in which the activity maximum occurred at the sediment/water interface. Again, the effect on calculated apparent

diffusion coefficients was small: the calculated coefficients were 16 - 21 x 10^{-8} cm^2/sec for ^{63}Ni and 12 - 22 x 10^{-8} cm^2/sec for ^{60}Co.

To derive the results described below, it has been assumed that the point-source model can be applied to the metal migration data. The assumption is based on the argument that the inadequacy of the model is greater, the larger is the dimensionless time parameter describing an experiment. The reason for the breakdown in the model is not understood. It appears that a 2-dimensional model, including an impermeable barrier at the probe surface and a sediment/water interface, is necessary to describe the experiments in detail. Although enough ^{36}Cl dispersion experiments were not carried out to prove the validity of the calculation method used, the trends observed in the ln (C) vs. R^2 plots for ^{36}Cl and metal ion migration experiments are consistent with it. In addition, independent evidence has been gathered to show that the ^{54}Mn experiments are consistent with transport of ^{54}Mn in solution at a rate described by the molecular diffusion coefficient for Mn. The evidnece is discusssed in detail below; it is based on the agreement between directly-measured ^{54}Mn solid:solution distribution coefficients and distribution coefficients calculated from the dispersion of ^{54}Mn tracer.

In the analysis that follows, ^{63}Ni and ^{60}Co results will be subjected to less detailed analysis than ^{54}Mn and ^{59}Fe; their distributions will be used primarily as indicators of the rate of particle dispersion during the experiments.

^{63}Ni and ^{60}Co Results

In Chapter 1, and again in Chapter 3, it was shown that the relative solubilities in reducing, sulfide-containing systems of the metals included in this study proceed in the order, Mn>Fe>Co,Ni. The dispersion rates of ^{54}Mn, ^{59}Fe, ^{60}Co, and ^{63}Ni can be expected to follow the same order. If a tracer is so insoluble that it precipitates quantitatively when introduced into the sediment/pore water system, its dispersion will depend only on the particle mixing rate and the particulate tracer concentration gradient. Because particle mixing rates at the Buzzards Bay study site are about 10 times slower than solution phase diffusion coefficients for the first-row transition metals, and because all tracers were introduced at similar activities, so that their concentration gradients were similar, tracers which precipitated as solids at the beginning of an experiment would disperse more slowly than soluble tracers. In addition, if tracers reach equilibrium between solid and solution phases rapidly, tracers with smaller solid:solution distribution coefficients disperse more rapidly than tracers with larger distribution coefficients. Anticipating a result which will be derived in the next section of the chapter, the apparent diffusion coefficient of a tracer in equilibrium with respect to solid:solution exchange reactions is related to the distribution coefficient and the solid-phase and solution-phase mixing coefficients by

$$D_{app} = D_B + D_{sed}/(1 + K) \qquad \text{(IV.3)}$$

D_{app} = apparent diffusion coefficient of tracer
D_B = bioturbation mixing coefficient
D_{sed} = molecular diffusion coefficient, corrected for tortuosity
K = dimensionless solid:solution distribution coefficient

Variations in the apparent diffusion coefficient with K are shown in Figure IV.8: the apparent diffusion coefficient (and, therefore, the dispersion rate of the tracer) decreases dramatically as K increases from 0 to 100 in a system with $D_{sed}/D_B = 10$. If K for a transition metal is related to the metal's solubility, then the tracer dispersion rate is related to solubility regardless of whether irreversible precipitation reactions or equilibrium solid:solution exchange reactions determine the distribution of tracer between solid and solution phases.

In this study, the distribution coefficients follow the trend of solubilities in reducing sediments, with K decreasing in the order, Co,Ni>Fe>>Mn. For ^{63}Ni and ^{60}Co, only lower limits on K can be determined from transport studies of the kind undertaken. There is some uncertainty as to the reason for the large K values for Co and Ni, because the stable metals were introduced with the tracers in large excess of natural pore water concentrations. Thus, the tracer partitioning may reflect precipitation upon introduction into the sediments. Nonetheless, ^{63}Ni and ^{60}Co dispersion are consistent with transport entirely with the particulate phase.

The apparent diffusion coefficients derived from the experimental distributions of ^{63}Ni and ^{60}Co are listed in Table IV.9. Before comparing them with excess ^{234}Th-derived mixing rates,

Figure IV.8

Variation in D-app with K

The variation in the apparent diffusion coefficient of a tracer in rapid exchange equilibrium between solid and solution phases. The calculation is based on equation IV.3

Figure IV.8

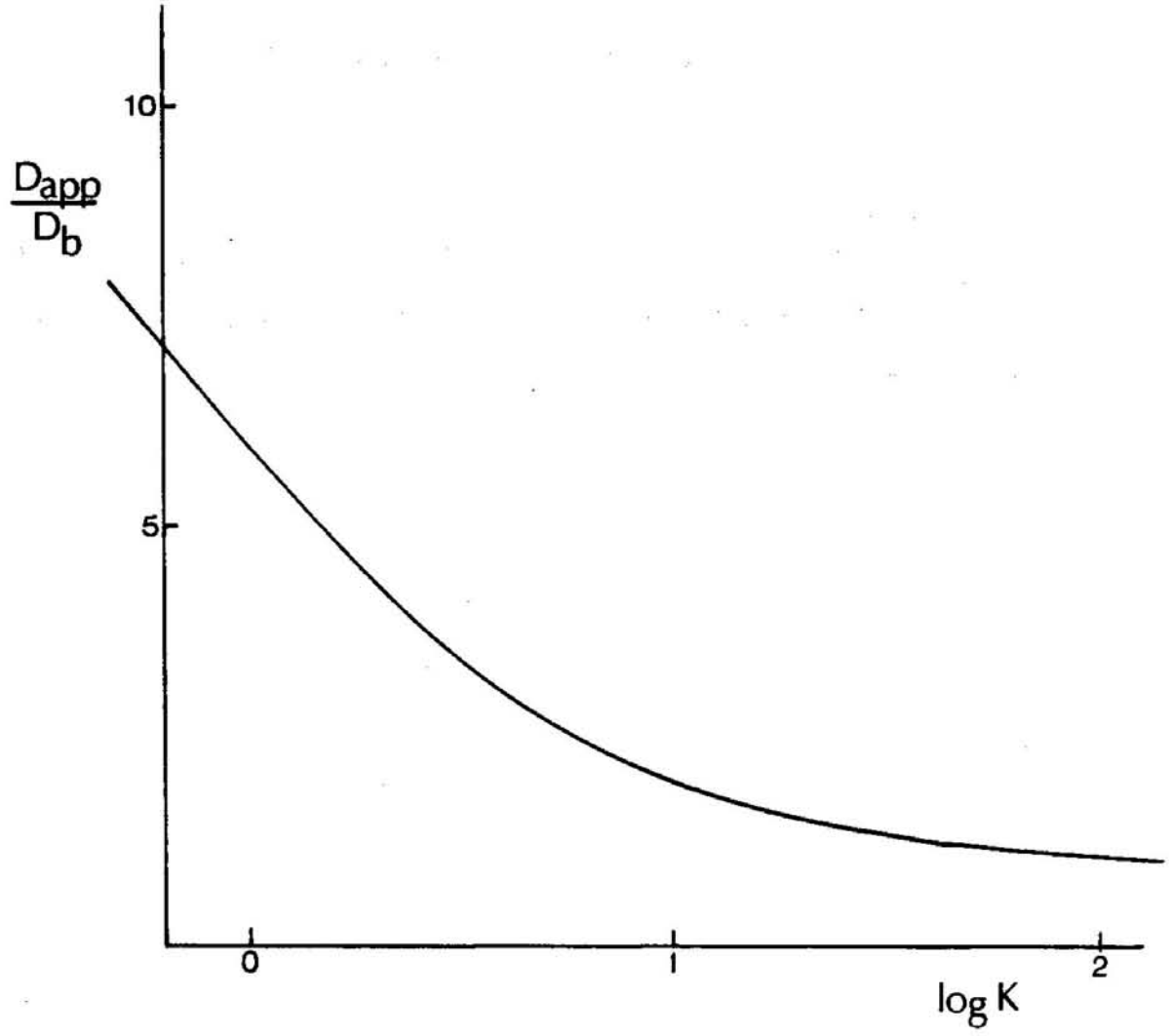

Table IV.9

Apparent Diffusion Coefficients for Co-60 and Ni-63

Apparent diffusion coefficients calculated from the results of the tracer migration experiments. Values are in $10^{-8}cm^2/sec$. ^{63}Ni was not measured for experiment 3B. No diffusion coefficient was calculated for ^{60}Co in experiment 6.

	D-app x 10^{-8} (cm^2/sec)	
Experiment	Ni-63	Co-60
3B	-	13.9±2.5
3C	13.2±1.7	15.1±2.1
1C	48.4±6.9	72.3±8.9
3	16.3±5.6	12.2±2.1
6	15.0±4.6	-

several differences between the two measurements should be noted. While ^{234}Th-derived rates are averaged over the upper 2-2.5 cm of the sediment column, the results for most of the tracer experiments depend on mixing deeper in the sediments. The activity maxima ranged from 0.3 to 7.75 cm below the interface (Table IV.7). Further, the depth range in the sediment column over which each experiment took place extends 2-3 cm deeper than the activity maximum. Because the tracer experiments took place largely below the depth of penetration of excess ^{234}Th, rates derived from the tracers can be expected to be slower than the ^{234}Th-derived rates. There are also important differences in scale between ^{234}Th and tracer-derived rates. ^{234}Th-derived rates are averages over about 90 days and over the area of a 20 cm-diameter core liner (300 cm^2); the tracer experiments ranged from 4-30 days in length, and the area of sediment over which ^{63}Ni and ^{60}Co were dispersed rarely exceeded 30 cm^2. Thus, because of their limited temporal and areal extent, the tracer-derived mixing rates can be expected to be more variable than the ^{234}Th rates.

Recalling results from Chapter 2, ^{234}Th bioturbation rates ranged from 9-34x10^{-8} cm^2/sec during the cold months, averaging 24x10^{-8} cm^2/sec. They ranged from 33-81x10^{-8} cm^2/sec in the warm months, averaging 44x10^{-8} cm^2/sec. Radiotracer experiments 3A, 3B, and 6 took place during spring, and should reflect "cold water" mixing rates. Experiment 3A rates were 12-16x10^{-8} cm^2/sec for ^{60}Co and ^{63}Ni. Experiments 3B (with an injection of tracer at the base of the excess ^{234}Th zone) and 6 (with tracer release below detectable excess

^{234}Th) yielded similar rates: 14-15x10^{-8} cm^2/sec. These rates are at the low end of the range of cold-water rates measured using ^{234}Th.

Experiments 1C and 3C took place during July, when ^{234}Th distributions indicate more rapid mixing. Experiment 1C yielded rates of 72 and 48x10^{-8} cm^2/sec for ^{60}Co and ^{63}Ni, respectively, near the average warm-month value measured using ^{234}Th. 3C gave rates of 15 and 13x10^{-8} cm^2/sec. As with the cold-water results, the tracer results obtained in the warm season are consistent with a particle mixing model of dispersion at rates similar to those of excess ^{234}Th-bearing particles. The range in transport rates measured from ^{63}Ni and ^{60}Co distributions is too small to be correlated with spatial and temporal variability in excess ^{234}Th-derived mixing rates, but, as shown in Figure IV.8, transport rates fall within the range of rates measured for excess ^{234}Th. Consistent with their position deeper in the sediment column, the tracer-derived rates tend to be slower than the ^{234}Th-derived rates.

Figure IV.9

D-app for Ni-63 and Co-60 Plotted on the Trend of Th-234 Mixing Rates

Figure IV.9

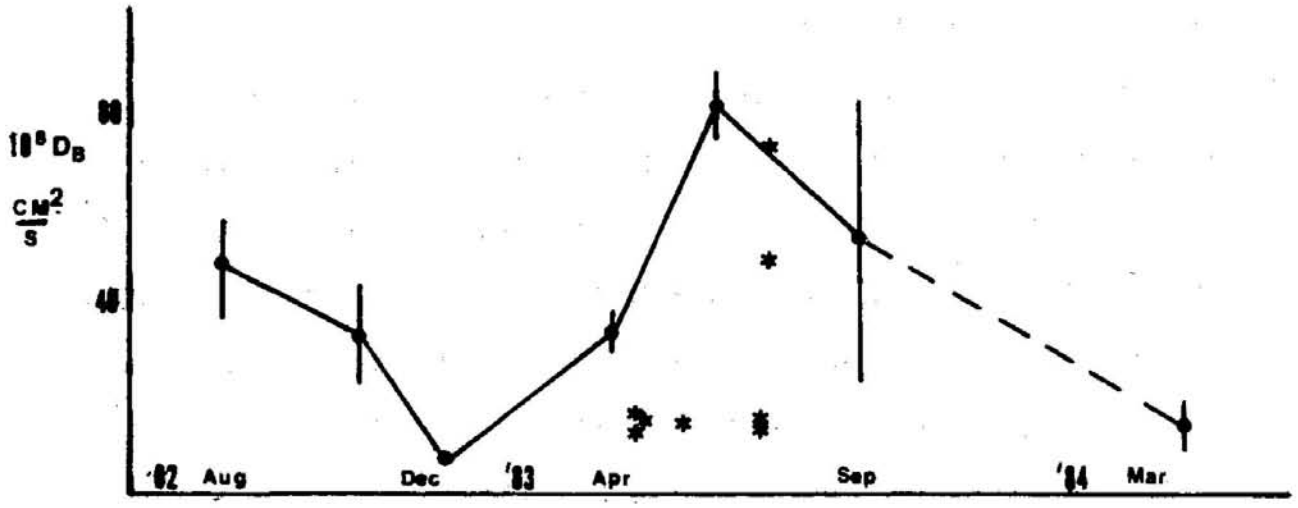

^{54}Mn and ^{59}Fe Results

In this section, the transport rates observed for ^{54}Mn and ^{59}Fe are used to determine the solid:solution partitioning of these tracers under in situ conditions. A simple model relating solid:solution distribution coefficients to transport rates is derived and used to obtain distribution coefficients; these results are then combined with direct measurements of ^{54}Mn distribution coefficients to demonstrate the internal consistency of the transport experiments. Finally, the results obtained from this study are compared with results from other transport rate experiments carried out in nearshore sediment systems.

The time rate of change of bulk concentration (that is, the sum of amounts of a species in the solid and solution phases, divided by volume of sediment) of a species at a point in the sediment column is determined by a balance between the gradient of the flux of the species at the point and the rates of reactions changing the bulk concentration,

$$\partial C_{tot}/\partial t = - \partial F_{tot}/\partial x + \Sigma R_{tot}$$

(Berner, 1980). The only reaction of interest affecting the bulk concentration is radioactive decay; Adler (1981) has shown that, given a differential equation and boundary conditions of the types governing the tracer experiments described here, the distributions of different species depend on their differing transport properties, not on differing decay rates, so that radioactive decay need not be considered here. Thus, $\Sigma R_{tot} = 0$ is assumed.

The total flux is assumed to have two components, a

bioturbation flux due to mixing of particles plus solution by organisms, and a solution phase flux due to molecular diffusion. The bioturbation flux is driven by the bioturbation mixing coefficient, D_B, and the bulk concentration gradient of the species:

$$F_B = -D_B(\partial C_t^*/\partial x)$$

C_t^* = bulk concentration, in dpm/vol. of sediment

The solution phase flux is

$$F_W = -\phi \cdot D_{sed}(\partial C_W/\partial x) = -D_{sed}(\partial C_W^*/\partial x)$$

C_W = solution phase concentration, dpm/vol. pore water. Note that ϕ is assumed constant.

C_W^* = solution phase concentration in (dpm in pore water)/volume sediment

D_{sed} = solute diffusion coefficient, corrected for porosity and tortuosity

The concentrations of the species in bulk sediment, in pore water, and in the solid phase are related through the dimensionless distribution coefficient,

$$K = C_S^*/C_W^*$$

C_S^* = (dpm in solid phase)/vol. of sediment

With concentrations defined in this way,

$$C_T^* = C_S^* + C_W^*.$$

Then, the total flux is given by

$$F_{tot} = F_B + F_W$$

$$= -D_B \cdot \partial C_t^*/\partial x - D_{sed} \cdot \partial/\partial x(C_t^*/(1+K))$$

Therefore, if D_B, D_{sed}, and K are constant,

$$\partial C_t^*/\partial x = (D_B + D_{sed}/(1+K)) \cdot \partial^2 C_t^*/\partial x^2$$

and, from equation IV.1, there is a relationship between the apparent diffusion coefficient derived from the tracer distribution (D_{app}), D_B, D_{sed}, and K:

(IV.3) $$D_{app} = D_B + D_{sed}/(1+K)$$

This relationship has been used to determine K for ^{54}Mn and ^{59}Fe. K values derived in this way have been converted to gravimetric distribution coefficients (dpm/gm dry wt ÷ dpm/gm pore water) using average values for weight percent water for the depth intervals used to deternmine D_{app} in each experiment and the relationship,

$$K_{grav} = K \cdot W/(1-W)$$

W= weight % water

In deriving K, the assumption was made that D_B is equal to the apparent diffusion coefficients measured for ^{60}Co and ^{63}Ni. These results were considered more appropriate than D_B from ^{234}Th measurements because they should reflect particle mixing at the time and place in the sediment column at which the experiment took place, rather than particle mixing averaged over larger areas and longer times. D_{sed} for ^{54}Mn and ^{59}Fe were determined from the data for the molecular diffusion coefficients in seawater as a function of temperature in Li & Gregory (1974). They were corrected for tortuosity and porosity using the relationships,

$$D_{sed} = D_{free\ soln}/(\phi F)$$

F = formation factor = (resistivity of free soln)/(resistivity of seds)

and

$$F = \phi^{-2.5}$$

The relationship between F and ϕ was determined from porosity and resistivity measurements made at the study site (see Chapter II). The values used for D_{sed} are shown in Table IV.12.

Calculated K_{grav} values are in Table IV.10. ^{54}Mn results are very similar for all experiments except experiment 6, which was carried out deeper in the sediment column than the others. The K_{grav} value for experiment 3B is changed from 8.7 to 6.7 if the largest D_{app} value calculated from an individual depth hoirizon (10×10^{-7}) is used instead of the value of 6.9×10^{-7}, derived by fitting a single line to all the data. Thus, the effect of the deviation of the ln (C) vs. R^2 plot from linearity on the distribution coefficient calculation does not change the nature of the results. Distribution coefficient estimates ranged from 5.2 to 8.7 in the upper 4 cm of the sediment column; $K_{grav} = 17 \pm 5$ was found in experiment 6 (in which the ^{54}Mn distribution ranged from about 3-8 cm below the sediment/water interface). Similarly, K_{grav} for ^{59}Fe was found to be significantly greater in experiment 6 than in the other experiments. Except for the very short experiment, 1C, K_{grav} for ^{59}Fe was always about 15 times K_{grav} for ^{54}Mn. In the short experiment, the ^{59}Fe distribution coefficient was only about 7 times the distribution coefficient for ^{54}Mn. It should be noted that the large uncertainty for K_{grav}(Fe) in

Table IV.10

Results of Mn-54 and Fe-59 Migration Experiments

A. Calculated molecular diffusion coefficients for Fe and Mn in pore water. Values are listed in 10^{-7} cm^2/sec. ϕ = .83 was used in the calculation.

B. Tracer migration experiment results. D_{app} is listed in 10^{-7} cm^2/sec; K_{grav} has dimensions,
(dpm in solid/gm dry wt)/(dpm in pore water/gm pore water).
Only a lower limit on $K_{grav}(^{59}Fe)$ could be calculated for experiment 6.

Table IV.12A

Expt	Temp (°C)	D-sed (10^{-7} cm^2/sec)	D-sed (Fe) (10^{-7} cm^2/sec)
3	6	27.3	29.3
6	6	27.3	29.3
3B	12	33.5	35.3
1C	18	39.6	41.5
3C	19	40.9	42.5

Table IV.12B

Expt	Activ. max (cm)	D-app		K-grav	
		Mn-54	Fe-59	Mn-54	Fe-59
1C	2.5	15.0±.8	7.83±.58	5.2±.8	34±30
3C	2.2	9.25±.47	3.03±.03	7.7±1.2	110±30
3B	2.5	6.92±.48	2.17±.23	8.7±1.2	125±90
3	0.3	6.73±.49	1.71±.12	6.9±1.0	121±65
6	5.7	3.37±.15	1.46±.32	15±5	>300

this experiment reflects the greater importance of the uncertainty in D_B in the determination of K when D_{app} is close in magnitude to D_B. In this case, the denominator in IV.3 is a small difference between two imprecisely known numbers. Thus, although $K_{grav}(Fe)$ is poorly known, $D_{app}(Mn)$ is clearly greater than $D_{app}(Fe)$, and $K_{grav}(Fe)$ is clearly larger than $K_{grav}(Mn)$.

These differences between the ^{54}Mn and ^{59}Fe distribution coefficients may reflect the difference in the saturation state of the pore waters with respect to Fe and Mn minerals. It was shown in Chapter 3 that the pore water Fe concentration appears to be in equilibrium with Fe solid phases throughout the sediment column: with oxides at the sediment/water interface, with phosphates above about 3 cm, and with sulfides below 3 cm. In addition, there is evidence that Fe sulfides form in the upper 3 cm of the sediment column. In contrast, the pore waters do not reach saturation with respect to pure Mn phases in at least the upper 10 cm of the sediments (although evidence for an insoluble Mn sulfide phase, not yet identified, in anoxic marine basins, has been given by Jacobs,1984). Scavenging and coprecipitation were proposed as means of removing dissolved Mn to solids in the upper 3 cm of the sediment column.

It is not clear why the distribution coefficient for ^{59}Fe should have been lower for experiment 1C than for experiment 3C: the two experiments were carried out at the same time, at the same depth relative to the sediment/water interface, and within a few meters of each other. The fact that 1C, the shorter experiment (4 days), yielded a

significantly smaller distribution coefficient than all the other experiments may indicate that K for Fe is not constant over time in these experiments; this may indicate that an irreversible precipitation reaction, occurring over a period of a few days, determines the ^{59}Fe distribution over short time periods.

Direct measurements of the solid:solution distribution coefficient for ^{54}Mn were made as part of experiments 1C and 3C. The results are shown in Table IV.11 and in Figure IV.10. $K_{grav}(^{54}Mn)$ is very nearly constant below 0.5 cm in each experiment. 1C yields an average of 8.7±1.0, while the average from 3C is 6.7±1.2. K_{grav} at the sediment/water interface is significantly larger than it is below 0.5 cm and is larger after 11 days (17.7) than after 4 days (14.3).

The constancy of $K_{grav}(Mn)$ over time and space below 0.5 cm in the sediment column indicates that the rapid-equilibrium-exchange model used to describe the ^{54}Mn distribution is appropriate for both the short-term and the longer-term experiments (from 4 to at least 30 days). The consistency of the model used can be tested further by comparing the directly measured K_{grav} to the results calculated from the ^{54}Mn transport model. They agree quite well:

Experiment	K_{grav} (direct meas.)	K_{grav} (transport expt.)
3C	6.7±1.2	7.7±1.2
1C	8.7±1.0	5.9±1.4

(the directly measured values are averages, excluding the 0-0.5 cm values; the uncertainty shown is the 1σ error).

From equation IV.3, it can be seen that K depends directly on

Figure IV.10

Directly Measured K-grav for Mn-54

Results of measurements made as part of experiments 1C and 3C. 1C is plotted on the right (the 4 day experiment), and 3C is plotted on the left (the 11 day experiment).

Figure IV.10

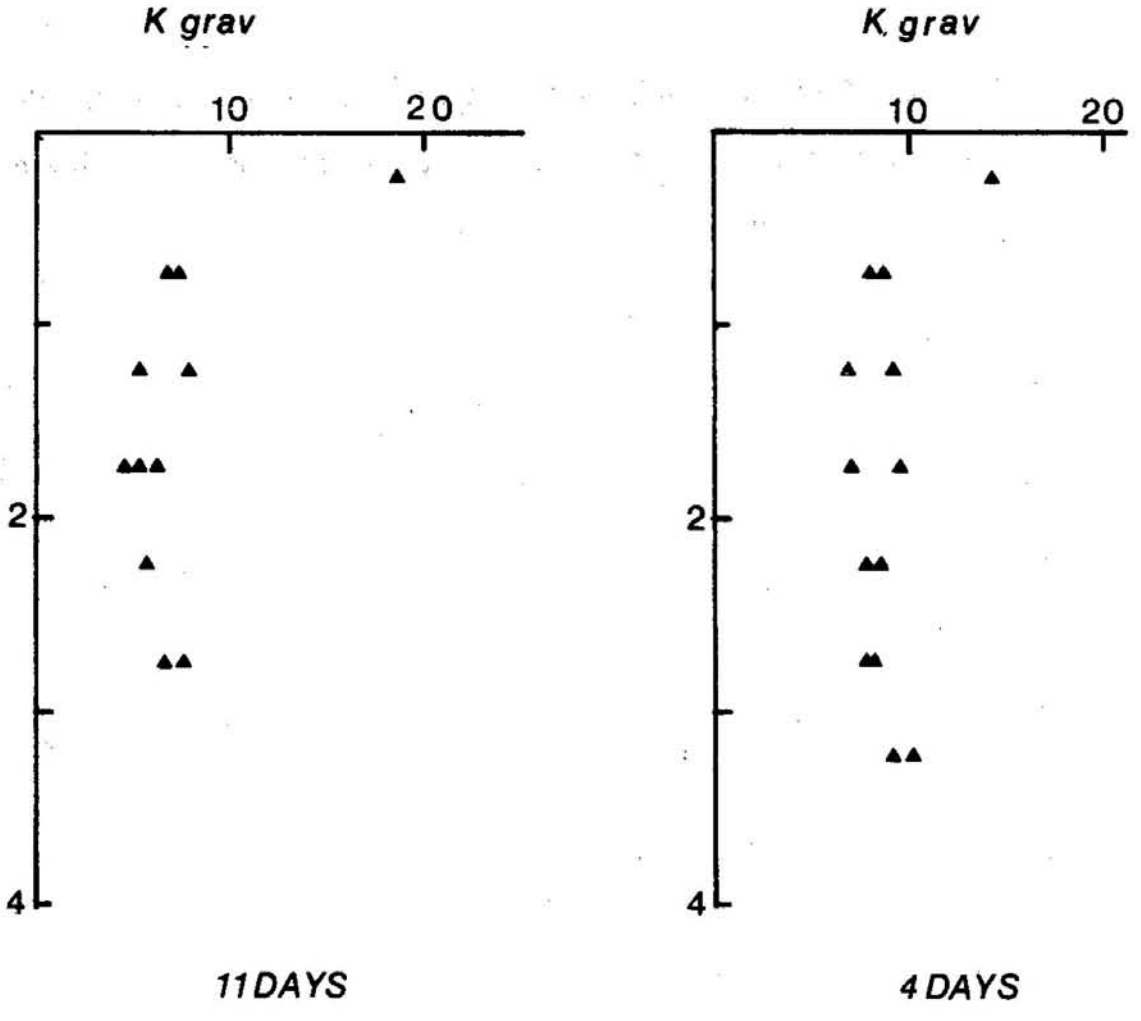

Table IV.11

Directly Measured Mn-54 Distribution Coefficients

In the table, samples are identified by their (z,ρ), as in Table IV.9. Units of K-grav are the same as for Table IV.10.

Experiment # 1C

Sample (z,ρ)	K-grav
0.25,0.25	14.3
0.80,0.75	8.85
0.80,0.25	8.26
1.38,0.75	7.30
1.38,0.25	9.01
1.95,0.75	7.25
1.95,0.25	9.80
2.63,0.75	8.20
2.63,0.25	8.85
3.33,0.75	8.13
3.33,0.25	8.47
3.93,0.75	9.09
3.93,0.25	10.8

Experiment # 3C

0.15,0.25	17.7
0.55,1.25	7.63
0.55,0.75	7.19
0.55,0.25	7.81
1.00,0.75	5.62
1.00,0.25	8.26
1.48,1.75	5.46
1.48,0.75	6.41
1.48,0.25	4.72
2.05,0.25	5.81
2.68,0.25	6.80
2.68,0.75	7.75

the value chosen for the solution phase diffusion rate of the tracer, D_{sed}. In the above comparison of K values, the molecular diffusion coefficient for ^{54}Mn was used to define its solution phase transport rate. The fact that this value produces a K_{grav} in agreement with the directly measured value is an indication that the simple point-source model of the tracer distribution provides a reasonable means of calculating apparent diffusion coefficients from the experimental ^{54}Mn distributions. The agreement lessens the uncertainty introduced by the ^{36}Cl migration results. Further, the close agreement found argues against the use of an enhanced diffusion coefficient to describe solute transport in the presence of irrigation; the experiments were carried out in July, when irrigation is significant at the study site (see Chapter 2). The contour plots of the tracer distributions for experiment 3C do appear to show some effect of irrigation, as preferential transport along a horizontal axis and along a vertical axis was noted (Figure IV.3); however, its effect was apparently too small and too localized to affect the transport rate calculation.

To summarize, then, the ^{54}Mn and ^{59}Fe transport experiments show that ^{54}Mn is considerably more mobile than ^{59}Fe and that this difference is due to a larger solid:solution distribution coefficient for the latter. This result is consistent with the hypothesis that the saturation state of the pore waters with respect to solid phases is a good indicator of the solid:solution distribution coefficients for ^{54}Mn and ^{59}Fe. The ^{59}Fe experiments showed some evidence of a time-varying distribution coefficient over short time

periods, indicating that an irreversible reaction occurring over a few days at the start of an experiment may affect its solid:solution distribution. The ^{54}Mn results, on the other hand, agreed very well with the rapid equilibrium exchange model of tracer transport. They showed consistency with the use of a molecular diffusion coefficient to describe solute transport in pore waters; and they agreed with the use of D_{app} for ^{63}Ni and ^{60}Co as an approximation to D_B, confirming the earlier conclusion that, under the conditions of these experiments, ^{63}Ni and ^{60}Co behave as particle tracers.

One other aspect of the ^{54}Mn distribution coefficient data is important: the existence of a larger distribution coefficient for ^{54}Mn in the upper 0.5 cm of sediment. This fact indicates that, over the short time scale of these experiments, a fraction of the ^{54}Mn may be oxidized at the sediment/water interface and trapped within the sediments. In the study of pore water Mn presented in Chapter 3, a 0.5 cm sampling interval was used to determine fluxes of dissolved Mn across the sediment/water interface. The dissolved Mn maximum always occurred in the 0-0.5 cm pore water sample. The results of the ^{54}Mn tracer experiments show that it may be necessary to measure pore water Mn at less than 0.5 cm intervals in reducing, nearshore sediments to get an accurate measurement of the dissolved Mn flux across the sediment/water interface.

Experiments to determine distribution coefficients for ^{54}Mn, ^{59}Fe, and ^{60}Co between marine sediments and O_2-containing seawater typically yield very large distribution coefficients, on the order of

10^3 (Duursma & Bosch, 1970). However, it has been demonstrated, in this work as well in others, that these elements are much more soluble in seawater under reducing conditions than they are in the presence of O_2. The radiotracer experiments of Luedtke & Bender (1979), carried out by introducing tracers into the seawater overlying box cores taken in Narragansett Bay, demonstrated this effect for ^{54}Mn in reducing sediments: they found that, of the ^{54}Mn present in the sediments after the completion of 14-day incubations, about 7% was in the pore water. In agreement with the results presented here, they found ^{59}Fe to be less mobile, with less than 1% present in pore water. Another set of radiotracer experiments has been carried out by Adler (1981) in Narragansett Bay sediments contained in the MERL microcosms. In these experiments, ^{60}Co, ^{54}Mn, and ^{59}Fe were introduced into overlying water and allowed to disperse for 90 days. Adler found that Mn could be included in a group of "very mobile" elements, while Co and Fe were included in a group of elements showing "some mobility". His results for ^{54}Mn and ^{59}Fe are in good agreement with the results of the experiments described in this work. For ^{54}Mn, he measured $K_{grav} \simeq$ 25 in the upper 0.5 cm of the sediments and values of 10-15 below 0.5 cm. These are somewhat larger than the values determined in Buzzards Bay, but are in good agreement, despite the important difference in the mode of introduction of ^{54}Mn into the sediments. While, in Adler's experiments, ^{54}Mn was introduced at the oxidizing sediment/water interface, in the Buzzards Bay experiments, it was introduced in the reducing zone of the sediments. The two sets of experiments agree less

closely for ^{59}Fe. Adler found K_{grav} (^{59}Fe) ≃ 1000-1500 near the sediment/water interface and 100-200 at 4-5 cm below the interface. No direct measurements of K_{grav}(^{59}Fe) were made in Buzzards Bay. Therefore, all values were determined from tracer dispersion rates, and are averages over several cm of the sediment column; values at the sediment/water interface cannot be distinguished. Adler's value of 100-200 at 4-5 cm is in good agreement with the values of 100-200 reported here.

Adler (1980) found ^{60}Co to be more mobile than it was found to be in the experiments reported here. This result may be due to the differing modes of introduction of tracers. Adler's experimental results depend more heavily on the near-interface cycling of the tracers. In chapter 3 of this work, it was shown that stable Co is recycled from the sediments to the water column with an efficiency similar to that found for Mn; stable Co was found to be recycled more efficiently than either Ni or Fe. These results from stable Co measurements tend to confirm Adler's finding that Co is "somewhat mobile" in a sediment/seawater system. In my tracer migration experiments, ^{60}Co was introduced below the sediment/water interface, where its low solubility relative to that of Mn and Fe appears to determine its dispersion rate. The effect of its insolubility may have been enhanced in my experiments because stable Co was introduced in large excess over pore water Co concentrations.

Conclusions

Using the results of the tracer dispersion experiments carried out *in situ* in Buzzards Bay and by Adler(1981) in the MERL microcosms, a picture of the depth dependence of ^{54}Mn and ^{59}Fe distribution coefficients emerges. Both isotopes have relatively large distribution coefficients at the sediment/water interface, where the presence of O_2 limits dissolved Mn and Fe concentrations; Fe, which is oxidized more rapidly in seawater than Mn (Murray & Gill, 1978; Emerson et al., 1979) has a distribution coefficient 40-60 times that of Mn. The distribution coefficients decrease to a minimum in the upper 4 cm of the sediments at the Buzzards Bay study site, with K_{grav}(Fe) about 15 times K_{grav}(Mn). The distribution coefficients increase deeper in the sediments, when solubility controls limit the concentrations of the metals to lower levels. Because the solubilities of Mn and Fe depend strongly on the presence of O_2 and on the presence of anionic products of organic matter degradation during early diagenesis, the depths of the regions of differing solid:solution distribution coefficients should vary as the depths of onset of Mn, Fe and SO_4 reduction vary.

The internal consistency of the experimental system used to determine K_{grav} at the Buzzards Bay site was demonstrated with comparisons of directly-measured and transport-determined distribution coefficients. Although they agreed well, there remains some uncertainty as to the adequacy of the model used to determine K_{grav}. In particular, ^{36}Cl dispersion experiments showed that the molecular

diffusion coefficient for Cl^- described only a portion of the ^{36}Cl distribution. Thus, further confirmation of the experimental results, from the development of a more sophisticated model and from more detailed ^{36}Cl dispersion experiments, would be useful in confirming the ^{54}Mn and ^{59}Fe distribution coefficient determinations.

A somewhat different picture emerges for ^{60}Co. While my experiments show ^{60}Co to be essentially completely particle-bound within the sediment column, Adler's results indicate that it may have some, limited mobility in a seawater/sediment system, similar to that of ^{59}Fe, presumably because of its Mn-like cycling near the sediment/water interface. At least below the sediment/water interface, ^{63}Ni behaves similarly to ^{60}Co, being particle-bound. The order of mobilities among the suite of tracers examined in these experiments is Mn>>Fe>Co,Ni; this order is in agreement with the solubility trend for these metals in reducing sediments.

Appendix IV.1

Table IV.9

Results of Tracer Release Experiments

Each sample is identified by its (z,ρ), with $z = 0$ at the sediment/water interface and $\rho = 0$ at the edge of the probe. The (z,ρ) are the midpoints of the sample intervals. Also included is $R = ((z-z_0)^2 + (\rho-\rho_0)^2)^{1/2}$, where (z_0,ρ_0) is the release position. The activities listed are the ratios,

$$\frac{A(z,\rho)}{A(z_0,\rho_0)}$$

for ^{54}Mn, ^{59}Fe, ^{60}Co, and ^{63}Ni.

The table begins on the following page

Experiment # 1C

Z	ρ	R	R^2	MN	FE	CO	NI
0.250	0.250	2.250	5.063	0.088	0.013	0.000 *	
0.250	0.750	2.305	5.312	0.079		0.003*	
0.250	2.750	3.363	11.313	0.007*	0.002*	0.002 *	
0.800	0.250	1.700	2.890	0.199	0.034	0.013	0.006
0.800	0.750	1.772	3.140	0.173	0.039	0.007	
0.800	1.750	2.267	5.140	0.067	0.004		
1.375	0.250	1.125	1.266	0.410	0.184	0.090	0.049
1.375	0.750	1.231	1.516	0.338		0.046	0.025
1.375	1.750	1.875	3.516	0.123	0.009		0.000
1.950	0.250	0.550	0.303	0.857	0.686	0.716	0.579
1.950	0.750	0.743	0.553	0.615	0.412	0.379	
1.950	1.250	1.141	1.302	0.355	0.165	0.083	0.063
1.950	2.250	2.074	4.302	0.058	0.012	0.002	0.003
2.625	0.250	0.125	0.016	1.000	1.000	1.000	1.000
2.625	0.750	0.515	0.266	0.802	0.602	0.493	0.423
2.625	1.250	1.008	1.016	0.433	0.194	0.123	
2.625	1.750	1.505	2.266	0.245	0.111	0.121	0.141
2.625	2.750	2.503	6.266	0.084	0.027	0.002	
3.325	0.250	0.825	0.681	0.713	0.273	0.130	0.091
3.325	0.750	0.965	0.931	0.523	0.140	0.058	0.053
3.325	1.750	1.712	2.931	0.195	0.048	0.006	0.004
3.925	0.250	1.425	2.031	0.349		0.021	0.017
3.925	0.750	1.510	2.281	0.273	0.026	0.082	0.012
3.925	1.750	2.069	4.281	0.097	0.007		
4.600	0.250	2.100	4.410	0.083	0.021	0.013	
4.600	1.250	2.326	5.410	0.039			

Experiment # 3C

Z	ρ	R	R^2	MN	FE	CO	NI
0.150	0.250	1.916	3.672	0.500*			0.003
0.150	0.750	1.916	3.672		0.040		
0.150	2.750	2.945	8.672	0.078*			
0.550	0.250	1.521	2.313	0.210	0.067	0.005	0.004
0.550	0.750	1.521	2.313	0.255		0.004	0.001
0.550	1.250	1.677	2.812	0.274			0.001
0.550	1.750	1.953	3.813	0.183	0.031		
0.550	3.500	3.354	11.250	0.033*	0.014*	0.008*	
1.000	0.250	1.079	1.165	0.433	0.149	0.022	0.031
1.000	0.750	1.079	1.165	0.469	0.175	0.022	0.012
1.000	1.250	1.290	1.665			0.006	0.003
1.000	2.250	2.041	4.165	0.182	0.025	0.002	
1.475	0.250	0.627	0.393	0.554	0.358	0.168	0.169
1.475	0.750	0.627	0.393	0.604	0.407	0.312	0.323
1.475	1.250	0.945	0.893	0.445	0.260	0.041	
1.475	1.750	1.376	1.893	0.264	0.094	0.003	0.002
1.475	3.500	3.055	9.331	0.048	0.005*	0.004*	
2.050	0.250	0.250	0.062	0.874	0.951	0.972	0.974
2.050	0.750	0.250	0.062	0.734	1.000	1.000	1.000
2.050	1.250	0.750	0.562	0.577	0.574	0.589	0.562
2.050	2.250	1.750	3.063	0.222	0.060	0.004	0.003
2.675	0.250	0.673	0.453	1.000	0.904	0.285	0.309
2.675	0.750	0.673	0.453	0.869	0.712	0.369	0.396
2.675	1.250	0.976	0.953	0.604	0.318	0.030	0.041
2.675	1.750	1.398	1.953	0.486	0.060	0.006	0.006
3.400	0.250	1.373	1.885	0.667	0.202	0.041	0.040
3.400	0.750	1.373	1.885	0.658	0.102	0.002	
3.400	1.250	1.544	2.385	0.260	0.015		
3.400	1.750	1.840	3.385	0.158	0.007		

Experiment # 3

Z	ρ	R	R^2	MN	FE	CO	NI
0.300	0.250	0.000	0.000	1.000	1.000	1.000	1.000
0.300	0.750	0.500	0.250	0.565*	0.641	0.443	0.535
0.300	1.250	1.000	1.000	0.743	0.385	0.186	0.167
0.300	1.750	1.500	2.250	0.535	0.186	0.074	0.062
0.300	2.250	2.000	4.000	0.381	0.083	0.027	0.026
0.300	2.750	2.500	6.250	0.372	0.056	0.014	0.011
0.300	3.750	3.500	12.250	0.137			
0.900	0.250	0.600	0.360	0.994	0.374	0.070	0.028
0.900	0.750	0.781	0.610	0.938	0.253	0.079	0.048
0.900	1.250	1.166	1.360	0.769	0.136	0.035	0.018
0.900	1.750	1.616	2.610	0.582	0.085	0.011	
0.900	2.250	2.088	4.360	0.261	0.041	0.003	0.003
0.900	3.250	3.059	9.360	0.165			
1.550	0.250	1.250	1.562	0.945	0.118	0.006	0.003
1.550	0.750	1.346	1.813	0.848	0.071	0.002	0.001
1.550	1.250	1.601	2.563	0.712	0.042	0.002	0.000
1.550	1.750	1.953	3.813	0.505	0.027	0.001	0.000
1.550	2.250	2.358	5.563	0.416	0.012	0.000	0.000
1.550	3.750	3.717	13.813	0.128			
2.300	0.250	2.000	4.000	0.696	0.031	0.001	0.001
2.300	0.750	2.062	4.250	0.663	0.014	0.000	0.000
2.300	1.750	2.500	6.250	0.654	0.012		
2.300	1.750	2.500	6.250	0.449	0.006	0.000	
2.300	2.750	3.202	10.250	0.172			
3.000	0.250	2.700	7.290	0.526		0.000	0.000
3.000	0.750	2.746	7.540	0.464	0.002		
3.000	1.250	2.879	8.290	0.273			
3.600	0.250	3.300	10.890	0.264	0.006*	0.001*	
3.600	0.750	3.338	11.140	0.230			
3.600	1.750	3.625	13.140	0.079			
3.600	2.750	4.140	17.140	0.052			
4.350	0.250	4.050	16.402	0.014*	0.003*	0.002*	

Experiment # 3B

Z	ρ	R	R^2	MN	FE	CO
0.250	0.250	2.250	5.063	0.042 *		
0.250	1.250	2.462	6.063	0.035 *		
0.725	0.250	1.775	3.151	0.374	0.057	0.005
0.725	0.750	1.844	3.401	0.296	0.031	0.006
0.725	1.750	2.324	5.401	0.201	0.010	0.008 †
0.725	3.250	3.486	12.151	0.089		
1.225	0.250	1.275	1.626	0.516	0.161	0.025
1.225	1.250	1.620	2.626	0.328	0.073	0.050
1.225	2.250	2.372	5.626	0.238	0.015	0.005 †
1.225	3.750	3.725	13.876	0.109	0.006 *	
1.800	0.250	0.700	0.490	0.830	0.526	0.589
1.800	0.750	0.860	0.740	0.590	0.236	0.300
1.800	1.250	1.221	1.490	0.551	0.132	0.056
1.800	1.750	1.655	2.740	0.437	0.076	0.014
2.550	0.250	0.050	0.002	1.000	1.000	1.000
2.550	0.750	0.502	0.252	0.647	0.256	0.269
2.550	1.250	1.001	1.002	0.521	0.136	0.044
2.550	1.750	1.501	2.252	0.519	0.066	0.022
2.550	2.750	2.500	6.252	0.294	0.018	0.002 †
2.550	3.750	3.500	12.252	0.146		
3.400	0.250	0.900	0.810	0.701	0.171	0.029
3.400	0.750	1.030	1.060	0.637	0.113	0.006
3.400	1.250	1.345	1.810	0.573	0.047	0.008
3.400	1.750	1.749	3.060	0.528	0.045	0.002
3.400	3.250	3.132	9.810	0.229		
4.050	0.250	1.550	2.402	0.516	0.042	0.005
4.050	1.250	1.845	3.402	0.509		
4.050	2.250	2.530	6.402	0.393		
4.650	0.750	2.207	4.872	0.417		0.001
4.650	1.750	2.622	6.872	0.331		
4.650	3.250	3.691	13.622	0.143		
5.200	0.250	2.700	7.290	0.282	0.012	
5.200	1.250	2.879	8.290	0.210		0.001 †
5.700	0.250	3.200	10.240	0.111		
5.700	1.750	3.534	12.490	0.080		

Experiment # 6

Z	ρ	R	R^2	MN	FE	CO *	NI
0.300	0.250	5.400	29.160	0.005			
1.550	0.250	4.150	17.222	0.004			
2.150	1.250	3.688	13.602	0.010			
2.750	0.250	2.950	8.702	0.025		0.002	0.002 *
2.750	1.750	3.309	10.952	0.019		0.000	
3.450	0.250	2.250	5.063	0.072	0.004	0.007	0.005
3.450	1.250	2.462	6.063	0.050	0.006	0.008	
4.150	0.250	1.550	2.403	0.188	0.011	0.010	0.010
4.150	0.750	1.629	2.653	0.152		0.000	0.000
4.150	1.750	2.157	4.653	0.083	0.004	0.002	
4.850	0.250	0.850	0.722	0.460	0.065	0.035	0.030
4.850	0.750	0.986	0.972	0.347	0.016	0.006	0.008
4.850	1.250	1.312	1.722	0.256	0.002	0.001	0.003
4.850	1.750	1.724	2.972	0.161	0.022	0.005	
5.600	0.250	0.100	0.010	1.000	1.000	1.000	1.000
5.600	0.750	0.510	0.260	0.725	0.413	0.390	0.326
5.600	1.250	1.005	1.010	0.507	0.182	0.117	0.156
5.600	1.750	1.503	2.260	0.358		0.093	0.105
6.350	0.250	0.650	0.423	0.971	0.315	0.189	0.222
6.350	0.750	0.820	0.673	0.659	0.180	0.099	0.120
6.350	1.250	1.193	1.422	0.404		0.164	0.247
6.350	2.250	2.103	4.422	0.193	0.064	0.039	
6.350	2.750	2.583	6.672	0.130	0.068	0.019	
7.000	0.250	1.300	1.690	0.636	0.283	0.222	0.217
7.000	0.750	1.393	1.940	0.408	0.018	0.007	0.009
7.000	1.250	1.640	2.690	0.327		0.004	0.005
7.000	2.250	2.385	5.690	0.172	0.007	0.002	
7.650	0.250	1.950	3.802	0.256	0.024	0.016	0.016
7.650	0.750	2.013	4.052	0.212	0.003	0.000	0.000
7.650	1.750	2.460	6.052	0.086		0.000	
7.650	2.750	3.171	10.052	0.030		0.014	
8.350	0.750	2.697	7.272	0.054			
8.350	1.750	3.045	9.272	0.028		0.001	
9.800	0.250	4.100	16.810	0.002			

Experiment # 1C Cl-36

z	ρ	R^2	ln (C/C0)
0.25	0.25	5.64	-2.341
0.25	1.25	6.64	-2.707
0.25	1.75	7.89	-2.834
0.25	2.25	9.64	-2.889
0.25	2.75	11.89	-2.839
0.80	0.25	3.33	-1.434
0.80	0.75	3.58	-1.423
0.80	1.75	5.58	-2.019
0.80	2.25	7.33	-2.144
0.80	2.75	9.58	-2.271
1.375	0.25	1.56	-0.774
1.375	0.75	1.81	-0.931
1.375	1.25	2.56	-1.371
1.375	1.75	3.81	-1.507
1.375	2.25	5.56	-1.617
1.375	2.75	7.81	-1.826
1.95	0.25	0.456	-0.150
1.95	0.75	0.706	-0.237
1.95	1.25	1.46	-0.763
1.95	2.25	4.46	-1.153
1.95	2.75	6.71	-1.518
2.625	0.25	0.0	1.0
2.625	0.75	0.25	-0.115
2.625	1.25	1.00	-0.376
2.625	1.75	2.25	-0.418
2.625	2.25	4.00	-1.063
2.625	2.75	6.25	-1.402
3.325	0.25	0.490	-0.293
3.325	0.75	0.740	-0.444
3.325	1.25	1.49	-0.709
3.325	1.75	2.74	-1.097
3.325	2.25	4.49	-1.157
3.325	2.75	6.74	-1.356
3.925	0.25	1.69	-0.701
3.925	1.25	2.69	-1.129
3.925	1.75	3.94	-1.153
3.925	2.75	7.94	-1.524
4.60	0.25	3.90	-1.153
4.60	0.75	4.15	-1.129
4.60	1.25	4.90	-1.279
4.60	1.75	6.15	-1.361
4.60	2.25	7.90	-1.512

Experiment # 3C Cl-36

z	ρ	R^2	ln (C/C0)
0.15	1.25	4.61	-2.454
0.55	0.25	2.25	-1.389
0.55	0.75	2.50	-1.277
0.55	1.25	3.25	-1.619
0.55	1.75	4.50	-3.946
0.55	2.25	6.25	-3.169
0.55	2.75	8.50	-3.255
0.55	3.50	12.81	-3.299
1.00	0.25	1.103	-1.706
1.00	0.75	1.35	-0.529
1.00	1.75	3.35	-2.459
1.00	2.25	5.103	-2.611
1.00	3.50	11.67	-2.944
1.475	0.25	0.331	-0.405
1.475	0.75	0.581	-0.151
1.475	1.25	1.33	-0.688
1.475	1.75	2.58	-0.718
1.475	2.25	4.33	-1.427
1.475	2.75	6.58	-1.511
1.475	3.50	10.89	-2.041
2.05	0.25	0.0	1.0
2.05	0.75	0.250	-0.010
2.05	1.25	1.00	0.656
2.05	1.75	2.25	-0.086
2.05	2.25	4.00	-1.062
2.675	0.25	0.391	-0.289
2.675	0.75	0.641	-0.209
2.675	1.25	1.39	-0.973
2.675	1.75	2.64	-1.429
2.675	2.25	4.39	-1.952
2.675	2.75	6.64	-1.915
3.40	0.25	1.82	-1.634
3.40	0.75	2.07	-0.904
3.40	1.25	2.82	-1.466
3.40	1.75	4.07	-1.912
3.90	0.75	4.45	-1.476
3.90	1.25	5.20	-2.352

Chapter 5

Summary and Conclusions

The focus of this work has been on rates of transport of metals both across the sediment/water interface and within the sediment column of nearshore sediments. It has been shown that, at the Buzzards Bay site, rates of particle mixing are about ten times slower than the molecular diffusion rates of dissolved first-row transition metals. Thus, key factors in metal transport are the rates and depths in the sediment column of solid:solution exchange reactions. In addition, it has been shown that both the rate and mechanism of solute transport vary seasonally, and that the effects of these variations on metal transport must be considered. The rate of particle transport is also an important consideration, as bioturbation redistributes the particulate sources of dissolved metals in the upper 2.5 cm of the sediment column. When these factors are taken into consideration -- solid:solution exchange reactions and rates and mechanisms of solute and particle transport -- then, conclusions can be drawn about the mechanisms determining the involvement of early diagenetic reactions in nearshore sediments in coastal ocean metal cycles.

Solid:Solution Exchange Reactions

Solid:solution exchange reactions are important because of the rapidity of solute relative to particle transport. Because mechanisms and rates of solute transport vary with depth below the sediment/water interface, it is convenient to group solid:solution exchanges according to their position in the sediment column. Oxidation reactions may be important close to the interface; reactions producing dissolved metals from particulate sources occur next; then, reactions involving precipitation of reduced metals with the products of organic matter degradation occur.

The pore water chemistry studies presented in Chapter 3 showed that the flux of dissolved Fe across the sediment/water interface varied seasonally, with the largest Fe fluxes occurring when the redox potential at the sediment/water interface was lowest. An important reason for this pattern is the rapid oxidation of Fe(II) to insoluble Fe(III) in the presence of O_2. O_2 can penetrate furthest below the interface -- to about 1 cm -- in late winter and spring, when the low temperature and supply of organic matter limit the rate of benthic metabolic activity. Thus, oxidation reactions, removing Fe from solution, are important to the transport of Fe across the sediment/water interface.

The pore water chemistry study did not show oxidation to be important for Mn. However, in situ ^{54}Mn migration experiments showed a secondary maximum in the ^{54}Mn distribution at 0-0.5 cm below the sediment/water interface and a larger solid:solution distribution coefficient for Mn in the same interval. Both results are evidence for removal of Mn from

solution near the sediment/water interface; oxidation of Mn(II) to insoluble Mn(IV) is the most likely mechanism. Although 0.5 cm interval pore water samples do not show removal of Mn from solution at the sediment/water interface, such removal may be occurring, and may limit the Mn flux across the interface.

When Mn and Fe are oxidized, there is the possibility of adsorption of other transition metals to the freshly precipitated oxide surfaces (Parks, 1975). Therefore, although 0.5 cm interval pore water samples showed no removal of Co, Ni, or Cu above their pore water maxima (which occurred in the first sanple interval, 0-0.5 cm), such removal may occur. Either finer sample intervals or direct flux measurements would be necessary to determine if there is Mn and trace metal removal by oxidation reactions at the interface of nearshore sediments.

The production of dissolved Mn, Co, Cu, and Ni occurs in the upper 0.5-1.5 cm of the sediment column at the Buzzards Bay site. For Mn and Co, net production is always observed, to depths of up to 1.5 cm when sulfate reduction is least important near the interface (late winter/spring), and to 0.5 cm or less under the most reducing conditions (during the summer or fall). Net dissolved Ni and Cu production show greater variability with the depth of sulfate reduction. Dissolved Ni production is similar to that of Mn and Co when the interface is relatively oxidizing, but is only just significant when sulfate reduction occurs very near the interface. Net production of Cu in the 0-0.5 cm sample interval is observed only when sulfate reduction is limited to deeper in the sediment column: in 6/84, when sulfides were present in the

upper 0.5 cm, a zone of net dissolved Cu production could not be resolved with a 0.5 cm sample interval.

The depth of net dissolved Fe production is more variable. The position of the dissolved Fe maximum ranges from the 0-0.5 cm interval in cores taken in the fall to the 2-2.5 cm interval in late winter/spring cores.

Dissolved metals are produced by both "primary" and "secondary" mechanisms. The primary mechanisms are those that result directly from the oxidation of organic matter. Mn (IV) and Fe(III) are used as electron acceptors during the oxidation of organic matter, and are produced rapidly during early diagenesis. Cu is released to solution from carrier phases during oxic diagenesis; Ni and Co are released when Mn(IV) is reduced. The secondary mechanisms of dissolved metal production occur when particle mixing redistributes particulate metals that form when dissolved metals react with organic matter breakdown products. When the reduced metals precipitate near the interface of nearshore sediments, the bioturbating macrobenthos can cycle the metals from layers where precipitation is favored back to layers where dissolution is favored. In Chapter 3, this cycling was shown to be important at the Buzzards Bay site for Mn and Fe. Depending on the accumulation rates of Co, Ni, and Cu at the study site, it may also be important fro these trace metals.

Except for Fe, whose transport across the sediment/water interface is limited by its rapid oxidation to Fe(III), the variability in fluxes of the metals studied depends largely on their solubility in reducing marine systems. At various points in this thesis, evidence concerning the

relative solubilities of the metals studied, from measured equilibrium constants, from observed behavior in marine anoxic basins, and from in situ radiotracer migration studies in Buzzards Bay, was presented. Although quantitative results from the radiotracer migration study are preliminary in that ^{36}Cl experiments indicated that there is uncertainty as to the adequacy of the model applied to the data, the qualitative results from this study, along with the other evidence cited, showed that the metals' solubility decreased in the order, Mn>Fe>>Co,Ni,Cu. The pore water chemistry study agreed with these results in most respects, the ecxeption being that Co behaves very similarly to Mn near the sediemt /water interface.

Calculated dissolved metal fluxes showed that solubility in suboxic and anoxic systems is an inportant factor for Mn, Co, Ni, and Cu, as the fluxes of all four are reduced when sulfides are present in the upper 0.5 cm of the sediments. It is most important for Cu. The rate of removal of the dissolved metals to the solid phase decreases in the order, Cu>Ni>Co,Mn under very reducing conditions; Ni is removed at a rate similar to that for Mn and Co when conditions are less reducing. It is difficult to distinguish the phasess to which the metals are removed. However, it appears likely that the sulfide-forming metals, Cu, Ni, and Co, are removed to sulfides, either by precipitation or by sorption onto Fe sulfides. Mn may be removed to either a sulfide or a phosphate phase near the sediment/water interface.

To summarize, solid:solution exchange reactions for Fe, Mn, Co, Ni, and Cu can be divided into three groups in nearshore sediments. Oxidation

reactions very near the interface cause precipitation of Fe, and perhaps of Mn. Reactions producing dissolved Mn, Co, Ni, and Cu occur in the upper 0.5 cm, and as deep as 1.5 cm when benthic metabolism is relatively slow; net production of dissolved Fe occurs at depths ranging from 0-0.5 cm to depths greater than 2 cm. Precipitation of the metals with sulfide and with organic matter breakdown products is an important determinant of metal fluxes across the sediment/water interface for Cu and Ni, especially, and also for Mn and Co.

Solute Transport

Solute transport is the most important mechanism moving reactive metals in nearshore sediments. It occurs by two mechanisms: molecular diffusion and exchange of solutes across the walls of rapidly flushed tube and burrow structures. The $^{222}Rn/^{226}Ra$ disequilibrium measurements presented in Chapter 2 showed that molecular diffusion is the dominant mode of transport during cold months (December through at least March), that rapid irrigation to at least 20 cm occurs in early summer, and that irrigation is important to depths of about 10 cm in late summer/fall (September, October). When using the ^{222}Rn deficit to infer the depth to which irrigation removes solutes, it is important to remember that the ^{222}Rn distribution depends on events occurring over only about a 2-week period; irrigation to greater depths may be important when longer time scales are considered.

Dissolved maxima for Mn, Co, Ni, and Cu occur in the upper 0.5 cm of

the sediment column at the study site. In this case, the distance from the position of dissolution to the sediment/water interface is less than or equal to the distance to burrow walls. This fact, coupled with the large concentration gradients across the sediment/water interface, implies that diffusion across the interface is the primary means by which dissolved metals are transfered between pore waters and overlying water. Calculated fluxes confirm the prediction: for Mn, the nonlocal exchange flux never ranged from 0% to 45% of the vertical diffusion flux at the Buzzards Bay site. For the trace metals, Co, Ni, and Cu, pore water concentrations below the upper cm of the sediments were similar to bottom water concentrations, and nonlocal exchange produced only very small net transfers. Nonlocal exchange may be important for Fe, which often has a dissolved maximum below the upper centimeter of the sediments. In one case (6/84), a dissolved Fe concentration of 600μM at 2 cm below the interface yielded a calculated nonlocal exchange flux that was 20% of the diffusion flux. The importance of the nonlocal exchange flux for Fe may be limited by Fe oxidation in O_2-containing burrow water. Aller (1976), for instance, has measured solid phase enrichments in the sediments surrounding burrow walls. Determination of the importance of irrigation to Fe cycling must await further field measurements and experimental determination of the permeability of burrow walls to Fe diffusion (Aller, 1983).

Determination of the nonlocal exchange served an important purpose in this study: it removed ambiguity as to the mechanism of dissolved Mn, Co, Ni, and Cu removal operating at 0.5-3cm below the interface. Because

nonlocal exchange could account for only a fraction of the metal removed from the pore waters, it could be unambiguously determined that removal to solid phases was of primary importance.

Particle Transport

Particle transport at the Buzzards Bay site was found to occur at rates ranging from about 10-80x10^{-8} cm^2/sec in the upper 2-2.5 cm of the sediment column using excess ^{234}Th measurements. Use of ^{60}Co and ^{63}Ni as particle tracers in in situ tracer migration experiments allowed the determination of particle mixing rates of about 10x10^{-8} cm^2/sec to a depth of 5 cm. These mixing rates, coupled with solution-phase transport by molecular diffusion and assumption of a rapid equilibrium exchange model, were consistent with directly measured ^{54}Mn solid:solution distribution coefficient measurements. This consistency was important to the interpretation of the results of the tracer migration experiments because of uncertainties concerning the model used to interpret the data. The uncertainties arose from the interpretation of ^{36}Cl migration in the experiments; finalization of the results will require development of a more sophisticated model and further ^{36}Cl dispersion experiments.

The primary importance of particle transport by bioturbation to metal cycling in nearshore sediments is as a redistributor of solids from layers favoring metal precipitation to layers favoring metal dissolution. Thus, Fe sulfides can be returned to layers in which they can contact

O_2, so that their sulfur is oxidized and Fe is either released to solution or oxidized to Fe(III). Similarly, particulate Mn (and perhaps Co, Cu, and Ni) can be mixed from their zones of formation to zones in which they are undersaturated. This mixing has been proposed to be an important process maintaining the Mn distribution in the upper 3 cm of the Buzzards Bay site. By enhancing solution phase concentrations near the sediment/water interface, it may contribute in an important way to metal regeneration during early diagenesis in bioturbated sediments.

Regeneration of Mn, Fe, Ni, Cu, and Co in Nearshore Sediments

When considering their regeneration during early diagenesis in nearshore sediments, these metals can be divided into three groups. Fe stands alone, as its cycling is different from that of the other four. Cu and Ni are grouped together, as are Mn and Co.

Fe(III) is used after Mn(IV) in the sequence of electron acceptors for the microbial oxidation of organic matter. Dissolved Fe production occurs deeper in the sediment column than Mn production; it is oxidized more rapidly in seawater. It is recycled to the water column more efficiently, the more rapidly organic matter oxidation occurs at the sediment/water interface. When the interface underlying oxygenated bottom water is most reducing, the dissolved Fe maximum is in the upper few mm of the sediment column, and, barring oxidation in a very thin layer at the interface, the dissolved Fe flux is large. Then, siginficant enrichments in Fe can be observed in water column particulate matter

(Murray & Gill, 1978).

The efficiency of the cycling of Cu, especially, and also of Ni, varies inversely to that of Fe. These metals are very insoluble in the presence of sulfide, and are removed rapidly from pore waters of nearshore sediments when sulfate reduction occurs very near the interface. Cu is especially insoluble; if the dissolved Cu flux is calculated based on 0.5 cm sampling intervals, it is directed into the sediments when sulfides are present in the upper 0.5 cm (6/84 at the Buzzards Bay site). When sulfides are not present at the interface, there is a small but possibly significant dissolved Cu flux. At the Buzzards Bay site, the maximum Cu flux observed, in a late winter core, was 10^{-7} nmol/cm^2.sec (3/84); if the average concentration in the 15 m water column is assumed to be 5 nM (the measured bottom water concentration), then this flux would imply a minimum turnover time for dissolved Cu of about 2 years. The calculated Ni flux in 3/84 (22×10^{-8} nmol/cm^2.sec) implies a similar minimum turnover time for dissolved Ni. The Ni flux decreased to very near the detection limit under very reducing conditions (6/84). These results are tentative, in that they are based on only two cores from a single site. However, the two cores represent a period when the effects of sulfate reduction near the interface dominated the pore water characteristics (6/84), and a period when its effects were relatively minor (3/84). Thus, they can be considered to represent extremes of conditions at the Buzzards Bay site. The observation of a minimum turnover time of two years for dissolved Ni and Cu relative to their benthic fluxes is an indicator that regeneration of these metals

within the sediment column in the fine-grained sediments of Buzzards Bay is probably a secondary factor in their local cycling.

The third group is Mn and Co. As is true for Cu and Ni, the fluxes of these metals decrease when sulfides are present in the upper 0.5 cm of the sediment column. However, the decrease is small. From 3/84 to 6/84, the Co flux decreased only from 23 to 19×10^{-8} nmol/cm^2.sec, not a significant change. The efficiency with which the dissolved Co produced in the sediments was recycled to the water column decreased from 82 to 56%. Similar variations were observed for Mn. Throughout this study, the range of calculated Mn fluxes was $6\text{-}11 \times 10^{-7}$ μmol/cm^2.sec; the efficiency of dissolved Mn recycling varied from 59% (6/84) to 84% (9/83). The dissolved Mn flux is very important to Mn cycling in the coastal ocean. It implies very significant enrichments of Mn on water column particulates (up to 10,000 ppm); such enrichments have been observed in coastal waters (Yeats et al., 1979). The dissolved Co concentration in Buzzards Bay water is not well known, but if the measured bottom water concentration (5 nM) is assumed to equal the average concentration, the residence time of dissolved Co relative to the benthic flux is 1 year. This flux may be significant in the dissolved Co cycle.

It has been shown that there is active cycling of first-row transition metals between solids and solution near the interface of nearshore sediments. While the regeneration of Mn and Co is, to a first approximation, independent of season, that of Fe, Cu, and Ni varies significantly. Fe regeneration is most important when the interface is

reducing, in summer and fall. Cu and Ni regeneration are most important when the interface is relatively oxidizing, in winter and spring. The flux of dissolved Mn is very significant to the coastal Mn cycle, producing large enrichments of Mn on water column particles. The Fe flux may have a similar effect at some times of year. The fluxes of the trace metals may not be primary factors in coastal trace metal budgets. However, at least for Co, the flux is significant, as it implies a turnover time of dissolved Co in the water column of a year or less. Similarly calculated residence times for dissolved Ni and Cu are greater than two years.

In considering the calculated fluxes, it is important to remember that their accuracy depends on the accuracy with which the average pore water concentration in the upper 0.5 cm of the sediment column reflects the interfacial dissolved metal concentration. An important goal of future research will be to test the accuracy of the average value, either by sampling pore waters at finer intervals or by direct flux measurements.

REFERENCES

Adler, D.M. 1981 Tracer Studies in Marine Microcosms: Transport Processes Near the Sediment/Water interface. PhD Thesis, Columbia University.

Aller, R.C. 1977 The influence of macrobenthos on chemical diagenesis of marine sediments. PhD Thesis, Yale University, New Haven, CT.

Aller, R.C., 1980a Diagenetic processes near the sediment-water interface of Long Island Sound. I. Decomposition and nutrient element geochemistry (S,N,P). in B. Saltzman, ed., Estuarine Physics and Chemistry: Studies in Long Island Sound, Advances in Geophysics 22, 237-349.

Aller, R.C. 1980b Diagenetic Processes near the sediment-water interface of Long Island Sound. II. Fe and Mn. in B. Saltzman, ed., Estuarine Physics and Chemistry: Studies in Long Island Sound, Advances in Geophysics 22, Academic Press, pp. 351-415.

Aller, R.C. 1980c Quantifying solute distributions in the bioturbated zone of marine sediments by defining an average microenvironment. Geochim. Cosmochim. Acta 44, 1955-1965.

Aller, R.C. 1982 The effects of macrobenthos on chemical properties of marine sediment and overlying water, in P.L.McCall and M.J.S. Teveez, eds., Animal-Sediment Relations, Plenum Publishing Corporation

Aller, R.C. 1983 The importance of the diffusive permeability of animal burrow linings in determining marine sediment chemistry J. Mar. Res. 41, 299-322

Aller, R.C., and Cochran, J.K. 1976 $^{234}Th/^{238}U$ disequilibrium in nearshore sediments: particle reworking and diagenetic time scales. Earth Planet. Sci. Lett. 29, 37.

Aller, R.C., and Yingst, J.Y. 1978 Biogeochemistry of tube dwellings: a study of the sedentary polychaete Amphitrite ornata (Leidy). J. Mar. Res. 36, 201-254

Aller, R.C., Benninger, L.K., and Cochran, J.K. 1980 Tracking particle-associated processes in nearshore environments by use of $^{234}Th/^{238}U$ disequilibrium. Earth Planet. Sci. Lett. 47, 161.

Aller, R.C., Yingst, J.Y., and Ullman, W.J. 1983 Comparative biogeochemistry of water in intertidal Onuphis (polychaeta) and Upogebia (crustacea) burrows: temporal patterns and causes J. Mar. Res. 41, 571-604

Aller, R.C. and DeMaster, D.J. 1984 Estimates of particle flux and reworking at the deep-sea floor using $^{234}Th/^{238}U$ disequilibrium. Earth Planet. Sci. Lett. 67, 308-318.

Andrews, D., and Bennett, A. 1981 Measurements of diffusivity near the sediment-water interface with a fine-scale resistivity probe Geochim. Cosmochim. Acta 45, 2169-2175

Balistrieri, L.S. and Murray, J.W. 1984 Marine Scavenging: trace metal adsorption by interfacial sediment from MANOP Site H. Geochim. Cosmochim. Acta 48, 921-929

Bender, M.L., Klinkhammer, G.P., and Spencer, D.W. 1977 Manganese in seawater and the marine manganese balance. Deep-Sea Res. 24, 799-812.

Bender, M.L., and Heggie, D.T. 1984 Fate of organic carbon reaching the deep sea floor: a status report. Geochim. Cosmochim. Acta 48, 977-986.

Benninger, L.K., Aller, R.C., Cochran, J.K., and Turekian, K.K. 1979 Effects of biological sediment mixing on the ^{210}Pb chronology and trace metal distribution in a Long Island Sound sediment core. Earth Planet. Sci. Lett. 43, 241-259

Berelson, W.M., Hammond, D.E., & Fuller, C. 1982 Radon-222 as a tracer for mixing in the water column and benthic exchange in the southern California borderland. Earth Planet. Sci. Lett. 61, 41-54

Berger, W.H. and Heath, G.R. 1968 Vertical mixing in pelagic sediments. J. Mar. Res. 26, 134

Berner, R.A. 1970 Sedimentary pyrite formation. Am. Jour. Sci. 268, 1-23.

Berner, R.A. 1980 Early Diagenesis: A Theoretical Approach. Princeton University Press, Princeton, New Jersey.

Bevington, P.R. 1969 Data Reduction and Error Analysis for the Physical Sciences, McGraw-Hill

Boudreau, B.P. 1984 On the equivalence of nonlocal and radial-diffusion models for pore water irrigation J. Mar. Res. 42, 731-735

Boyle, E.A. 1983 Manganese carbonate overgrowths in foraminifera tests. Geochim. Cosmochim. Acta 47, 1815-1819.

Boyle, E.A., and Edmond, J.M. 1975 Determination of trace metals in aqueous solution by APDC coprecipitation. in Gibb, ed., Analytical Methods in Chemistry, Advances in Chemistry Series, #147, ACS, Washington, D.C., pp. 44-55.

Boyle, E.A., Edmond, J.M., and Sholkovitz, E.R. 1977 The mechanism of iron removal in estuaries Geochim. Cosmochim. Acta 41, 1313-1324

Boyle, E.A., Sclater, F.R., and Edmond, J.M. 1977 The distribution of dissolved copper in the Pacific. Earth Planet. Sci. Lett. 37, 38-54

Boyle, E.A., Huested, S.S., and Jones, S.P. 1981 On the distribution of copper nickel and cadmium in the surface waters of the North Atlantic and North Pacific Ocean. J. Geophys. Res. 86, 8048-8066.

Boyle, E.A., Huested, S.S., and Grant, B. 1982 The chemical mass balance of the Amazon plume --II. Copper, nickel, and cadmium. Deep-Sea Research 29, 1355-1364

Boyle, E.A., Reid, D.F., Huested, S.S., Hering, J. 1984 Trace metals and radium in the Gulf of Mexico: an evaluation of river and continental shelf sources. Earth Planet. Sci. Lett. 69, 69-87.

Broecker, W.S. 1965 The application of natural radon to problems in ocean circulation. Symposium on Diffusion in the Oceans and Fresh Waters, ed. T. Ichiye, pp. 116-145, Lamont-Doherty Geological Observatory, Palisades, NY.

Broecker, W.S. and Peng, T.-H. 1974 Gas exchange rates between air and sea. Tellus 26, 21-35.

Bruland, K.W. 1980 Oceanographic distributions of cadmium, zinc, nickel, and copper in the North Pacific. Earth Planet. Sci. Lett. 47, 176-198.

Bruland, K.W., and Franks 1979 Sampling and analytical methods for the determination of copper, cadmium, zinc, and nickel at the nanogram per liter level in seawater, Anal. Chim. Acta 105, 233-245.

Bruland, K., and Franks 1983 Mn, Ni, Cu, Zn, and Cd in the western North Atlantic, in Trace Metals in Seawater, C.S. Wong, E. Boyle, K.W. Bruland, J.D. Burton, and E.D. Goldberg, eds. pp. 395-414, Plenum Press, New York, NY.

Callender, E., and Bowser, C.J. 1980 Manganese and copper geochemistry of interstitial fluids from manganese nodule-rich pelagic sediments of the northeastern equatorial Pacific Ocean. Am. Jour. Sci. 280, 1063-1096.

Carpenter, R. 1983 Quantitative electron spin resonance (ESR) determination of forms and total amounts of Mn in aqueous environmental samples. Geochim. Cosmochim. Acta 47, 875-885

Chester, R. and Aston, S.R. 1976 The geochemistry of deep-sea sediments. in Riley and Chester, eds., Chemical Oceanography, vol. 6, Academic Press, London, pp. 281-390.

Cochran, J.K., and Aller, R.C. 1979 Particle reworking in sediments from the New York Bight Apex: Evidence from $^{234}Th/^{238}U$ disequilibrium. Estuar. Coast. Mar. Sci. 9, 739-747.

Collier, R.W. 1981 The trace metal geochemistry of marine biogenic particulate matter. PhD Thesis, MIT/WHOI, WHOI-81-10.

Crank. J. 1975 The Mathematics of Diffusion, 2nd edition Oxford University Press

Davison, W. 1980 A critical comparison of the measured solubility of ferrous sulfide in natural waters Geochim. Cosmochim. Acta 44, 803-808

DeMaster, D.J. and Cochran, J.K. 1982 Particle mixing rates in deep-sea sediments determined from excess ^{210}Pb and ^{32}Si profiles. Earth Planet. Sci. Lett. 61, 257-271

Duursma, E.K. & Bosch, C.J. 1970 Theoretical, experimental, and field studies concerning diffusion of radioisotopes in sediments and suspended particles of the sea Part B: Methods and experiments Neth. J. Sea Res. 4, 395-469

Elderfield, H. 1976 Manganese fluxes to the oceans. Mar. Chem. 4, 103-132.

Elderfield, H. 1981 Metal-organic associations in interstitial waters of Narragansett Bay sediments. Am. Jour. Sci. 281, 1184-1196.

Elderfield, H., McCaffery, R.J., Luedtke, N., Bender, M., and Truesdale, V.W. 1981a Chemical diagenesis in Narragansett Bay sediments. Am. Jour. Sci. 281, 1021-1055.

Elderfield, H., Luedtke, N., McCaffery, R.J., and Bender, M. 1981b Benthic flux studies in Narragansett Bay. Am. Jour. Sci. 281, 768-787.

Emerson, S., Cranston, R.E., and Liss, P.,S. 1979 Redox species in a reducing fjord: equilibrium and kinetic considerations. Deep-Sea Research 26, 859-878.

Emerson, S. Jahnke, R. and Heggie, D. 1984 Sediment-water exchange in shallow water estuarine sediments. J. Mar. Res. 42, 709-730.

Evans, D.W., Cutshall, N.H., Cross, F.A., and Wolfe, D.A. 1977 Manganese cycling in the Newport River estuary, North Carolina. Estuar. Coast. Mar. Sci. 5, 71-80

Farrington, J.W., Henrichs, S.M., and Anderson, R. 1977 Fatty acids and ^{210}Pb geochronology of a sediment core from Buzzards Bay, MA. Geochim. Cosmochim. Acta 41, 289-296.

Fonselius 1976 Determination of hydrogen sulfide, in K. Grasshoff, ed. Methods of Seawater Analysis, Verlang Chemie, Weinheim.

Fritz, J.S. & Pietrzyk, D.J. 1961 Non-aqueous solvents in anion-exchange separations. Talanta 8, 143-162

Froelich, P.N., Klinkhammer, G.P., Bender, M.L., Luedtke, N.A., Heath, G.R., Cullen, D., Dauphin, P., Hammond, D., Hartman, B., and Maynard, V. 1979 Early oxidation of organic matter in pelagic sediments of the eastern equatorial Atlantic: suboxic diagenesis. Geochim. Cosmochim. Acta 43, 1075-1090.

Garrels, R.M. & Thompson, M.E. 1962 A chemical model for seawater at 25°C and one atmosphere pressure Am. Jour. Sci. 260, 57-66

Gibbs, R.J. 1977 Transport phases of transition metals in the Amazon and Yukon Rivers. Geological Society of America Bulletin 88, 829-843

Giblin, A.E., and Howarth, R.W. 1984 Porewater evidence for a dynamic sedimentary iron cycle in salt marshes. Limnol. Oceanogr. 29, 47-63.

Gilboa-Garber 1971 Direct spectrophotometric determination of inorganic sulfide in biological materials and in other complex mixtures Anal. Biochem. 43, 129-133

Goldberg, E.D. & Koide, M. 1962 Geochronological studies of deep-sea sediments by the ionium-thorium method Geochim. Cosmochim. Acta 26, 417

Goldhaber, M.B., Aller, R.C., Cochran, J.K., Rosenfeld, J.K., Martens, C.S., and Berner, R.A. 1977 Sulfate reduction, diffusion, and bioturbation in Long Island Sound sediments: Report of the FOAM group. Am. Jour. Sci. 277, 193-237.

Gordon, R.M., Martin, J.H., and Knauer, G.A. 1982 Iron in north-east Pacific waters Nature 299, 611-612

Graham, W.F., Bender, M.L., and Klinkhammer, G.P. 1976 Manganese in Narragansett Bay. Limnol. & Oceanogr. 21, 665-673

Graybeal, A.L. & Heath, G.R. 1984 Remobilization of transition metals in surficial pelagic sediments from the eastern Pacific Geochim. Cosmochim. Acta 48, 965-975

Guinasso, N.L. and Schink, D.R. 1975 Quantitative estimates of biological mixing rates in abyssal sediments. J. Geophys. Res. 80, 3032

Hammond, D.E., Simpson, J.H., & Mathieu, G. 1977 Radon-222 distribution and transport across the sediment-water interface in the Hudson River estuary J. Geophys. Res. 82, 3913-3920

Hammond, D.E., and Fuller, C. 1979 The use of radon-222 to estimate benthic exchange and atmospheric exchange rates in San Francisco Bay. in T.J. Comas, ed., San Francisco Bay: The Urbanized Estuary, AAAS, San Francisco, Ca, pp. 213-230.

Heggie, D.T. 1982 Copper in surface waters of the Bering Sea. Geochim. Cosmochim. Acta 46, 1301-1306.

Heggie, D.T., and Lewis, T. 1984 Cobalt in pore waters of marine sediments. Nature 311, 453-455.

Hornbeck, R.W. 1975 Numerical Methods, Quantum Publishers, Inc.

Howarth, R.W. 1984 The ecological significance of sulfur in the energy dynamics of salt marsh and coastal marine sediments. Biogeochemistry 1, 5-27.

Hydes, D.J. 1980 Reduction of matrix effects with a soluble organic acid in the carbon furnace atomic spectrometric determination of cobalt, copper, and manganese in seawater. Anal. Chem. 52, 959-963.

Ingle, S.E. 1975 Solubility of calcite in the ocean Mar. Chem. 3, 301-319

Jacobs, L. 1984 Metal Geochemistry in Anoxic Marine Basins. PhD Thesis, University of Washington.

Jacobs, L. and Emerson, S. 1982 Trace metal solubility in an anoxic fjord. Earth Planet. Sci. Lett. 60, 237-252.

Johnson, K.S. 1982 Solubility of rhodochrosite ($MnCO_3$) in water and seawater. Geochim. Cosmochim. Acta 46, 1805-1809.

Key, R.M., Guinasso, N.L., Schink, D.R. 1979 Emanation of radon-222 from marine sediments. Mar. Chem. 7, 221-250.

Klinkhammer, G.P. 1980 Early diagenesis in sediments from the eastern equatorial Pacific, II. Pore water metal results. Earth Planet. Sci. Lett. 49, 81-101.

Klinkhammer, G.P., and Bender, M.L. 1980 The distribution of manganese in the Pacific Ocean. Earth Planet. Sci. Lett. 46, 361

Klinkhammer, G. Heggie, D.T., Graham, D.W. 1982 Metal diagenesis in oxic marine sediments. Earth Planet. Sci. Lett. 61, 211-219.

Kraus, K.A. & Moore, G.E. 1953 Anion exchange studies VI. The divalent transition elements manganese to zinc in hydrochloric acid J. Am. Chem. Soc. 75, 1460-1462

Kremling, K. 1983 The behavior of Zn, Cd, Cu, Ni, Co, Fe, and Mn in anoxic Baltic waters. Mar. Chem. 13, 87-108.

Krom, M.D., and Sholkovitz, E.R. 1977 Nature and reactions of dissolved organic matter in the interstitial water of marine sediments. Geochim. Cosmochim. Acta 41, 1565-1573.

Landing, W.M. & Bruland, K.W. 1980 Manganese in the north Pacific Earth Planet. Sci. Lett. 49, 45-56

Li, Y-H., and Gregory, S. 1974 Diffusion of ions in sea water and in deep-sea sediments. Geochim. Cosmochim. Acta 38, 703-714.

Luedtke, N.A. and Bender, M.L. 1979 Tracer study of sediment-water interactions in estuaries. Estuar. Coast. Mar. Sci. 9, 643-651

Lyle, M., Heath, G.R., & Robbins, J.M. 1984 Transport and release of transition elements during early diagenesis: sequential leaching of sediments from MANOP Sites M and H. Part I. pH 5 acetic acid leach Geochim. Cosmochim. Acta

Martens, C.S., Berner, R.A., and Rosenfeld, J.K. 1978 Interstitial water chemistry of anoxic Long Island Sound sediments. II. Nutrient regeneration and phosphate removal. Limnol. Oceanogr. 23, 605-617.

Martens, C.S., Kipphut, G.W., and Klump, J.V. 1980a Sediment-water chemical exchange in the coastal zone traced by in situ Radon-222 flux measurements. Science 208, 285-288

Martens, C.S., and Klump, J.V. 1980b Biogeochemical cycling in Cape Lookout Bight-I. Methane sediment-water exchange processes. Geochim. Cosmochim. Acta 44, 471-490.

Martin, J.H., and Knauer, G.A. 1984 Vertex: manganese transport through oxygen minima. Earth Planet. Sci. Lett. 67, 35-47.

Mathieu, G. 1977 Radon-222/radium-226 technique of analysis. App I in Annual report to ERDA, Transport and Transfer Rates in the Waters of Continental Shelf, Contract EY76-S-02-2185, 30 pp.

McCaffrey, R.L., Myers, A., Davey, E., Morrison, C., Bender, M., Luedtke, N., Cullen, D., Froelich, P., and Klinkhammer, G. 1980 The relation between pore water chemistry and benthic fluxes of nutrients and manganese in Narragansett Bay. Limnol. Oceanogr. 25, 31-44.

Moore, J.R. 1963 Bottom sediment studies, Buzzards Bay. Jour. Sed. Pet. 33, 511-558.

Mucci, A. 1983 The solubility of calcite and aragonite in seawater at various salinities, temperatures, and one atmosphere total pressure Am. Jour. Sci. 283, 780-799

Murray,J.W. and Brewer, P.G. 1977 The mechanisms of removal of iron, manganese and other trace metals from sea water. In Glasby, ed., Marine Manganese Deposits, Elsevier, pp.291-326

Murray, J.W., Grundmanis, V., & Smethie, W.H. 1978 Interstitial water chemistry in the sediments of Saanich Inlet, British Columbia Geochim. Cosmochim. Acta 42, 1011-1026

Murray, J.W., and Gill, G. 1978 The geochemistry of iron in Puget Sound, Geochim. Cosmochim. Acta 42, 9-19.

Nozaki, Y., Cochran, J.K., Turekian, K.K., and Keller, G. 1977 Radiocarbonand ^{210}Pb distributions in submersible-taken deep-sea cores from Project FAMOUS. Earth Planet. Sci. Lett. 34, 167

Parks, G.A. 1975 Adsorption in the marine environment. In Riley & Skirrow, eds., Chemical Oceanography, vol.1, Academic Press, pp.241-308

Pedersen, T.F., and Price, N.B. 1982 The geochemistry of manganese carbonate in Panama Basin sediments. Geochim. Cosmochim. Acta 47, 1815-1819.

Rhoads, D.C. 1967 Biogenic reworking of intertidal and subtidal sediments in Barnstable Harbor and Buzzards Bay, MA. Jour. Geol. 75, 461-476.

Rickard, D.T. 1975 Kinetics and mechanism of pyrite formation at low temperatures. Am. Jour. Sci. 275, 636-652.

Robbins. J.A. 1984 A model for tracers in sediments with conveyor-belt deposit feeders. EOS 65, 960

Roman, M.R., and Tenore, K.R. 1978 Tidal resuspension in Buzzards Bay, Massachusetts. I. Seasonal changes in the resuspension of organic matter and chlorophyll a. Estuar. Coast. Mar. Sci. 6, 37-53

Rosenfeld, L.K., Signell, R.P., Gawarkiewicz, G.G. 1984 Hydrographic study of Buzzards Bay, 1982-1983. Technical Report WHOI-84-5, Woods Hole Oceanographic Institution, Woods Hole, MA.

Sanders, H.L. 1958 Benthic studies in Buzzards Bay. I. Animal-sediment relationships, Limnol. Oceanogr. 3, 245-258.

Santschi, P.H., Adler, D.M., Amdurer, M. Li, Y.-H., and Bell, J. 1980 Thorium isotopes as analogs for "particle-reactive" pollutants in coastal marine environments Earth Planet. Sci. Lett. 47, 327-335

Sawlan, J.J., and Murray, J.W. 1983 Trace metal remobilization in the interstitial waters of red clay and hemipelagic marine sediments. Earth Planet. Sci. Lett. 64, 213-230.

Sclater, F.R., Boyle, E.A., & Edmond, J.M. 1976 On the marine geochemistry of nickel Earth Planet. Sci. Lett. 31, 119-128

Sholkovitz, E.R., Boyle, E.A., and Price, N.B. 1978 Removal of dissolved humic acid and iron during estuarine mixing. Earth Planet. Sci. Lett. 41, 77-86

Sholkovitz, E.R. and Copland, D. 1981 The coagulation, solubility, and adsorption properties of Fe, Mn, Cu, Ni, Cd, Co, and humic acids in a river water. Geochim. Cosmochim. Acta 45, 181-189

Smethie, W.M., Nittrouer, C.A. and Self, R.F.L. 1981 The use of radon-222 as a tracer of sediment irrigation and mixing on the Washington Continental Shelf. Mar. Geol. 42, 173-200.

Spencer, D.W., and Brewer, P.G. 1971 Vertical advection, diffusion, and redox potentials as controls on the distribution of manganese and other trace metals dissolved in the waters of the Black Sea. J. Geophys. Res. 76, 5877-5892.

Strickland, J.D.H., and Parsons, T.R. 1972 A Practical Handbook of Seawater Analysis, 2nd edition, Fisheries Research Board of Canada, Ottawa.

Stumm, W. & Morgan, J.J. 1970 Aquatic Chemistry John Wiley & Sons, Inc.

Suess, E. 1979 Mineral phases formed in anoxic sediments by microbial decomposition of organic matter. Geochim. Cosmochim. Acta 41, 1565-1573.

Talvitie, N.A. 1971 Radiochemical determination of plutonium in environmental and biological samples by ion exchange Anal. Chem. 43, 1827-1830

Trefry, J.H. & Presley, B.J. 1982 Manganese fluxes from Mississippi Delta sediments Geochim. Cosmochim. Acta 46, 1715-1726

Turekian, K.K. and Imbrie, J. 1966 The distribution of trace elements in deep-sea sediments of the Atlantic Ocean. Earth Planet. Sci. Lett. 1, 161-168.

Yeats, P.A., Sundby, B., and Bewers, J.M. 1979 Manganese recycling in coastal waters, Mar. Chem. 8, 43-55.

BIOGRAPHICAL NOTE

The author was born in Pittsburgh, Pa., on 17 November, 1951. After living in London, New York, and Los Angeles, he settled in Paris. He graduated from the American School in Paris in 1969. His itinerant lifestyle continued through his college career: after earning a bachelor's degree, with major in economics, at Brown University in 1973, and after a brief stop at UCLA, he earned a B.S. in chemistry and a B.S. in oceanography at the University of Washington. Since 1979, he has been a student in the MIT/WHOI Joint Program in Oceanography.